UNIVERSITÀ
DEGLI STUDI
DI PALERMO

Sintesi di complessi metallici e studio della loro interazione con acido desossiribonucleico

Tesi di Dottorato del
Dott. Alessio Terenzi

Tutor
Dott. Giampaolo Barone

Co-Tutor
Dott. Andrea Pace

Coordinatore
Prof. Michelangelo Gruttadauria

Dottorato di Ricerca in Scienze Chimiche
XXII CICLO
CHIM/03

UNIVERSITÀ
DEGLI STUDI
DI PALERMO

The interaction of transition metal complexes with deoxyribonucleic acid

Tesi di Dottorato del
Dott. Alessio Terenzi

Tutor
Dott. Giampaolo Barone

Co-Tutor
Dott. Andrea Pace

Coordinatore
Prof. Michelangelo Gruttadauria

Dottorato di Ricerca in Scienze Chimiche
XXII CICLO
CHIM/03

Contents

Abbreviations

[DNA] Molar polynucleotide concentration in monomer units

BePI Benzo[e]pyridoindole derivative

BfPQ benzo[f]pyrido[3,4-b]quinoxaline

bipyOXA 3,5-bis(2′-pyridyl)-1,2,4-oxadiazole

BQQ benzo[f]quino[3,4-b]quinoxaline

CD Circular Dichroism

COSY Correlation Spectroscopy

ct- Calf Thymus

DAzP 2-(4-(pyridin-4-ylmethyl)phenyl)benzo[lmn][3,8]phenanthrolin-2-ium

DNA Deoxyribonucleic acid

EB Ethidium Bromide

H_2Salen N,N′-bis (salicylidene) ethylenediamine

H_2Salphen N,N′-bis (salicylidene) phenylenediamine

Hepes 4-(2-hydroxyethyl)-1-piperazineethanesulfonic acid

HMBC Heteronuclear Multiple Bond Correlation

Hoechst 33258 4-(6-(4-methylpiperazin-1-yl)-1H,3′H-[2,5′-bibenzo[d]imidazol]-2′-yl)phenol

HSQC Heteronuclear Single Quantum Correlation

ICD Induced Circular Dichroism

ILD Induced Linear Dichroism

LD Linear Dichroism

PCR Polymerase Chain Reaction

pyOXA 3-(2′-pyridyl)5-(phenyl)-1,2,4-oxadiazole

RNA Ribonucleic acid

TBAN Tetrabutylammonium nitrate

Tris-HCl Tris-hydroxymethyl-amino-methane

UV Ultraviolet

vis Visible

Sommario

La presente tesi è suddivisa in quattro capitoli. Il Capitolo 1 è di carattere introduttivo. Nel Capitolo 2 viene trattata la sintesi e la caratterizzazione strutturale dei complessi di Cu^{II}, Ni^{II} e Zn^{II} con il legante N,N'-Bis-5-(trietil ammonio metil salicilidene)-1,2-fenilendiammina. Inoltre, vengono riportati e confrontati i risultati dello studio della loro interazione con DNA nativo. Viene in particolare mostrato come l'interazione con DNA aumenti la stabilità fotochimica del complesso di Zn^{II}. Infine, vengono evidenziati gli effetti del confinamento in cristalli liquidi sull'interazione del complesso di Cu^{II} e DNA.Nel Capitolo 3 è riportata la sintesi e la caratterizzazione strutturale dei complessi di Cu^{II}, Zn^{II} e Ni^{II} con due leganti 1,2,4-ossadiazolici sostituiti. Viene inoltre riportato il primo studio sull'attività biologica di un complesso di rame(II) con un legante di questo tipo. I saggi biologici mostrano che, sebbene uno dei due leganti non sia efficace, il suo complesso di rame riduce la vitalità di linee cellulari umane di epatoblastoma e di carcinoma colorettale. I risultati dei saggi biologici trovano riscontro negli studi di interazione con DNA dello stesso complesso. Infine, nel Capitolo 4 è riportata la sintesi e la caratterizzazione strutturale di un legante derivato dal 2,7-diazapirenio e di un suo metallociclo binucleare di Pt^{II} oltre che lo studio, spettroscopico ed elettroforetico, della loro interazione con DNA nativo. Sono infine riportati risultati di saggi *in vitro* che dimostrano la citotossicità di tali composti nei confronti di diverse linee cellulari tumorali.

Abstract

This thesis is divided in four chapters. The aim of the work and a general introduction on the main DNA-drugs binding modes are reported in Chapter 1. In Chapter 2, the synthesis and structural characterization of Cu^{II}, Ni^{II} e Zn^{II} complexes of N,N'-Bis-5-(triethyl ammonium methyl salicylidene)-1,2-phenylenediamine will be described. Furthermore, the results of the investigation of their interaction with native DNA will be reported and compared. In particular, it will be shown that the interaction with DNA increases the photochemical stability of the Zn^{II} complex. Finally, the confinement effects of tetraethylene glycol monododecyl ether liquid crystals on the interaction of the Cu^{II} complex with DNA will be highlighted. The synthesis and structural characterization of Cu^{II}, Zn^{II} and Ni^{II} complexes of two 1,2,4-oxadiazole ligands is presented in Chapter 3. Moreover, the first study of the biological activity of a copper(II) complex of 1,2,4-oxadiazole ligands is reported. In this respect, biological assays show that, despite the free ligand is not being effective, its Cu^{II} complex reduces the vitality of human hepatoblastoma and colorectal carcinoma cells in a dose- and time-dependent manner. The results of the biological assays receive a positive feedback in the DNA binding studies performed for the same complex. Finally, in Chapter 4, the synthesis and structural characterization of a 2,7-diazapyrenium derivate and of his binuclear Pt^{II} metallacycle is reported, as well as the spectroscopic and electrophoretic study of their interaction with native DNA. Finally, *in vitro* essays are reported that show the cytotoxic effect of such compounds toward tumor cell lines.

Chapter 1

Introduction

Contents

> Life is what happens to you while you're busy making other plans.
>
> J. Lennon, 1980

1.1 Introduction

The argument of this thesis is the synthesis and characterization of metal complexes and the study of their interaction with native deoxyribonucleic acid (DNA). It is in fact known that DNA is a major target of anticancer drugs and that the most common clinically used metallo-based anticancer-drugs are today platinum compounds able to covalently bind to the DNA macromolecule [1]. Nevertheless, platinum anticancer drugs often present serious side-effects. For such reason, nowadays there is a growing research interest in the study of the reversible interaction of small molecules with DNA [2–4]. In this context, an interesting aspect of this work is that the metal compounds synthesized interact with DNA through the three principal non-coordinative modes of binding recognized up to our days: (i) intercalation, (ii) groove binding and (iii) the recently discovered metallo-supramolecular groove binding [2–4]. A short description of the three DNA-binding modes is reported below (see Section 1.2). Furthermore, each of the main chapters concerns one of these three DNA-binding modes.

In particular, three DNA-intercalators are considered in Chapter 2. These are Cu^{II}, Ni^{II} e Zn^{II} complexes of a Schiff base tetradentate ligand, called H_2L^{2+}. In the same chapter it is shown that DNA intercalation inhibits the photooxidation occurring to $Zn^{II}L^{2+}$ in buffered water solution and that the $Cu^{II}L$-DNA interaction is deeply affected by confinement in reverse micelles, mimicking the intracellular environment.

Chapter 3 deals with Cu^{II}, Ni^{II} e Zn^{II} complexes of two 1,2,4-oxadiazole chelating ligands (called bipyOXA and pyOXA). It is there shown that $[Cu(bipyOXA)_2(H_2O)_2]^{2+}$ has the characteristics of a DNA groove binder and that it reduces the vitality of human hepatoblastoma and colorectal carcinoma cells lines.

Finally, a metallo-supramolecular groove binder, a binuclear Pt^{II} 2,7-diazapyrenium metallacycle, is discussed in Chapter 4. Specifically its effect on the DNA structure as well as its cytotoxicity against human cancer cell lines are highlighted.

Each of the three chapters is independent from the others and can be read in any order. Detailed introductions and specific conclusions are reported.

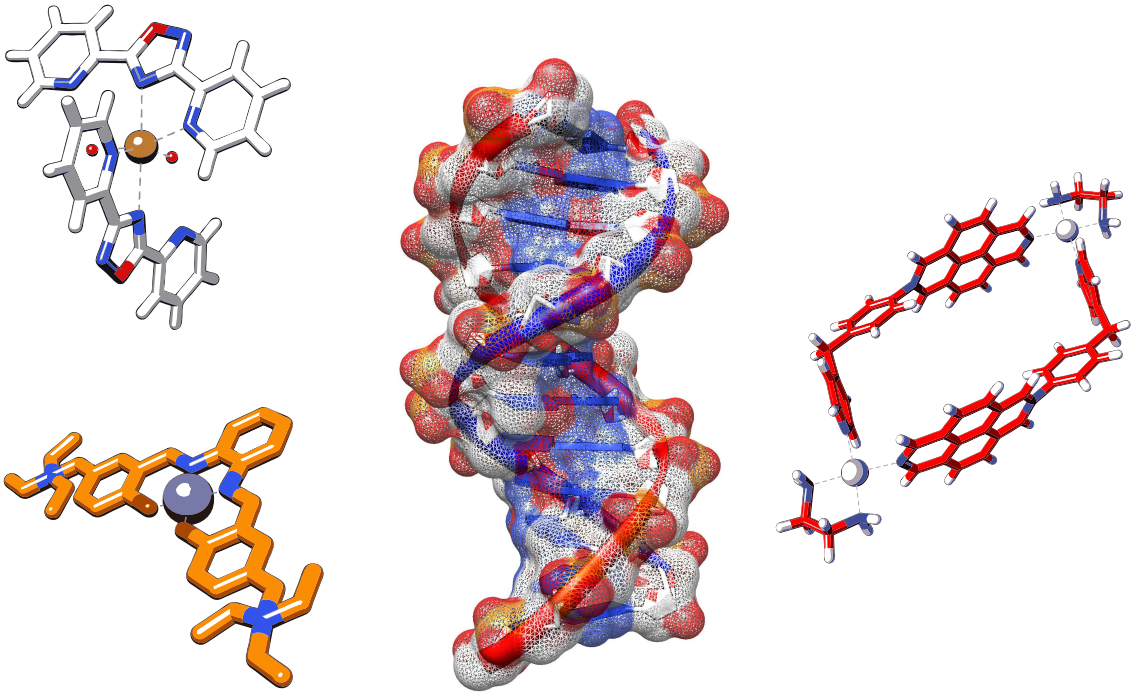

Figure 1.1: Illustration of the metal compounds whose interaction with DNA was investigated in this thesis.

Different techniques were used to monitor the DNA-metal complex interactions, for example: UV-visible absorption and fluorescence spectroscopy, circular and linear dichroism and gel electrophoresis. Among these, linear dichroism and polymerase chain reaction (PCR) electrophoresis will be shortly described in Chapter 2, because of their peculiarity and novelty.

The results described in the present thesis have been obtained at the University of Palermo, at the University of La Coruña (Spain) and at the University of Birmingham (UK). In particular, in 2009 I have spent about seven months working with the group of Professor José M. Quintela Lopez, University of La Coruña. There, I have performed the synthesis of dinuclear square metallacycles of Pt^{II} with the 2,7-diazapyrenium ligand. Furthermore, I have spent six months with the group of Professor Michael J. Hannon at the University of Birmingham, in particular exploiting linear dichroism and PCR as tools to investigate the interaction between metal compounds and native DNA.

1.2 DNA-drug interactions

The double-helical structure of DNA was first published by Watson and Crick in 1953 [5, 6]. Only few years later, Lerman reported the first studies of the interaction between small molecules and DNA, demonstrating that acridine dyes intercalate between DNA base pairs [7] (Figure 1.2). Moreover, Rosenberg et al. indicated cisplatin, a DNA covalent binder, as a highly effective agent in eliminating tumours [8] (Figure 1.2). Since then the research of small molecules able to interact with DNA has attracted the interests of many chemists.

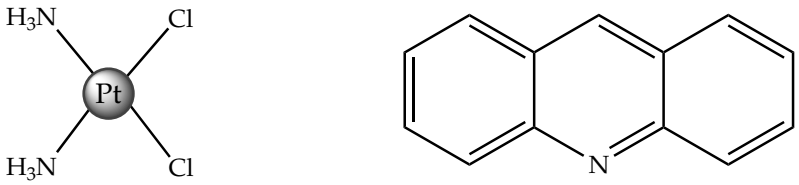

Cisplatin Acridine

Figure 1.2: Structure of two important molecules able to interact with DNA: cisplatinum and acridine.

DNA-binding drugs can be classified according to the type of association with DNA: covalent binding agents, major- or minor-groove-binders, intercalators, and external binders (phosphodiester backbone-binders). It is well known that one of the most successful anticancer drugs, cisplatin, acts through the formation of coordination bonds with the N7 nitrogen atoms on two neighbouring guanine DNA bases [1]. In this form, DNA cannot be processed or correctly repaired by cellular proteins, the cell is therefore unable to replicate and dies. Despite its success, cisplatin is efficient in only a limited range of cancers, has lot of severe side-effects and for some other tumours often induces "resistance" during the treatment [9]. During the past years a number of platinum-based drugs with less side-effects and improved pharmacological properties were synthesized (Figure 1.3), but the research is now oriented also toward less toxic molecules, able to interact reversibly with the polynucleotide.

1.2.1 Intercalation

This binding mode involves the insertion of a planar aromatic ring between the base pairs of DNA, leading to significant π overlap and for this reason is usually favoured

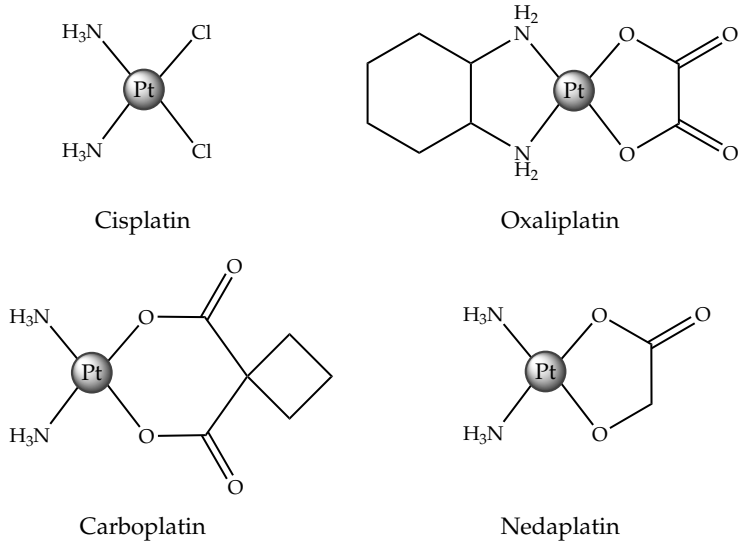

Figure 1.3: Structure of Platinum complexes clinically used as anticancer drugs.

by the presence of an extended electron-deficient planar aromatic ligand. Many different compounds have been proven to be DNA-intercalators, for example proflavine, ethidium bromide and daunomycin (Figure 1.4).

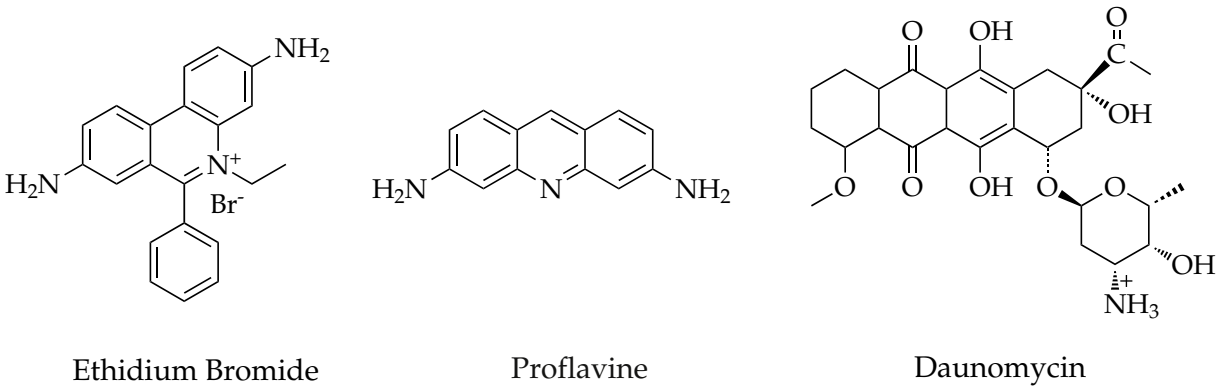

Figure 1.4: Structure of three classic DNA-intercalators.

Intercalating compounds distort the native structure of the DNA double helix. There is a decrease in the twist angle between the base pairs around the intercalation site, and the length of the biopolymer is increased. All of these effects are reversible upon removal of the intercalator at room temperature [10, 11]. The biological effects of the intercalators are exerted mainly through interference with the recognition and function of DNA-binding proteins (for example polymerases and topoisomerases), which are probably responsible of drug-selectivity at the cellular level [12].

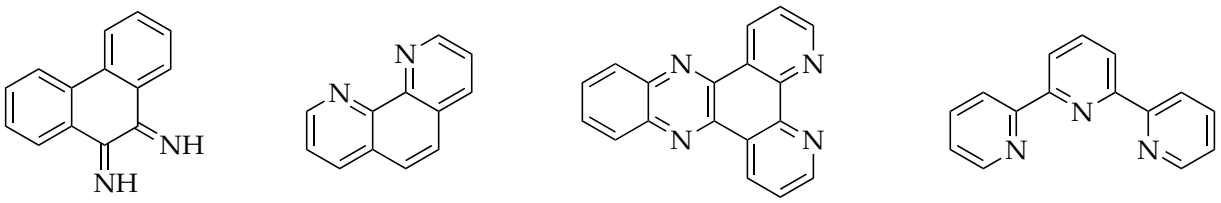

phi phen dppz terpy

Figure 1.5: Structure of classic ligands used in metallo-intercalators: phi (9,10-phenanthrenequinone diimine), phen (1,10-phenanthroline), dppz (dipyrido[3,2-a:2′,3′-c]phenazine) and terpy (2,2′:6′,2″-terpyridine).

Since the DNA phosphate backbone is negatively charged, a suitable method to improve the affinity for DNA of an organic molecule is to incorporate it as a ligand in a cationic metal complex [2, 13–15]. Moreover, metal compounds usually present interesting features such as luminescence and DNA cleavage properties. The aromatic ligands shown in Figure 1.5 are among the most used ligands in metal complexes that are well known as effective non-covalent DNA binders [2, 4]. Barton *et al.*, for example, found that ruthenium(II) polypyridine octahedral complexes, produce what has become known as ”light switch effect”: they only emit when are bound to DNA [16]. As another example, the rhodium(II) complex of the phi ligand (see Figure 1.5) was the first DNA-metallo-intercalator binding complex whose structure was characterized by X-ray crystallography [2, 17]. In the same context, during the first part of my Ph.D. I have concluded the investigation of the DNA interaction with a Fe^{III} complex with the ligand dppz, which was found to be a strong DNA-intercalator [18]. Such investigation was the argument of my thesis for the master degree in Chemistry.

Although intercalation mechanism was proposed years ago, its ”appeal” is still untouched. For instance, it has been recently reported that human telomeric quadruplex DNA structure, a potential target of novel anticancer drugs [19, 20], is stabilized by metal-Salphen complexes that are known intercalators [21, 22]. Even more recently, Hepes (4-(2-hydroxyethyl)-1-piperazineethanesulfonic acid) was found to stabilize by intercalative interaction a Z-Z junction, a potential target of a number of anticancer drugs during DNA replication [23].

DNA junctions are formed when two or more duplexes come together and exchange strands. The Z-Z junction is formed at a discontinuity point of the double strand, where a single nitrogen base is present without its complementary counterpart, producing Z-DNA double helices. Hepes is inserted in the junction region of the left-handed helix,

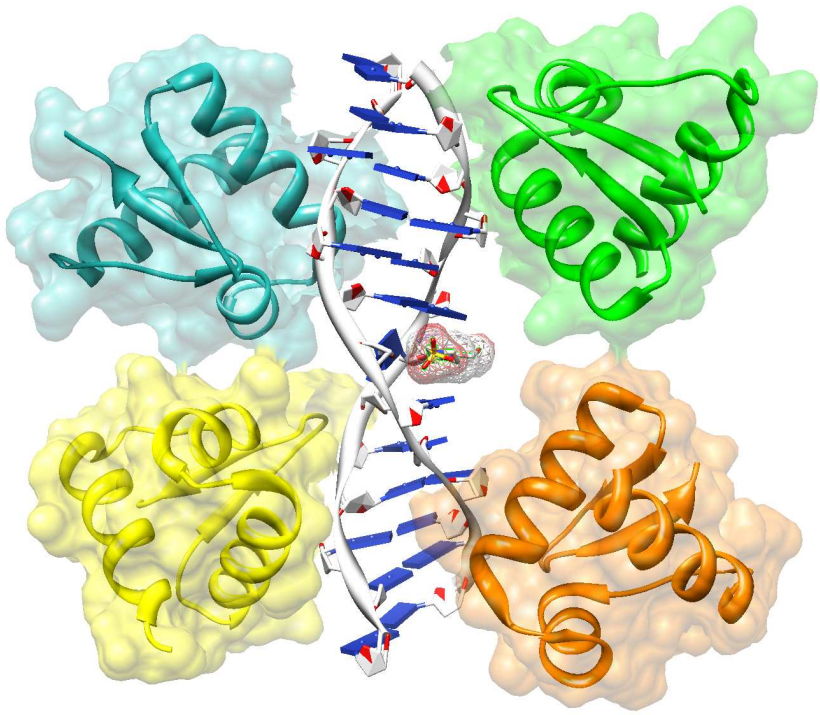

Figure 1.6: Adapted picture of Hepes intercalated in a DNA duplex. Overall structure of a Z-Z junction. The DNA duplex is shown as a skeletal model. Four Zα protein domains are bound to the duplex $(CG)_3A(CG)_3$ DNA oligonucleotide and shown as ribbon diagrams. The molecular surface of each chain is shown transparent [23].

which is otherwise resistant to intercalation. The unexpected Hepes intercalation stabilizes the left-handed conformation by restoring base stacking to some extent and may have deleterious effects for cancer cells resulting in lethal DNA rearrangements. Moreover, this finding could explain one of the mechanisms through which intercalating agents exert their anticancer action [23].

1.2.2 Groove-binding

B-DNA has two distinct grooves in the double-helical structure, termed minor and major. Proteins and large molecules, for example oligonucleotides, bind DNA preferentially through the major groove, because it is a good receptor in terms of size, flexibility and possibility to form H-bonding [2, 24, 25]. Small molecules typically bind DNA through the minor groove, where sequence recognition is limited compared to the major groove, in large part due to less varied H-bonding patterns and more limited shape vari-

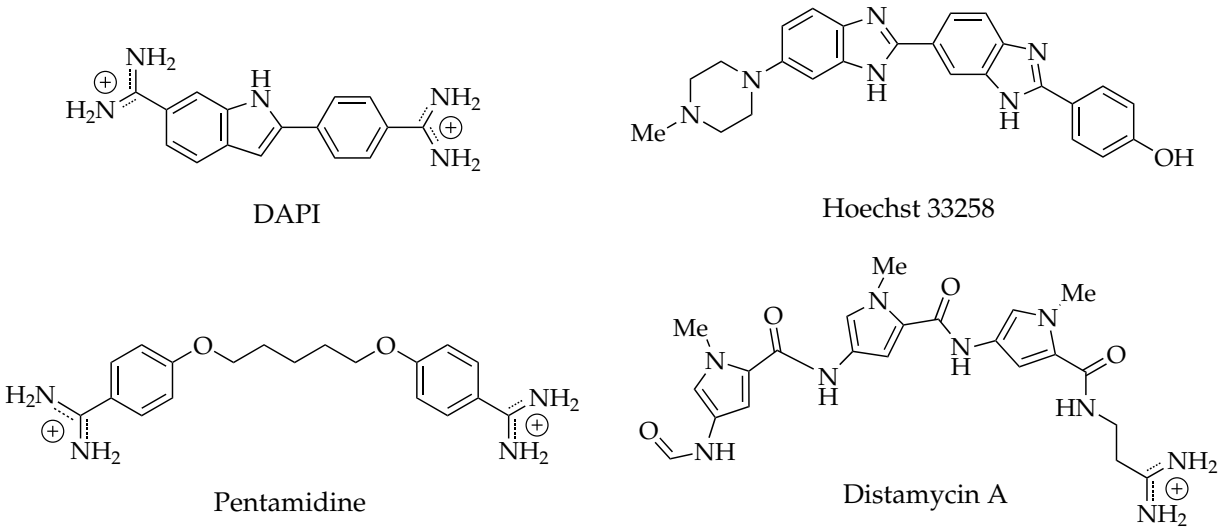

Figure 1.7: Minor groove binding agents.

ations with sequence. The natural compound distamycin A, synthetic diarylamidines (such as DAPI and pentamidine) and bis-benzimidazoles (such as Hoechst 33258) are among the most common groove binders (see Figure 1.7).

Minor groove binders are characterized by a high level of sequence specificity. They are among the most widely studied class of DNA-binding agents and exhibit several biological activities. Some of them, for example, have found clinical application in treating cancers, protozoal diseases, as anti-viral and anti-bacterial agents [26]. DAPI and

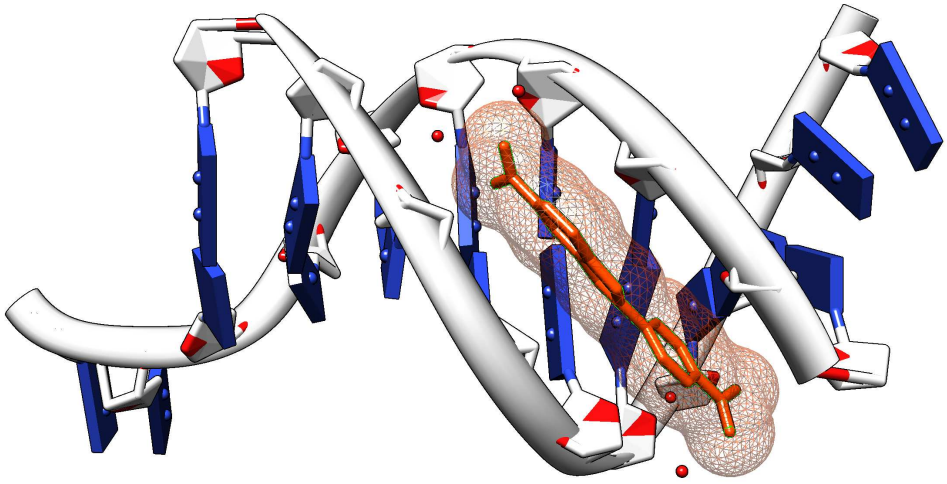

Figure 1.8: View of DAPI (orange with transparent surface) binding in the minor groove of DNA [27].

pentadimine, two proved DNA groove binders (see Figure 1.7 and Figure 1.8), reached the clinical trial phase because of their effective antiparasitic activity, especially against trypanosomes [26,28]. DAPI was shown to inhibit DNA and RNA polymerase and was found to bind specifically to AT-rich regions of double-stranded DNA [26,29].

Recently, a series of 1,3,4-oxadiazoles, an important class of heterocyclic compounds with a broad spectrum of biological activities, were found to induce apoptosis in cultured breast cancer cells [30]. Interestingly, several metal complexes are DNA-groove binders. For example, Pt^{II} complexes of substituted 1,2,4-oxadiazole derivatives, that are DNA-groove binders, have shown antitumor activity towards human ovarian cancer cell lines [31].

1.2.3 Metallo-supramolecular groove binding

Chemistry-biology interfaced research groups have been in the last years interested in finding novel types of drug-DNA recognition modes. Molecules able to interact with B-DNA *via* conventional binding processes, were found to recognize and stabilize triplex and quadruplex DNA structures as well [2].

Cationic benzopyridoindole ligand BePI and the analogous BfPQ and BQQ, for instance (see Figure 1.9), were found to have a strong preference for triplex over duplex DNA [2,32,33].

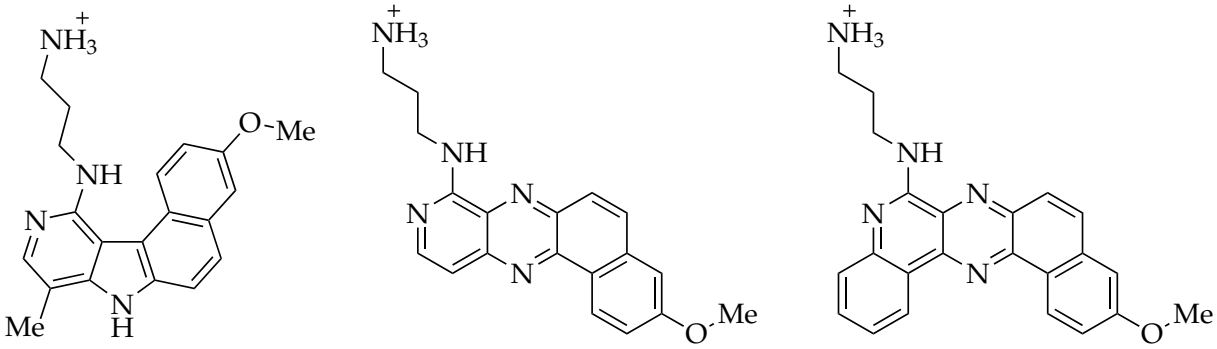

BePI BfPQ BQQ

Figure 1.9: Triplex-binding intercalators. BePI (benzo[e]pyridoindole derivative), BfPQ (benzo[f]pyrido[3,4-b]quinoxaline) and BQQ (benzo[f]quino[3,4-b]quinoxaline) [32,33].

Even more interesting is the possibility to stabilize DNA junction structures through synthetic agents specifically designed. Cardin *et al.* have recently described the crystal

structure of two bis-acridine intercalators combined with eight oligonucleotides, simulating a 4-way junction (the so called Holliday junction) [2, 34].

The role of triplex and quadruplex junction DNA structures in cells is not yet clear and the design of specific chemical probes which recognize only one of the many possible structures could help to this aim. In this context, supramolecular assemblies, such as those constituted by metal complexes fitting the size of the DNA major groove, have been recently considered. The self-assembly approach, and in particular the use of metal ions to control it, has led to the synthesis of topologically novel molecular structures, including, knots, grids, boxes and cylinders [35–39]. These so called metallo-supramolecular agents, bigger than the usual DNA binders, can mimic the dimensions of protein DNA recognition motifs. Hannon *et al.*, for example, have designed an iron(II) tetracationic triple-stranded cylinder (see Figure 1.10) with dimensions similar to those of the alpha-helical DNA recognition unit of zinc fingers proteins. It has been demonstrated, in particular by X-ray crystallography, that this cylindrical molecule binds in the major groove of DNA duplex and that it fits in the heart of a DNA 3-way junction, the first completely new way of DNA recognition in the last 40 years [2, 40].

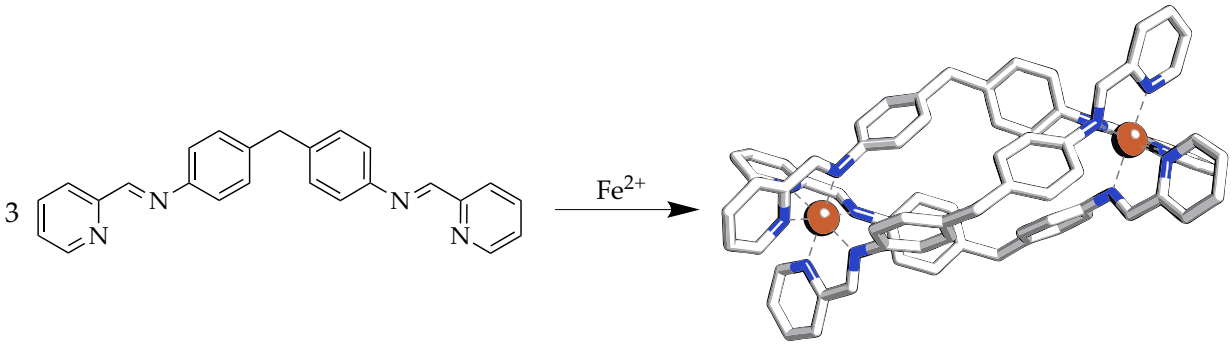

Figure 1.10: The metallo-supramolecular iron cylinder synthesized by Hannon *et al.* [2, 40].

Chapter 2

The interaction of DNA with Ni^{II}, Cu^{II} and Zn^{II} Schiff base complexes

Contents

But the fool on the hill sees the sun
going down, and the eyes in his head
see the world spinning round.

Lennon/McCartney, 1967

2.1 Introduction

The condensation of an amine with an aldehyde, forming a Schiff base, is one of the oldest reactions in chemistry [41, 42]. The condensation of a salicylaldehyde with 1,2-diaminoethane gives what is called "Salen", an acronym widely used to denote a family of Schiff base compounds having a structure derived from N,N′-bis (salicylidene) ethylenediamine (see Figure 2.1). In particular, when 1,2-phenylendiamine derivatives instead of the 1,2-diaminoethane are used, the final products are generally called "Salphen" ligands.

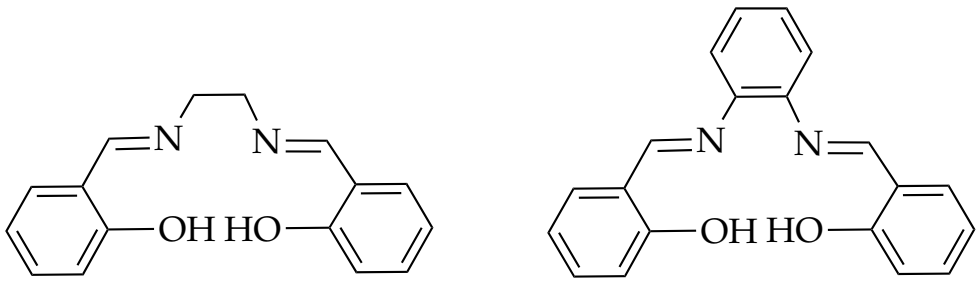

H_2Salen H_2Salphen

Figure 2.1: Geometries of H_2Salen (N,N′-Bis-salycilidene-ethylenediamine) and of H_2Salphen (N,N′-Bis-salicylidene-1,2-phenylenediamine) ligands

Schiff bases are among the most popular nitrogen donor ligands. In fact, because of its Lewis basicity, the imino nitrogen is well suited to form coordination bonds with metal ions [43, 44]. When the two hydroxy groups are deprotonated, these ligands present four coordination sites, two oxygens and two nitrogens, in an almost square planar array. For this reason, they are suitable for the equatorial coordination of transition metals, leaving two axial sites open for the potential coordination of ancillary ligands. Salen and Salphen ligands are easy to prepare, inexpensive and generally stable. The salicylidene imino group of the isolated ligand may undergo acid-catalyzed hydrolysis, reverting to the corresponding salicylaldehyde and diamine in the presence of

water [44]. However, Salen- and Salphen-metal complexes are even more stable and can be used in aqueous media without undergoing hydrolysis. In 1889 Combes prepared the first Salen-type ligand and its Cu complex [45]. Since then, Salen derivatives and their metal complexes have been extensively used in transition-metal chemistry for a large variety of applications, especially in catalysis [42, 44, 46]. In homogeneous and heterogeneous catalysis they have been used in numerous organic conversions including the epoxidation of olefins and asymmetric ring opening of epoxide [47].

In particular, metal complexes of the ligand shown in Figure 2.2 have been successfully applied to a broad range of industrially important asymmetric reactions. The Mn^{III} complex of this ligand, for example, is known as "Jacobsen's catalyst" and is currently the most efficient catalyst available for the enantioselective epoxidation of unfunctionalized olefins [46, 48].

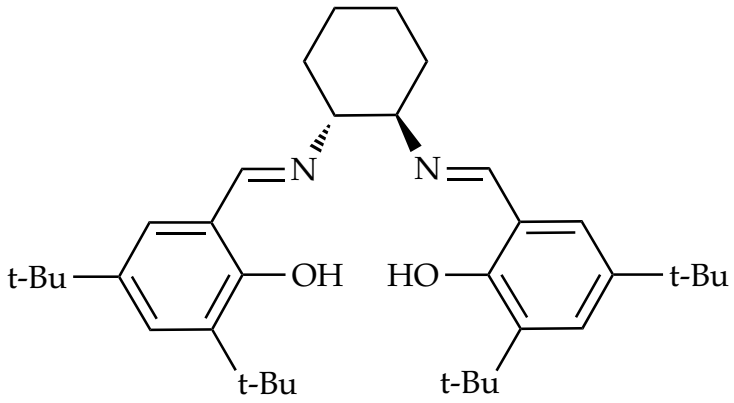

Figure 2.2: The Salen-type ligand used for the "Jacobsen's catalyst"

Salen and Salphen complexes have been recently used as molecular building blocks in material science. For example, they have been incorporated into a wide variety of structures and devices such as sensors, multimetallic systems useful for cooperative catalysis and molecular templates for organic and inorganic synthesis [49].

Moreover, several Salen metal complexes have found biomedical applications, for instance as potent anti-inflammatory or anti-viral drugs, as models for superoxide dismutase and as markers for several pathological conditions including ovarian cancer [42, 50, 51]. For example, a Fe^{III}-Salphen complex is a potent growth-suppressing agent *in vitro* for ovarian cancer cell lines, with a potential therapeutic use in the treatment of such tumors *in vivo* [51, 52]. Mn-Salphen (EUK178) and different Mn-Salen derivatives display cytoprotective features in fibroblast cultures via hydrogen peroxide scavenging [51, 53].

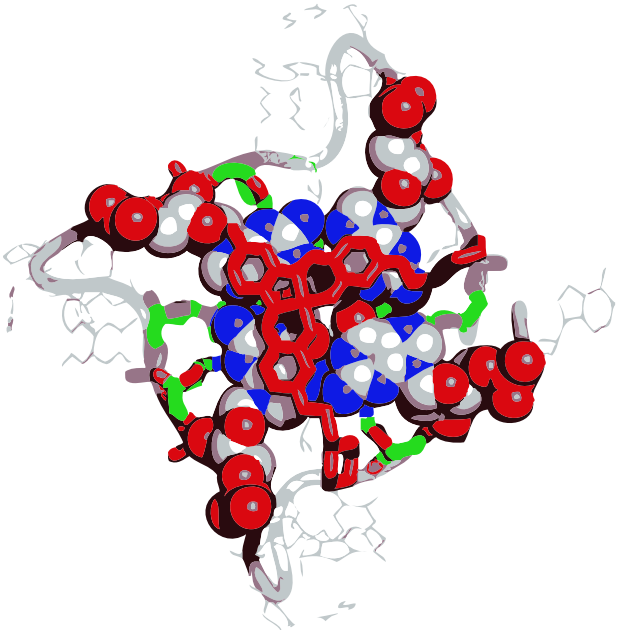

Figure 2.3: A Salphen-type complex (red coloured, in the middle) proposed by Vilar et. al [19, 20], that produce quadruplex DNA stabilization.

Among the various mechanisms through which Salen metal complexes carry out their action in bioenvironments, of utmost importance is their direct interaction with DNA. Salen, Salphen and their functionalized water-soluble ligands coordinate transition metal atoms via a square planar N_2O_2 system and are characterized by an extended nearly planar area. These properties make Salphen metal complexes potential candidates as DNA intercalators, while Salen metal complexes, lacking the aromatic phenyl moiety, are usually external DNA binders [54]. As a matter of fact, several DNA binding studies of metal complexes of Salen-type ligands have been reported in the literature [19, 55–60]. For example, it has been recently reported that some metal-Salphen complexes are able to stabilize human telomeric quadruplex DNA structures (see Figure 2.3), potential targets of novel anticancer drugs [19, 20].
In this context, the interaction between native DNA and Cu^{II} and Zn^{II} complexes of N,N'-Bis-5-(triethyl ammonium methyl salicylidene)-1,2-phenylenediamine (H_2L^{2+}, see Figure 2.4) has been recently investigated [21]. The results obtained collectively show that ZnL^{2+} and CuL^{2+} strongly interact with native DNA, by a combined electrostatic and intercalative mechanism and that CuL^{2+} is a stronger DNA binder than ZnL^{2+}. In the first pargraph (Section 2.2) of the present chapter further insights into this interaction are presented, as well as that between DNA and the nickel(II) complex of the same

ligand [22].

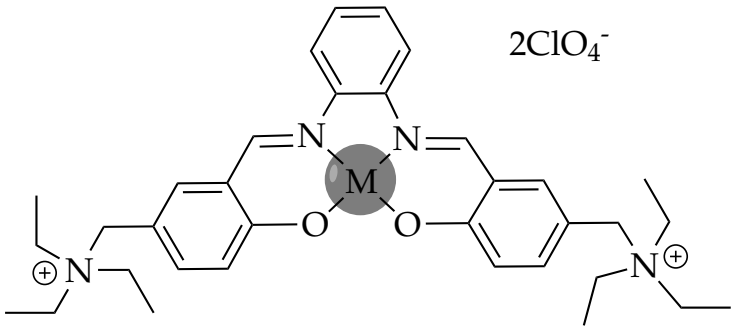

Figure 2.4: Structure of the ML^{2+} complex (M = Cu, Ni, Zn, H_2L^{2+} = N,N'-Bis-5-(triethyl ammonium methyl salicylidene)-1,2-phenylenediamine).

The structural characterization of the three complexes and the spectroscopic study of their interaction with the DNA macromolecule are the core of the first part of this chapter. For what concerns the study of the DNA-metal complex interaction, the following spectroscopic techniques were mainly used as investigation tools: variable temperature UV-visible absorption, fluorescence emission, circular and linear dichroism. Moreover, the effect of the complexes on the DNA processing was further investigated by performing *in vitro* experiments as gel-electrophoresis and polymerase chain reaction (PCR) assays. On the basis of all these techniques, which afford an indirect and complementary evidence of the interaction occurrence, a DNA-intercalation mechanism was confirmed for the three metal complexes, with a decreasing interaction strength in the order: $NiL^{2+} > CuL^{2+} > ZnL^{2+}$.

Furthermore, a detailed investigation of the photophysical and photochemical properties of ZnL^{2+}, due to its exposition to tungsten lamp light and of how these properties are influenced by its interaction with DNA is presented in the second paragraph (Section 2.3). Fluorescence spectroscopy measurements were mainly exploited for this purpose. Moreover, quantum chemical calculations were performed to support the hypothesis that the effect of the photoexposition is to partially oxidize ZnL^{2+} to ZnL^{4+} [61].

Finally, the study of the interaction of the CuL^{2+} with DNA in a micro-heterogeneous system, able to segregate the biomolecule in a nanoscopic domain made by tetraethylene glycol monododecyl ether liquid crystals, is reported in the third paragraph (Section 2.4). Such inverse micellar system was intended as a "biomimetic" model of the intra-cellular environment [62].

2.2 The interaction of DNA with NiL^{2+}, CuL^{2+} and ZnL^{2+}

The interaction between native DNA and CuL^{2+} and ZnL^{2+} cationic complexes in aqueous solution has been previously described [21]. Here the investigation is extended to the NiL^{2+} complex, with the aim to evaluate the role of the metal atom on the DNA binding properties of Ni^{II}, Cu^{II} and Zn^{II} complexes of the same Schiff base ligand [22]. In details, the UV-visible absorption, circular dichroism and fluorescence spectroscopic techniques have been used to investigate NiL-DNA solutions. Furthermore, flow linear dichroism titrations of DNA aqueous solutions in the presence of increasing amounts of the NiL^{2+}, CuL^{2+} and ZnL^{2+} complexes are reported. Finally, their effect on the DNA processing was tested through *in-vitro* experiments, such as gel-electrophoresis and polymerase chain reaction (PCR) assays.

2.2.1 Structural characterization of NiL^{2+}, CuL^{2+} and ZnL^{2+}

NiL^{2+}, CuL^{2+} and ZnL^{2+} were characterized by elemental analysis, ESI mass experiments and 2D-NMR, including COSY, HSQC and HMBC spectra (see Experimental, Section 2.5 and Appendix A). The NMR spectra of the paramagnetic CuL^{2+} complex were not reported, while its structure was characterized in the solid state by X-ray crystallography. In fact, suitable crystals for X-ray diffraction analysis were obtained only for the copper complex (see below and Appendix B). The NiL^{2+} crystals were too small while it was not possible to crystallize the Zn^{II} complex. Considering that Ni^{II} has a d^8 electronic configuration, the square planar N_2O_2 coordination around the Ni atom can be also inferred on the basis of the diamagnetic nature of the compound, typical of planar nickel compounds. According to the literature, the diamagnetism of Ni-Salen is also maintained in solutions of coordinating and non-coordinating solvents [63]. This evidence is confirmed by the NMR spectra obtained. The ^{1}H-NMR of NiL^{2+} and its labelling are shown in Figure 2.5.

Concerning the coordination geometry of ZnL^{2+}, a comparison between calculated and experimental electronic spectra (see Section 2.3) suggests the presence of an apical water molecule coordinating the metal atom, creating a pentacoordinated aquo-complex, in agreement with the structure of ZnSalphen complexes reported in the literature [63].

The crystal structure of CuL^{2+} (see Figures 2.6 and B.1) has been obtained from single crystal X-ray diffraction data and confirms the expected molecular conformation

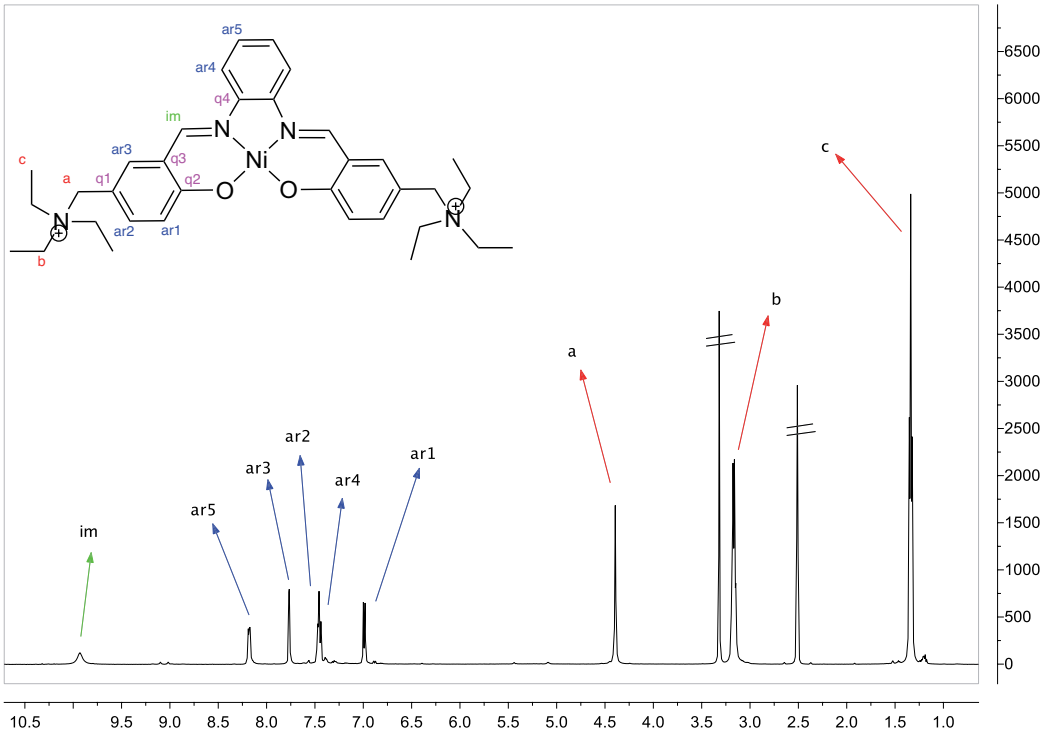

Figure 2.5: ^{1}H NMR (500 MHz, DMSO) of the NiL^{2+} complex. Further NMR spectra of NiL^{2+} and ZnL^{2+} are reported in Appendix A.

as shown in Figure 2.4. The structure contains two crystallographically independent copper complexes which display the same molecular configuration and similar geometries that fall within the normal ranges for these types of species, although the poor data quality does affect the accuracy with which geometric parameters can be determined from this structure. As expected, the structure contains two perchlorate ions per copper complex as well as benzene, nitromethane and highly disordered water molecules (see Experimental Section 2.5). The two crystallographically independent copper complexes form columns through intermolecular π-π stacking interactions with an interplanar distance of approximately 3.3 Å(see Figure B.2). In one of the unique copper complexes (see Figure B.1) three methyl groups, C(124)/C(24′), C(126)/C(26′) and C(128)/C(28′) are disordered over two positions each, at percentage occupancy ratios of 71 (4):29 (4), 56 (4):44 (4) and 60:40 respectively. Most of the water molecules are highly disordered and it was not possible to refine them all anisotropically or locate all the hydrogen atoms

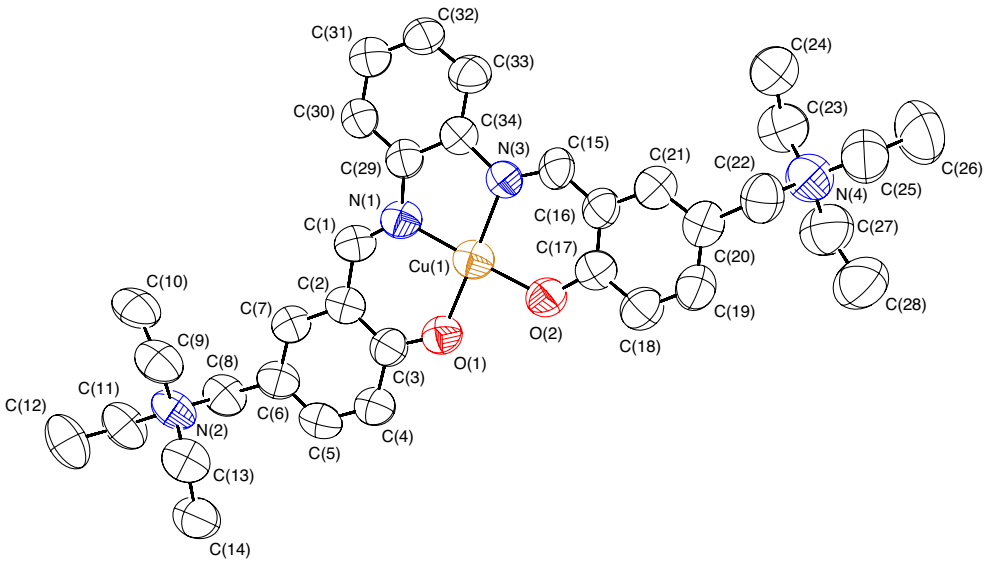

Figure 2.6: Ortep view of one of the two crystallographically independent copper complexes of CuL^{2+} with ellipsoids drawn at the 50% probability level. The perchlorate ions, benzene, nitromethane and water molecules and hydrogen atoms have been omitted for clarity. The color labelling scheme is as follows: carbon (black), copper (orange), nitrogen (blue) and oxygen (red).

belonging to them in the electron density. As a result of this it was not possible to list all the hydrogen bonding. All hydrogen atoms not belonging to water molecules were added at calculated positions and refined by use of a riding model with isotropic displacement parameters based on the equivalent isotropic displacement parameter (U_{eq}) of the parent atom. The hydrogen atoms belonging to water molecule H(81A)-O(801)-H(81B) were located in the electron density and their positions refined subject to O-H (0.88 (2) Å) and H-H (1.41 (4) Å) bond distance restraints.

2.2.2 UV-visible absorption of NiL-DNA solutions

The UV-vis absorption spectrum of NiL^{2+} in aqueous solution (black solid line in Figure 2.7) shows an intense band at about 261 nm and a weaker band in the range 330–400 nm, attributable to a metal perturbed infra–ligand electronic transition [21]. Such spectrum is significantly modified by the addition of increasing amounts of calf thymus DNA (ct-DNA). In details, the absorption band of NiL^{2+} at 352 nm (see Figure 2.7) is red shifted by about 10 nm and shows hypochromism of about 40% at [DNA]:[NiL^{2+}] molar ratio equal to 10. Furthermore, the intensity of the absorption band at 260 nm is lowered by the addition of DNA up to [DNA]:[NiL^{2+}] molar ratio of 0.75 and in-

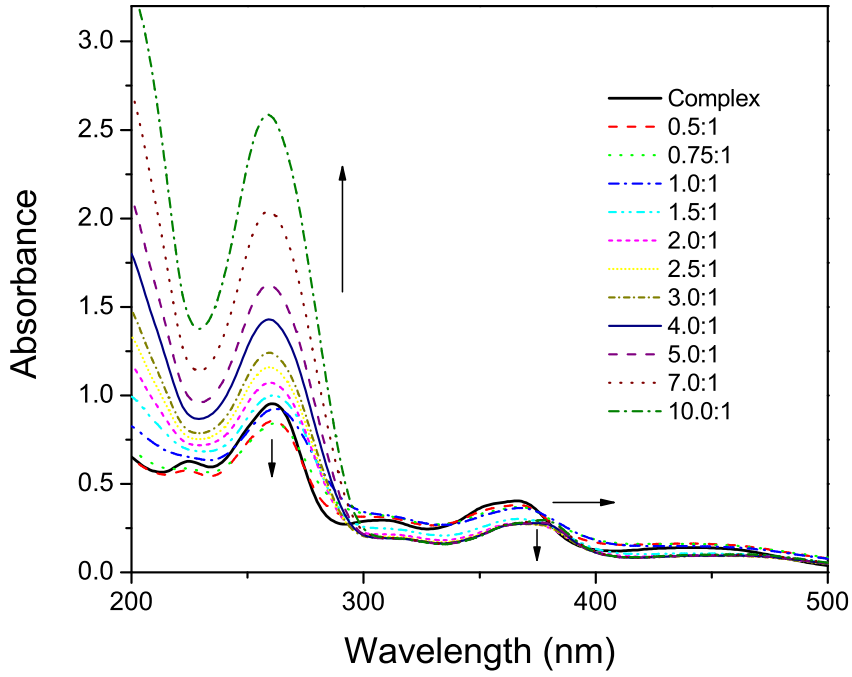

Figure 2.7: Uv-vis of 20 μM NiL^{2+} (1 mM Tris-HCl buffer) in the presence of increasing concentration of ct-DNA, in the range [DNA]:[NiL^{2+}] = 0.5:1 - 10:1 as shown.

creases at higher molar ratios. These evidences collectively suggest that Ni^{II} complex is a DNA intercalator [54, 64]. To determine the intrinsic binding constant (K_b) and the stoichiometry of the NiL^{2+}–DNA system, the quantity y (see Eq. 2.1) at 352 nm has been plotted, in Figure 2.8, as a function of the molar concentration of DNA. The quantity y contains the molar extinction coefficients of NiL^{2+}, free (ϵ_f) and bound to DNA (ϵ_b) and of the solution containing both free and bound NiL^{2+} (ϵ_a). In details, ϵ_f is determined by a calibration curve of the isolated metal complexes in aqueous solution, following the Beer-Lambert law; ϵ_b is found out from the plateau of the DNA titration (Figure 2.8), where addition of DNA did not result in further changes in the absorption spectrum [21]; finally, ϵ_a is obtained as the ratio between the measured absorbance and the NiL^{2+} molar concentration [21]. The values of the intrinsic binding constant (K_b) and of the binding size in base pairs (s) of the NiL^{2+} complex were obtained by using

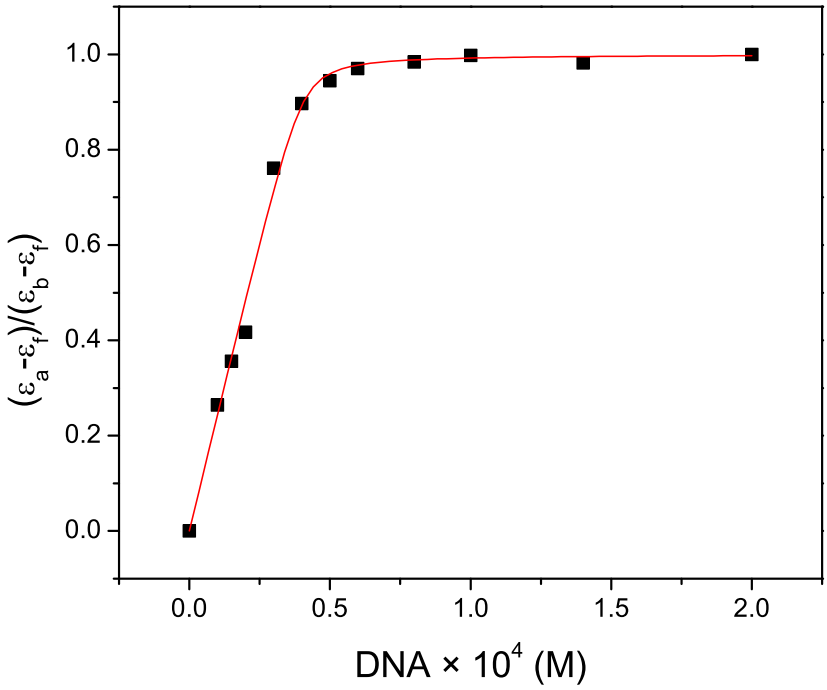

Figure 2.8: Spectrophotometric titration of NiL^{2+}, at 352 nm, with ct-DNA in aqueous solution; [NiL^{2+}] = 20 μM, [DNA] = 0 - 200 μM. The solid line is the fit of the experimental data by Eq. 2.1.

Eqs. (2.1) and (2.2) [21, 65, 66]:

$$y = \frac{\epsilon_a - \epsilon_f}{\epsilon_b - \epsilon_f} = \frac{b - \sqrt{(b^2 \cdot \frac{2K_b^2 C_t[\mathrm{DNA}]}{s})}}{2K_b C_t} \tag{2.1}$$

$$b = 1 + K_b C_t + \frac{K_b[\mathrm{DNA}]}{2s} \tag{2.2}$$

where C_t is the total concentration of the metal complex. It is known that the model leading to Eqs. (2.1), (2.2), proposed by Carter et al. [65], is valid in the assumption of a non–cooperative and non–specific binding to DNA. The K_b and s values obtained by non linear fits of the experimental data by Eqs. (2.1), (2.2) were $K_b = (4.2 \pm 0.4) \times 10^6$ M^{-1} and $s = 1.01 \pm 0.04$. These results confirm that the metal complex strongly interacts with DNA. In particular, NiL^{2+} shows an interaction stoichiometry of approximately 1 mol of

DNA base pairs per 1 mol of metal complex. Interestingly, the binding of NiL^{2+} to DNA is slightly higher than that relative to the CuL-DNA system and more than 10 times higher than that relative to the ZnL-DNA system (see Table 2.1). These comparisons suggest that the binding capability to the DNA backbone is critically influenced by the specific electronic and geometrical structures of similar complexes of the same ligand differing only in the nature of the metal atom.

Table 2.1: Comparison of K_b and s values of ML-DNA systems

	NiL-DNA	**CuL-DNA** [21]	**ZnL-DNA** [21]
K_b (M^{-1})	$(4.2 \pm 0.4)\times10^6$	$(1.28 \pm 0.05)\times10^6$	$(7.35 \pm 0.01)\times10^4$
s	1.01 ± 0.04	0.73 ± 0.01	0.69 ± 0.01

2.2.3 DNA Thermal Denaturation Analysis of NiL-DNA solutions

The thermal behavior of DNA offers some information about its binding affinity toward small molecules. The melting temperature (T_m) of DNA, which is defined as the temperature at which half of the double-stranded DNA is dissociated into single strands [67], is strictly related to the stability of the macromolecule and may be altered by the interaction with chemicals. For example, it has been reported [68, 69] that the stacking interactions, typical of intercalation processes, produce a stabilization of the DNA double helix followed by a considerable increase in the melting temperature. Thermal denaturation profiles of ct-DNA solutions, in the presence of increasing amounts of NiL^{2+}, were obtained by plotting the absorbance at 258 nm as a function of temperature (see Figure 2.9 and Table 2.2). It can be seen that T_m of ct-DNA (46 ± 1°C) increases of about 33 and 36 °C, at [DNA]:[NiL^{2+}] molar ratios 10:1 and 5:1. These results are consistent with the hypothesis of DNA-intercalation of the metal complex leading to a more compact structural arrangement of the DNA double helix. Furthermore, the presence of a positive charge on the NiL^{2+} complex should furnish further contributions to the stabilization of the double helix as a consequence of the partial neutralization of the negatively charged phosphate groups. Finally, as highlighted by the data collected in Table 2.2, the increase of the DNA melting temperature (ΔT_m) caused by addition of NiL^{2+} to the DNA solution, compared to that caused by CuL^{2+} and ZnL^{2+} [21], leads to the same conclusions drawn by comparing the binding constants of three parent com-

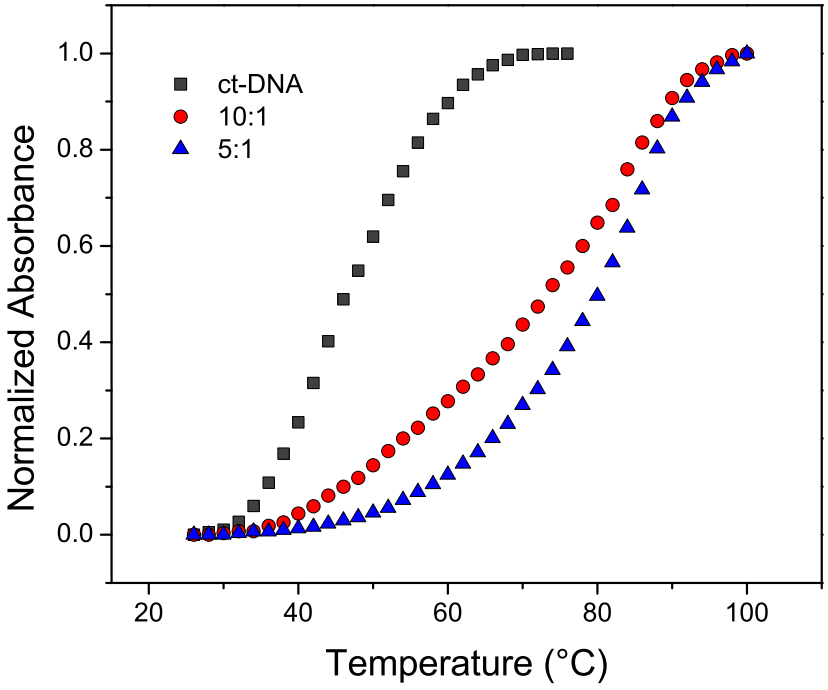

Figure 2.9: Thermal denaturation profiles of ct-DNA in the presence of increasing amounts of NiL^{2+}, in 1 mM Tris-HCl buffer; [DNA] = 100 μM; [NiL^{2+}] = 0 (squares, T_m = 46 $\pm$ 1 °C), 10 μM (circles, T_m = 79 $\pm$ 1 °C), 20 μM (triangles, T_m = 82 $\pm$ 1 °C).

Table 2.2: Comparison of ΔT_m values of ML-DNA systems

[DNA]:[ML^{2+}]	**NiL-DNA** (°C)	**CuL-DNA** [21] (°C)	**ZnL-DNA** [21] (°C)
10:1	33	21	14
5:1	36	37	17

plexes. In fact, at [DNA]:[ML^{2+}] = 10:1 the ΔT_m decreases in the order: NiL^{2+} > CuL^{2+} > ZnL^{2+}. On the other hand, NiL^{2+} and CuL^{2+} at [DNA]:[ML^{2+}] = 5:1 induce the same ΔT_m.

2.2.4 Circular Dichroism of NiL-DNA solutions

Circular dichroism (CD) refers to the differential absorption of the two circularly polarized components, one rotating counter-clockwise (left handed) and the other clockwise (right handed) of a plane polarized light. The idea behind CD is that the interaction between left and right handed photons and a chiral molecule will be different, thus only chiral molecules are able to produce a CD signal [70].

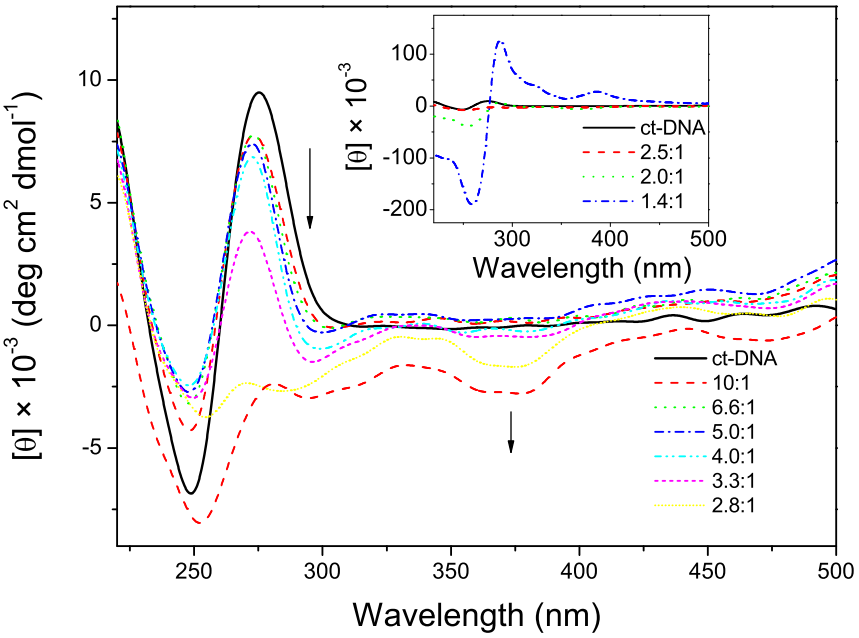

Figure 2.10: Circular dichroism spectra of 40 μM ct-DNA in the presence of increasing amounts of NiL^{2+} in 1.0 mM Tris-HCl, in the range [DNA]:[NiL^{2+}] = 10:1 - 1.4:1 as shown.

CD spectra of ct-DNA were recorded in the presence of increasing amounts of NiL^{2+}, up to [DNA]:[NiL^{2+}] molar ratios of approximately 1.4 (see Figure 2.10 and inset). Due to its right-handed helicity, the CD of native DNA (black solid line in Figure 2.10) exhibits a positive band centered at 275 nm and a negative band centered at 245 nm. Similarly to what observed for the CuL-DNA and ZnL-DNA systems [21], this typical spectrum is modified by the addition of increasing amounts of NiL^{2+} suggesting the occurrence of DNA structural modifications following the metal complex-DNA interaction. In particular, a decrease of the intensity and a blue shift of the positive CD band of DNA are observed and a weak induced CD negative band appears in the range 350-400 nm. The

latter finding can be interpreted by considering that the NiL^{2+} moiety supplies a further chromophore appended to the chiral backbone of DNA [71].

Noteworthy, the intensity of the positive band of DNA monotonously decreases with the addition of metal complex and becomes negative at NiL^{2+} concentrations higher than 14 μM, corresponding to a [DNA]/[NiL^{2+}] molar ratio equal to 2.8. Moreover, the intensity and shape of CD spectrum in the presence of [NiL^{2+}]$\geq$ 20 μM is dramatically different from that of native DNA (see inset in Figure 2.10) and it is characterized by two extremely intense negative and positive bands at about 260 and 290 nm, which can be attributed to the presence of supramolecular DNA aggregates in solution [72].

To analyze the spectral changes induced by the addition of NiL^{2+}, the molar ellipticity (a) and the UV absorbance (b) at 248 nm as a function of the NiL^{2+} concentration are reported (see Figure 2.11). The values of the absorbance follow a linear trend with

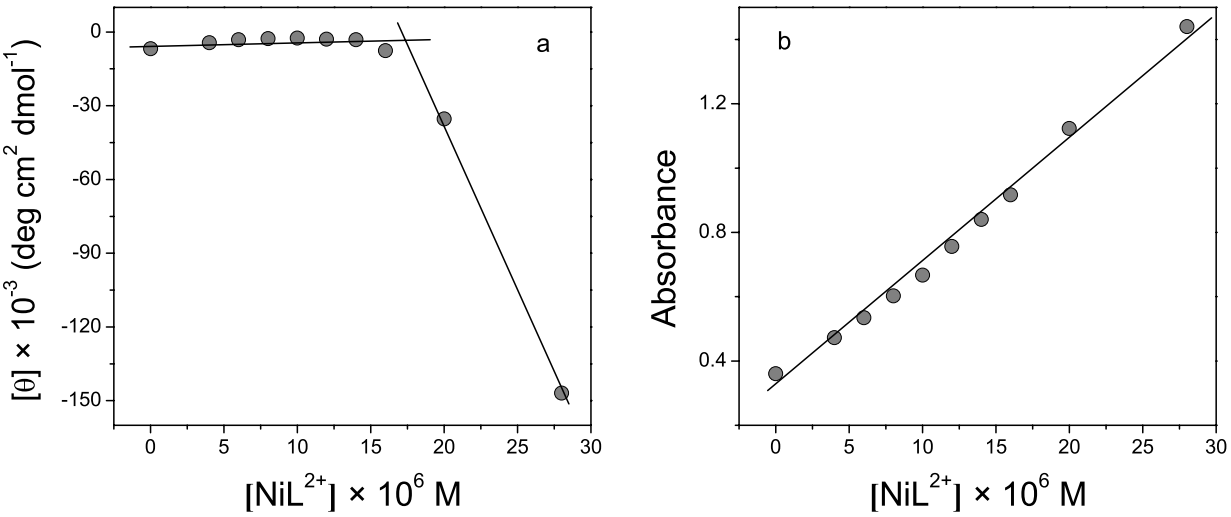

Figure 2.11: Molar ellipticity (a) and UV absorbance (b), both at 248 nm, of NiL-DNA aqueous solutions in the presence of increasing amounts of NiL^{2+}; [DNA] = 40 μM, [NiL^{2+}] =0-28 μM.

the metal complex concentration, confirming that the Lambert-Beer law is fulfilled in the investigated concentration range. On the other hand, the molar ellipticity can be described by two trends that intersect at about 18 μM, corresponding to approximately 1 NiL^{2+} per 2 DNA monomeric units, that roughly coincides with the stoichiometry value obtained by both fluorescence (see below) and UV-vis measurements. From these findings it can be argued that: i) a tight binding exists between the metal complexes and DNA; ii) the conformational changes of the DNA double helix are dramatic when the complex concentration is higher than 14 μM, probably due to the formation of DNA aggregates [72].

2.2.5 Ethidium bromide displacement assay of NiL-DNA solutions

It is known that ct-DNA does not give fluorescence, while the emission intensity is greatly enhanced in the presence of ethidium bromide (EB). EB is also weakly fluorescent, but the EB-DNA complex is remarkably more fluorescent giving an emission band at about 600 nm, as a consequence of the intercalation of EB between adjacent DNA base pairs [73]. The enhancement of the EB fluorescence is due to the inhibition of the amino

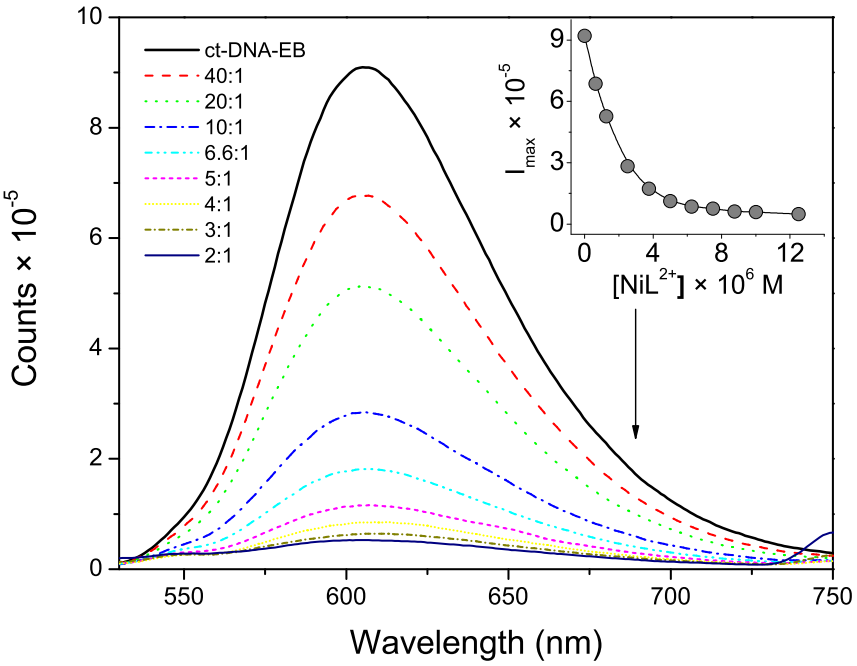

Figure 2.12: Fluorescence spectra of the EB-DNA complex in the presence of increasing amounts of NiL^{2+}. [EB] = 4 μM, [DNA] = 25 μM, range [DNA]:[NiL^{2+}] = 40:1 - 2:1 as shown. Inset: fluorescence intensity at 600 nm vs. the NiL^{2+} molar concentration.

proton transfer to the solvent occurring when EB is segregated within the DNA molecule. This phenomenon is accompanied by an increase of the EB excited state lifetime. In particular, several thorough investigations have established that a model based on triexponential function is the most appropriate to describe the fluorescence decay kinetics of EB in DNA solutions [74–76]. Such model involves that two kinds of EB molecules with different lifetimes, bound with low and high affinity to DNA sites, respectively, coexist with free EB in DNA aqueous solutions. Then, it follows that steady state and

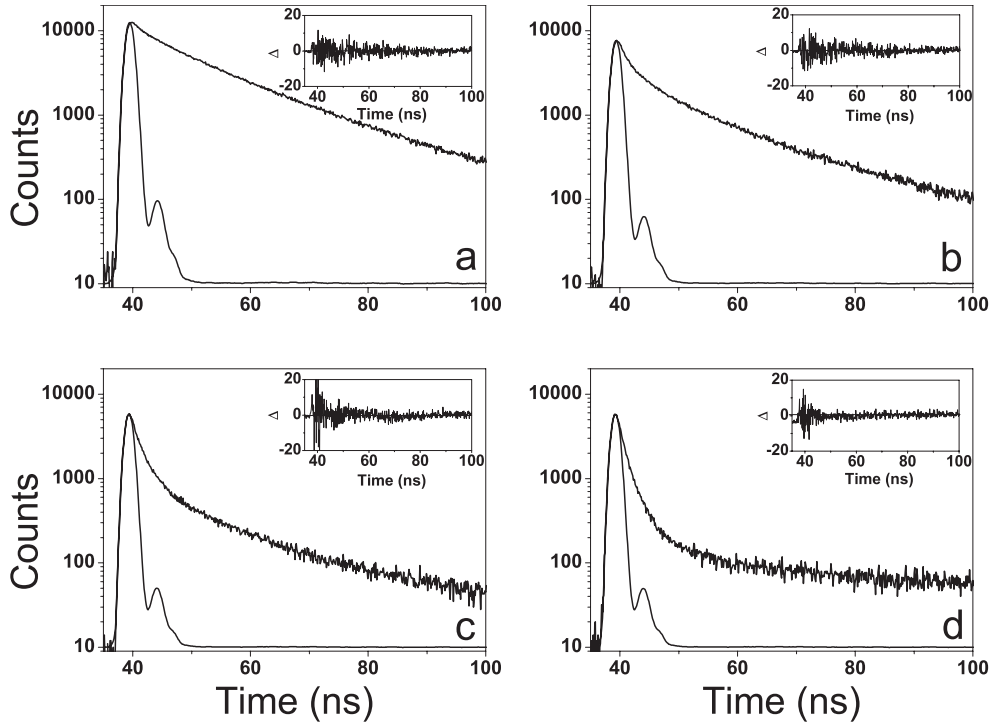

Figure 2.13: Representative decays of the investigated systems. [EB] = 4 μM, [DNA] = 25 μM; [DNA]:[NiL^{2+}] = 0 (a); 10:1 (b); 5:1 (c); 2.5:1 (d). In each panel, the inset shows the residuals.

time-resolved fluorescence spectra of EB in DNA aqueous solutions in the presence of various amounts of competitive non-fluorescent species could be useful to study the affinity of the added molecule to DNA [77]. The emission spectra of the EB-DNA complex in Tris-HCl 1 mM, in the presence of increasing amounts of the non-fluorescent NiL^{2+}, are shown in Figure 2.12. It can be noted that the intensity of the fluorescence spectrum of the EB-DNA complex is lowered by the addition of increasing amounts of the complex. In particular, by plotting the fluorescence intensity at 600 nm vs. the NiL^{2+} molar concentration (see the inset in Figure 2.12), an initial steep decrease of the signal is noticed in the range 0-4 μM, trending to level off at higher NiL^{2+} concentration. Taking into account that the EB concentration is 4 μM, this behavior is consistent with the hypothesis that NiL^{2+} competes effectively with EB for the same DNA binding sites with a displacement stoichiometry of approximately 1 mole of metal complex per 1 mole of EB.

Concerning the time-resolved fluorescence experiments, according to literature, the spectrum of EB in aqueous solution of ct-DNA can be consistently described in terms of three exponential decay functions [74–76]. Moreover, as highlighted in Figure 2.13,

Table 2.3: Fitting parameters resulting from three exponential function analysis of the fluorescence decay profiles of NiL^{2+}/EB/DNA aqueous solutions at various [DNA]:[NiL^{2+}] molar ratios and fixed EB (4 μM) and DNA (25 μM) concentrations

[DNA]:[NiL^{2+}]	τ_1 (ns)	$\mathbf{A}_1$ (%)	τ_2 (ns)	$\mathbf{A}_2$ (%)	τ_3 (ns)	$\mathbf{A}_3$ (%)
ct-DNA	1.6	26.1	9.1	43.1	20.5	30.8
40:1	1.3	33.9	8.0	35.6	20.0	30.5
20:1	1.4	44.6	7.3	30.4	19.4	25.0
10:1	1.3	57.8	6.0	26.7	19.9	15.6
6.6:1	1.4	69.0	5.5	20.2	20.0	10.7
5:1	1.3	74.7	4.2	19.2	20.8	6.0
4:1	1.3	83.9	4.6	12.9	19.8	3.2
3.3:1	1.3	81.2	3.5	16.2	20.8	2.6
3:1	1.2	83.6	3.3	14.6	20.8	1.8
2.5:1	1.3	87.6	3.3	10.6	20.8	1.8
2:1	1.2	88.9	3.3	9.2	20.4	1.9

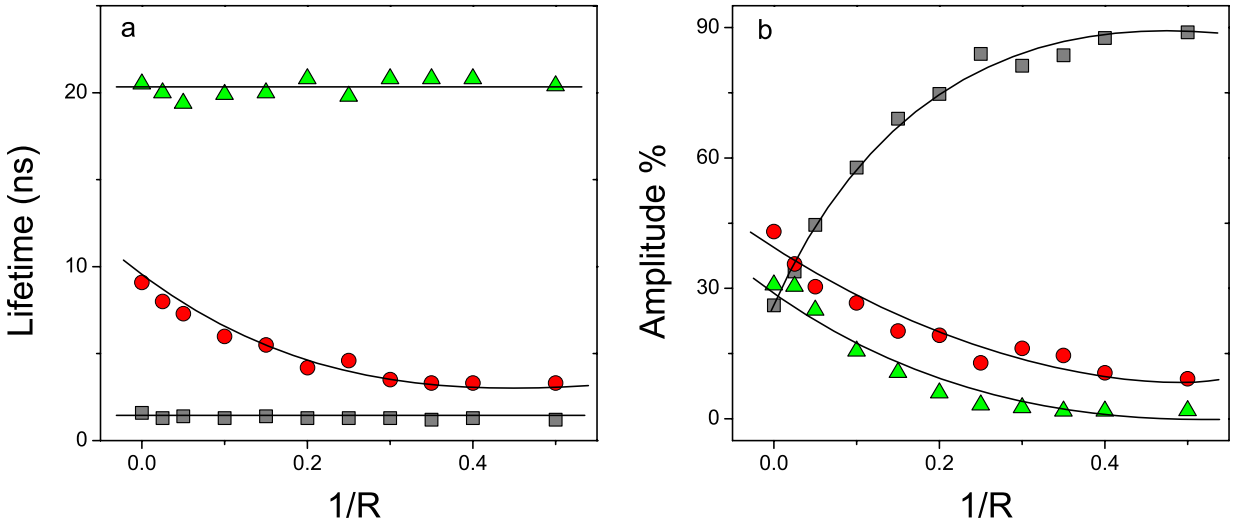

Figure 2.14: 1/R dependence of the (a) lifetimes (τ_1, squares; τ_2, circles; τ_3, triangles) and of the (b) component amplitude (A_1, squares; A_2, circles; A_3, triangles) of the three EB species in NiL^{2+}/EB/DNA aqueous solutions.

also the spectra of EB in aqueous solution of ct-DNA containing increasing amounts of NiL^{2+} are well-described by three exponential decay functions. The fitting parameters (component amplitude, $A\%$; lifetime, τ) for all the investigated samples are collected in Table 2.3.

By analyzing the data of Table 2.3 and their 1/R dependence (R = [DNA]:[NiL^{2+}]),

shown in Figure 2.14, some observations can be made: i) the lifetime of deeply intercalated EB is practically unaffected by an increase of the NiL^{2+} concentration emphasizing the nature of this binding site, while that of free EB shows a moderate decrease attributable to medium induced quenching effects; ii) the lifetime of EB molecules bonded to low affinity DNA sites decreases smoothly with $1/R$ emphasizing that these sites are accessible to species present in the solution able to quench EB; iii) as expected, the component amplitude of free EB increases with $1/R$ whereas those of EB bound at low and high affinity DNA sites decrease. It must be pointed out that the simultaneous decrease of the component amplitudes of the two types of bonded EB suggests that NiL^{2+} competes effectively and with comparable strength for both sites; iv) even at the lower [DNA]:[NiL^{2+}] values investigated, the component amplitudes of the two kind of bonded EB do not vanish, implying that some changes occur hindering a total exchange with the NiL^{2+} species.

2.2.6 Linear Dichroism of ML-DNA solutions (M = Ni, Cu, Zn)

Linear dichroism (LD) has been largely used for studying DNA-drugs interactions and is defined as the difference in absorption of light linearly polarized parallel and perpendicular to an orientation axis at a given wavelength [70,78]:

$$LD(\lambda) = A_{\parallel} - A_{\perp} \tag{2.3}$$

Linear dichroism can be used with systems that are either intrinsically oriented or are oriented during the experiment. In experiments that involve ct-DNA, the long polymer is oriented by the viscous drag caused when a solution flows between narrow walls (see Figure 2.15) [70,78]. The orientation of the small molecules bound to DNA are then probed by comparing the absorption of light linearly polarized parallel to and perpendicular to the direction of flow. Small molecules that are unbound or randomly bound to the polymer will not be oriented and will show no differential absorption. However, small molecules bound in a specific orientation(s) to the polymer, will themselves become oriented by the flow and the orientation of their spectroscopic transitions can then be probed [70,78].

.

Due to the fact that the base pairs are almost perpendicular to the helical axis, B-DNA exhibits a characteristic negative band between 220 nm and 300 nm (black solid

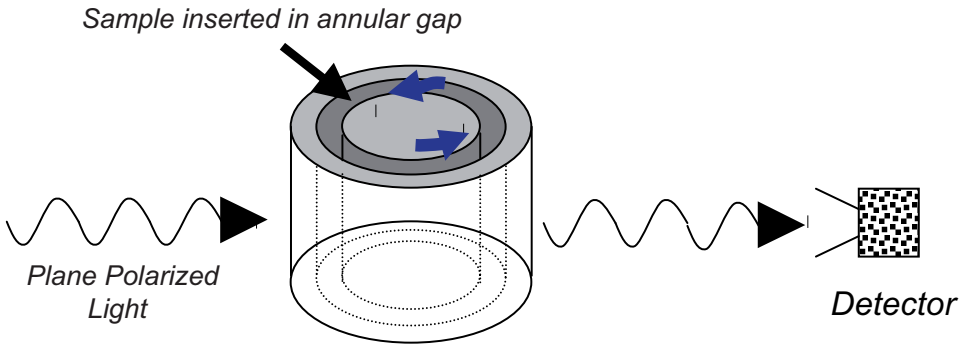

Figure 2.15: Schematic diagram of Couette flow cell.

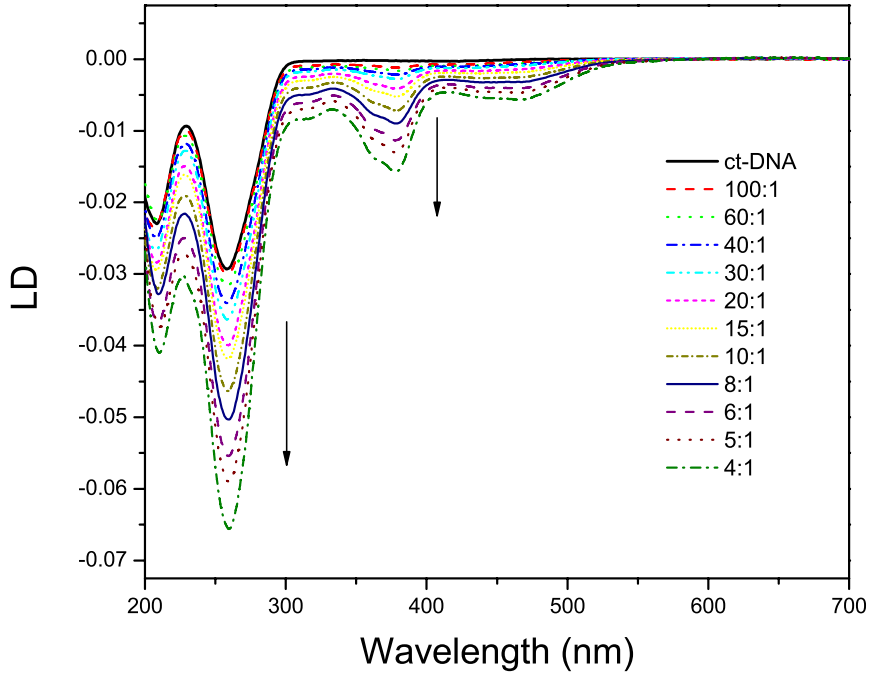

Figure 2.16: LD of 280 μM ct-DNA in 20 mM NaCl and 1 mM cacodylate buffer in the presence of increasing concentration of NiL^{2+}, in the range [DNA]:[NiL^{2+}] = 100:1 - 4:1 as shown.

line in Figures 2.16, 2.17 and 2.18) caused by $\pi - \pi^*$ transitions [70]. Molecules that are able to interact with the DNA could produce a decrease of the intensity, due for example to coiling effect, or an increase of the same band, generally caused by intercalation of aromatic rings between the bases of the DNA ("stiffening") [70,78].

In these experiments a ct-DNA solution was injected in the annular gap between the rotating and the fixed coaxial cylinder of a Couette flow apparatus (Figure 2.15).

During the spinning process (the rotation gradient was maintained constant over all the experiment) increasing amounts of the complexes solution were added in order to obtain different [ct-DNA]:[complex] ratios.

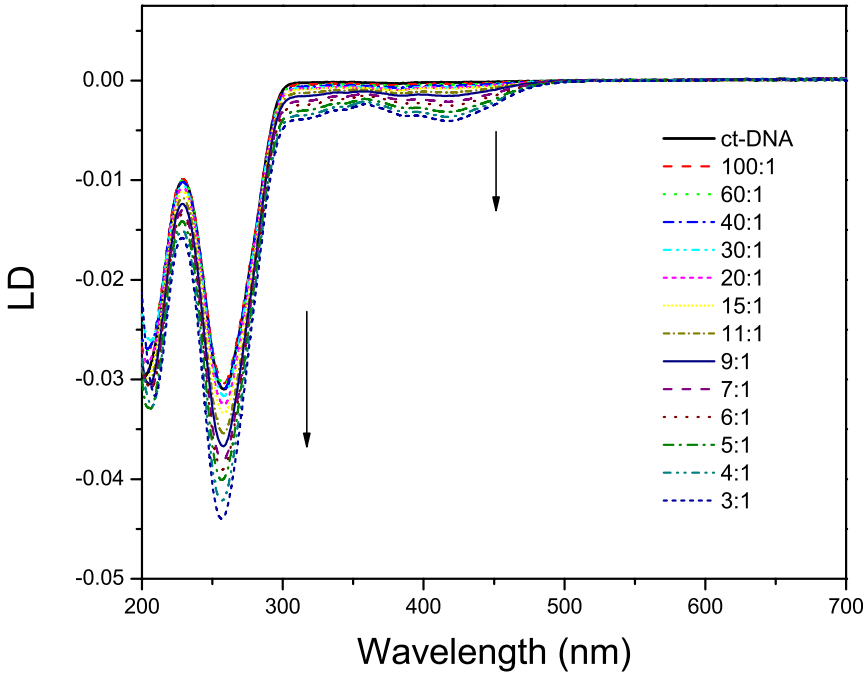

Figure 2.17: LD of 300 μM ct-DNA in 20 mM NaCl and 1 mM cacodylate buffer in the presence of increasing concentration of CuL^{2+}, in the range [DNA]:[CuL^{2+}] = 100:1 - 3:1 as shown.

The LD spectra of ct-DNA in presence of increasing amounts of NiL^{2+}, CuL^{2+} and ZnL^{2+} are shown in Figures 2.16, 2.17 and 2.18 respectively. The presence of the two induced LD bands in the metal to ligand charge transfer region (centered at 376 and 455 nm for NiL^{2+}, at 330 and 417 nm for CuL^{2+} and 330 and 385 nm for ZnL^{2+}), indicates firstly that there is an interaction between the three metal compounds and the DNA and that these compounds are oriented in a specific way by the polynucleotide. More interestingly, all the complexes induce an enhancement of the DNA negative band indicating an intercalative binding mode. This result definitively confirms the DNA-intercalating nature of the three complexes, obtained by the complementary CD, UV-vis and fluorescence measurements [21, 22]. The effect of the Ni^{II} compound on the DNA structure is larger with respect to that of both Cu^{II} and Zn^{II}, as can be argued by the shape of the titration spectra and by the linear trend of the plot in Figure 2.19. In the latter Figure the differential DNA LD signal at 260 nm (obtained by subtracting from each LD value at this wavelength the DNA signal at the same wavelength) is reported as a function of

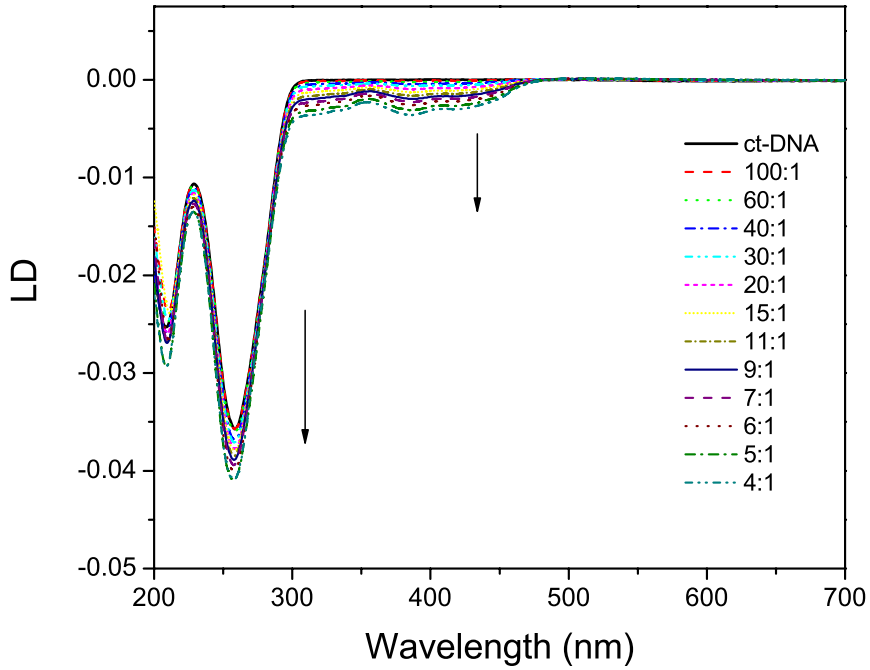

Figure 2.18: LD of 320 μM of ct-DNA in 20 mM NaCl and 1 mM cacodylate buffer in the presence of increasing concentration of ZnL^{2+}, in the range [DNA]:[ZnL^{2+}] = 100:1 - 4:1 as shown.

the NiL^{2+}, CuL^{2+} and ZnL^{2+} concentration. The differential LD decreases with a higher slope for the Ni^{II} compound. This latter finding is also in good agreement with the results previously obtained, where a bigger binding constant (K_b) for the Ni^{II} compound was obtained (see Table 2.1) [22]. As a matter of fact, Ni^{II} Salphen compounds present a more planar coordination with respect to Cu^{II} and Zn^{II} complexes. In details, while it is well know that the stability of the square planar Ni^{II} site prevents coordination of the Ni^{II} ion with moderately strong axial ligands [63,79], there may be an equilibrium with axial hydration of the copper ion and a slightly distorted square planar geometry (see Figure 2.6 and B.1) that reduce to some extent the intercalation of CuL^{2+} into the DNA. Furthermore, the even lower ability to intercalate DNA of Zn^{II} Salphen complexes can be explained by the non-planar square-based pyramidal geometry where a molecule of water is in the axial position (see Section 2.3) [19,63].

2.2.7 Gel electrophoresis of ML-DNA solutions (M = Ni, Cu, Zn)

Plasmid Gel Electrophoresis. Gel electrophoresis of negative-supercoiled and open-circle plasmid DNA can be used to assess unwinding of the DNA helix caused by small molecules [80]. The ability of the three complexes here synthesized to induce DNA

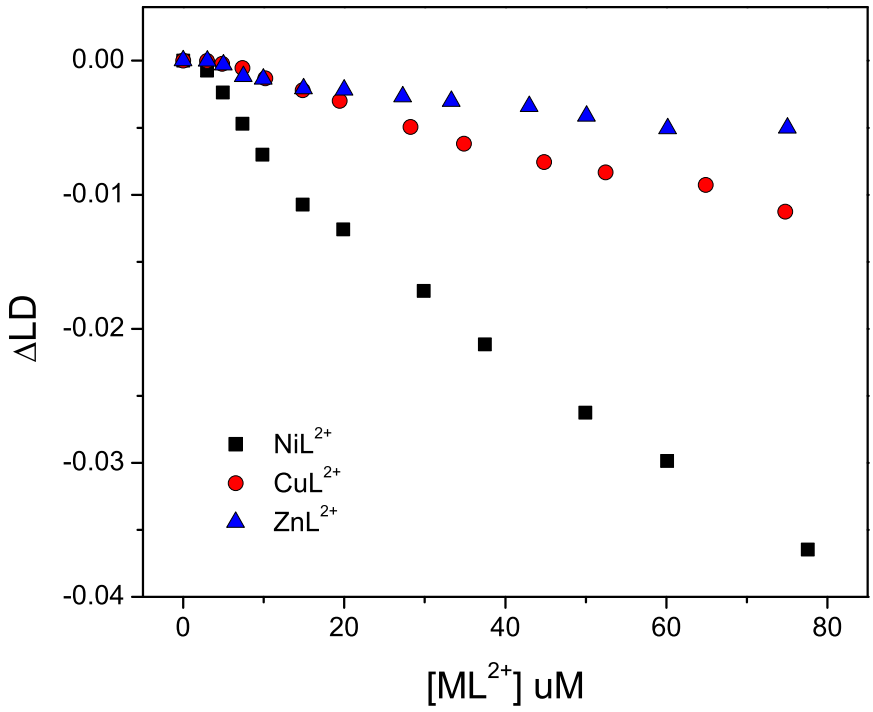

Figure 2.19: Differential DNA LD signal at 260 nm as a function of the NiL^{2+} (squares), CuL^{2+} (circles) and ZnL^{2+} (triangles) concentration.

unwinding was studied by gel electrophoresis using negatively supercoiled plasmid DNA pBR322. The characteristic agarose gel pattern of plasmid DNA consists of two bands, one corresponding to the negatively supercoiled form and the other to the open circle form.

It is known that molecules that are able to bind DNA, such as intercalators, induce an unwinding of the duplex supercoils, giving rise to a decrease of the DNA density, thus a decrease in the rate of migration through agarose gel [80, 81]. Moreover, if there is a double strand cleavage, a linear form that migrates between circular and supercoiled will be generated [82,83]. In Figure 2.20 the 2% agarose gel patterns of the plasmid DNA pBR322 and the changes caused by the addition of increasing amounts of compounds NiL^{2+}, CuL^{2+} and ZnL^{2+} are shown. While the Zn^{II} and Cu^{II} complexes induce just a weak unwinding of the supercoiled DNA, NiL^{2+} not only induces a strong unwinding even at low concentrations (lanes 2,3 Figure 2.20a) but, unexpectedly, produces a cleavage of the plasmid in his circular form with formation of linear DNA at higher concen-

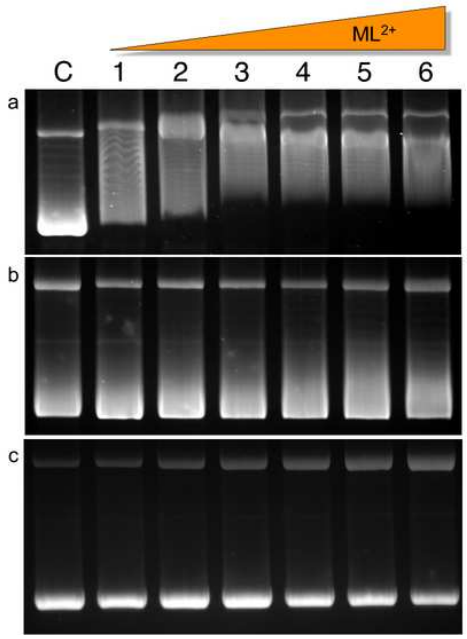

Figure 2.20: Agarose gel electrophoresis patterns for cleavage/unwinding of supercoiled pBR322 plasmid DNA by NiL^{2+} (a), CuL^{2+} (b) and ZnL^{2+} (c). In each gel the top bands correspond to the circular plasmid form while the bottom bands to the supercoiled one. In picture (a) the middle band correspond to the linear form. Lane C: DNA control; Lanes 1-6: [DNA]/[complex] 20:1; 12:1; 8:1; 6:1; 5:1; 3:1.

trations (lanes 3-6 Figure 2.20a). The geometry of the complexes could play a key role in determining the activity toward plasmidic DNA. In fact, as described by the linear dichroism and by the structural features (Sections 2.2.6 and 2.2.1), the slightly uncoplanar geometry of CuL^{2+} and ZnL^{2+} may affect the binding to DNA. The stronger interacalation of NiL^{2+} could explain the larger unwinding effect and the nuclease activity of this compound, as also reported in literature [84].

Polymerase chain reaction (PCR). The polymerase chain reaction, considered a milestone of molecular biology, is a procedure developed for the *in vitro* amplification of DNA sequences. It is a technique which has been performed as model of DNA replication in cells in many studies [85]. Furthermore, PCR is currently used to allow analysis of DNA extracted from very small amounts of biological samples [85].

In PCR amplification, two oligonucleotide primers are designed to be complementary to the ends of a sequence which has to be amplified and they are mixed in molar

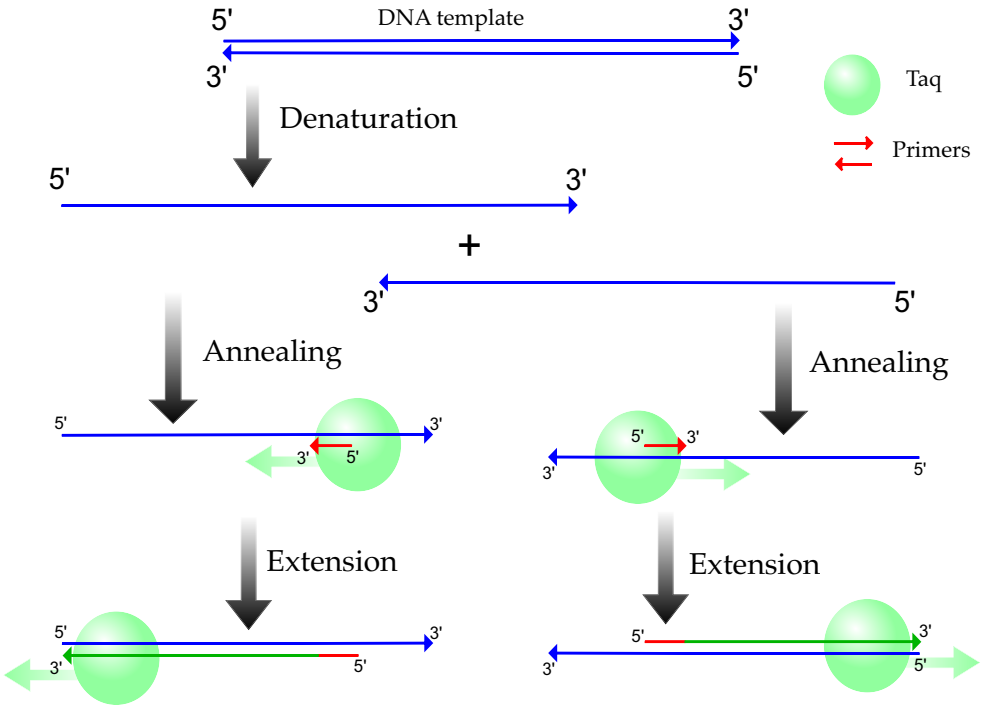

Figure 2.21: Schematic representation of the first cycle of PCR.

excess with the DNA template and the deoxyribonucleotide triphosphates in a proper buffer. The solution is first heated to denature the original strands and then cooled to promote the primer annealing to each different strand of the target fragment. The positioned primers can be then extended by the action of a DNA polymerase, and the newly synthesized strands will overlap the binding site of the opposite oligonucleotide. The steps of denaturation, annealing and extension are repeated cyclically and the primers bind continuously to both the original DNA template and complementary sites in the newly synthesized strands and are extended to produce new copies. That leads to an exponential increase in the total number of DNA fragments, where the majority of the products synthesized are double strand DNA fragments of a discrete length.

PCR is possible thanks to the presence of a heat resistant DNA polymerase (an enzyme) from the thermophilic bacterium Thermus aquaticus (Taq) [85]. In a recent important work, developed in the M. Hannon research group, where I've been as visiting student, PCR was used for the first time to evaluate the interference of DNA binders with the biological polymer replication [86]. In this context, polymerase chain reaction assays were performed to check whether the intercalation of the three metal complexes could interfere with DNA amplification. In particular, the plasmidic pUC19 DNA was

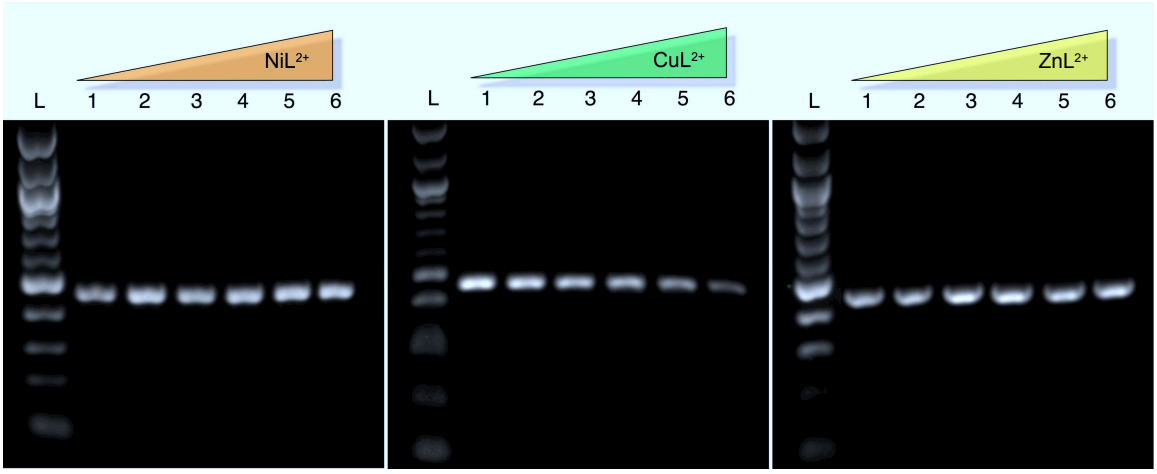

Figure 2.22: PCR inhibition assay with ML^{2+} (M = Ni, Cu, Zn, as shown). 100 bp oligonucleotide ladders (L); control (1); ML^{2+} 0.05 μM (2); 0.1 μM (3); 0.3 μM (4); 0.5 μM (5); 1.0 μM (6).

first incubated with increasing concentrations of NiL^{2+}, CuL^{2+} and ZnL^{2+} for 5 minutes at room temperature, then amplified by Taq DNA polymerase. Agarose gel electrophoresis patterns of the reaction products after 35 cycles, followed by ethidium bromide staining and UV visualization, showed a single DNA product of the expected length (Figure 2.22). It can be seen from the intensities of the product bands that just the copper complex affects drastically the amplification of the DNA. CuL^{2+} reduces the amplification up to 70% with the higher concentration used in the PCR solution. This result was obtained by measuring the intensities of the bands relative to the control. On the other hand, both NiL^{2+} and ZnL^{2+} do not affect the PCR at the considered concentrations. In a further experiment the PCR product was incubated with increasing concentrations of CuL^{2+} even higher than those used in the first PCR assays to exclude any affection on the visualization by ethidium bromide (Figure 2.23). The agarose gel (Figure 2.23) did not show any significant reduction of band intensities. This confirms that CuL^{2+} interferes with the amplification of the DNA without preventing the ethidium bromide intercalation during the staining step. Although the spectroscopic studies indicate that the intercalation strength is higher for NiL^{2+} than for CuL^{2+} and ZnL^{2+}, only CuL^{2+} interferes with the DNA amplification. Likely, the combination of the intercalation strength and the distorted geometry of the copper(II) compound have a significant consequence on the Taq DNA polymerase activity. The zinc(II) complex has a pyramidal square planar coordination, it is not a good intercalator. Analogously, the nickel(II) compound is an excellent DNA-intercalator, but apparently it does not present the proper

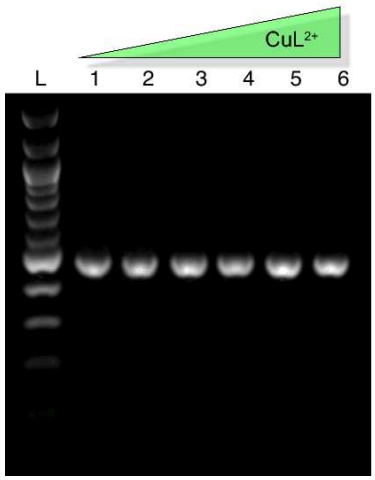

Figure 2.23: Incubation of CuL^{2+} complexes with PCR products. Control (1); CuL^{2+} 0.5 μM (2); 1.0 μM (3); 3.0 μM (4); 5.0 μM (5); 10.0 μM (6).

geometrical features to interfere with the polymerase.

2.2.8 Conclusions

The structural characterization of the NiL^{2+} and ZnL^{2+} complexes in aqueous solution was performed by NMR spectroscopy, while the solid state structure of the CuL^{2+} complex was established by X-ray crystallography. Concerning the metal complexes-DNA interaction, spectroscopic studies and, especially, linear dichroism titrations confirmed that these compounds are certainly DNA-intercalators. The DNA binding affinity decreases in the order: $NiL^{2+} > CuL^{2+} > ZnL^{2+}$. In particular, the DNA interaction strength is slightly weaker for the copper(II) than for the nickel(II) complex probably due to the slightly distorted square planar structure of the former, as shown by its X-ray structure. The geometry distortion from coplanarity produces an even weaker DNA-binding for the zinc(II) compound. Plasmid-DNA gel electrophoresis experiments indicated that while the CuL^{2+} and ZnL^{2+} complexes induce a poor unwinding of supercoiled DNA, the NiL^{2+} complex has a nuclease activity without the addition of external agents. On the other hand, the PCR assays demonstrated that only CuL^{2+} is able to inhibit the DNA amplification mediated by Taq DNA polymerase. The results obtained collectively show that the compromise between intercalation strength and geometry distortion of the copper(II) complex has a key role in interfering with the processivity of the polymerase.

2.3 Fluorescence emission and enhanced photochemical stability of ZnL^{2+} interacting with native DNA

Schiff base ligands and their metal complexes show interesting photophysical properties and display comparable fluorescence with excitation maxima at about 300 nm and emission maxima at about 420 nm [87]. For Salphen and Salen ligands, fluorescence occurs through the proton transfer between the hydroxy and azomethine groups in the chromophore. Consequently, the polarity of the solvent has a marked effect [88]. Fluorescence emission from intraligand excited states of metal-Salen complexes has also been detected [89]. In particular, Zn-Salen and related complexes are highly fluorescent and their spectra are consistent with singlet emission in competition with efficient singlet-to-triplet intersystem crossing [90,91]. Concerning the photochemical properties of Zn^{II} complexes of Salen-type Schiff bases, these undergo a Zn^{II} mediated two-electron oxidation, due to simultaneous one-electron oxidation of the two imine moieties of the bridging ligand. In fact, two redox processes at positive potential have been detected: the first oxidation process is likely localized on the phenolate ring of the Schiff base ligand while the second oxidation process may be a subsequent oxidation to form dicationic species [92]. Furthermore, when dissolved in relatively acid organic solvents, in the presence of water, able to coordinate the Zn metal in the apical position, Zn-Salphen complexes are known to lead to demetallated structures [93].

The photophysical, photochemical and solution properties of Zn^{II} complexes recently reported [87–93] were an incitement to revisit the issue of stability of the ZnL^{2+} and further investigate the effect of light on its water solutions, also in the presence of native DNA. Considering the photophysical properties of Zn^{II}-Schiff base complexes described above, fluorescence spectroscopy measurements were mainly exploited and supported by quantum chemical calculations.

2.3.1 Photochemistry of ZnL^{2+} and protective effect of DNA

Preliminary experiments were carried out to ascertain the feasibility of the spectrofluorimetric investigation of the photophysical and photochemical properties of ZnL^{2+} intercalated in native ct-DNA. First of all, the absorption spectra of a buffered aqueous solution of DNA ([DNA] = 50 μM) and of ZnL^{2+} ([ZnL^{2+}] = 50 μM) were collected to select the best suited excitation wavelength. Such spectra are shown in Figure 2.24. Since

the complex shows an absorption band centered at about 370 nm in a region where DNA does not absorb, this excitation wavelength was selected for the fluorescence experiments. After detecting a fluorescence band in the 360-700 nm region, suitable ex-

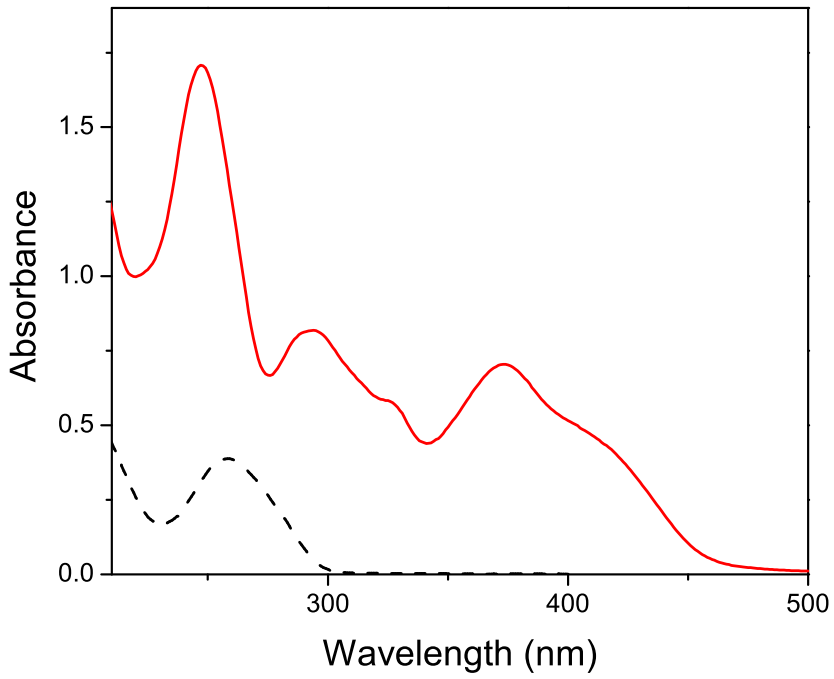

Figure 2.24: Absorption spectra of buffered aqueous solutions of DNA, [DNA] = 50 μM, (- - -) and of ZnL^{2+}, [ZnL^{2+}] = 50 μM, (—).

perimental conditions and apparatus set up were searched, in order to collect the fluorescence spectra without significant sample photodegradation. It was found that, using the excitation wavelength of 370 nm, an entrance slit width of 0.24 mm and a scan rate of 6 nm/s nearly identical replicate spectra were collected. Furthermore, in order to evaluate the photochemical stability of ZnL^{2+}, the fluorescence spectra of some selected samples at various R values (R = [DNA]:[ZnL^{2+}]) were collected at t = 0 h (freshly prepared samples) and after 24 h by maintaining the samples at room temperature i) in the dark or ii) under the illumination of a tungsten lamp (100 watt) placed at a fixed distance of 30 cm from the quartz cuvette (10 mm path length) containing the sample. The comparison among these spectra is shown in Figure 2.25. It can be noted that, after 24 h, all the samples maintained in the dark are only marginally affected. On the other

hand, while the sample without DNA (R = 0) after illumination displays a marked enhancement of its fluorescence intensity, by increasing the amount of DNA this effect progressively disappears being negligible at R = 5. Taking into account that ZnL^{2+} is intercalated within the DNA structure [21] (see Section 2.2), quite surprisingly this finding indicates that the insertion of the Zn^{II} complex in the DNA double helix involves an efficient protection against the observed photochemical process. Moreover, it emphasizes a novel and interesting functionality of the DNA molecules which could be exploited for biomedical applications.

In fact, being ZnL^{2+} representative of potentially interesting DNA intercalating drugs, this finding could suggest the formulation of photounstable drugs that become photostable after DNA intercalation. Therefore, it should be of utmost interest to speculate i) on the nature of this photochemical process and ii) on the ability of the DNA double helix to hinder it. Measurements performed at different light exposition times show that the fluorescence intensity of the ZnL^{2+} solutions exposed to light has a drastic enhancement within the first 24 h. After this period, further exposition to light negligibly changes both the fluorescence intensity and the band shape. Moreover, the fluorescence spectra of the samples stored in the dark for several days, after prolonged light exposition, are essentially coincident with those registered immediately after light exposition. These results allow to conclude that: 1) the photoproduct is stable and 2) the process is irreversible. Interestingly, the same dramatic intensity enhancement was observed, after exposure to tungsten light for 24 h, for deoxygenated solutions of the ZnL^{2+} complex in Tris-HCl 1 mM. The latter were obtained by extensively insufflating nitrogen gas in the solvent and keeping it under nitrogen atmosphere.

The striking increase in the fluorescence quantum yield of the illuminated ZnL^{2+} in the free state strongly suggests the occurrence of a photochemical process resulting in an increase of the structural rigidity of the zinc(II) complex that remarkably reduces the radiationless decay rate from the excited to the ground state [94]. An additional support to this hypothesis comes from the light sensitivity observed in a Co^{II}-Salen-type complex, that is irreversibly photooxidized to a cationic species and in which the electron is not removed from the metal but from the ligand [95]. Moreover, it has been reported that a Mn^{III} complex of a Salen-type ligand in $CHCl_3$ is photooxidized to a Mn^{IV} complex although, in addition, secondary processes can lead to various photoproducts [96]. Concerning the latter remark, it is known that visible light promotes the oxidation of the ligand in a Mn^{III} Salen-type complex, followed by the hydrolysis and rearrangement of

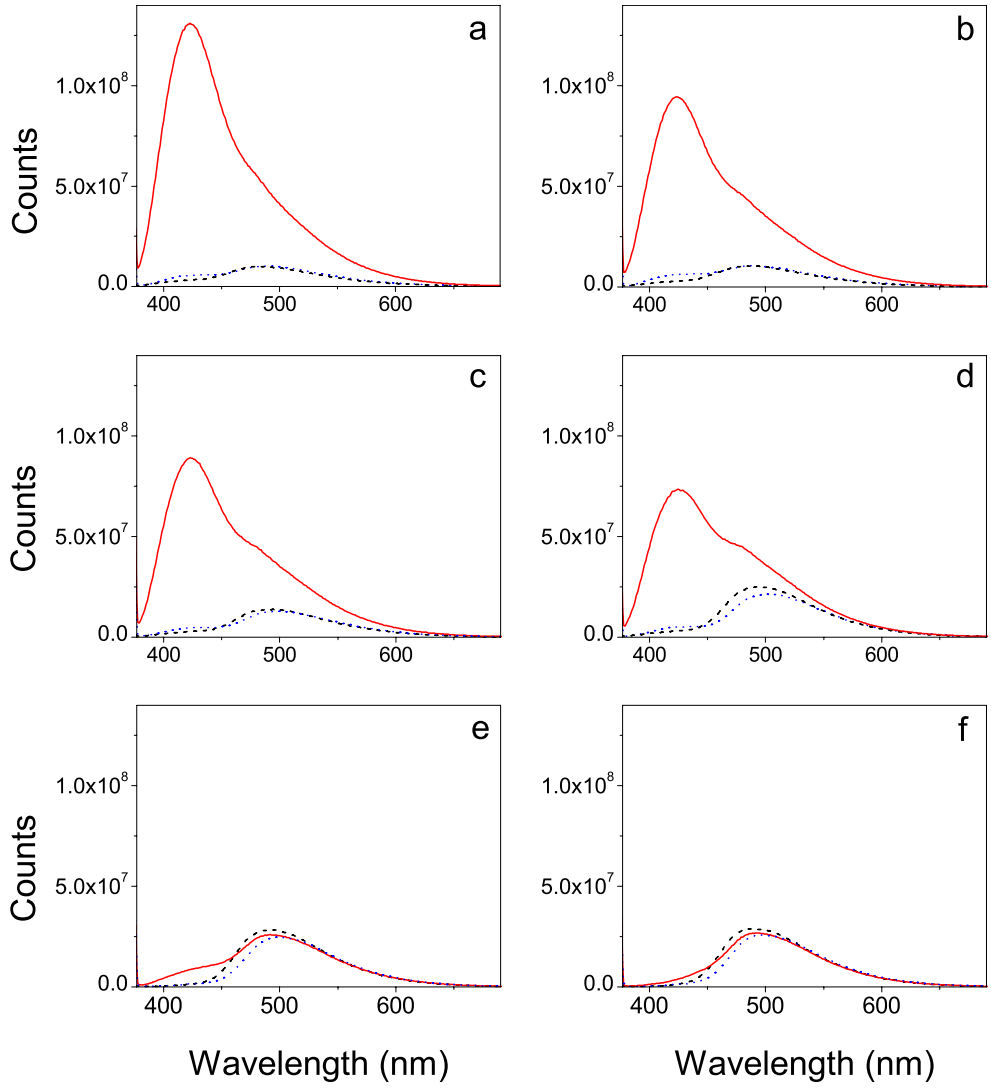

Figure 2.25: Fluorescence spectra of samples at fixed ZnL^{2+} concentration,$[ZnL^{2+}]$ = 50 μM and various R ([DNA]:$[ZnL^{2+}]$) values: a, R = 0; b, R = 0.2; c, R = 0.8; d, R = 2.0; e, R = 5.0; f, R = 10.0, for t = 0h (- - -), stored in the dark for t = 24h (· · ·) and exposed to tungsten lamp light for t = 24h (—).

the coordinated Schiff base ligand [97].

According to these considerations and recalling the results by Germain et al. [92], proving that Salen-type Schiff bases may undergo a Zn^{II} mediated two-electron oxidation, the rationalization of the experimental findings was attempted in terms of the photooxidation of the ZnL^{2+} complex, by comparing experimental spectra with those obtained through TD-DFT calculations.

It should also be noted that the fluorescence spectrum of the aqueous H_2L^{2+} ligand

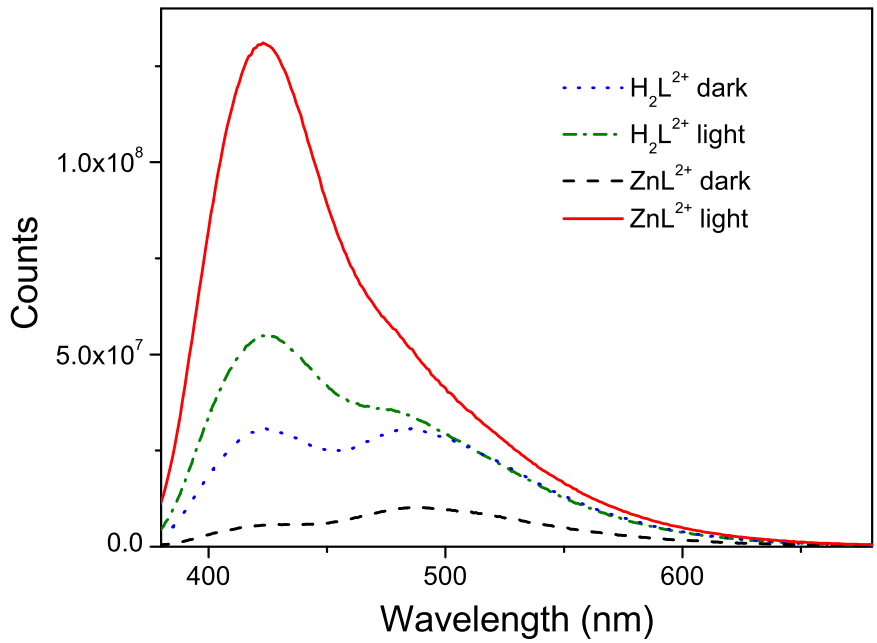

Figure 2.26: Fluorescence spectra of aqueous solutions of ZnL^{2+} and H_2L^{2+}, $[ZnL^{2+}] = [H_2L^{2+}] = 50\ \mu M$, stored in the dark and exposed to tungsten lamp light for 24 h.

is also somewhat influenced by light exposure but, remarkably, it is strongly different from that of the illuminated ZnL^{2+} sample at R = 0 (see Figure 2.26). This leads us to exclude that the observed photochemical process consists in the complex demetallation. An explanation of the latter evidence may be given by considering that bulk water is known to be a base less strong than water traces dissolved in apolar solvents (or in relatively acidic solvents such as $CHCl_3$). Moreover, the presence of the Tris-HCl buffer at neutral pH may enhance the stability of the ZnL^{2+} complex towards demetallation [93]. To further investigate photochemical stability in water solutions of ZnL^{2+}, ^{1}H-NMR spectra were recorded in D_2O for samples stored in the dark and exposed to tungsten lamp light for 24 h (see Figure 2.27). Remarkably, the ^{1}H-NMR spectrum of ZnL^{2+} exposed to light shows the same peaks of the sample stored in the dark. Considering that the photooxidation of the ZnL^{2+} complex does not modify significantly its structure, these findings are consistent with the hypothesis that light exposure causes partial photooxidation of the ZnL^{2+} complex.

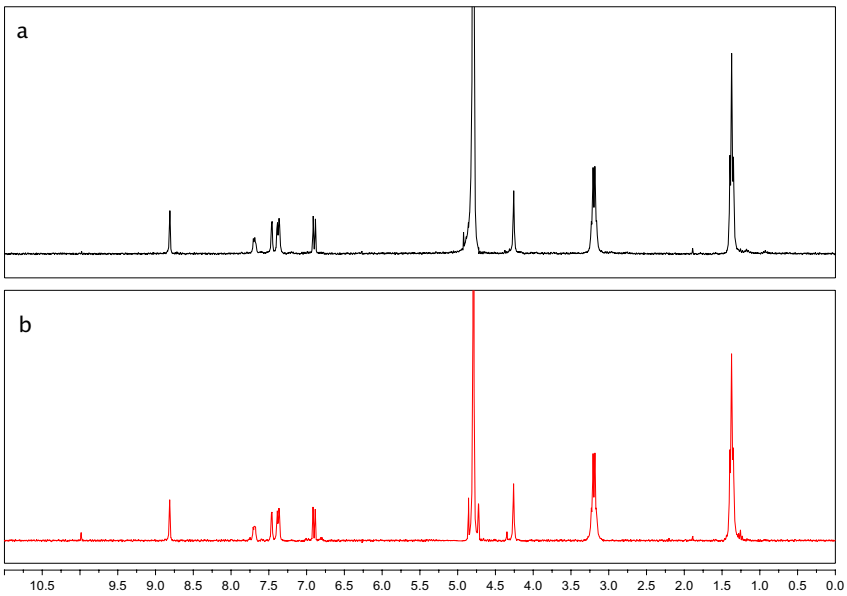

Figure 2.27: ^{1}H-NMR spectra of ZnL^{2+} in D_2O, stored in the dark (a) and exposed to tungsten lamp light for 24 h (b)

2.3.2 Comparison between experimental and calculated absorption and emission spectra of ZnL^{2+} and ZnL'

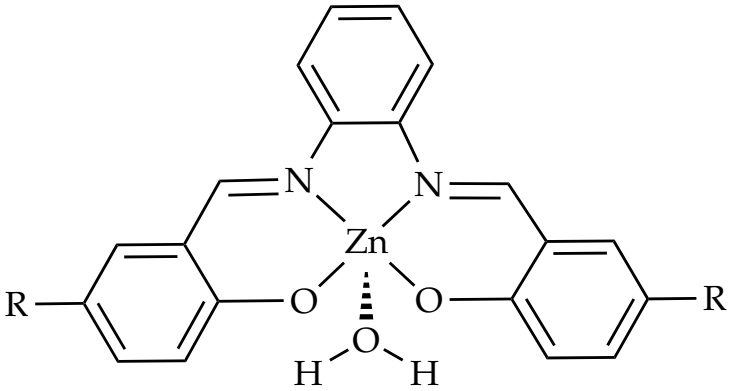

Figure 2.28: Structure of the pentacoordinated aquo-complexes $ZnL^{2+}\cdot H_2O$ (H_2L^{2+} = 5-triethyl ammonium methyl salicylidene ortho-phenylendiimine, R = $CH_2NEt_3^+$) and $ZnL'\cdot H_2O$ (H_2L'=N,N'-phenylene-bis(salicylideneimine), R = H).

The geometry of the H_2L^{2+} Schiff base ligand and of ZnL^{2+} ground states, both the square planar and the pentacoordinated aquo-complexes (see Figure 2.28) [98] as well as those of their mono and dioxidized forms, was fully optimized by the spin un-

restricted Density Functional Theory (DFT) B3LYP method [99], using the all-electron double-zeta split-valence plus polarization (DZVP) basis set [100, 101]. The spin state of the considered species was singlet (S0) for the lowest oxidation state, doublet (D0) for the monooxidized form and both singlet (S0) and triplet (T0) spin states for the dioxidized forms, respectively. Their absorption spectra were calculated by the Time Dependent DFT (TD-DFT) method, by using the same functional and basis set described above [102–105].

To evaluate the emission spectra of the ZnL^{2+} aquo-complexes, in the reduced and dioxidized forms, TD-DFT calculations were performed on the first singlet excited states (S1) of the Zn^{II}-Salphen simplified model complex, ZnL' (see Figure 2.28), obtained by substitution of the two triethyl ammonium methyl cationic groups by two hydrogen atoms, whose geometry was optimized by the Configuration Interaction Singles (CIS) method and using the DZVP basis set [106, 107]. Although it is known that the accuracy of the CIS method is comparable to that of the Hartree-Fock method for the ground state [108], nevertheless the main structural differences between the ground and first excited states are consistently reproduced by the CIS approach [109]. Implicit solvent effects in the electronic transitions were considered by single point calculations within the conductor-like polarized continuum model [110]. All calculations were performed using the Gaussian03 program package. The calculated absorption and emission electronic spectra were reproduced by the help of the GaussSum-2.1.6 program package [111].

The absorption spectra of the H_2L^{2+} ligand, of the ZnL^{2+} tetracoordinated complex and of the $ZnL^{2+}\cdot H_2O$ pentacoordinated complex (Figure 2.28) were calculated by the TD-DFT method, in the spin states S0 for the lowest oxidation state, D0 for the monooxidized form and S0 and T0 for the dioxidized forms. The comparison between calculated and experimental absorption spectra shown in Figure 2.29, induces the consideration that in water solution ZnL^{2+} should be coordinated by an axial water molecule and the presence of square planar ZnL^{2+} and/or of the H_2L^{2+} ligand can be safely excluded. In fact, there is a better matching between the experimental absorption spectrum of ZnL^{2+}, stored in the dark (Figure 2.29 d) and that calculated for $ZnL^{2+}\cdot H_2O$ in the singlet spin ground state (Figure 2.29 b, see also Figure 2.30 dashed lines).

The latter conclusion is better illustrated by Figure 2.30, where the absorption spectrum of $ZnL^{2+}\cdot H_2O$ S0 and the average of the two spectra corresponding to the reduced $ZnL^{2+}\cdot H_2O$ S0 and dioxidized $ZnL^{2+}\cdot H_2O$ T0 state are reported in Figure 2.30 b. In par-

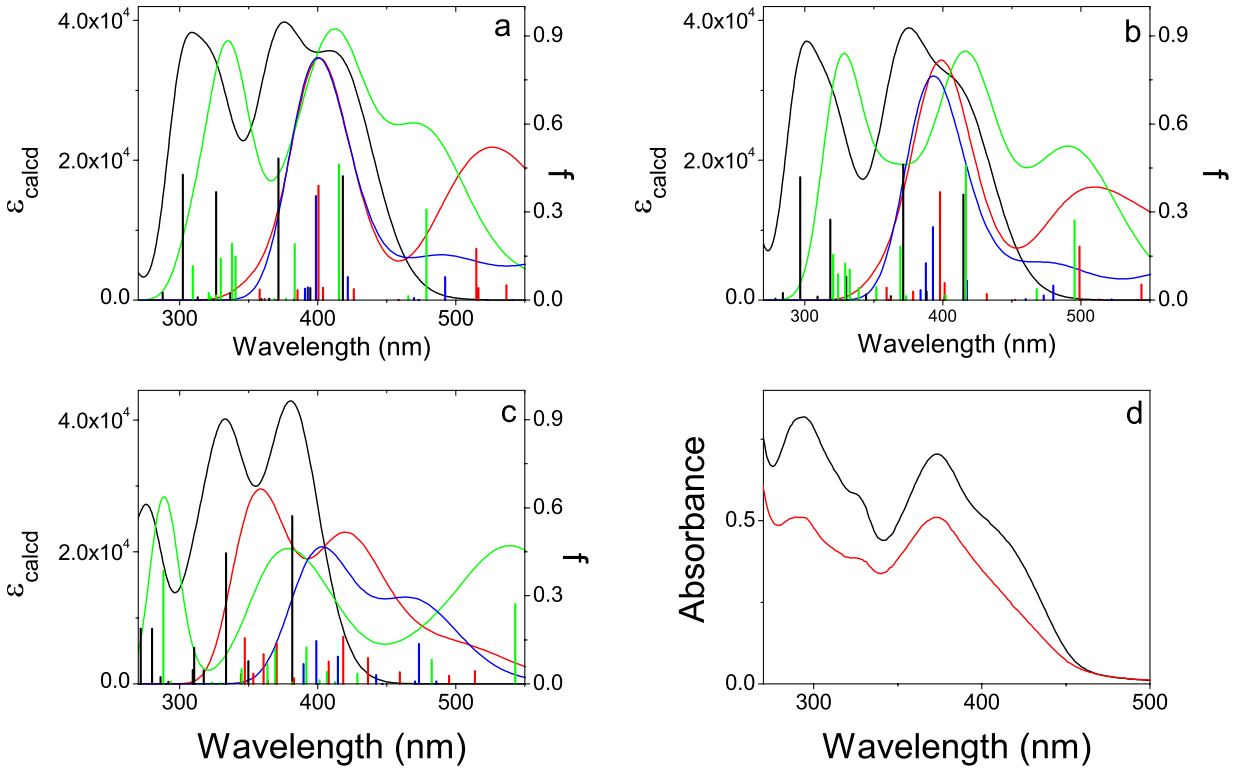

Figure 2.29: Calculated absorption spectra (ϵ_{calcd}) and oscillator strengths (f) of ZnL^{2+} (a), $ZnL^{2+}{\cdot}H_2O$ (b) and H_2L^{2+} (c) in the reduced S0 state (—), in its monooxidized D0 state (—) and in the dioxidized S0 (—) and and T0 (—) spin states, within the implicit water solvent; (d) experimental absorption spectra of ZnL^{2+} ([ZnL^{2+}] = $5{\times}10^{-5}$ M), stored in the dark (—) and exposed to the tungsten lamp light for 24 h (—).

ticular, the similarity between the calculated absorption spectrum obtained by a 50% mixture of the S0 $ZnL^{2+}{\cdot}H_2O$ and T0 ZnL^{4+} ${\cdot}H_2O$ with experimental absorption spectrum of illuminated ZnL^{2+} in water solution, supports the hypothesis that the effect of the tungsten lamp light for 24 h is to partially oxidize ZnL^{2+} to ZnL^{4+}, up to an approximately equimolar ratio between the two forms. To understand the role of light exposure on the fluorescence emission of ZnL^{2+} water solutions, the structure of the first excited state of simplified model complexes $ZnL'{\cdot}H_2O$ and $ZnL'^{2+}{\cdot}H_2O$ (see Figure 2.28) was calculated by the CIS method, in the S1 spin states for both the reduced and the dioxidized states (see Experimental Section 2.5). Their emission spectra calculated by the TD-DFT method are shown in Figure 2.31. Despite the remarkable difference between the experimental fluorescence intensities of ZnL^{2+} solutions stored in the dark and illuminated, due to their different nonradiative decay rates, the shape of the calculated emission spectra in Figure 2.31 reproduces the two key spectral changes accompanying

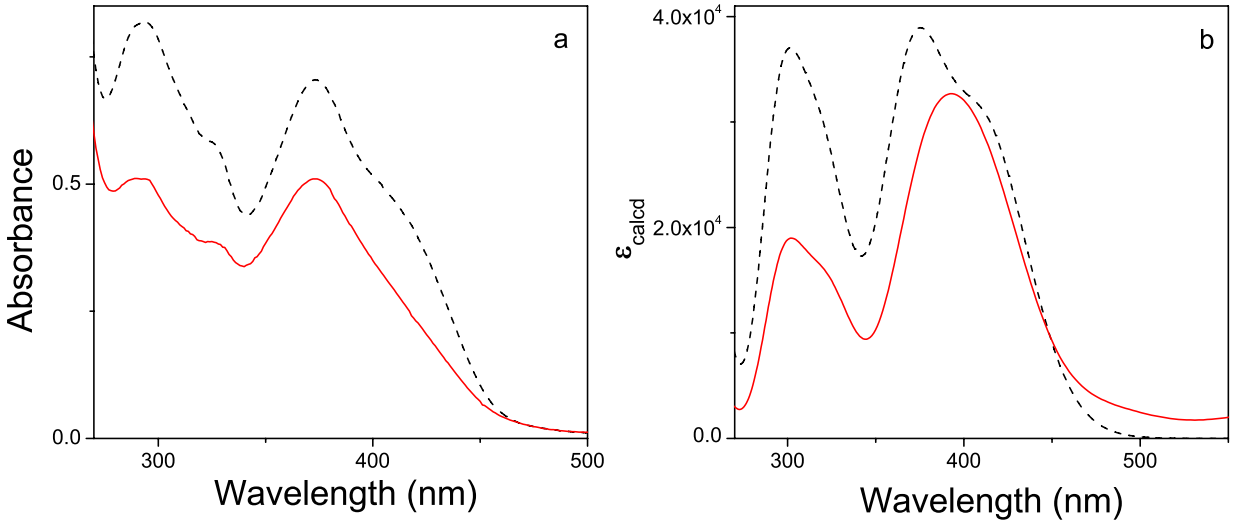

Figure 2.30: Experimental absorption spectra of ZnL^{2+} (a) and calculated spectra of $ZnL^{2+}\cdot H_2O$ within the implicit water solvent (b): (a) experimental ($[ZnL^{2+}] = 5\times10^{-5}$ M), stored in the dark (- - -) and exposed to the tungsten lamp light for 24 hours (—); (b) reduced S0 state (- - -) and 50% mixture of the reduced S0 state and dioxidized T0 state (—)

the exposure to light. In fact, in the experimental spectrum (Figure 2.31 a) the peak at 420 nm is red shifted in the illuminated ZnL^{2+} solutions and the intensity of the peak at 480 nm decreases compared to that at 420 nm. Moreover, the analysis of Figures 2.29 and 2.31 shows that the ground state of the dioxidized ZnL^{2+} aquo-complex is a triplet spin state, while the emission from the first excited state of the dioxidized species occurs from the S1 singlet spin state, presumably following a triplet to singlet intersystem crossing.

Noteworthy, the increase in the positive charge accompanying the two-electron oxidation process, may well explain the increase of the photoinduced structural rigidity of the cationic zinc(II) complex, as deduced above from the analysis of the experimental spectra (see Figure 2.25 a). The most intense electronic transitions of the absorption spectra calculated for $ZnL^{2+}\cdot H_2O$ S0 and for $ZnL^{4+}\cdot H_2O$ T0 (see Figure 2.29 b) and of the emission spectra calculated for $ZnL'\cdot H_2O$ S1 and for $ZnL'^{2+}\cdot H_2O$ S1 (see Figure 2.31 b), can be attributed to electronic transitions among the Molecular Orbitals (MOs) depicted in Figure 2.32, as detailed in Table 2.4.

Interestingly, it can be noticed that the contribution of the orbitals centered on the metal ion is negligible in all the MOs represented Figure 2.32. This result shows that the calculated electronic transitions, of both the absorption and emission spectra, involve intraligand states, in agreement with the attributions reported in the literature [89].

Table 2.4: Attribution of the most intense calculated absorption and emission transitions of the considered Zn^{II} complexes (see Figures 2.29 b and 2.31 b) to the frontier molecular orbitals essentially involved (see Figure 2.32).

Compound	λ (nm)	Attribution
$ZnL^{2+}\cdot H_2O$-S0	297	HOMO-4 $\mapsto$ LUMO 61%
	371	HOMO $\mapsto$ LUMO+1 69%
	415	HOMO $\mapsto$ LUMO 89%
$ZnL^{4+}\cdot H_2O$-T0	388	HOMO-6 $\mapsto$ LUMO+1 35%
	393	HOMO-6 $\mapsto$ LUMO+1 31%
	480	HOMO $\mapsto$ LUMO 39%
$ZnL'\cdot H_2O$-S1	398	HOMO-1 $\mapsto$ LUMO 44%
		HOMO $\mapsto$ LUMO+1 36%
$ZnL'^{2+}\cdot H_2O$-S1	489	HOMO $\mapsto$ LUMO 87%
	410	HOMO-5 $\mapsto$ LUMO 89%
	490	HOMO $\mapsto$ LUMO+1 57%

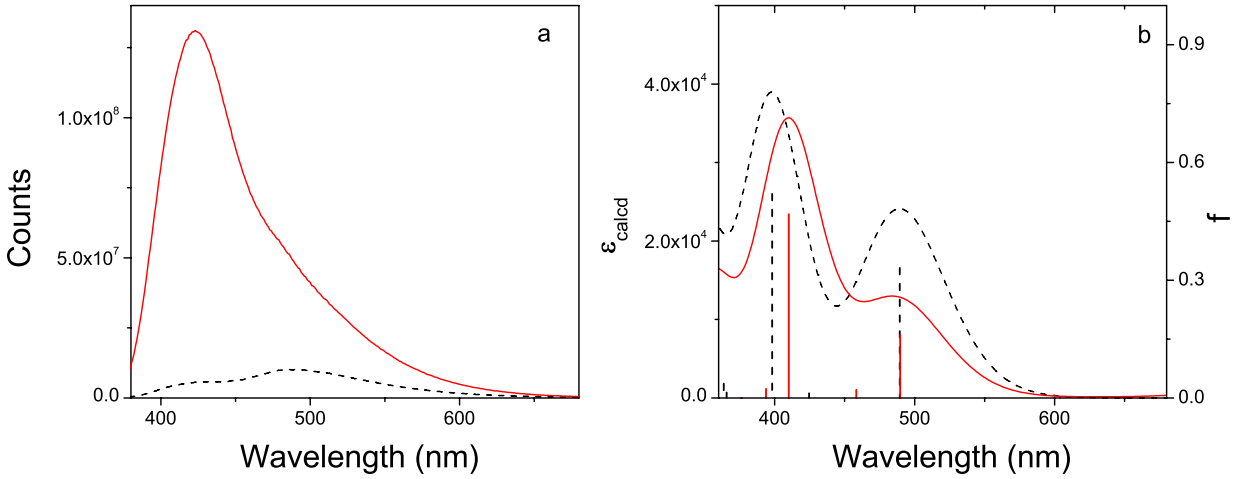

Figure 2.31: (a) Experimental fluorescence spectra of ZnL^{2+}, $[ZnL^{2+}] = 5\times10^{-5}$ M, stored in the dark (- - -) and exposed to the tungsten lamp light for 24 hours (—)); (b) calculated emission spectra (ϵ_{calcd}) and oscillator strengths (f) for the simplified $ZnL'\cdot H_2O$ complex, within the implicit water solvent, reduced S1 state (- - -) and dioxidized S1 state species (—)).

Moreover, it is worth considering that the triethyl ammonium methyl groups are essentially not involved in the MOs of both $ZnL^{2+}\cdot H_2O$ and $ZnL^{4+}\cdot H_2O$ shown in Figure 2.32. This suggests that $ZnL'\cdot H_2O$ is a reliable model for describing the excited state of $ZnL^{2+}\cdot H_2O$. Table 2.5 shows the relevant bond lengths and angles involving the oxygen and nitrogen atoms coordinated to the Zn atom in the four metal complexes

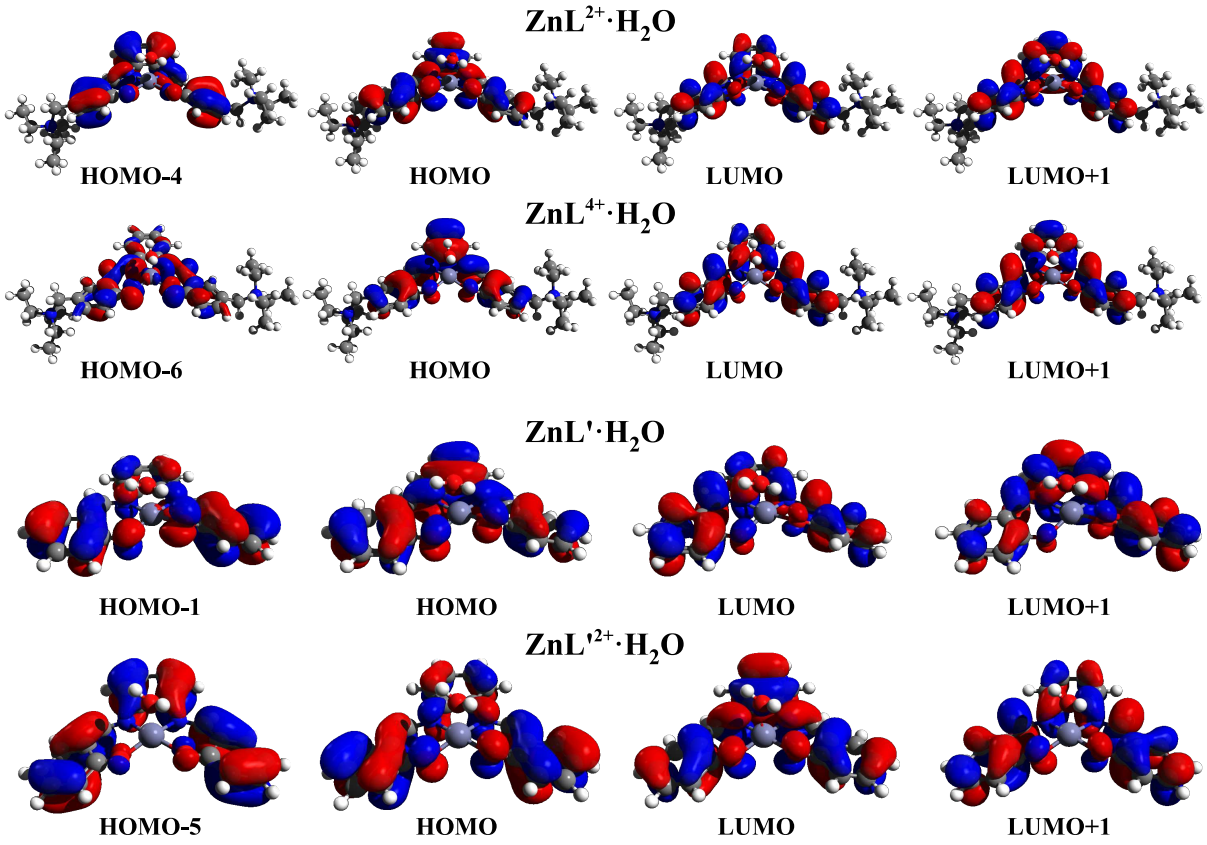

Figure 2.32: Molecular orbitals involved in the electronic transitions calculated for the absorption spectra of the $ZnL^{2+}\cdot H_2O$ S0 and of the dioxidized $ZnL^{4+}\cdot H_2O$ T0 (top rows) and for the emission spectra of the corresponding simplified models, $ZnL'\cdot H_2O$ S1 and $ZnL'^{2+}\cdot H_2O$ S1 excited states (bottom rows).

$ZnL^{2+}\cdot H_2O$, $ZnL^{4+}\cdot H_2O$, $ZnL'\cdot H_2O$ and $ZnL'^{2+}\cdot H_2O$. The geometry of the first singlet excited state of the reduced and oxidized forms of the Zn^{II} complex has been obtained on a simplified system (see Figure 2.28) and using the CIS method. The latter is less accurate than the B3LYP method used for the description of the reduced and oxidized forms in the ground state. Nevertheless the analysis of Table 2.5 suggests that only minor structural modifications occur on the coordination site of the title complex when it is photooxidized and/or when it is photoexcited. However, interestingly, such small distortions largely take into account of the remarkable spectral differences, experimentally detected both in the absorption and in the emission electronic transitions (see Figures 2.29 and 2.30).

According to this picture, the protective action of DNA toward the intercalated ZnL^{2+} can be attributed to the inhibition of the ZnL^{2+} photooxidation through an ef-

Table 2.5: Relevant geometrical parameters (Å and °) of the compounds $ZnL^{2+}\cdot H_2O$ S0 and $ZnL^{4+}\cdot H_2O$ T0, optimized by the B3LYP/DZVP method and of the compounds $ZnL'\cdot H_2O$ S1 and $ZnL'^{2+}\cdot H_2O$ S1, optimized by the CIS/DZVP method (see Fig. 1 for atom labels).

	$ZnL^{2+}\cdot H_2O$ S0	$ZnL^{4+}\cdot H_2O$ T0	$ZnL'\cdot H_2O$ S1	$ZnL'^{2+}\cdot H_2O$ S1
Zn-O1	1.994	2.043	1.985	1.985
Zn-O2	2.001	2.042	1.988	1.989
Zn-N1	2.117	2.113	2.124	2.153
Zn-N2	2.122	2.112	2.113	2.155
Zn-OH_2	2.178	2.103	2.230	2.143
O1-Zn-O2	100.2	94.5	105.2	102.6
N1-Zn-N2	78.0	79.3	78.2	75.7
O1-Zn-N2	89.0	88.2	88.2	87.0
N1-Zn-O2	161.2	156.2	166.0	156.8

fective stabilization of its ground S0 state (see Figure 2.25). The occurrence of ZnL^{2+} photooxidation in bulk water solution induces to hypothesize that an electron transfer takes place from each of the salicylideneimine groups to a water molecule. It is worth in fact recalling that the same photooxidation process also occurs in deoxygenated solutions (see above). Hence, a possible explanation of the way by which DNA hinders this process and protects ZnL^{2+} from the photooxidation, can be given considering that the DNA-intercalated ZnL^{2+} compound is in a more hydrophobic region, less accessible to water molecules (see below). Then, in agreement with the above reported findings, to investigate the photophysical properties of intercalated ZnL^{2+}, all the subsequent fluorescence experiments were carried out using samples prepared and stored in the dark before each measurement.

2.3.3 Steady-state and time-resolved photophysical properties of ZnL^{2+} intercalated in native DNA

Under excitation at 370 nm, ZnL^{2+} aqueous solutions show an intense structured emission band centered at 483 nm, whose intensity increases in the presence of DNA. The increase of the fluorescence intensity is accompanied by a red-shift of the fluorescence maximum (see Figure 2.33). These findings are typical clues of the occurrence of an intercalation process and in particular indicates that in the intercalated state the complex experiences (i) an environment less polar than water or (ii) a restriction of molecular

motions or (iii) solvent relaxation that deactivates the excited state without emission of a photon [112]. In particular, by adding increasing amounts of DNA at fixed complex concentration, the emission intensity at the band maximum is progressively enhanced reaching a plateau at R = 3 (R = [DNA]:[ZnL^{2+}]) corresponding to a binding size of about 0.7 per base pairs which is in fair agreement with the literature value [21] (see Section 2.2).

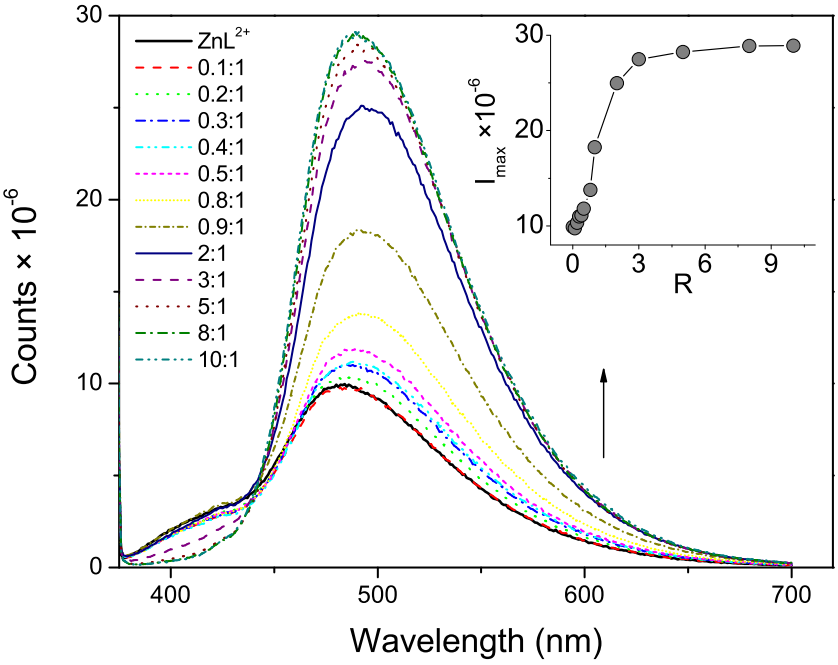

Figure 2.33: Fluorescence spectra of solutions of the ZnL^{2+} complex, stored in the dark, in the presence of increasing amounts of DNA at fixed ZnL^{2+} concentration ([ZnL^{2+}] = 50 μM). In the inset the intensity (I_{max}) at the emission band maximum is reported as a function of R.

By plotting the fluorescence intensity at the band maximum as a function of R (inset in Figure 2.33), it can be noted that a short induction regime (phase 1) in the region 0<R<0.8 was characterized by a nearly linear increase followed by a rapid increase (phase 2) and finally a trend toward a plateau (phase 3). This peculiar behaviour reveals the existence of different binding regimes of ZnL^{2+} to the DNA double helix. It is worth to note that during phase (1), although the fraction of intercalated ZnL^{2+} is small, the DNA is completely saturated by ZnL^{2+} while the major part of the complex is in the aqueous medium or surrounding the DNA molecule. Accordingly, regime (1) could be

attributed to the depletion of ZnL^{2+}-layers nearest the DNA surface [91]. Then, further increasing of the DNA concentration in the region 0.8<R<3, together with an increase of the fraction of DNA-intercalated Zn^{II} complex, the concentration of ZnL^{2+} outside tends to vanish. Finally, when the DNA concentration is very high all the ZnL^{2+} molecules are totally secluded within the DNA double helix. On the other hand, by considering the behavior of the wavelength at the maximum of the emission band (see Figure 2.34a), a bathochromic shift occurs in the 0<R<2 range followed by a hypsochromic shift at R>2. This finding indicates that this parameter monitors a different aspect of the intercalation process. Specifically, it is a fine probe of the environment experienced by ZnL^{2+}. The region where the bathochromic shift occurs corresponds to an increase of the fraction of the complex intercalated. On the other hand, the region of the hypsochromic shift reveals that, during the dilution process of ZnL^{2+} among the DNA binding sites, some changes of the DNA interior, involving an increase of its polarity, occur.

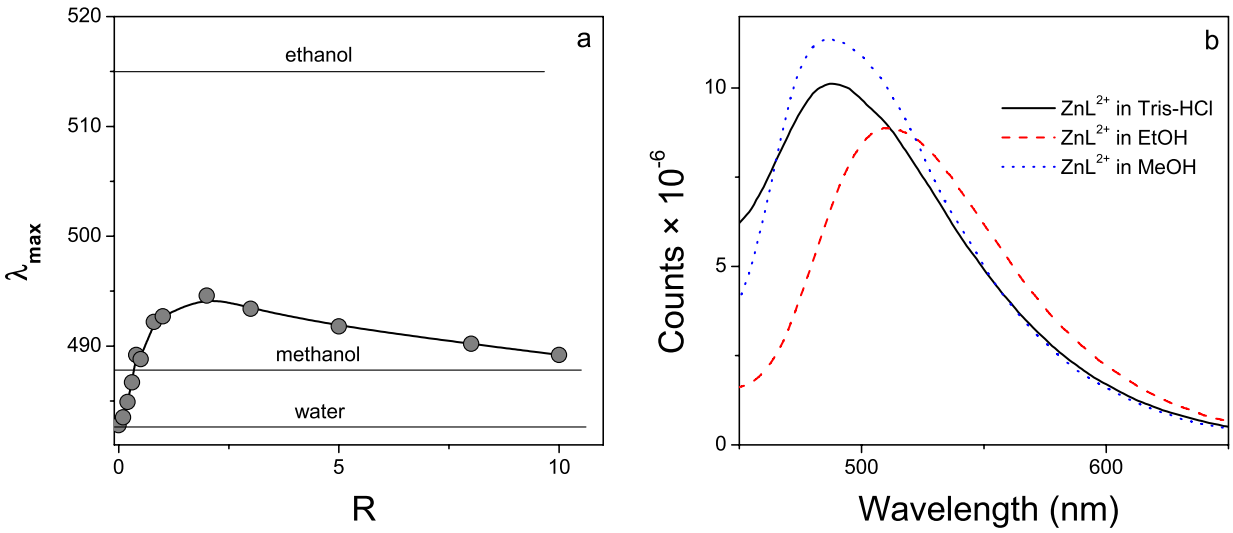

Figure 2.34: (a) Wavelength at the band maximum as a function of R (horizontal lines indicate the max value of ZnL^{2+} in the specified solvent medium). (b) Fluorescence spectra of ZnL^{2+} at fixed concentration ($[ZnL^{2+}]$ = 50 μM) in the specified solvent medium.

In order to estimate the environment sensed by the intercalated complex, its spectrum was also collected in methanol and ethanol. The comparison with that in aqueous solution is shown in Figure 2.34b. It can be noted that the wavelength at the band maximum in water (482 nm, dielectric constant 78) shifts to about 488 nm in methanol (dielectric constant 32.6) and to 510 nm in ethanol (dielectric constant 24.3). Considering that the highest wavelength value at the band maximum observed in the presence

of DNA is 495 nm, it can be concluded that the intercalated complex experiences an environment whose polarity is between that of methanol and ethanol. Further insights on the environment sensed by the intercalated complex were searched by monitoring the time-resolved fluorescence spectra of the complex in aqueous solution of native DNA. These spectra can be consistently described in terms of two exponential decay functions where, according to the literature, the faster decay characterized by a quite constant relaxation time of about 0.2 ns can be attributed to the sample scattering [74–76]. On the other hand, the second decay, attributable to the excited ZnL^{2+} complex, is characterized by a relaxation time which changes little going from the bulk aqueous phase (1.1 ns) to the DNA-intercalated state (0.9 ns). This piece of experimental result can be taken as an indication that the complex intercalation does not involve significant restriction of its molecular motions which should lead to a decrease of the nonradiative decay rate [113]. Moreover, the existence of a single decay time for the intercalated complex points toward the existence of nearly homogeneous binding sites.

2.3.4 Conclusions

The fluorescence intensity of the cationic complex ZnL^{2+}, in water solution at neutral pH, dramatically increases in the range 360-700 nm by exposure of the solution samples to tungsten light. Surprisingly, experimental results indicate that, in the intercalated state, ZnL^{2+} is effectively protected from this photochemical process. Quantum chemical calculations allowed us to suggest that in the free state ZnL^{2+} undergoes a photoinduced two-electron oxidation process and, consequently, the protective action of DNA toward the intercalated ZnL^{2+} can be attributed to an effective inhibition of the ZnL^{2+} photooxidation. The latter conclusion is in agreement with the result that DNA-intercalated ZnL^{2+} is confined in a region less polar than water and inaccessible to this solvent, possibly being water the electron acceptor molecule of the ZnL^{2+} photooxidation. Information achieved by steady state and time-resolved fluorescence spectroscopy indicates that the polarity of the environment probed by ZnL^{2+}, intercalated within DNA, is between that of methanol and ethanol and shows a continuous variation with the DNA to complex molar ratio. Indirectly, this finding allows to hypothesize that the structure of the DNA double helix progressively changes by increasing the fraction of occupied binding sites. From a more general perspective, the capability of DNA molecules to protect intercalated species from photodegradation processes seems to be of utmost importance from a biological point of view and could be amenable to biomedical

applications.

2.4 Confinement effects on the interaction of native DNA with CuL^{2+} in $C_{12}E_4$ liquid crystals

Among the various topics concerning the deoxyribonucleic acid macromolecule, its confinement in reduced space and its interaction with intercalating molecules are of current scientific interest and have been separately widely investigated [114–120]. While confinement investigations attempt to characterize the peculiar structural and dynamic properties of DNA, mimicking the conditions experienced *in vivo*, those on the intercalation aim to define the specific interactions and the microscopic mechanisms involved in the binding of chemical species, thus allowing to state the molecular features they should possess to effectively stick to the DNA backbone. This knowledge is thus pivotal to select substances that could be employed as diagnostic, protective or therapeutic agents or to develop novel specialized molecules able to control genetic information and/or to avoid growth and replication of cancerous cells by transcription inhibition [121–125]. However, it is reasonable to foresee that the intercalation process could be influenced by the chemical environment in which the DNA is located and, in particular, by the compaction degree of its tertiary structure [126]. But, in spite of the relevant interest in this specific research field, studies focused on the intercalation of transition metal complexes characterized by ideal intercalative features (extended aromatic moiety and planarity) in the backbone of DNA confined in biomimetic nanoscopic domains are absent in the literature.

Prompted by this consideration, the interaction of CuL^{2+} with DNA was studied in a microheterogeneous system, to segregate DNA in a nanoscopic domain (tetraethylene glycol monododecyl ether liquid crystals). The experimental techniques selected for the investigation were UV absorption spectrophotometry, circular dichroism and small angle X-ray scattering (SAXS). The comparison of the experimental results with those previously obtained in aqueous solution allows to emphasize the role of the confinement effects on the structure of DNA and on its interaction with the Cu^{II} cationic complex [21] (see Section 2.2).

Tetraethylene glycol monododecyl ether ($C_{12}E_4$), an amphiphilic substance with formula $CH_3(CH_2)_{11}(OCH_2CH_2)_4OH$, was chosen for the present study because it has been suggested that non-ionic surfactants show low affinity with polyelectrolytes such as

DNA, thus allowing confinement effects to be studied without the introduction of specific electrostatic interactions, which greatly contribute to the observed behaviour [127]. Furthermore, in the investigated temperature and composition range, $C_{12}E_4$ forms a dense phase of reverse micelles entrapping in their core water molecules [128, 129]. The solubilization of increasing amounts of water or aqueous solutions in $C_{12}E_4$ liquid crystals causes a progressive increase of the micellar radius until a structural transition to a lamellar phase occurs [130, 131]. Generally, the presence of few small-size molecules does not significantly alter the reverse micellar structure. However, the entrapment of macromolecules is expected to alter drastically the size and shape of the hosting aggregate [132].

Only a few studies on DNA confined in reverse micelles have been published [133, 134]. It has been shown that DNA within reverse micelles is condensed in compact structures (size 50-400 nm) and this process is accompanied by a hypochromic effect, a red shift of the absorption maximum and changes in the CD spectra. For anionic and cationic reverse micelles, electrostatic interactions have been invoked to rationalize these experimental findings while, for non-ionic surfactants, it has been suggested that the spatial restriction imposed by reverse micelles and the relatively low dielectric constant of its polar core are the main contributions [133, 134].

Finally, this study could shed some light on the peculiarity of drug-DNA interactions occurring within the intracellular environment. This section is organized as follows: each paragraph reports and discusses the results of the title technique applied to DNA in water and in $C_{12}E_4$, then to CuL^{2+} in water, DNA + water and DNA + $C_{12}E_4$.

2.4.1 UV-visible absorption

Lyophilized ct-DNA displays in aqueous solution an absorption band centred at 258 nm characterized by a molar extinction coefficient at the band maximum (ϵ_{max}) of 7000 M^{-1} cm^{-1} [135–138]. On the other hand (see Figure 2.35), when it is solubilized in $C_{12}E_4$ liquid crystals (DNA, W/$C_{12}E_4$ at $R_{w/s}$ = 3, where $R_{w/s}$ = [Water]/[$C_{12}E_4$]), the band is red shifted (λ_{max} = 260 nm) and ϵ_{max} diminishes (ϵ_{max} = 5849 M^{-1} cm^{-1}).

Taking into account that this band is due to $\pi \rightarrow \pi^*$ and $n \rightarrow \pi^*$ electronic transitions involving the aromatic rings of the DNA base pairs and that the related transition moments decrease by increasing the interactions among adjacent base pairs, the observed ϵ_{max} change suggests that the DNA confinement within $C_{12}E_4$ reverse micelles and/or the reduced hydration of DNA cause a closer approach, along the double helical axis

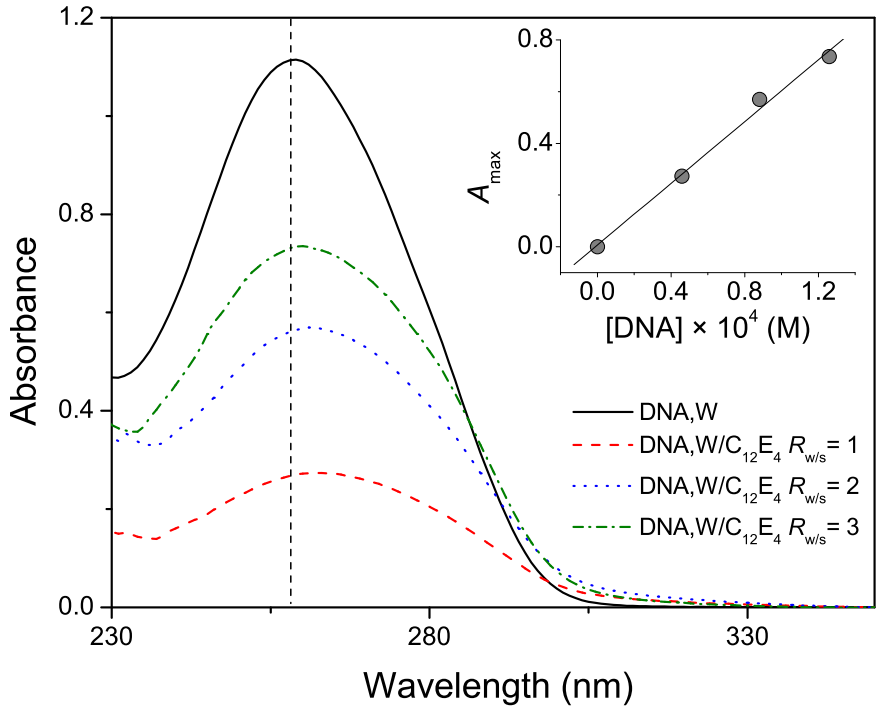

Figure 2.35: UV spectra of DNA, W ([DNA] = 146 μM) and DNA, W/$C_{12}E_4$ system at various $R_{w/s}$ values ($R_{w/s}$ = 1 and [DNA] = 46 μM, $R_{w/s}$ = 2 and [DNA] = 88.1 μM, $R_{w/s}$ = 3 and [DNA] = 126 μM). The inset shows the absorbance at the band maximum (A_{max}) as function of DNA concentration.

and/or a more favourable orientation of the base pairs. The red shift of the band maximum indicates that also the energetic gap of the molecular orbitals involved in the transition is consequently affected by DNA confinement and/or reduced hydration.

Table 2.6: Wavelength (λ_{max}) and molar extinction coefficient (ϵ_{max}) at the band maximum of DNA in aqueous solution and in $C_{12}E_4$ reverse micelles at various $R_{w/s}$

$R_{w/s}$	λ_{max} (nm)	ϵ_{max} (M^{-1} cm^{-1})
1	262	5956
2	261	6470
3	260	5849
Aqueous Solution	258	7000

The effect of the water content of the $C_{12}E_4$ reverse micelles on the DNA band para-

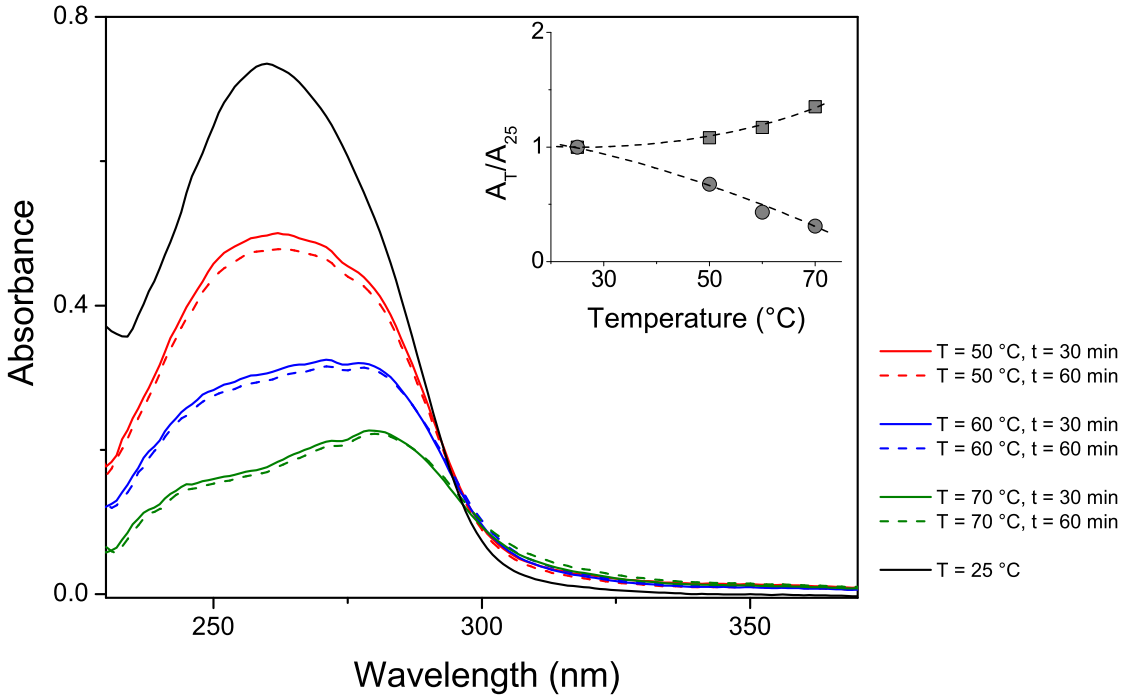

Figure 2.36: DNA band of the DNA, W/$C_{12}E_4$ at $R_{w/s}$ = 3 sample at 25 °C and after the thermal treatment shown.Inset: absorbance at the band maximum as function of temperature for DNA, W (squares) and DNA, W/$C_{12}E_4$ (circles, $R_{w/s}$ = 3). [DNA] = 126 μM.

meters was investigated by recording the UV spectra of samples at various $R_{w/s}$ values shown in Figure 2.35 and collecting the λ_{max} and ϵ_{max} values summarized in Table 2.6. The linear trend of the band intensity (A_{max}) with the DNA molar concentration, in the inset of Figure 2.35, shows that the Lambert-Beer law is fulfilled in all the samples implying the absence of a DNA structural transition in the investigated $R_{w/s}$ range. From an inspection of Table 2.6, it can be argued that by decreasing $R_{w/s}$, i.e. by reducing the water content of reverse micelles, there is an increasing deviation of λ_{max} with respect to the value in aqueous solution while ϵ_{max} does not show a definite trend. This suggests that λ_{max} is more sensitive to change of the DNA hydration whereas ϵ_{max} is sensitive to base pair interactions.

Further information on the state of DNA confined in $C_{12}E_4$ reverse micelles has been gained by holding for 30 and 60 minutes the DNA, W/$C_{12}E_4$ sample at $R_{w/s}$ = 3 at 50, 60 and 70 °C in a thermostatic bath and immediately after collecting the UV spectra at 25 °C (see Figure 2.36). Surprisingly, a marked and irreversible decrease of the band

intensity by increasing the temperature of the thermal treatment and a modest reduction with its duration was observed. This indicates the occurrence of DNA condensation in a more compact structure at increasing values of the temperature. This behaviour is opposite to that occurring in aqueous solutions where an increase of the temperature above the DNA melting point ($T_m \approx 53$ °C) causes an absorbance increase, attributed to a separation of DNA into single filaments (denaturation) [21] (see Section 2.2).

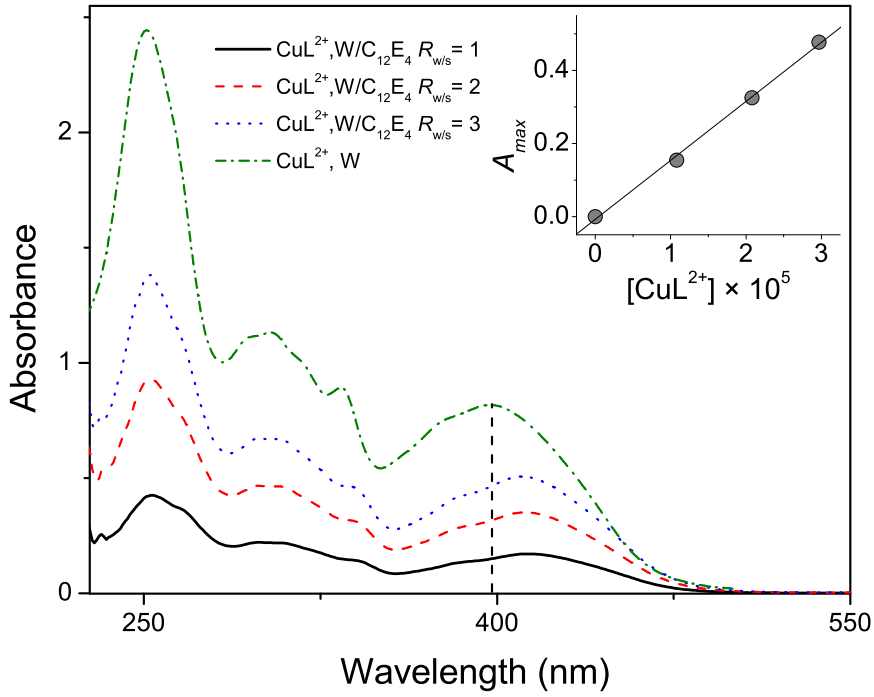

Figure 2.37: UV spectra of CuL^{2+}, W ([CuL^{2+}] = 53.0 μM) and CuL^{2+}, W/$C_{12}E_4$ at $R_{w/s}$ = 1 ([CuL^{2+}] = 10.8 μM), $R_{w/s}$ = 2 ([CuL^{2+}] = 20.8 μM) and $R_{w/s}$ = 3 ([CuL^{2+}] = 29.7 μM) systems. The inset shows the absorbance (A_{max}) at the maximum of the band at $\approx$ 400 nm as function of CuL^{2+} concentration.

The diametric behaviour is also emphasized in the inset of Figure 2.36, where the absorbance at the band maximum (normalized with respect to the value at 25 °C) of the systems DNA/W and DNA, W/$C_{12}E_4$ at $R_{w/s}$ = 3 are shown as a function of temperature. Taking into account that the monolayer of oriented surfactant molecules surrounding the DNA macromolecule applies a surface tension on it, it can be hypothesized that the thermal treatment of the DNA, W/$C_{12}E_4$ at $R_{w/s}$ = 3 makes accessible DNA transitions toward more compact structures.

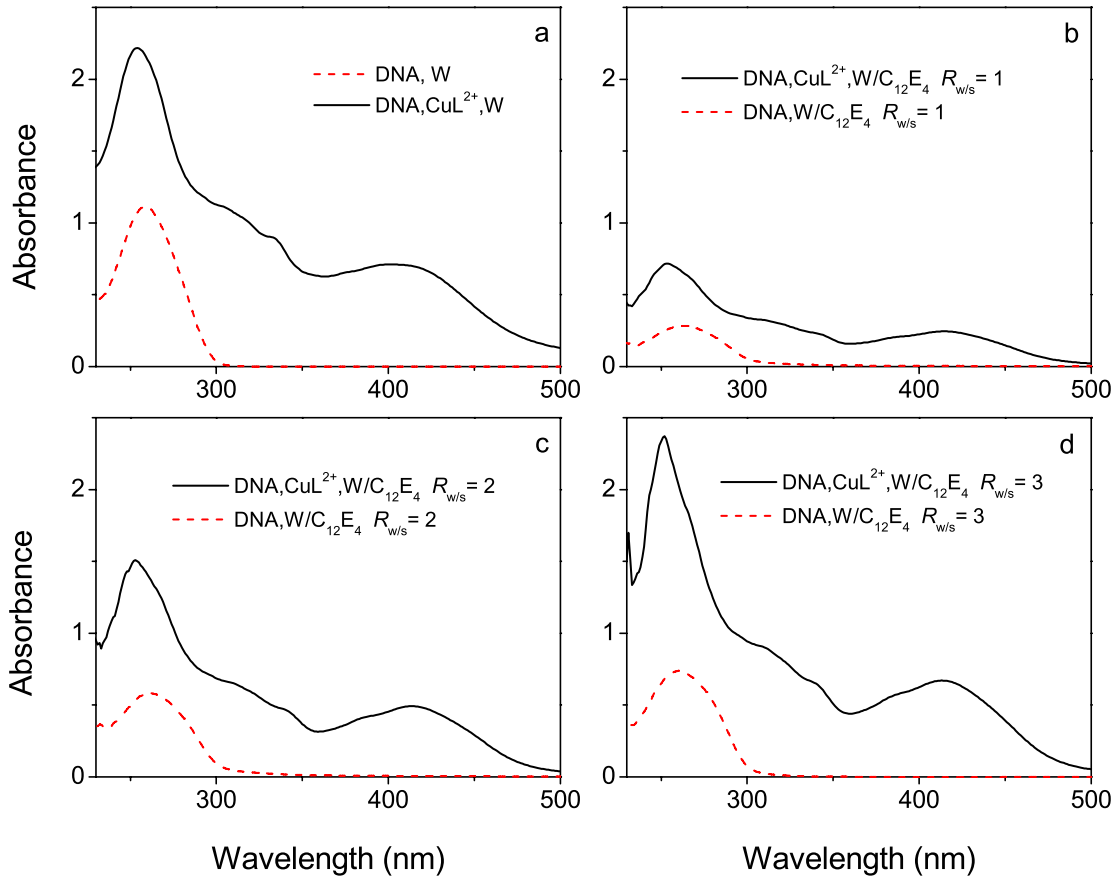

Figure 2.38: UV-vis spectra of: panel (a) DNA, W ([DNA] = 150 μM) and DNA, CuL^{2+}, W ([CuL^{2+}] = 53.0 μM); panel (b) DNA, $W/C_{12}E_4$ and DNA, CuL^{2+}, $W/C_{12}E_4$ at $R_{w/s}$ = 1 and [CuL^{2+}] = 19.5 μM; panel (c) DNA, $W/C_{12}E_4$ and DNA, CuL^{2+}, $W/C_{12}E_4$ at $R_{w/s}$ = 2 and [CuL^{2+}] = 37.2 μM; panel (d) DNA, $W/C_{12}E_4$ and DNA, CuL^{2+}, $W/C_{12}E_4$ at $R_{w/s}$ = 3 and [CuL^{2+}] = 53.2 μM. In all samples containing CuL^{2+} R = 1 (R = [DNA]:[CuL^{2+}]).

Confinement effects on the intercalation of CuL^{2+} in the DNA structure were emphasized by collecting the UV spectra of CuL^{2+} and of the CuL-DNA system in water and in $C_{12}E_4$ reverse micelles at various $R_{w/s}$. These spectra are shown in Figures 2.37 and 2.38. Among the various features, the band at about 400 nm entirely attributable to CuL^{2+} is of utmost importance because DNA spectral contributions are absent in this region. The λ_{max} and ϵ_{max} parameters of this band are summarized in Table 2.7.

The linear trend shown in the inset of Figure 2.37 shows that the Lambert-Beer law is fulfilled in the investigated systems. Moreover, an analysis of the band parameters of Table 2.7 concerning CuL^{2+} and the CuL-DNA system in water and in $C_{12}E_4$ reverse micelles at various $R_{w/s}$ indicates intercalation through the stacking interaction of the aromatic rings of CuL^{2+} and the base pairs of DNA mainly leading to band red shift [21].

Table 2.7: Wavelength (λ_{max}) and molar extinction coefficient (ϵ_{max}) at the band maximum of CuL^{2+} (about 400 nm) and of the system DNA-CuL^{2+} in water and in $C_{12}E_4$ reverse micelles at various $R_{w/s}$

$R_{w/s}$	λ_{max} (nm) CuL^{2+}	ϵ_{max} (M^{-1} cm^{-1}) CuL^{2+}	λ_{max} (nm) DNA-CuL^{2+}	ϵ_{max} (M^{-1} cm^{-1}) DNA-CuL^{2+}
1	413	1.59×10^4	414	1.26×10^4
2	412	1.70×10^4	414	1.31×10^4
3	411	1.72×10^4	414	1.27×10^4
Aqueous Solution	396	1.55×10^4	401	1.34×10^4

In $C_{12}E_4$ reverse micelles, the mean change of λ_{max} ($\Delta\lambda_{max}$ = 2 nm) due to intercalation is lower than that in aqueous solution ($\Delta\lambda_{max}$ = 5 nm) while that of ϵ_{max} ($\Delta\epsilon_{max} \approx -0.4\times 10^4$) is greater ($\Delta\epsilon_{max} = -0.21 \times 10^4$). These departures from the behaviour observed in aqueous solution emphasize that the CuL^{2+} interaction with DNA is influenced by different microscopic events.

Further information on the state of the CuL-DNA system confined in $C_{12}E_4$ reverse micelles has been gained by holding for 30 and 60 minutes the DNA, CuL^{2+}, W/$C_{12}E_4$ sample at $R_{w/s}$ = 3 at 60 and 70 °C in a thermostatic bath and immediately after collecting the UV spectra at 25 °C (see Figure 2.39). It is of interest that the spectrum of confined DNA + CuL^{2+} complex is slightly affected by the thermal treatment. This means that CuL^{2+} intercalated in the DNA confined within $C_{12}E_4$ reverse micelles partially neutralizes the negative charges of the phosphate groups, stabilizing its double-helical structure and thus inhibiting the changes induced by the thermal treatment. Together with the intrinsic importance of this finding, it confirms the CuL^{2+} intercalation in the DNA double helix.

2.4.2 Circular Dichroism

The CD spectrum of lyophilized ct-DNA in buffered aqueous solution displays a positive band centred at 270 nm due to the stacking of base pairs and a negative band at 240 nm due to the characteristic helicity of right-handed DNA in the B form.

In the case of Z-DNA, DNA with left-handed helicity, a positive band is observed at 260-280 nm and a negative band at 300-350 nm. Moreover, in confined systems at low water content where DNA takes a compact form (called Ψ-DNA), a strong enhancement of the band intensity in the region at about 280 nm is observed [133].

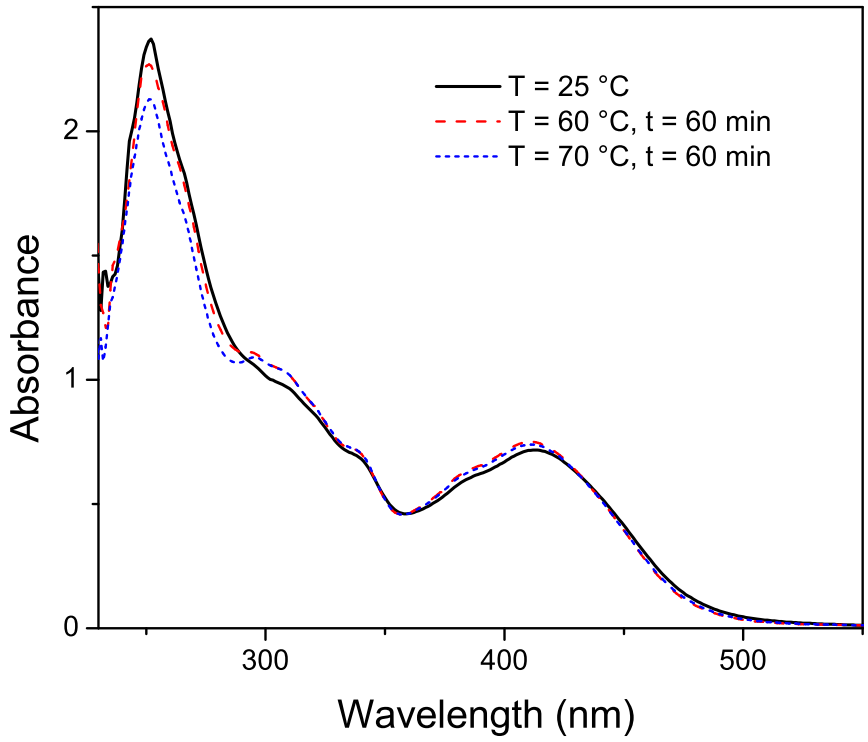

Figure 2.39: UV-vis spectra of the DNA, CuL^{2+}, $W/C_{12}E_4$ at $R_{w/s}$ = 3 sample at 25 °C and after the thermal treatment shown ([CuL^{2+}] = 53.2 μM and R = 1, (R = [DNA]:[CuL^{2+}]).

The CD spectra of native DNA in aqueous solution and in $W/C_{12}E_4$ at various $R_{w/s}$ are shown in Figure 2.40. It can be noted that there are marked differences in the spectral shape with respect to that registered in aqueous solution: a very intense positive band at 267 nm and the appearance of a negative band at about 300 nm both linearly related to the DNA concentration (see inset of Figure 2.40). This finding suggests that DNA confined in $C_{12}E_4$ reverse micelles undergoes a compaction presumably accompanied by a transition from a right- to left-handed helix.

A further contribution could arise from the chiral binding of the surfactant to the DNA double strands. It can be hypothesized that DNA condensation is driven by the low local dielectric constant of the reverse micellar cores that increasing the electrostatic interactions causes a partial neutralization of the charges residing on the DNA backbone. Additional contributions might arise from the tension on its surface due to the monolayer of adsorbed surfactant molecules. Moreover, looking to the CD spectra at

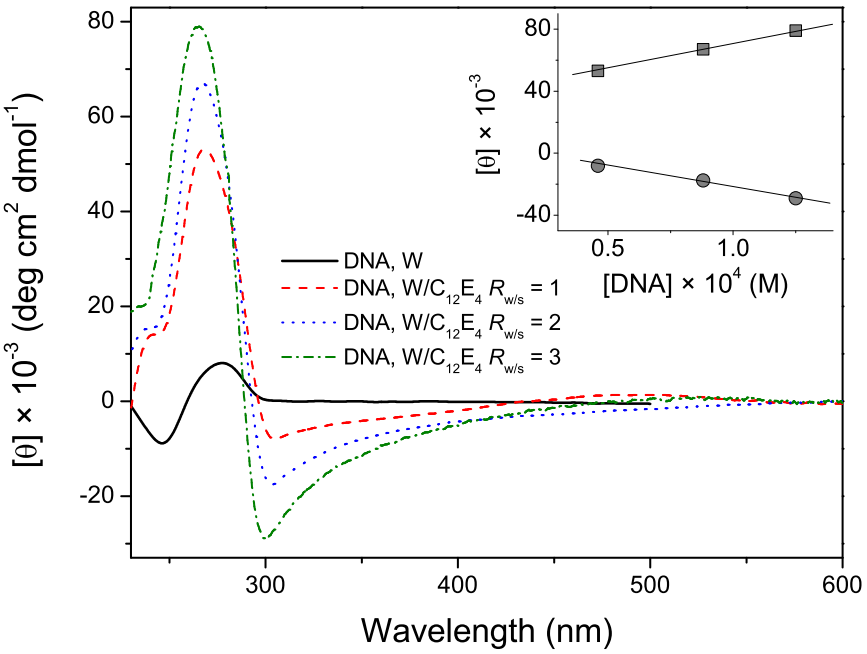

Figure 2.40: CD spectra of DNA, W/$C_{12}E_4$ at $R_{w/s}$ = 1 ([DNA] = 46.0 μM), $R_{w/s}$ = 2 ([DNA] = 88.1 μM) and $R_{w/s}$ = 3 ([DNA] = 125.0 μM) and DNA, W ([DNA] = 100 μM) systems. The inset shows molar ellipticity values at the positive band maximum (circles) and at the negative band minimum (squares) as a function of the DNA concentration.

various $R_{w/s}$, it seems reasonable to conclude that in the investigated $R_{w/s}$ range the compaction of DNA is favoured by an increase of its hydration degree. On the other hand, the transition from B to Z-DNA can be considered to be a consequence of its confinement in the reverse micellar core.

Further information on the state of ct-DNA confined in $C_{12}E_4$ reverse micelles has been gained by holding for 30 minutes the DNA, W/$C_{12}E_4$ sample at $R_{w/s}$ = 3 at 50, 60 and 70 °C in a thermostatic bath and immediately after collecting the CD spectra at 25 °C (see Figure 2.41). It can be noted that the intensity of the positive band at 280 nm, after an initial decrease, at T $>$ 60 °C increases dramatically while the negative band at 300 nm disappears. This behaviour emphasizes that the thermal treatment causes different effects: increases the DNA compaction and at the same time inhibits the B- to Z-DNA transition.

Confinement effects on the CuL^{2+} interaction with the DNA macromolecule were

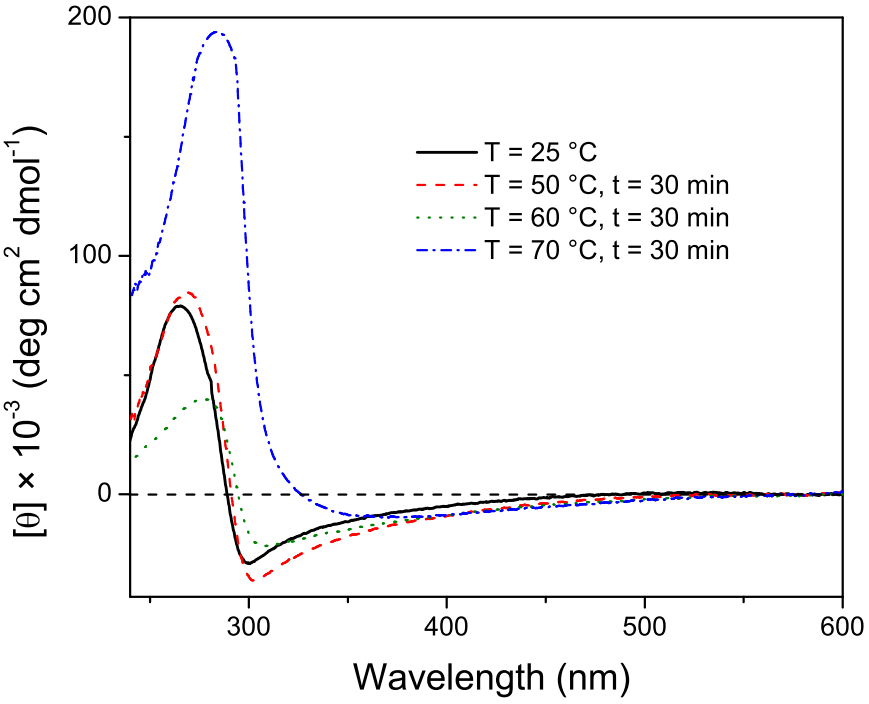

Figure 2.41: CD spectra of DNA, W/$C_{12}E_4$ at $R_{w/s}$ = 3 sample at 25 °C and after the thermal treatment shown.

also emphasized by recording the CD spectra of CuL^{2+} and of the CuL-DNA system in water and in $C_{12}E_4$ reverse micelles at various $R_{w/s}$. These spectra, with the solvent contribution subtracted, are shown in Figure 2.42. Comparing these spectra with those shown in Figure 2.40, it can be noted that there are marked changes in the shape of the CD spectra induced by the presence of CuL^{2+}. These findings suggest unequivocally the occurrence of a DNA-interaction by CuL^{2+} and, at the same time, of significant perturbations of the DNA helicoidal structure. Moreover, notwithstanding that CuL^{2+} is not chiral, its binding to the DNA determines an induced CD band occurring at $\lambda > 380$ nm, i.e. in a spectral region where the DNA does not show CD contributions. This finding suggests that CuL^{2+} is tightly bonded and adopts the dominating chiral organization of the DNA double helix [139].

Other effects due to CuL^{2+} intercalation are shown in Figure 2.43 where the CD spectra of the DNA, CuL^{2+}, W/$C_{12}E_4$ sample at $R_{w/s}$ = 3 at 25 °C and after the thermal treatment at 60 and 70 °C for 30 minutes are reported. It can be noted that at T = 60 °C,

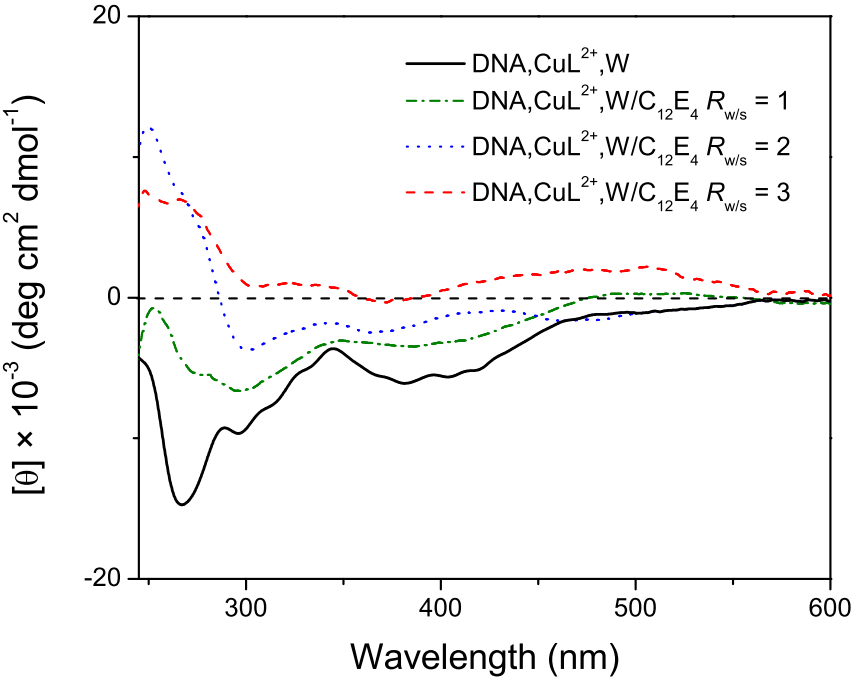

Figure 2.42: CD spectra of DNA, CuL^{2+}, $W/C_{12}E_4$ at $R_{w/s}$ = 1 ([DNA] = 42.0 μM), $R_{w/s}$ = 2 ([DNA] = 81.1 μM) and $R_{w/s}$ = 3 ([DNA] = 114.0 μM) and DNA, CuL^{2+}, W ([DNA] = 100.0 μM); R = 2 (R = [DNA]:[CuL^{2+}])

the CD spectrum is slightly affected with respect to that at 25 °C while at T = 70 °C a dramatic change with the formation of a highly compact and ordered DNA superstructure.

2.4.3 Small Angle X-Ray Scattering

Figure 2.44 shows the scattering profiles of $W/C_{12}E_4$ and DNA, $W/C_{12}E_4$ samples at the investigated $R_{w/s}$ and of the DNA, CuL^{2+}, $W/C_{12}E_4$ sample at $R_{w/s}$ = 3. It can be noted that all the spectra are characterized by an intense absorption at the lower q due to the beam stop and an interference peak with a maximum at about $q^* \approx 0.17$ Å^{-1} whose position decreases with $R_{w/s}$. Taking into account that in the investigated composition range $C_{12}E_4$ forms a dense L2 phase of reverse micelles, the Bragg distance ($d = 2\pi/q$) can be identified with the micellar core diameter [128, 129]. The q and d values are collected in Table 2.8.

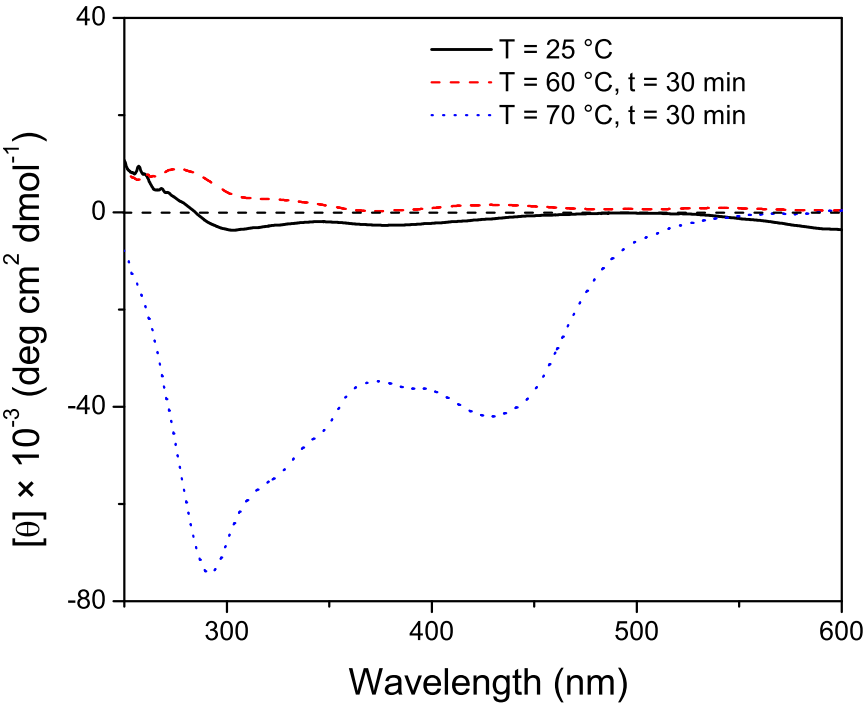

Figure 2.43: CD spectra of DNA, CuL^{2+}, $W/C_{12}E_4$ ($R_{w/s}$ = 3; [DNA] = 114.0 μM; [CuL^{2+}] = 53.2 μM) sample at 25 °C and after the thermal treatment shown.

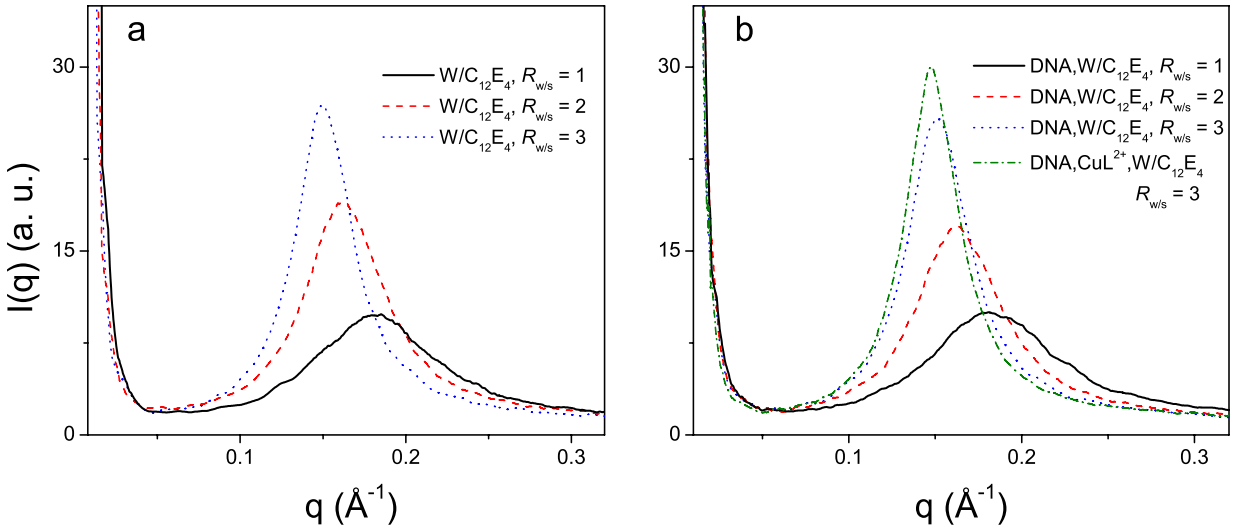

Figure 2.44: SAXS patterns of $W/C_{12}E_4$ and DNA, $W/C_{12}E_4$ samples at various $R_{w/s}$ and of the DNA, CuL^{2+}, $W/C_{12}E_4$ sample at $R_{w/s}$ = 3.

A linear increase of the reverse micelle diameter (d) and a decrease of the peak width (w) with $R_{w/s}$ have been found. These findings are consistent with a progressive increase of the aqueous micellar core size accompanied by a parallel increase of the local structural order in the $C_{12}E_4$ liquid crystals [140].

Table 2.8: Structural parameters of the investigated samples

System	q (Å^{-1})	d (Å)	w (Å^{-1})
W/$C_{12}E_4$, $R_{w/s}$ = 1	0.182	34.5	0.068
DNA, W/$C_{12}E_4$, $R_{w/s}$ = 1	0.184	34.1	0.069
W/$C_{12}E_4$, $R_{w/s}$ = 2	0.163	38.5	0.048
DNA, W/$C_{12}E_4$, $R_{w/s}$ = 2	0.164	38.3	0.051
W/$C_{12}E_4$, $R_{w/s}$ = 3	0.148	42.4	0.037
DNA, W/$C_{12}E_4$, $R_{w/s}$ = 3	0.149	42.2	0.039
CuL^{2+},DNA, W/$C_{12}E_4$, $R_{w/s}$ = 3	0.148	42.4	0.037

The extrapolated d value at $R_{w/s}$ = 0 is 31.3 Å, which is in agreement with the literature value (32.5 Å) [131]. It is worth noting that the d values are always much smaller than the ct-DNA size [141–143]. This indicates that the micellar aggregates containing this macromolecule are bigger than empty micelles.

Comparing the structural parameters of samples at the same $R_{w/s}$, it can be also noted that the d value of the DNA, W/$C_{12}E_4$ samples is slightly lower than that of the W/$C_{12}E_4$ samples whereas the peak width is slightly larger. These findings suggest that the hydration of the DNA macromolecule diminishes the amount of water disposable for empty reverse micelles while its presence involves an increase of the local disorder. Finally, the d and w values concerning the DNA, CuL^{2+}, W/$C_{12}E_4$ sample at $R_{w/s}$ = 3 indicate that the intercalation of CuL^{2+} in the DNA backbone determines a decrease of its hydration degree.

2.4.4 Conclusions

This investigation shows that ct-DNA can be stably solubilized in the non-ionic surfactant $C_{12}E_4$ in the presence of small amounts of water and that this process determines dramatic changes of its structural properties. The experimental results obtained by UV-vis spectrophotometry, circular dichroism and small angle X-ray scattering consistently indicate that DNA is confined in the hydrophilic core of $C_{12}E_4$ reverse micelles, strongly perturbed by its presence. The confinement causes the formation of more compact and

thermoresistent DNA structure accompanied by a transition from right- to left- handed. It has been hypothesized that the DNA condensation in $C_{12}E_4$ reverse micelles is caused by the low local dielectric constant of the reverse micelle core which increasing the electrostatic interaction determines a partial neutralization of the DNA charges. Further contributions can arise from the tension on the DNA surface due to the monolayer of oriented surfactant molecules. It has been found that, as in aqueous solution, CuL^{2+} intercalates the DNA confined in $C_{12}E_4$ reverse micelles enhancing the stability of its structure. Within the $C_{12}E_4$ reverse micelles, both the DNA and the CuL-DNA system display a response to the thermal treatment different from that observed in aqueous solution. In particular, in aqueous solution and above a critical value, the thermal treatment determines the DNA denaturation whereas, surprisingly, in $C_{12}E_4$ reverse micelles a strong stabilization of the DNA double helix occurs. This behavior deserves further investigation for its theoretical and applicative relevance.

2.5 Experimental

2.5.1 Materials and Method

All chemicals and solvents were purchased from Sigma–Aldrich, Fisher or Alfa Aesar and used as received. Deuterated solvents for NMR were supplied by Cambridge Isotope Laboratories, Inc. and Goss scientific. Ultrapure water (18.2 MΩ, Fisher) was used in all UV-vis, circular and linear dichroism experiments and for electrophoresis gel. Lyophilized ct-DNA, purchased from Sigma-Aldrich, was resuspended in tris-hydroxymethyl-aminomethane (Tris-HCl) pH 7.5 and dialyzed as described in the literature [144]. The DNA concentration was determined by UV-vis measurements using the molar extinction coefficient of ϵ_{258} = 7000 mol^{-1} dm^3 cm^{-1} per DNA base [135–138].

Proton and carbon nuclear magnetic resonance spectra were recorded on Bruker AC300 or DRX500 spectrometers.

ESI mass spectra were recorded on a Micromass LCT Time of flight mass spectrometer.

Spectroscopic studies

Stock solutions of 1 M NaCl, 1 M Tris-HCl and 100 mM sodium cacodylate buffer ($Na(CH_2)_2AsO_2{\cdot}3H_2O$, pH 6.8) were prepared and, together with ct-DNA stock, were

used to obtain the final work solutions.

Absorption measurements were performed on a Varian Cary 5000 UV-vis double beam spectrophotometer or on a Varian UV–vis Cary 1E double beam spectrophotometer, both equipped with a Peltier temperature controller, using 1 cm pathlength cuvettes.

Circular dichroism spectra were recorded at 25 °C on a Jasco J-715 or Jasco J-810 spectropolarimeters, using 1 cm path–length quartz cells. sensitivity, 100 mdeg; wavelength range, 200 -750 nm; data pitch, 0.5 nm; scanning mode, continuous; scanning speed, 200 nm min^{-1}; response, 0.1 s; bandwidth, 1.0; accumulation, 6. Linear dichroism spectra were collected using a Jasco J-810 spectropolarimeter adapted for LD measurements with a flow Couette cell, ideal to give an orientation to long molecules such DNA [145]. The following parameters were used: sensitivity, 100 mdeg; wavelength range, 200-750 nm; data pitch, 0.5 nm; scanning mode, continuous; scanning speed, 500 nm min^{-1}; response, 0.25 s; bandwidth, 2.0; accumulation, 8.

Steady-state fluorescence measurements were made at 25 °C using a Horiba Jobin Yvon spectrofluorimeter (Fluoromax 4) arranged in T-shaped geometry. Time correlated single photon counting (TCSPC) measurements were carried out using the Fluoromax 4 apparatus equipped with a Single Photon Counting Controller (FluoroHub, Horiba Jobin Yvon) and a pulsed diode light source (Nanoled, repetition rate 1 MHz, pulse duration 1.27 ns, 368 nm); data fitting was accomplished using least-squares methods with DAS6 Fluorescence Decay Analysis Software. All spectra were made using a 10 mm path length cuvette and were corrected for buffer fluorescence.

Small angle X-ray scattering spectra have been collected at 25 °C by a Nanostar (Bruker) equipped with a copper anode Cu Kα, filtered with Ni (λ= 1.5418 Å) and a bidimensional detector. Experimental data, the scattering intensity I and the scattering vector q, related to the scattering angle θ by the equation

$$q = \frac{4\pi}{\lambda} \sin \frac{\theta}{2} \tag{2.4}$$

have been corrected by subtraction of the cell and solvent contributions.

X-ray crystallography

Crystal data for CuL^{2+}: $C_{34}H_{46}CuN_4O_2$, 2(ClO_4), 0.5(C_6H_6), 0.25(CH_3NO_2), 1.75(H_2O), M = 891.03, triclinic, space group P-1, T = 120 (2) K, a = 9.473 (12) Å, b = 17.12 (2) Å,

c = 28.27 (3) Å, α = 81.854 (14)°, β = 89.586 (14)°, γ = 79.222 (11)°, V = 4458 (9) Å^3, Z = 4, 25883 reflections measured, 10983 unique (R_int = 0.2081) which were used in all calculations. Final R1 (I>2σ(I)) = 0.1225, wR2 (all data) = 0.4126, goodness of fit = 0.947 on F^2.

The dataset was measured on a Crystal Logics diffractometer using a Rigaku Saturn 724+ detector at the Diamond synchrotron X-ray source, beamline I19 (λ = 0.6889 Å). The data collection was driven by CrystalClear [146] and unit cell refinement and data reduction was carried out in Apex2 [147]. An absorption correction was applied using SADABS [147]. The structure was solved in SIR97 and was refined by a full-matrix least-squares procedure on F^2 in SHELXL-97 [148,149]. All non-hydrogen atoms were refined with anisotropic displacement parameters. Figures were produced using ORTEP3 for Windows and Mercury 2.2 [150,151].

The crystal was the best quality that could be grown but was weakly diffracting, especially at higher 2θ angles and, despite use of the Diamond synchrotron X-ray source no diffraction was observed above 2θ 43°. The dataset was of rather poor quality and the structure contains highly disordered solvent molecules and these facts are reflected in the somewhat high agreement statistics.

Gel Electrophoresis

The electrophoresis experiments were performed through Electrophoresis Power Supply (EPS 301) system with the following parameters: voltage, 120 V; electric current, 190 mA; time, 2.5 h. Gel trays of 210 150 mm with a 15-toothed comb were used. In all of the electrophoresis experiments 1X Tris acetate (obtained by dilution of 10X TAE, supplied by SIGMA) was used as working buffer. In detail, the gel was prepared warming up 2 g of agarose (from USB corporation) in 200 mL of 1X TAE. pBR322 plasmide DNA (1mg/mL, New England Biolabs) was used to prepare the samples. Once incubated for 1.5 h at 37 °C, to each sample 4 μL of loading buffer (30% glycerol and 0.25% bromophenol blue in ultra pure water) were added and 16 μL of each final solution were loaded in the gel. After electrophoresis the gel was stained in 100 mL of 1X TEA buffer containing 400 μL of ethidium bromide solution (0.5 μg mL^{-1}) for 15-20 min followed by a washing with water for 5 min. The images of the gels were visualized and acquired using a UVtec-uvipro platinum system.

As concerns the PCR gel electrophoresis experiment, twelve reaction mixtures were prepared, all containing 1X NH_4 reaction buffer, $MgCl_2$ (1.5 mM), pUC19 plasmid DNA

substrate (50 ng, Sigma Aldrich), Taq DNA polymerase (5U; Bioline), dNTPs (3 mM), the primers (0.4 μM each) pUC19F (5′-CGGTGAAAACCTCTGACACA -3′) and M13 reverse (5′-CAGGAAACAGCTATGACC -3′; Alta Bioscience). The images of the gels were visualized and acquired using a UVtec-uvipro platinum system.

2.5.2 Synthesis and characterization

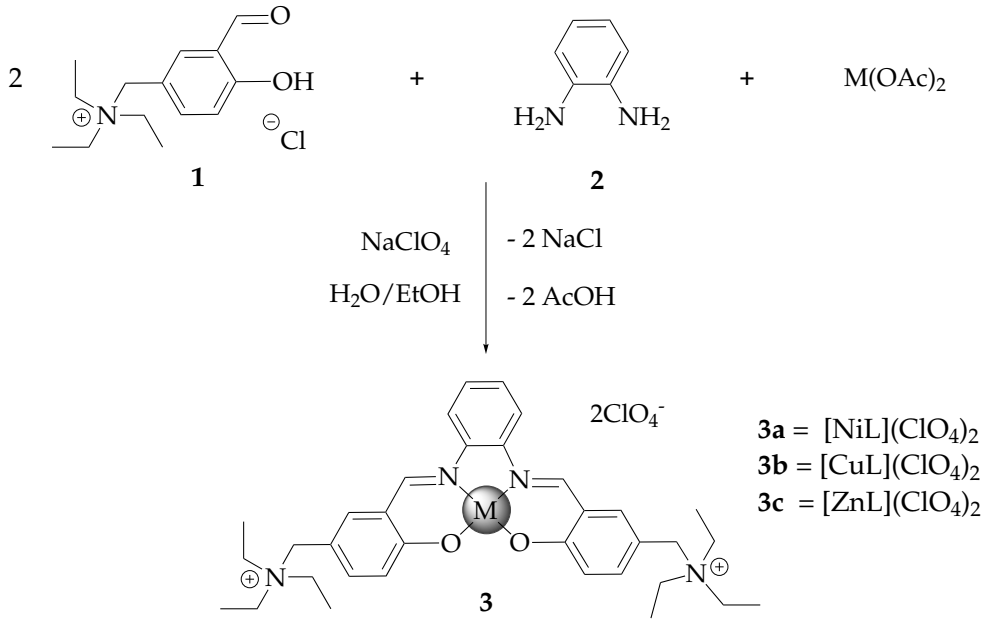

Figure 2.45: Reaction scheme of the ML^{2+} complex (M = Cu, Ni, Zn, H_2L^{2+} = N,N′-Bis-5-(triethyl ammonium methyl salicylidene)-1,2-phenylenediamine)

The Ni^{II} complex was synthesized as described previously [21, 22, 152]. In brief, 5-(triethylammoniummethyl) salicylaldehyde chloride (**1**) and 1,2 phenylendiamine (**2**) were mixed in ultrapure water in a 2:1 molar ratio. To this solution one equivalent of nickel(II) acetate was added and the resulting mixture was stirred for 1h at room temperature. Finally the compound was isolated as perchlorate salt adding sodium perchlorate. The orange precipitate was washed with methanol and diethyl ether to afford the compound as an orange solid. The 5–(triethylammoniummethyl) salicylaldehyde chloride ligand was prepared mixing 5–chloromethyl salicylaldehyde [153] and triethylamine in THF at room temperature for 5h [21].

N,N′-Bis-5-(triethylammoniummethylsalicylidene)-1,2-phenylenediamine-Ni^{II} (3a). The complex was characterized by elemental analysis, NMR, ESI mass analysis and UV-

vis spectroscopy.
^{1}H NMR (500 MHz, DMSO, 298 K) δ 9.93 (s, 1H, im), 8.18 (dd, J = 6.0, 3.4 Hz, 1H, ar5), 7.77 (s, 1H, ar3), 7.46 (dd, J = 12.2, 6.0 Hz, 2H, ar2 and ar4), 6.99 (d, J = 8.8 Hz, 1H, ar1), 4.39 (s, 2H, a), 3.17 (q, J = 6.8 Hz, 6H, b), 1.34 (t, J = 7.0 Hz, 9H, c).
^{13}C NMR (125 MHz, DMSO) δ 166.5 (q2), 157.8 (im), 142.0 (q4), 139.5 (ar3), 139.0 (ar2), 128.7 (ar4), 123.5 (ar1), 121.1 (q3), 117.4 (ar5), 114.6 (q1), 59.3 (a), 51.9 (b), 7.9 (c). For numbering scheme see Figure 2.5. ^{13}C DEPT, COSY, HSQC, HMBC NMR spectra are presented in Appendix A.
Elemental analysis calcd (%) for $NiC_{34}H_{46}N_4O_{10}C_{12}$ ($NiL(ClO_4)_2$) : C, 51.0; H, 5.8; N, 7.0; Cl, 8.9; found: C, 50.5; H, 5.7; N, 7.0; Cl, 9.0. MS-ESI (m/z): 300.2 $[NiL]^{2+}$.
UV-vis (Tris-HCl): $\epsilon = 4.76 \times 10^4$ (λ = 261 nm); $\epsilon = 1.87 \times 10^4$ (λ = 352 nm); $\epsilon = 2.01 \times 10^4$ (λ = 366 nm) $cm^{-1}M^{-1}$.

N,N′-Bis-5-(triethylammoniummethylsalicylidene)-1,2-phenylenediamine-Cu^{II} (3b). The general procedure for the synthesis is identical to the one of the compound NiL^{2+} and was previously reported [21, 152]. Green single crystals suitable for X–ray diffraction analysis were obtained by slow diffusion of diethyl ether into a solution of CuL^{2+} (4 mg) in acetonitrile (2 mL), or in CH_3NO_2/benzene (2 mL). The products were characterized by elemental analysis, ESI mass analysis and UV-Vis spectroscopy.
Elemental analysis calcd (%) for $CuC_{34}H_{46}N_4O_{10}Cl_2$ ($CuL(ClO_4)_2$): C, 50.72; H, 5.76; N, 6.96; Cl, 8.81; found: C, 49.22; H, 5.69; N, 6.86; Cl, 8.59. ESI mass analysis: m/z = 303.3 $[CuL]^{2+}$.
UV-vis (Tris-HCl): $\epsilon = 5.35 \times 10^4$ (λ = 252 nm); $\epsilon = 2.49 \times 10^4$ (λ = 304 nm); $\epsilon = 1.95 \times 10^4$ (λ = 334 nm); $\epsilon = 1.79 \times 10^4$ (λ = 397 nm) $cm^{-1}M^{-1}$.
N,N′-Bis-5-(triethylammoniummethylsalicylidene)-1,2-phenylenediamine-Zn^{II} (3c). The general procedure for the synthesis is identical to the one of the compound NiL^{2+} and was previously reported [21, 22, 61, 152]
^{1}H NMR (500 MHz, DMSO, 298 K) δ 9.08 (s, 1H, im), 7.94 (dd, J = 6.1, 3.5, 1H, ar5), 7.56 (d, J = 2.3, 1H, ar3), 7.47 (dd, J = 6.1, 3.4, 1H, ar4), 7.38 - 7.28 (m, 1H, ar2), 6.80 (d, J = 8.8, 1H, ar1), 4.36 (s, 2H, a), 3.16 (q, J = 6.9, 6H, b), 1.33 (t, J = 7.0, 9H, c).
^{13}C NMR (125 MHz, DMSO) δ 173.3 (q2), 163.5 (im), 141.4 (ar3), 139.7 (q4), 138.0 (ar2), 128.2 (ar4), 124.2 (ar1), 119.8 (q3), 117.3 (ar5), 111.7 (q1), 60.0 (a), 51.7 (b), 8.0 (c). For numbering scheme see Figure 2.5. ^{13}CC DEPT, COSY, HSQC, HMBC NMR spectra are presented in Appendix A.

ESI mass analysis: m/z = 303.1 $[ZnL]^{2+}$.

Chapter 3

The interaction of DNA with Ni^{II}, Cu^{II} and Zn^{II} 1,2,4-oxadiazole complexes

Contents

Doesn't have a point of view, knows not where he's going to, isn't he a bit like you and me?

Lennon/McCartney, 1965

3.1 Introduction

Many low molecular weight DNA-binding drugs possess interesting biological properties and have found therapeutical applications in chemotherapeutic anticancer therapy [154–156]. In particular, the observed cytotoxic properties can be due to either direct interaction with DNA, with topoisomerases or with DNA-topoisomerase complexes [157]. Metal complexes constitute an important subset of DNA binding compounds, often DNA intercalators and groove binders, characterized by non-covalent sequence-specific interactions [4, 26, 158, 159].

As far as transition metal complexes are concerned, besides the classic 2,2'-bipyridyl based ligands, five-membered ring heterocyclic chelators have been recently developed. This strategy takes advantage of the coordinating ability of pyridine-like nitrogens of azoles, opening the way to new geometrical structures considering the peculiar coordination angles of five-membered ring ligands [160].

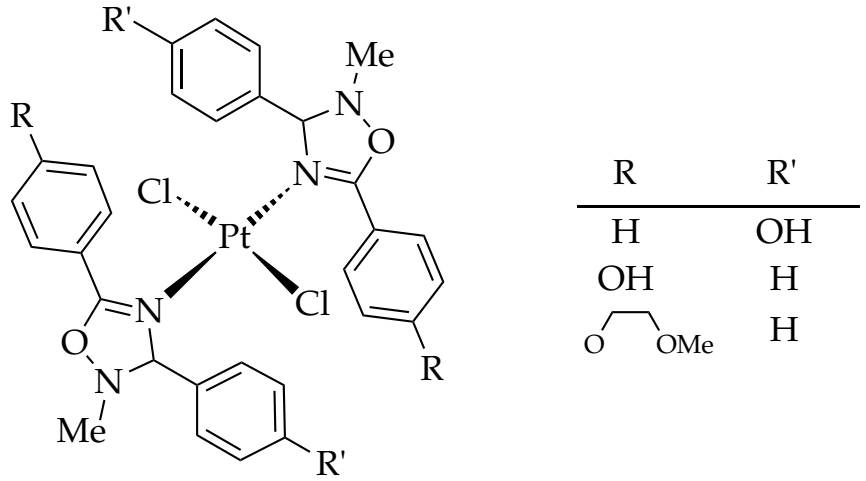

Figure 3.1: Structures of a series of Pt^{II} complexes of substituted 1,2,4-oxadiazole derivatives that have shown antitumor activity towards different human tumoral cell lines [31].

It is worth recalling that several five-membered heterocyclic compounds, such as 1,2,4- and 1,3,4-oxadiazoles, have shown a significant *in vitro* antitumor activity [30].

In particular, 1,2,4-oxadiazoles [161] have been employed as bioisosteres of bioactive compounds, as peptidomimetics and enzyme inhibitors, agonists or antagonist of different receptors, genotoxic compounds, apoptosis inducers, or as unnatural bases in the extension of DNA strands [162–168].

These heterocyclic systems are easily accessible and the modulation of their properties is achievable through the introduction of appropriate substituents on the central heterocycle. In particular, 1,2,4-oxadiazole ligands can be designed so as to chelate metal ions by the heteroatoms of the ring and of the side chain substituents in the ring positions 3 and 5.

Oxadiazole-based ligands have been used for complexation of metals such as platinum, silver, palladium and copper [160, 169, 170]. Recently, a series of Pt^{II} complexes of substituted 1,2,4-oxadiazole derivatives (Figure 3.1) have shown antitumor activity towards human ovarian cancer cell lines, as well as in colon and testicular cancer cell lines and the results have been correlated to their DNA-binding properties [31].

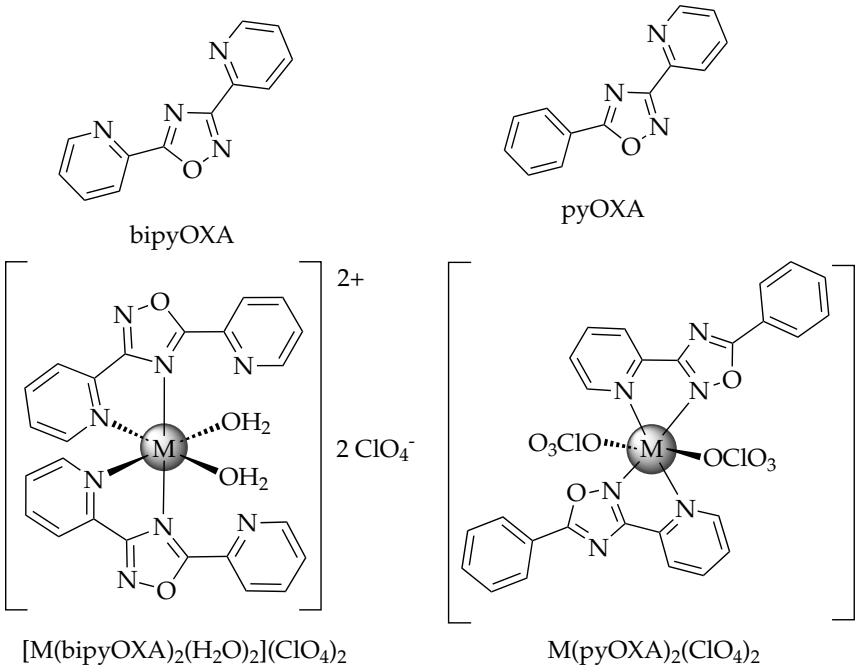

Figure 3.2: Structure of the bipyOXA and pyOXA ligands and of their metal complexes (M = Cu^{II}, Zn^{II}, Ni^{II})

Based in the considerations above, the synthesis and characterization of novel 1,2,4-oxadiazole complexes of Ni^{II}, Cu^{II} and Zn^{II} were performed, with the aim to obtain metal compounds with potential antitumor properties. In fact, the three metal ions are

present as essential elements in the biological intracellular environment of living organisms [171–174]. Moreover, their complexes with planar heterocyclic ligands are efficient DNA-binders and have a stronger affinity toward DNA than the corresponding isolated ligands [3, 49, 175]. In particular, two 1,2,4-oxadiazole ligands have been selected, opportunely substituted in both positions 3 and 5 of the ring, 3,5-bis(2'-pyridil)-1,2,4-oxadiazole (bipyOXA) and 3-(2'-pyridyl)5-(phenyl)-1,2,4-oxadiazole (pyOXA) (see Figure 3.2). Based on the results of the DNA binding studies, the most promising compound, $[Cu(bipyOXA)_2(H_2O)_2](ClO_4)_2$, was also tested against human hepatoblastoma and colorectal carcinoma cells lines [176].

3.2 Synthesis and structural characterization

The ligand bipyOXA was synthesized through a solvent-free reaction between amidoxime **5** and 2- cyanopyridine (**4**) (see Figure 3.3 and Section 3.6). The same amidoxime, together with benzoyl chloride (**9**) was used to synthesize the ligand pyOXA. The reaction was conducted in toluene at 130 °C (see Figure 3.4).

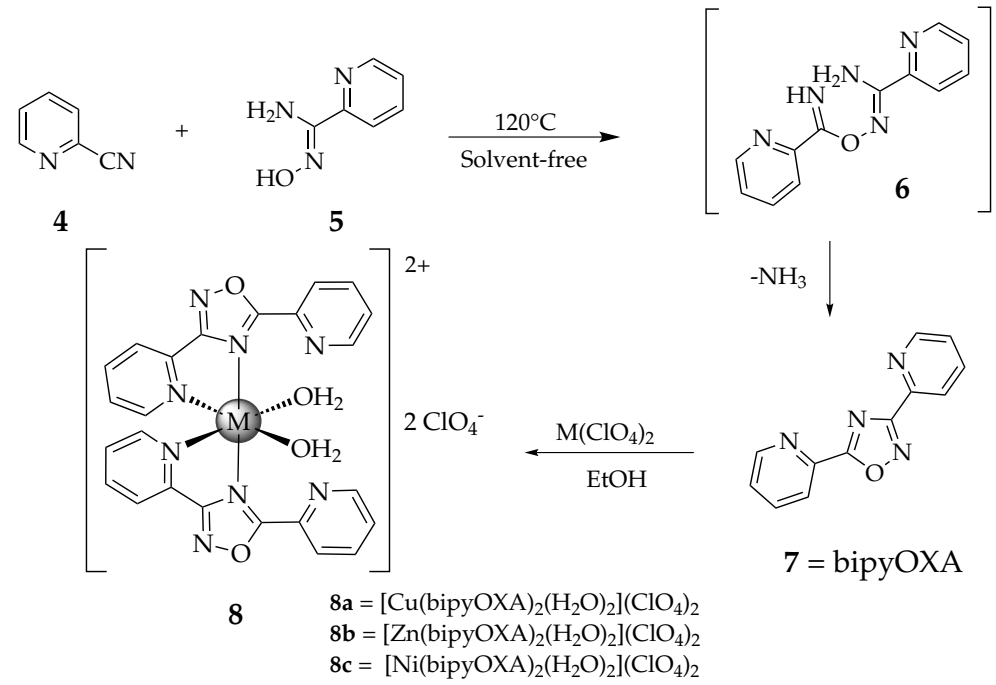

Figure 3.3: Synthesis of bipyOXA and of its Ni^{II}, Cu^{II} and Zn^{II} complexes.

The synthesized Cu^{II}, Zn^{II} and Ni^{II} complexes of the ligands bipyOXA (Figure 3.3)

and pyOXA (Figure 3.4) were characterized by elemental analysis, ESI mass spectrometry experiments and NMR, including COSY (see Experimental, Section 3.6, and Appendix A).

Due to their paramagnetism, it was not possible to acquire noiseless NMR spectra for the copper(II) and the nickel(II) complexes, both presenting an octahedral coordination geometry (see Figure 3.2) leading to open shell electron configurations. Suitable crystals for X-ray diffraction analysis were obtained only for the two copper complexes and their crystal structure is reported in the next paragraph. Nevertheless, elemental analysis data (see Section 3.6) confirm that the three metal complexes of bipyOXA contain two hydration water molecules, presumably coordinated as in the structure of the copper(II)-bipyOXA complex.

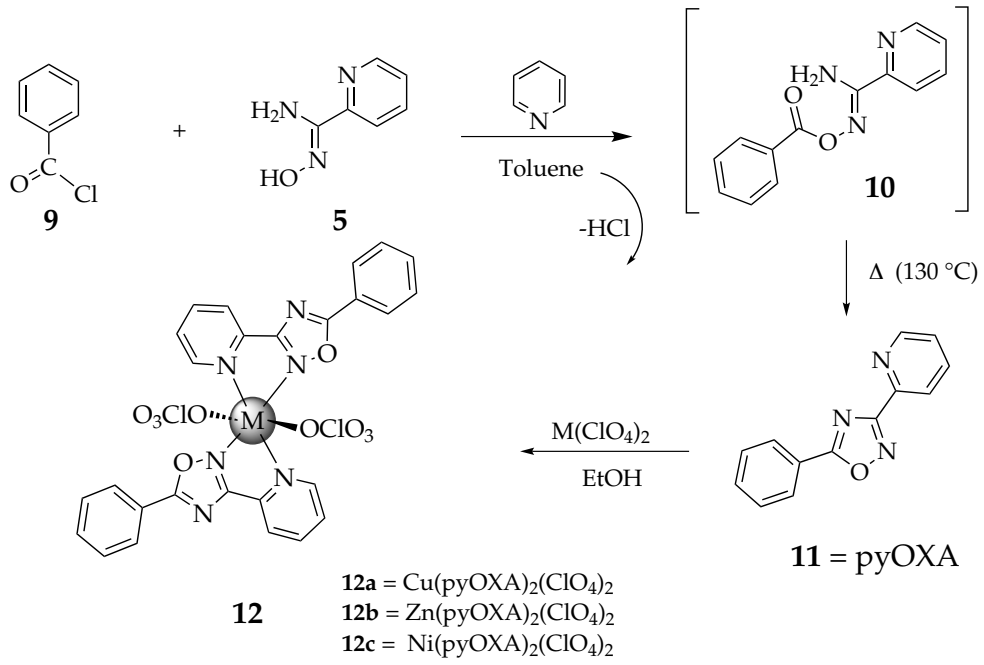

Figure 3.4: Synthesis of pyOXA and of its Ni^{II}, Cu^{II} and Zn^{II} complexes.

3.2.1 X-ray crystallography

The copper complex $[Cu(bipyOXA)_2(H_2O)_2]^{2+}$ was prepared in ethanol, crystallized from acetonitrile, and characterized by X-ray crystallography. Its structure consists of a discrete $[Cu(3,5\text{- bis}(2'\text{-pyridyl})\text{-}1,2,4\text{-oxadiazole})_2(H_2O)_2]^{2+}$ cation and two ClO_4^- anions (Figure 3.5a). The four crystallographically independent molecules constituting the

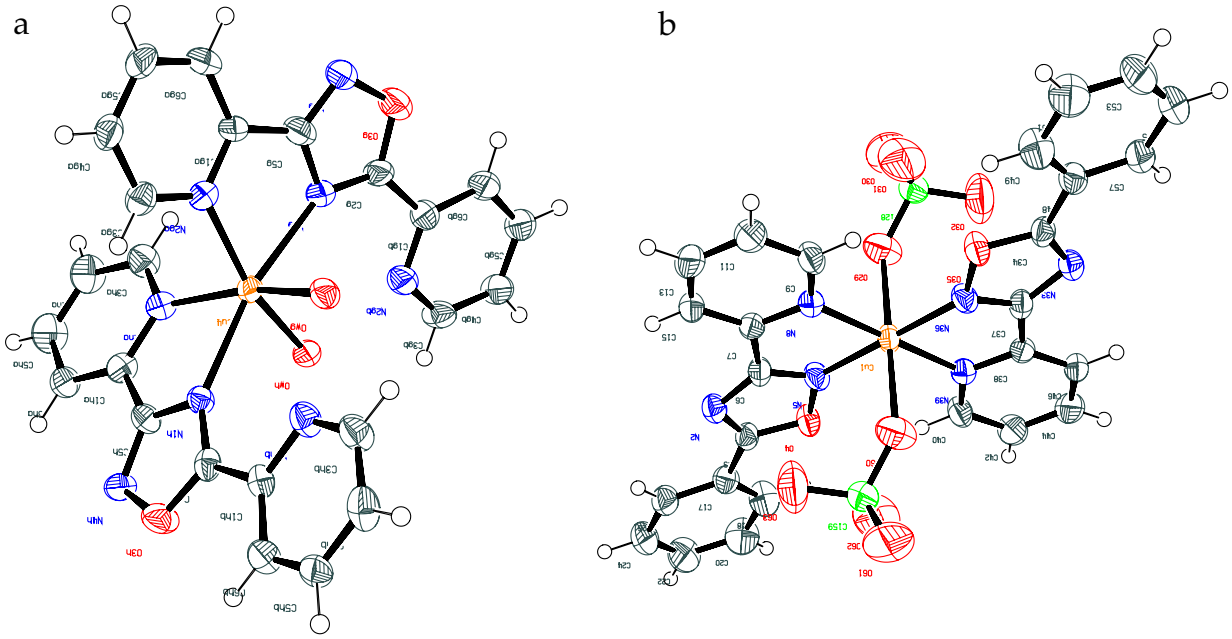

Figure 3.5: Crystal structures of the complexes (a) $[Cu(bipyOXA)_2(H_2O)_2]^{2+}$ and (b) $Cu(pyOXA)_2(ClO_4)_2$. The labelling colour scheme is as follows: hydrogen (small open circles), carbon (dark grey), nitrogen (blue), chlorine (green), copper (orange) and oxygen (red).

asymmetric unit of [Cu(3,5- bis(2'-pyridyl)-1,2,4-oxadiazole)$_2$(H_2O)$_2$]$^{2+}$ are illustrated in Figure B.3 (see Appendix B). Only few Cu^{II} complexes of 1,3,4-oxadiazole ligands have been synthesized up to now [177–179]. Their X-ray crystallographic structures show that the coordinated oxadiazoles are co-planar. Interestingly, the Cu^{II} ion of the complex $[Cu(bipyOXA)_2(H_2O)_2]^{2+}$ lies in a distorted octahedral environment, where each bipyOXA acts as bidentate ligand and the two ligands are not coplanar. Two coordinated water molecules occupy the cis positions in the equatorial plane. BipyOXA only uses two of its five potential donor atoms, acting as a typical bidentate chelator. It forms a five-membered Cu-N-C-C-N metallacycle with a N-Cu-N angle that averages 77.9(2)° in the four molecules. The equatorial Cu-N(pyridine) bond distances vary from 2.004(7) to 2.059(6) Å, and averaging 2.029(6) Å, while the axial Cu-N(oxadiazole) bond lengths range from 2.321(6) to 2.388(6) Å. The Cu-O(water) distances mean 1.987(6) Å, while the O-Cu-O angles average 91.7(3)°. The two non-coordinating ClO_4^- counter anions are involved in hydrogen bonds with the coordinated water molecules, with a O(water)-O(perchlorate) separation that averages 2.74(1) Å. The water molecules are also involved in intramolecular hydrogen bonding interactions with the uncoordinated nitrogen of one pyridine moiety thus forming a six-membered Cu-N-C-C-N-O metalla-

cycle. The two pyridine rings of bipyOXA are not coplanar with the oxadiazole ring and their orientation is forced by the coordination to Cu^{II}.

The ligand pyOXA was synthesized from benzoyl chloride and amidoxime **5** (see Figure 3.4 and Section 3.6). $[Cu(pyOXA)_2(ClO_4)_2]$ crystals, suitable for single crystal X-ray analysis, were obtained from acetonitrile. Differently from the complex with the ligand bipyOXA, $[Cu(pyOXA)_2(ClO_4)_2]$ has no coordinated water molecules (Figure 3.5b). PyOXA acts as bidentate ligand, and the two ligands are in the same plane and in *trans* disposition, with two perchlorate molecules occupying the two apical positions of the octahedral structure. This results in a neutral complex with a consistently lower water solubility compared to $[Cu(bipyOXA)_2](ClO_4)_2$. The ligand forms a five-membered Cu-N-C-C-N metallacycle with a N-Cu-N angle equal to 80.0(8)°. The Cu-N(pyridine) bond distances are equal to 2.00(8) Å, while Cu-N(oxadiazole) and Cu-O(perchlorate) bond lengths are 2.02(3) and 2.35(4) Å, respectively.

3.2.2 NMR spectroscopy

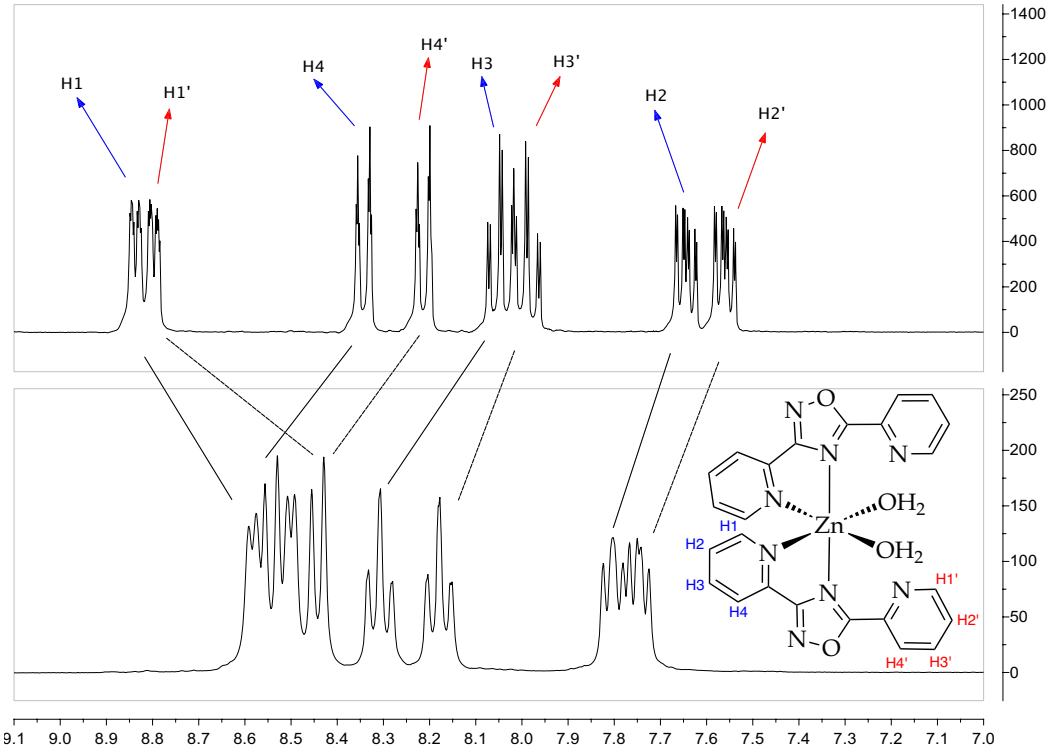

Figure 3.6: Partial ^{1}H-NMR (CD_3CN, 300 MHz) of bipyOXA (upper) and its Zn^{II} complex.

Figure 3.6 shows the comparison between the ^{1}H-NMR spectra of the ligand bipyOXA and of its Zn^{II} complex. The complexation of the ligand with the metal center can be argued by the upfield shift of the protons H1 and H1′ and the downfield shift of the remaining protons.

Analogously, the comparison between the ^{1}H-NMR spectra of the ligand pyOXA and its Zn^{II} complex is shown in Figure 3.7. It can be noticed that all the pyridine protons (H1-H4, Figure 3.7) are shifted to the left part of the spectrum (downfield shift) while the phenyl protons are slightly shifted to the right part of the spectrum (upfield shift) or remain essentially in the same position.

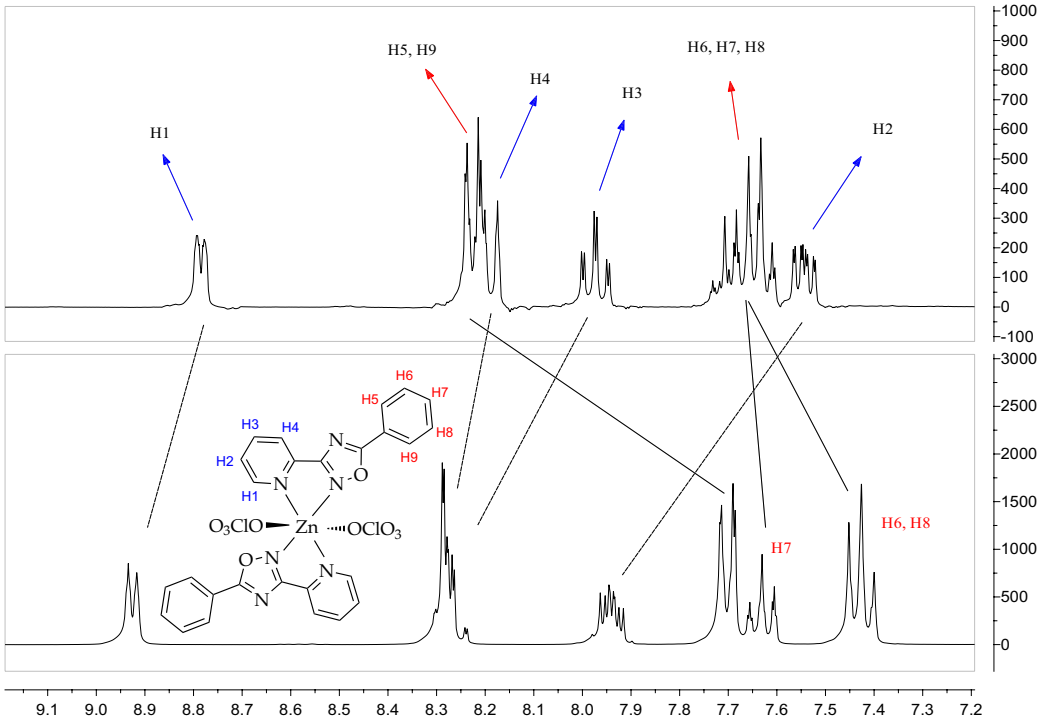

Figure 3.7: Partial ^{1}H-NMR (CD_3CN, 300 MHz) of pyOXA (upper) and its Zn^{II} complex.

Taking into account that, according to the crystal structure of its Cu^{II} complex (see Figure 3.5b), the coordinated pyOXA ligands are coplanar, the change in the chemical shift of the pyridine protons to lower fields can be attributed only to zinc coordination. In fact, a low field shift indicates that the electron density around the pyridine protons decreases. The observed chemical shift values of $[Zn(bipyOXA)_2(H_2O)_2]^{2+}$, compared to those of the isolated ligand, are more difficult to rationalize, because the two coordinated bipyOXA ligands are not coplanar, in analogy with the structure of

$[Cu(bipyOXA)_2(H_2O)_2]^{2+}$ (see Figure 3.5a). In this case, non bonding (or through space) interactions could indeed contribute to determine the observed shifts.

3.2.3 ESI Mass spectrometry

The ESI(+) mass spectrum of a methanolic solution of $[M(bipyOXA)_2](ClO_4)_2$ shows the presence of different ions attributed to $\{[M(bipyOXA)_2](ClO_4)\}^+$,$\{[M(bipyOXA)_2]-Cl\}^+$, $[M(bipyOXA)_2]^+$ and $\{[M(bipyOXA)](ClO_4)\}^+$, respectively and confirmed by the analysis of their isotopic clusters. Analogous results were obtained for methanolic solutions of $[M(pyOXA)_2](ClO_4)_2$. The data obtained suggest that, in the ionization/evaporation process, (i) the species formed in the gas phase are mainly singly positively charged ions while multiply charged species are not detectable; (ii) the two coordinated water molecules of the copper(II)-bipyOXA complex are easily lost; (iii) one perchlorate anion can be replaced by a chlorine; (iv) the copper ion undergoes a reduction process with the formation of Cu^I.

3.3 DNA interaction studies

Preliminary spectroscopic measurements indicated that the interaction between DNA and the isolated bipyOXA ligand is very weak. Furthermore, the shoulder at 340 nm in the UV-vis absorption spectrum of the Cu^{II}-bipyOXA complex was used to monitor the interaction with DNA.

However, such band is absent in Zn^{II}-bipyOXA and very weak in Ni^{II}-bipyOXA (see Figure 3.8a). As a consequence, only the interaction of DNA with $[Cu(bipyOXA)_2(H_2O)_2]^{2+}$ has been thoroughly investigated.

The pyOXA ligand and its Ni^{II}, Cu^{II} and Zn^{II} complexes are sparingly soluble in water solution, possibly as a consequence of the perchlorate coordination (see Figure 3.5b), that makes difficult to obtain a dicationic complex in solution, as observed for the bypyOXA complexes (see Figure 3.5a). In Figure 3.8b the UV-vis spectra of the ligand pyOXA and of its metal complexes in CH_3CN are reported. Here, it is even more evident the absence in all the compounds examined of a convenient band in a region where DNA does not absorb (Abs^{max}_{DNA} = 258 nm), that could be used to monitor the interaction with DNA through a spectrophotometric titration with the biologic polymer. These two conditions prevented the investigation of the interaction between DNA and the Ni^{II}, Cu^{II}

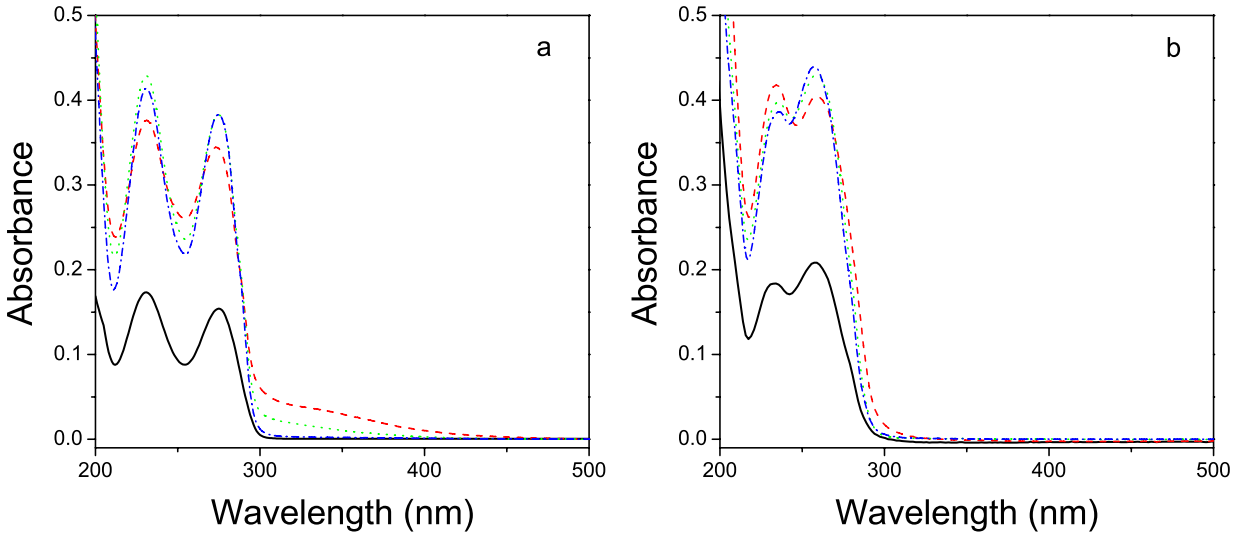

Figure 3.8: (a) Uv-vis spectra in 1 mM Tris-HCl buffer of bipyOXA (10 μM, —) and its 30 μM Cu^{II} (- - -), Ni^{II} (· · ·) and Zn^{II} (- · -) complexes; (b) Uv-vis spectra in CH_3CN of the ligand bipyOXA (10 μM, —) and its 10 μM Cu^{II} (- - -), Ni^{II} (· · ·) and Zn^{II} (- · -) complexes.

and Zn^{II} complexes of the pyOXA ligand.

3.3.1 UV-visible

$[Cu(bipyOXA)_2(H_2O)_2]^{2+}$ complex presents two strong absorption bands at 230 and 275 nm, attributable to the ligand, and a characteristic $d-d$ band at 340 nm. The absorbances at 340 and 275 nm follow the Lambert-Beer law in the concentration range 22 - 180 μM. The DNA-$[Cu(bipyOXA)_2(H_2O)_2]^{2+}$ interaction was studied by monitoring the spectral variations of the absorption band at 340 nm upon addition of increasing amounts of DNA to solutions of $[Cu(bipyOXA)_2(H_2O)_2]^{2+}$ (Figure 3.9).

The observed hypochromism (see Figure 3.9) with increasing DNA concentration, up to 47% at [DNA]/[complex] = 7.0, the absence of a red shift of the monitored band and the values of the intrinsic binding constant K_b suggests the groove binding and electrostatic binding nature of the complex to DNA in preference over an intercalative mode of binding [158, 159, 180].

The data have been analyzed by the following equation (inset in Figure 3.9):

$$\frac{[DNA]}{2(\epsilon_a - \epsilon_f)} = \frac{[DNA]}{2(\epsilon_b - \epsilon_f)} + \frac{1}{K_b(\epsilon_b - \epsilon_f)} \tag{3.1}$$

where ϵ_a is the ratio between the measured absorbance and the molar concentration of

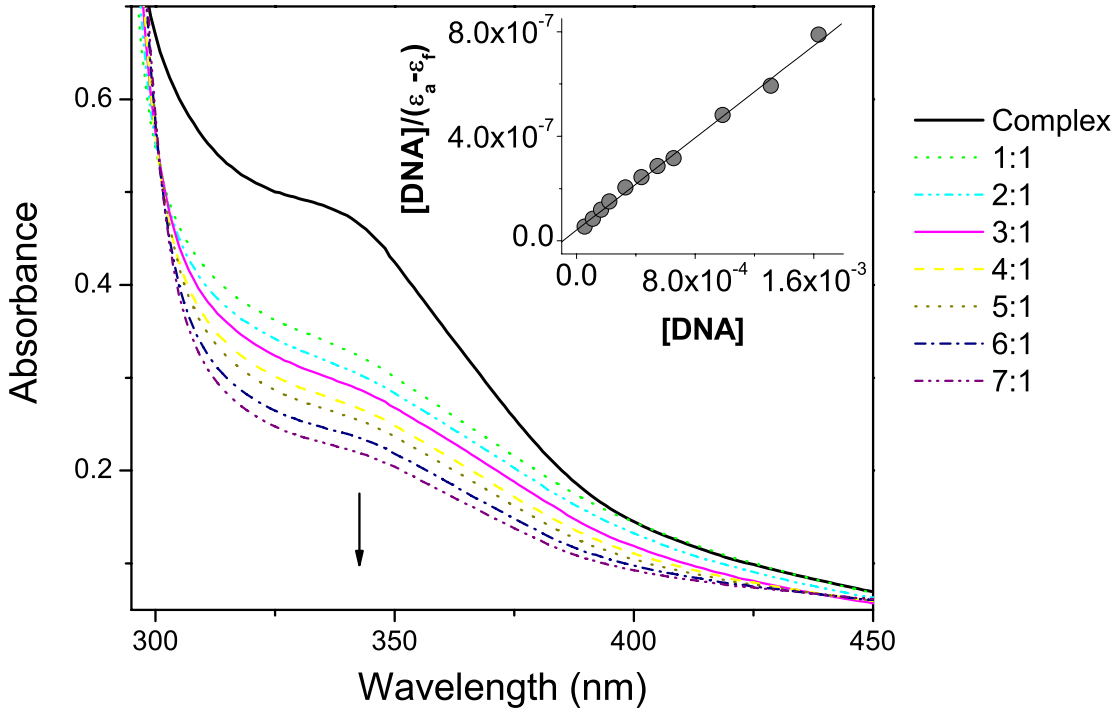

Figure 3.9: Uv-vis of the compound $[Cu(bipyOXA)_2(H_2O)_2]^{2+}$ ([complex] = 110 μM , 1 mM Tris-HCl buffer) in the presence of increasing concentration of ct-DNA, in the range [DNA]:[complex] shown in the legend. Inset: plot of $[DNA]/(\epsilon_a - \epsilon_f)$ vs. [DNA] from eqn. 3.1.

$[Cu(bipyOXA)_2(H_2O)_2]^{2+}$, ϵ_f is the molar extinction coefficient for the free metal complex and ϵ_b is the molar extinction coefficient for the metal complex bound to DNA [66, 181, 182].

Plotting $[DNA]/(\epsilon_a - \epsilon_f)$ $vs.$ [DNA], K_b is given by the ratio of slope to the intercept. The DNA-$[Cu(bipyOXA)_2(H_2O)_2]^{2+}$ binding constant K_b is equal to 2.2 $\times$ 10^4 M^{-1} and is comparable to that of DNA- groove binders [158, 159]. Indeed, the size of the cationic copper complex $[Cu(bipyOXA)_2(H_2O)_2]^{2+}$ is comparable to that of typical DNA groove binders [4]. The observed hypochromism with increasing DNA concentration, up to 47% at [DNA]:[complex] = 7.0, is also in agreement with an electrostatic groove binding nature of the complex to DNA [158, 159].

3.3.2 DNA Thermal Denaturation Analysis

The thermal denaturation profiles of native DNA in the presence of increasing amounts of $[Cu(bipyOXA)_2(H_2O)_2]^{2+}$, obtained by plotting the UV absorbance at 258 nm as a function of temperature, are reported in Figure 3.10.

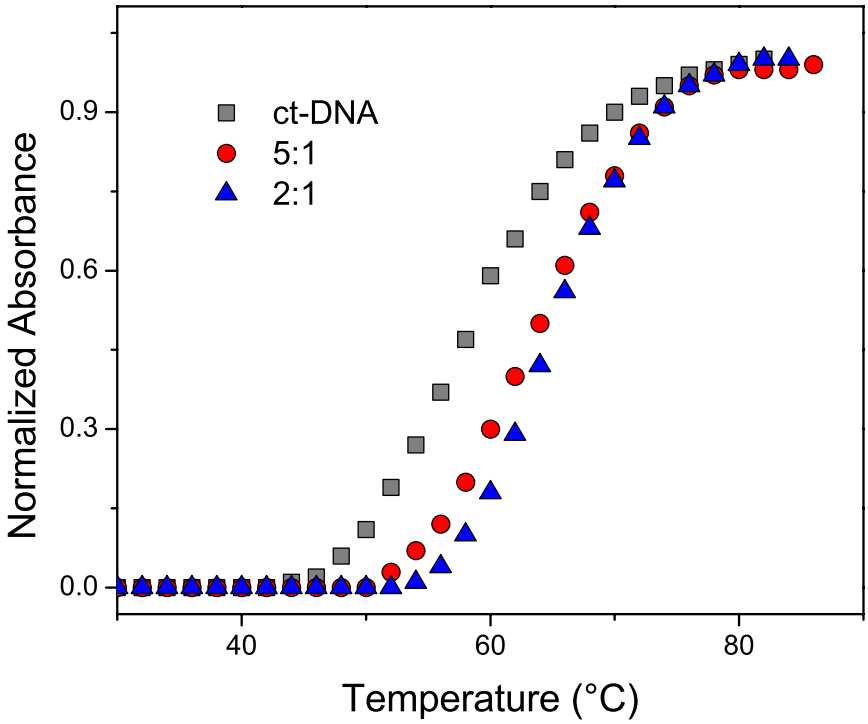

Figure 3.10: Thermal denaturation profiles of ct-DNA solutions (100 μM ct-DNA, 1.0 mM Tris-HCl) in the presence of increasing amounts of $[Cu(bipyOXA)_2(H_2O)_2]^{2+}$, in the range [DNA]:[complex] shown in the legend. ct-DNA, T_m= 58.5 $\pm$ 0.1; 5:1 T_m= 64.0 $\pm$ 0.1; 2:1, T_m= 65.3 $\pm$ 0.1 °C.

At [DNA]:[complex] molar ratios 5:1 and 2:1, the DNA melting temperature increases of 5.5 and 6.5 °C, respectively, confirming that the double helical structure is only slightly perturbed by the interaction with the complex. Considering that intercalative mode of binding to DNA normally gives significantly high positive ΔT_m values [183], these results suggest electrostatic and/or groove binding nature of the $[Cu(bipyOXA)_2(H_2O)_2]^{2+}$ complex, a result in agreement with the UV-vis titration (see Figure 3.9).

3.3.3 Circular Dichroism

The CD spectrum of B-DNA is characterized by a positive band centered at 275 nm, a negative band at 240 nm (black solid line in Figures 3.11a). Figure 3.11 shows that these bands are only weakly modified by the addition of increasing amounts of the complex $[Cu(bipyOXA)_2(H_2O)_2]^{2+}$, showing that the double helical structure is only slightly perturbed by the interaction with the metal complex. Nevertheless, the presence of an induced CD band in the range 300-375 nm (i.e around the UV absorption band

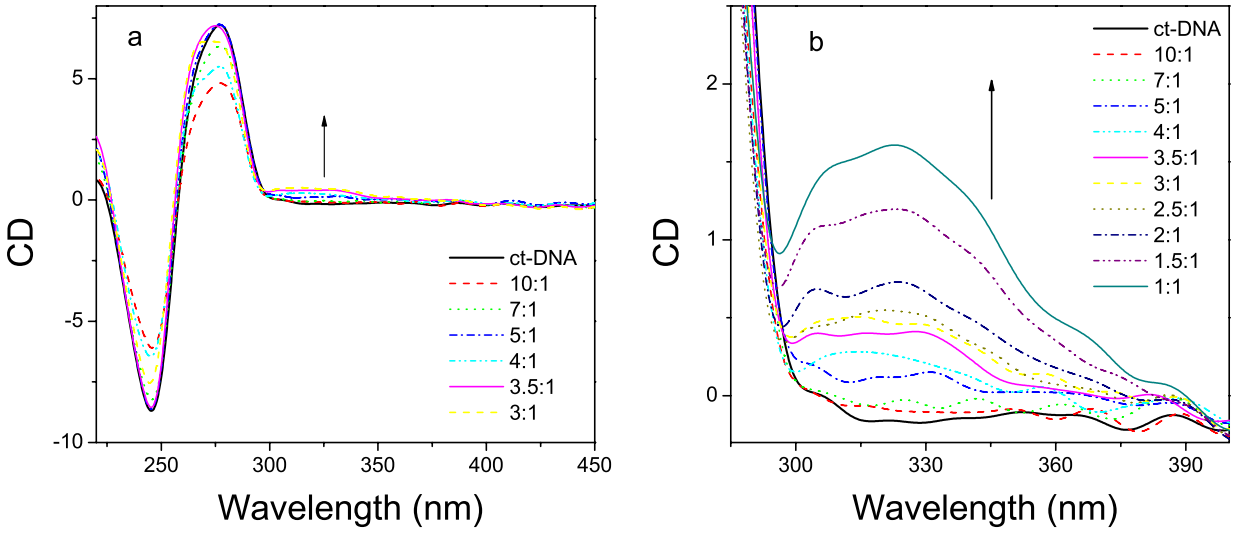

Figure 3.11: CD of 100 μM ct-DNA (1 mM Tris-HCl buffer) in the presence of increasing concentration of the complex $[Cu(bipyOXA)_2(H_2O)_2]^{2+}$, in the range [DNA]:[complex] shown in the legend.

of the metal complex, see Figure 3.9) points out that $[Cu(bipyOXA)_2(H_2O)_2]^{2+}$ tightly binds to the chiral scaffold of the DNA double helix, acting as a new CD chromophore.

Such evidence, in agreement with the value of the binding constant obtained by the spectrophotometric titration shown in Figure 3.9, can be interpreted by hypothesizing the existence of an electrostatic binding between the cationic metal complex and the negatively charged phosphate groups of DNA, in which $[Cu(bipyOXA)_2(H_2O)_2]^{2+}$ is a groove binder.

3.3.4 Gel electrophoresis

The characteristic agarose gel pattern of plasmid DNA consists generally in two bands, one intense corresponding to the negatively-supercoiled DNA and another one to the open-circle DNA.

Figure 3.12 shows the agarose gel electrophoresis pattern of pBR322 DNA (lane 1) treated with $[Cu(bipyOXA)_2(H_2O)_2]^{2+}$ at [DNA]:[complex] molar ratios equal to 2:1 and 1:1 (lane 2 and 3, respectively). The results obtained allowed to establish that, in the experimental conditions used, $[Cu(bipyOXA)_2(H_2O)_2]^{2+}$ does not degrade the DNA or even affect its mobility.

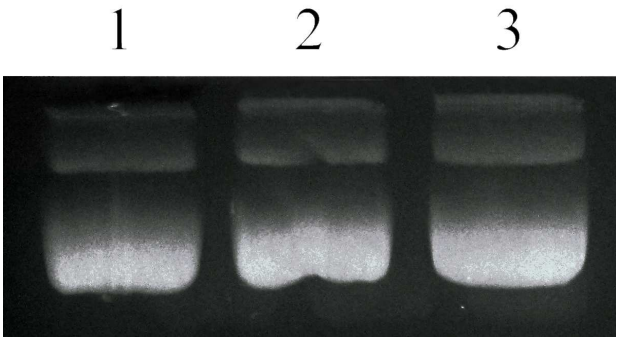

Figure 3.12: Agarose gel electrophoresis pattern of pBR322 DNA (lane 1) in the presence of $[Cu(bipyOXA)_2(H_2O)_2]^{2+}$ at different [DNA]:[complex] ratios: lane 2, 2:1; lane 3, 1:1

3.3.5 Viscosity

It is known that molecules that are able to intercalate DNA induce an unwinding of the duplex supercoils, giving rise to an increase of DNA viscosity and a decrease of the density of DNA, thus a decrease in the rate of migration through agarose gel [80, 184].

DNA viscosity experiments in the presence of $[Cu(bipyOXA)_2(H_2O)_2]^{2+}$ confirm the absence of DNA-intercalation and reinforce the conclusion that it is a groove binder. In fact, the relative viscosity of 100 μM DNA in Tris-HCl 1 mM, is not affected by the presence of the complex, at the molar ratio values [DNA]:[complex] equal to 2:1, 1.25:1 and 1:1. The average value of relative viscosity, $(\eta/\eta^0)^{1/3}$, where η^0 is the viscosity of the DNA solution alone, was 0.999 ± 0.001.

3.4 Cytotoxic Tests

The cytotoxicity of $[Cu(bipyOXA)_2(H_2O)_2]^{2+}$ and of bipyOXA, as control, on HepG2 and HT29 cells was evaluated by means of MTT cell viability/proliferation assay, as reported in Materials and Methods (see Section 3.6). While bipyOXA was not cytotoxic, inhibition of cell proliferation by the copper complex $[Cu(bipyOXA)_2(H_2O)_2]^{2+}$ was already evident (10%) at 8 h of treatment at 5 μM concentration and reached its maximum (85-90%) at 48 h of treatment at 40 μM concentration. The cytotoxicity was similar on both the cell lines as confirmed by the concentrations that kill and/or inhibit cell growth by 50% (IC_{50}) calculated at 24 h of treatment (Figure 3.13a).

Trypan blue was used to count viable cells with comparable results to those obtained by MTT test. Dramatic cell morphological changes were observed by light microscopy.

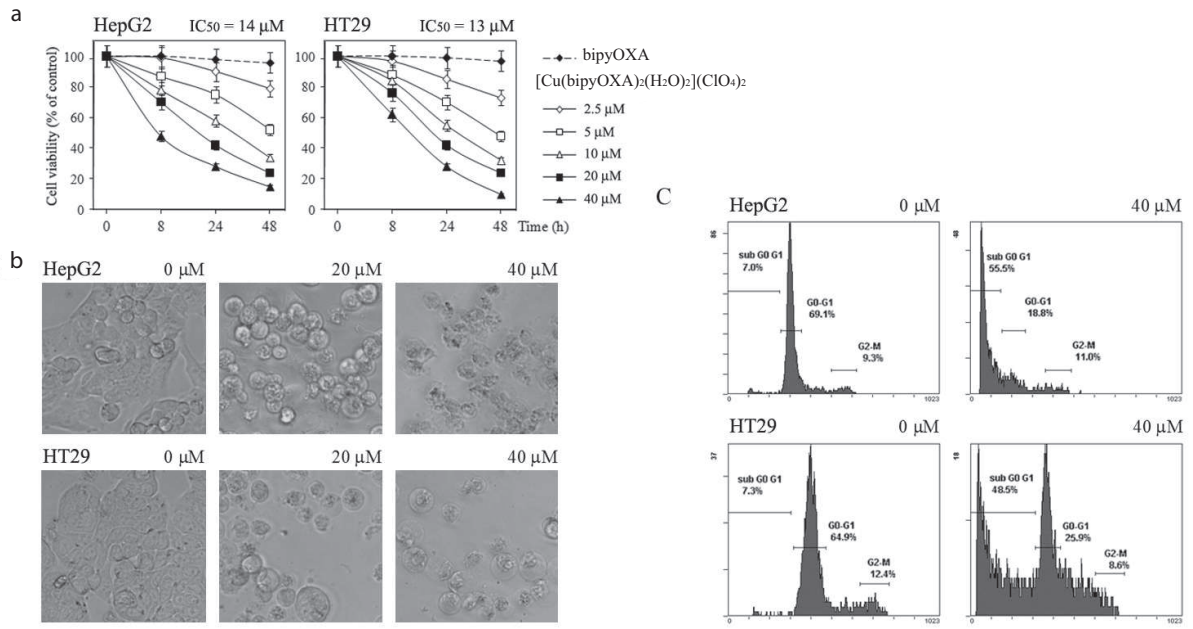

Figure 3.13: (a) Concentration- and time-dependent effect of bipyOXA and $[Cu(bipyOXA)_2(H_2O)_2]^{2+}$ on HepG2 and HT29 cell viability. (b) Cell morphological analysis at 24 h of treatment (magnification 40X). (C) Flow cytometric analysis of cell cycle distribution at 24 h of treatment.

Cells became rounded, detached from culture substrates and floated in the medium, indicating the commitment to apoptotic death (Figure 3.13b). This conclusion is also supported by flow cytometric analysis. Cytometric profiles of the propidium iodide-stained DNA showed that treatment of HepG2 and HT29 cells for 24 h with 40 μM of the copper complex $[Cu(bipyOXA)_2(H_2O)_2]^{2+}$ resulted in DNA fragmentation for a significant amount of cells, 55.5 and 48.5% respectively, confined in the sub-G0/G1 phase of cell cycle (Figure 3.13C). This result was considered as an index of apoptosis.

3.5 Conclusions

The novel copper complexes $[M(bipyOXA)_2(H_2O)_2]ClO_4)_2$ and $[M(pyOXA)_2ClO_4)_2]$ (M = Cu^{II}, Zn^{II} and Ni^{II}), were synthesized and structurally characterized in the solid state and in solution. The study of the interaction of $[Cu(bipyOXA)_2(H_2O)](ClO_4)_2$ with native DNA , through circular dichroism, variable temperature UV-visible absorption, gel electrophoresis and viscosity, was reported.

Cellular uptake experiments showed that, despite the inactivity of bipyOXA ligand,

its Cu^{II} complex reduces the vitality of human hepatoblastoma and colorectal carcinoma cells lines, in a dose- and time-dependent manner. The results of the biological assays receive a positive feedback in the DNA binding studies performed. The spectroscopic and hydrodynamic investigations showed that the copper(II) complex has the characteristics of a DNA groove binder, displaying good affinity while preserving the native B-DNA form.

This work represents the first study of the biological activity of a copper(II) complex of 1,2,4-oxadiazole ligands. Infact, despite the bioactivity of analogous platinum complexes, so far only a few metal complexes of 1,2,4-oxadiazole ligands have been considered for biological studies.

3.6 Experimental

3.6.1 Materials and Method

All chemicals and solvents were purchased from Sigma–Aldrich, Fisher or Alfa Aesar and used as received, without further purification.

Proton and carbon nuclear magnetic resonance spectra were recorded on Bruker AC300 spectrometer, solvent residual peaks were used as reference. Flash chromatography was performed by using silica gel (Merck, 0.040-0.063 mm) and mixtures of ethyl acetate and petroleum ether (fraction boiling in the range of 40-60 °C) in various ratios.

Mass spectrometry (MS) and MS/MS measurements of the complexes have been carried out by using electrospray ionization (ESI) with a LCQ-DECA ion trap (Thermo, Bremen, Germany). Operating conditions of the ESI source were as follows: spray voltage 4.5 kV; capillary temperature 200 °C; sheath gas (nitrogen) flow rate, $ca.$ 0.75 L min^{-1}. Ultra-pure helium was the collision gas. CID collision energy: 0.5-1.0 eV (laboratory frame). A methanol solution of the complex (1×10^{-4} M) was introduced into the mass spectrometer using a syringe pump at a flow rate of 5 μL min^{-1}.

Melting points were determined on a Reichart-Thermovar hot stage apparatus and are uncorrected. IR spectra were registered with a Shimadzu FTIR-8300 instrument.

Viscosity measurements were performed on a Ubbelodhe viscosimeter maintained at 25.0 ± 0.1 °C. Flow time was measured with a digital stopwatch.

Ultrapure water (18.2 MΩ, Fisher) was used in all UV-vis, circular and linear dichro-

ism experiments and for electrophoresis gel. Lyophilized calf thymus DNA, purchased from Sigma-Aldrich, was resuspended in Tris-HCl (pH 7.5) and dialyzed as described in the literature [144]. The DNA concentration was determined by UV-vis measurements using the molar extinction coefficient of ϵ_{260} = 7000 mol^{-1} dm^3 cm^{-1} per DNA base [135–138].

Spectroscopic studies

Absorption measurements were performed on a Varian Cary 5000 UV-vis double beam spectrophotometer or on a Varian UV–vis Cary 1E double beam spectrophotometer, both equipped with a Peltier temperature controller, using 1 cm pathlength cuvettes.

Circular dichroism spectra were recorded at 25 °C on a Jasco J-715 spectropolarimeter, using 1 cm path–length quartz cells.

X-ray crystallography

A Bruker-Nonius FR591 rotating anode diffractometer with graphite monochromated Mo-Ka radiation (λ = 0.71073 Å) was used for data collection at 120(2) K. The structure was solved by direct methods implemented in the SHELXS-97 program. The refinement was carried out by full-matrix anisotropic least-squares on F2 for all reflections for non-H atoms by using the SHELXL- 97 program [148,149].

The complex $[Cu(bipyOXA)_2(H_2O)_2]ClO_4)_2$ crystallizes in the triclinic crystal system, and in the $P\bar{1}$ space group. Four molecules constitute the asymmetric unit. A statistical disorder has been found for the N(1) and O(2) atoms of each oxadiazole ring and for a perchlorate anion.

Gel electrophoresis

Gel electrophoresis experiments of pBR322 DNA (0.5 mg mL^{-1}, Fermentas) were performed in a 2% agarose gel, through an electrophoresis system with the following parameters: voltage, 100 V; electric current, 250 mA; time, 1.5 h. TAE buffer 1X (obtained by dilution of 50X TAE, pH 8.0, SIGMA) was used as working buffer. In detail, 17 mL volume samples loaded in the gel contained a fixed concentration of pBR322 DNA (0.06 μg mL^{-1}) and increasing concentration of $[Cu(bipyOXA)_2(H_2O)_2]ClO_4)_2$. Once incubated for 1.5 h at 37 °C, to each sample 5 mL of loading buffer (Blue/Orange Loading Dye, 6X, 0.4% orange G, 0.03% bromophenol blue, 0.03% xylene cyanol FF, 15% Ficoll

400, 10 mM Tris-HCl, pH 7.5 and 50 mM EDTA, pH 8.0, Promega Madison USA) were added. The gel was revealed with ethidium bromide (0.5 μg mL^{-1}) and was finally visualized using a UV lamp.

Cytotoxic Test

Human hepatoblastoma HepG2 and colorectal carcinoma HT29 cells were grown as monolayers in RPMI 1640 medium, supplemented with 10% (v/v) heat-inactivated fetal calf serum (FCS) and 2.0 mM glutamine, in a humidified atmosphere of 95% air and 5% CO_2 at 37 °C. HepG2 culture medium also contained 1.0 mM sodium pyruvate.

HepG2 and HT29 cells (1×10^4) were grown in 200 μL medium in 96-well plate overnight. The cells were treated with $[Cu(bipyOXA)_2(H_2O)_2]^{2+}$ (2.5-40 μM) or with bipyOXA (40 μM), dissolved in 1 mM Tris-HCl buffer pH 7.4, for 8, 24 and 48 h. The cytotoxic effect was determined by MTT cell viability/proliferation test. Control samples were treated with vehicle only. MTT data (average of four independent experiments in triplicate) are expressed as percent of untreated control cells [185]. IC_{50} values were calculated at 24 h of treatment. Morphological changes were observed by means of light microscopy (magnification 40X). Colorimetric quantification was determined by an ELISA microplate reader at 570 nm (test WL) and 630 nm (reference WL), using lysis buffer as a blank. After treatment, cells (1×10^6) were harvested by trypsinization and incubated for 2-3 h at 4 °C in a hypotonic solution containing 50 μg mL^{-1} propidium iodide, 0.1% sodium citrate, 0.01% Nonidet P-40 and 10 μg mL^{-1} RNase A. After staining, cells were subjected to flow cytometric analysis of DNA content using a Beckman Coulter Epics XL cytometer. The percentage of cells in the different phases of the cycle was calculated using Expo32 software. Cell debris and aggregates were excluded by opportune gating and 5000 events/sample were analyzed.

3.6.2 Synthesis and characterization

bipyOXA ligand and its Cu^{II}, Zn^{II} and Ni^{II} complexes

3,5-bis(2'-pyridyl)-1,2,4-oxadiazole (bipyOXA): 1.00 g of 2-cyanopyridine (**4**) (8.14 mmol) and 0.56 g of 2- picolinamidoxime (**5**) [186] (4.07 mmol) were mixed in a sealed tube and heated at 120 °C for 8 h. The residue was chromatographed yielding 0.59 g of 3,5-bis(2'-pyridyl)-1,2,4-oxadiazole (65%): mp 173-176 °C (from EtOH) (lit. 173-175 °C) [187] ; ^{1}H NMR (300 MHz, $CDCl_3$) δ (ppm): 7.44 - 7.58 (m, 2H); 7.87 - 7.98 (m, 2H); 8.28 - 8.31

(d, 1H); 8.42 - 8.44 (d, 1H); 8.84 - 8.89 (m, 2H).
^{1}H NMR (300 MHz, CD_3CN) δ (ppm): 8.96 - 8.70 (m, 2H), 8.34 (dt, J = 7.9, 1.0 Hz, 1H), 8.21 (dt, J = 7.9, 1.1 Hz, 1H), 8.13 - 7.91 (dtd, J = 17.3, 7.8, 1.8 Hz, 2H), 7.64 (ddd, J = 7.7, 4.8, 1.2 Hz, 1H), 7.56 (ddd, J = 7.7, 4.8, 1.2 Hz, 1H).
^{13}C NMR (75 MHz, CD_3CN) δ (ppm): 176.1 (C), 170.0 (C), 151.5 (CH), 151.3 (CH), 147.3 (C), 144.5 (C), 138.7 (CH), 138.4 (CH), 128.1 (CH), 126.9 (CH), 125.3 (CH), 124.4 (CH).
UV (MeOH): $\epsilon = 1.7 \times 10^4$ (λ = 274 nm); $\epsilon = 1.5 \times 10^4$ (λ = 231 nm) $cm^{-1}M^{-1}$. UV (Tris-HCl, pH = 7.5): 1.5×10^4 (λ = 275 nm); $\epsilon = 1.7 \times 10^4$ (λ = 231 nm) $cm^{-1}M^{-1}$
[Cu(bipyOXA)$_2$(H$_2$O)$_2$]$^{2+}$(ClO$_4$)$_2$: A light blue solution of $Cu(ClO_4)_2 \cdot 6H_2O$ (0.09 g, 0.24 mmol) in absolute ethanol was added drop wise and under constant stirring to a colorless solution of 3,5-bis(2'-pyridyl)-1,2,4-oxadiazole (0.11 g, 0.50 mmol) in absolute ethanol and at room temperature. The mixture was let under stirring for 12 h, the precipitate filtered, washed with cold absolute ethanol and dried under vacuum (0.152 g; 85%). The solid was recrystallized from acetonitrile. After one week at 4 °C, blue crystals of $[Cu(bipyOXA)_2](ClO_4)_2 \cdot 2H_2O$, suitable for X-ray crystallographic analysis, were obtained.
MS-ESI (m/z): 609.73 ($[Cu(bipyOXA)_2]ClO_4^+$).
Elemental analysis calcd (%) for $CuC_{24}H_{20}N_8O_{12}Cl_2$: C, 38.59, H, 2.70, N, 15.00; found: C, 38.51, H, 2.69, N, 15.13. UV (Tris-HCl 1mM, pH = 7.5): $\epsilon = 4.2 \times 10^3$ (λ = 340 nm); $\epsilon = 3.3 \times 10^4$ (λ = 273 nm); $\epsilon = 3.8 \times 10^4$ (λ = 231 nm) $cm^{-1}M^{-1}$
IR (Nujol) ν (cm^{-1}) :1651 m, 1616 m, 1560 s, 1257 m, 1116 s, 1047 s, 1009 m, 923w, 807w, 756m, 624s.
[Zn(bipyOXA)$_2$(H$_2$O)$_2$]$^{2+}$(ClO$_4$)$_2$: A solution of $Zn(ClO_4)_2 \cdot 6H_2O$ (0.14 g, 0.4 mmol) in absolute ethanol was added dropwise and under constant stirring to a colorless solution of 3,5-bis(2'-pyridyl)-1,2,4-oxadiazole (0.179 g, 0.8 mmol) in absolute ethanol and at room temperature. The mixture was let under stirring for 12 h in the dark, the white precipitate filtered, washed with cold absolute ethanol and dried under vacuum (0.215 g; 72%). The solid was recrystallized from acetonitrile.
MS-ESI (m/z): 610.87 ($[Zn(bipyOXA)_2]ClO_4^+$); 386.93 ($[Zn(bipyOXA)]ClO_4^+$).
Elemental analysis calcd (%) for $ZnC_{24}H_{20}N_8O_{12}Cl_2$: C, 38.50, H, 2.69, N, 14.97; found: C, 38.31, H, 2.63, N, 15.06. UV (Tris-HCl 1mM, pH = 7.5): $\epsilon = 3.9 \times 10^4$ (λ = 273 nm); $\epsilon = 4.2 \times 10^4$ (λ = 231 nm) $cm^{-1}M^{-1}$
^{1}H NMR (300 MHz, CD_3CN) δ (ppm): 8.69 - 8.37 (m, 4H), 8.31 (t, J = 7.8 Hz, 1H), 8.18 (t, J = 7.8 Hz, 1H), 7.89 - 7.68 (m, 2H).

^{13}C NMR (75 MHz, CD_3CN) δ (ppm): 176.3 (C), 166.5 (C), 150.9 (CH), 150.0 (CH), 142.5 (CH), 142.1 (C), 140.8 (C), 140.6 (CH), 130.3 (CH), 130.0 (CH), 127.2 (CH), 125.1 (CH).
$[Ni(bipyOXA)_2(H_2O)_2]^{2+}(ClO_4)_2$: A light green solution of $Ni(ClO_4)_2 \cdot 6H_2O$ (0.15 g, 0.4 mmol) in absolute ethanol was added drop wise and under constant stirring to a colorless solution of 3,5-bis(2'-pyridyl)-1,2,4-oxadiazole (0.179 g, 0.80 mmol) in absolute ethanol and at room temperature. The mixture was let under stirring for 12 h in the dark, the precipitate filtered, washed with cold absolute ethanol and dried under vacuum (0.244 g; 83%). The solid was recrystallized from acetonitrile.
MS-ESI (m/z): 604.93 ($[Ni(bipyOXA)_2]ClO_4^+$); 380.9 ($[Ni(bipyOXA)]ClO_4^+$).
Elemental analysis calcd (%) for $NiC_{24}H_{20}N_8O_{12}Cl_2$: C, 38.85, H, 2.72, N, 15.10; found: C, 38.67, H, 2.68, N, 15.07. UV (Tris-HCl 1mM, pH = 7.5): $\epsilon = 1.0 \times 10^3$ (λ = 340 nm); $\epsilon = 3.9 \times 10^4$ (λ = 275 nm); $\epsilon = 4.4 \times 10^4$ (λ = 231 nm) $cm^{-1}M^{-1}$

pyOXA ligand and its Cu^{II}, Zn^{II} and Ni^{II} complexes

3-(2'-pyridyl)5-(phenyl)-1,2,4-oxadiazole (pyOXA): 1 g of 2- picolinamidoxime (**5**) [186] (7.3 mmol) and 1.12 g of benzoyl chloride (**9**, 8.03 mmol, d=1.2 g/mL) were mixed in 120 mL of toluene. 0.64 mL of pyridine (0.63 g, 8.03 mmol, d=0.98 g/mL) was added and the mixture was left refluxing for 12 h. The residue was chromatographed yielding 0.60 g of 3-(2'-pyridyl)5-(phenyl)-1,2,4-oxadiazole (70%) [188].
^{1}H NMR (300 MHz, CD_3CN) δ (ppm): 8.77 (dd, J = 11.8, 7.8 Hz, 1H), 8.30 - 8.15 (m, 3H), 8.04 - 7.91 (m, 1H), 7.76 - 7.59 (m, 3H), 7.59 - 7.49 (m, 1H).
^{13}C NMR (75 MHz, CD_3CN) δ (ppm): 177.1 (C), 169.8 (C), 151.3 (CH), 147.4 (C), 138.3 (CH), 134.1 (CH), 130.4 (CH), 128.9 (CH), 126.8 (CH), 125.1 (C), 124.3 (CH).
UV (CH_3CN): $\epsilon = 2.1 \times 10^4$ (λ = 259 nm); $\epsilon = 1.8 \times 10^4$ (λ = 234 nm) $cm^{-1}M^{-1}$.
$Cu(pyOXA)_2(ClO_4)_2$: a light blue solution of $Cu(ClO_4)_2 \cdot 6H_2O$ (0.15 g, 0.4 mmol) in absolute ethanol was added drop wise and under constant stirring to a colorless solution of pyOXA (0.178 g, 0.8 mmol) in absolute ethanol and at room temperature. The mixture was let under stirring for 12 h, the precipitate filtered, washed with cold absolute ethanol and dried under vacuum (0.230 g; 81%). The solid was recrystallized from acetonitrile. After one week at 4 °C, blue crystals of $Cu(pyOXA)_2(ClO_4)_2$ suitable for X-ray crystallographic analysis, were obtained.
MS-ESI (m/z): 607.8 ($[Cu(pyOXA)_2ClO_4]^+$); 385 ($[Cu(pyOXA)ClO_4]^+$).
Elemental analysis calcd (%) for $CuC_{26}H_{18}N_6O_{10}Cl_2$: C, 44.05, H, 2.56, N, 11.85; found:

C, 44.19, H, 2.35, N, 11.83. UV (CH_3CN): ϵ = 4.0 $\times$ 10^4 (λ = 259 nm); ϵ = 4.2 $\times$ 10^4 (λ = 234 nm) $cm^{-1}M^{-1}$.

Zn(pyOXA)$_2$(ClO$_4$)$_2$: a solution of $Zn(ClO_4)_2 \cdot 6H_2O$ (0.149 g, 0.4 mmol) in absolute ethanol was added drop wise and under constant stirring to a colorless solution of pyOXA (0.179 g, 0.8 mmol) in absolute ethanol and at room temperature. The mixture was let under stirring for 12 h in the dark but no precipitate was observed. The solution was let for 6 h at -18 °C the precipitate was filtered, washed with cold absolute ethanol and dried under vacuum (0.20 g; 70%). The solid was recrystallized from acetonitrile.

MS-ESI (m/z): 608.87 ($[Zn(pyOXA)_2ClO_4]^+$); 386.13 ($[Zn(pyOXA)ClO_4]^+$).

Elemental analysis calcd (%) for $ZnC_{26}H_{18}N_6O_{10}Cl_2$: C, 43.94, H, 2.55, N, 11.82; found: C, 42.48, H, 2.32, N, 11.37. UV (CH_3CN): ϵ = 4.4 $\times$ 10^4 (λ = 259 nm); ϵ = 3.9 $\times$ 10^4 (λ = 236 nm) $cm^{-1}M^{-1}$.

^{1}H NMR (300 MHz, CD_3CN) δ (ppm): 9.02 (d, J = 5.23 Hz, 1H), 8.47 - 8.25 (dd, J = 4.46, 8.32 Hz, 2H), 8.14 - 7.93 (dd, J = 4.91, 9.41 Hz, 1H), 7.88 - 7.60 (m, 3H), 7.49 (t, J = 7.80, 7.80 Hz, 2H).

^{13}C NMR (75 MHz, CD_3CN) δ (ppm): 178.7 (C), 165.3 (C), 150.2 (CH), 143.3 (CH), 141.6 (C), 135.1 (CH), 130.3 (CH), 130.1 (CH), 129.5 (CH), 124.8 (CH), 121.2 (C).

Ni(pyOXA)$_2$(ClO$_4$)$_2$: A light green solution of $Ni(ClO_4)_2 \cdot 6H_2O$ (0.15 g, 0.4 mmol) in absolute ethanol was added drop wise and under constant stirring to a colorless solution of pyOXA (0.179 g, 0.80 mmol) in absolute ethanol and at room temperature. The mixture was let under stirring for 12 h in the dark but no precipitate was observed. The solution was let for 6 h at -18 °C the precipitate was filtered, washed with cold absolute ethanol and dried under vacuum (0.210 g; 75%). The solid was recrystallized from acetonitrile.

MS-ESI (m/z): 602.9 ($[Ni(pyOXA)_2ClO_4]^+$); 379.9 ($[Ni(pyOXA)ClO_4]^+$).

Elemental analysis calcd (%) for $NiC_{26}H_{18}N_6O_{10}Cl_2$: C, 44.35, H, 2.58, N, 11.94; found: C, 44.05, H, 3.04, N, 11.22. UV (CH_3CN): ϵ = 4.3 $\times$ 10^4 (λ = 259 nm); ϵ = 4.0 $\times$ 10^4 (λ = 236 nm) $cm^{-1}M^{-1}$.

Chapter 4

The interaction of DNA with a dinuclear Pt^{II} diazapyrenium metallacycle

Contents

> Words are flying out like endless rain into a paper cup, they slither while they pass, they slip away across the universe
>
> Lennon/McCartney, 1969

4.1 Introduction

Deoxyribonucleic acid is the biomolecule that preserves the genetic information of most organisms and, for this reason, was identified as one of the principal targets for anticancer compounds. Synthetic molecules able to bind DNA have attracted a great interest in the last 50 years. The research was mostly focused on non-covalent recognition of DNA by small molecules, with particular emphasis for the intercalation mechanism [2] (see Introduction, Section 1.2). In recent years, the synthesis of metallo-supramolecular assemblies has prompted the research of alternative systems with a different chemical nature and different effects on the biologic polymer. For example, tetracationic supramolecular cylinders, which bind strongly and non-covalently in the major groove, cause remarkable intramolecular coiling of DNA [2,78,189].

Furthermore and more interestingly, these kind of molecules are able to recognize

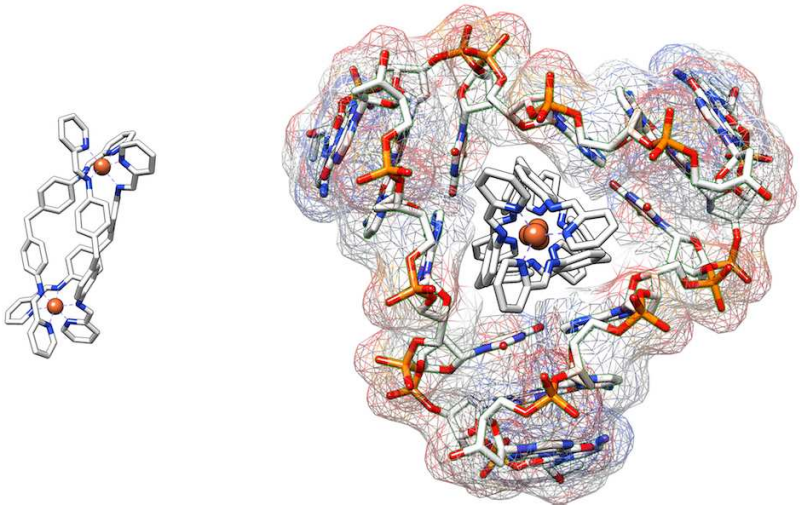

Figure 4.1: Three-dimensional structure of a tetracationic supramolecular cylinder inserted in a 3-way junction DNA [40]

a specific unusual DNA structure called three-way junction (see Figure 4.1), opening the possibility to overcome drug-resistance problems encountered with classical and nonspecific drugs with broad cytotoxic effects [40]. In this context, the self-assembly-

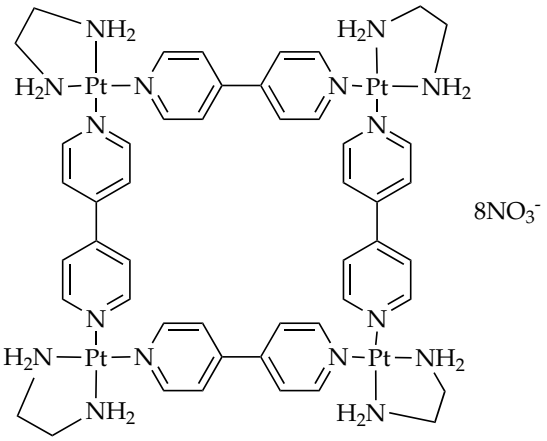

Figure 4.2: Fujita's platinum square

mediated synthesis of metallamacrocycles, such as molecular squares and rectangles, is a growing area at the forefront of supramolecular chemistry [190–195]. In particular, the combination of pyridyl ligands with Pd^{II} or Pt^{II} complexes has become a powerful tool to synthesize 2d and 3d suprastructures [190, 193, 196, 197]. These architectures display interesting applications in various fields, especially as host-guest chemistry [190, 198].

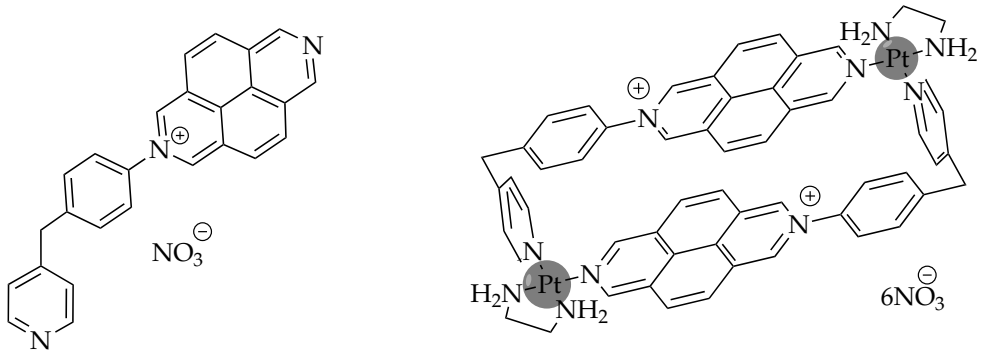

[DAzP]NO_3 $[Pt_2(DAzP)_2(en)_2](NO_3)_6$

Figure 4.3: Structure of [DAzP]NO_3 and $[Pt_2(DAzP)_2(en)_2](NO_3)_6$.

Recently, the self-assembled platinum molecular square extensively explored by the group of Fujita (see Figure 4.2) was found to bind ct-DNA, G-quadruplex DNA and to

inhibit telomerase [198–200]. Apart from the above mentioned studies, up to now, no DNA binding studies and cytotoxic tests are reported for this kind of molecules.

Prompted by these considerations, the DNA binding properties and the cytotoxicity of 2,7-diazapyrenium- based ligand and its Pt^{II} metallacycle (compounds $[DAzP]NO_3$ and $[Pt_2(DAzP)_2(en)_2](NO_3)_6$ respectively, see Figure 4.3) were investigated.

4.2 Structural characterization

The aromatic nucleophilic substitution of 4-chloro-1,3-dinitrobenzene with 2,7-diazapyrene produced the activated intermediate N-(2,4-dinitrophenyl)-2,7-diazapyrenium salt (**13** in the Figure 4.4, see Section 4.6).

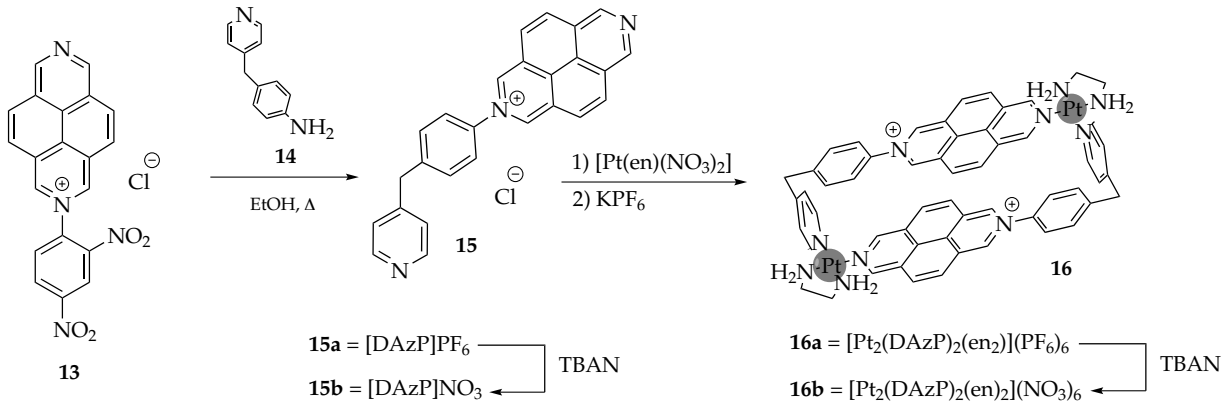

Figure 4.4: Reaction scheme for $[DAzP]NO_3$ and $[Pt_2(DAzP)_2(en)_2](NO_3)_6$ (see text for details).

For the preparation of $[DAzP]NO_3$ the Zincke reaction was used [201] being, up to now, the first example of this kind of reaction with a 2,7-diazapyrene derivative. The exchange of the 2,4-dinitroaniline moiety **13** by 4-(pyridin-4-ylmethyl)aniline (**14**) gave $[DAzP]PF_6$. This last step takes presumably advantage of an addition of the nucleophile, ring opening and ring closing (ANRORC) mechanism. The nitrate salt was prepared by metathesis of $[DAzP]PF_6$ with tetrabutylammonium nitrate (TBAN). $[DAzP]PF_6$ was characterized by ESI-HRMS mass spectrometry and 2D-NMR, including COSY, HSQC and HMBC spectra (see Experimental, Section 2.5 and Appendix A). The same NMR measurements were performed for $[DAzP]NO_3$.

The metallacycle was synthetized by the reaction of $[DAzP]NO_3$ with $Pt(en)(NO_3)_2$ in H_2O for 8 days at 100 °C. The Pt-N coordination bond inertness at low temperature is lost when the temperature is increased. This dual feature has been exploited by

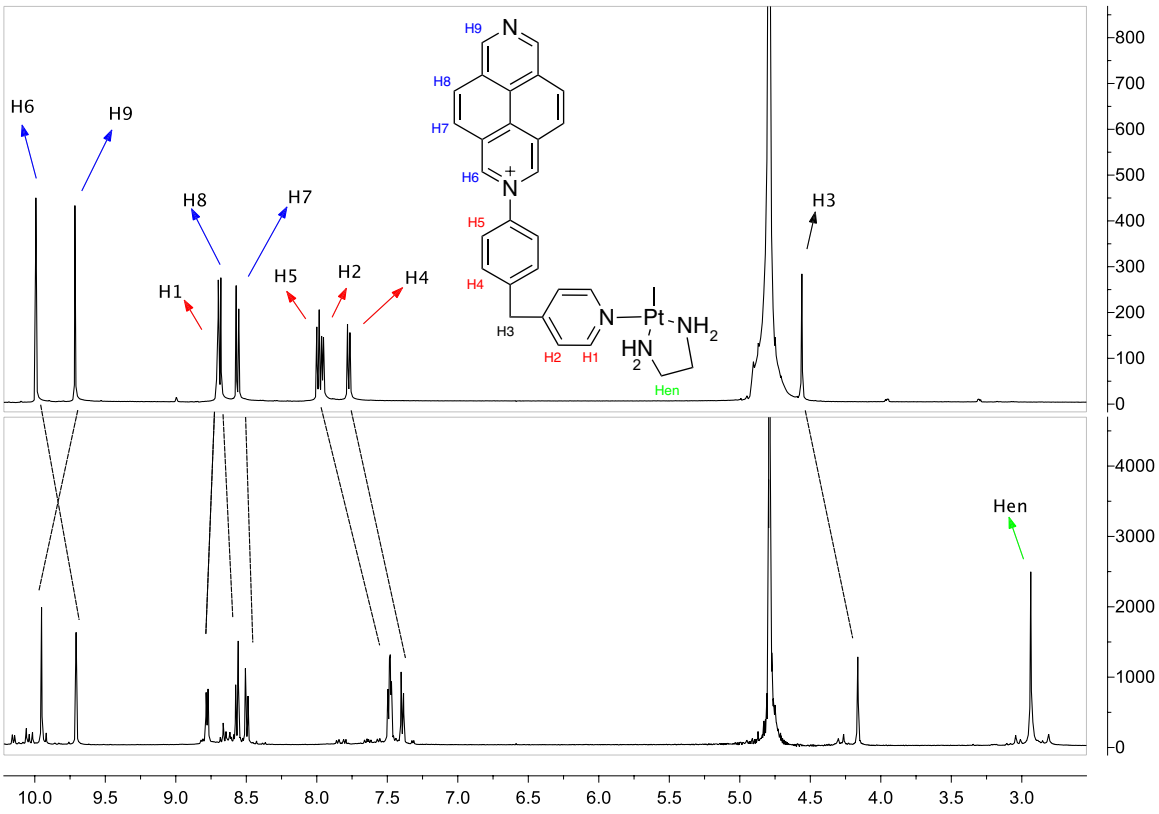

Figure 4.5: ^{1}H-NMR (D_2O, 500 MHz) of $[DAzP]NO_3$ (above) and $[Pt_2(DAzP)_2(en)_2](NO_3)_6$ (bottom).

Fujita to introduce the "molecular lock" concept [39]. Obviously, the reaction time and temperature were chosen to assure the thermodynamic control over the self-assembly. $[Pt_2(DAzP)_2(en)_2](PF_6)_6$ was characterized by ESI-HRMS mass experiments and 2d-NMR, including COSY, HSQC and HMBC spectra (see Experimental, Section 2.5 and Appendix A). The same NMR experiments were performed for $[Pt_2(DAzP)_2(en)_2](NO_3)_6$. Mass spectrometry showed peaks resulting from the loss of between two and five hexafluorophosphate anions. As concerns the NMR (Figure 4.5), the downfield shift of protons H1 and H9 and the upfield shift of H2, H4, H5 and H6 clearly suggested the complexation of DAzP ligand to the metal center and the formation of the rectangle (Figure 4.3). The presence of other cyclic structures was discarded by dilution experiments monitored by ^{1}H NMR spectroscopy.

4.2.1 X-ray crystallography

The structure of [DAzP]PF_6 was confirmed by means of X-ray crystallography of suitable single crystals obtained by vapor diffusion of diethyl ether into a CH_3CN solution of a monoprotonated form of the ligand. The dihedral angle between the planes defined by the phenylene and diazapyrene systems is 52°(Figure 4.6).

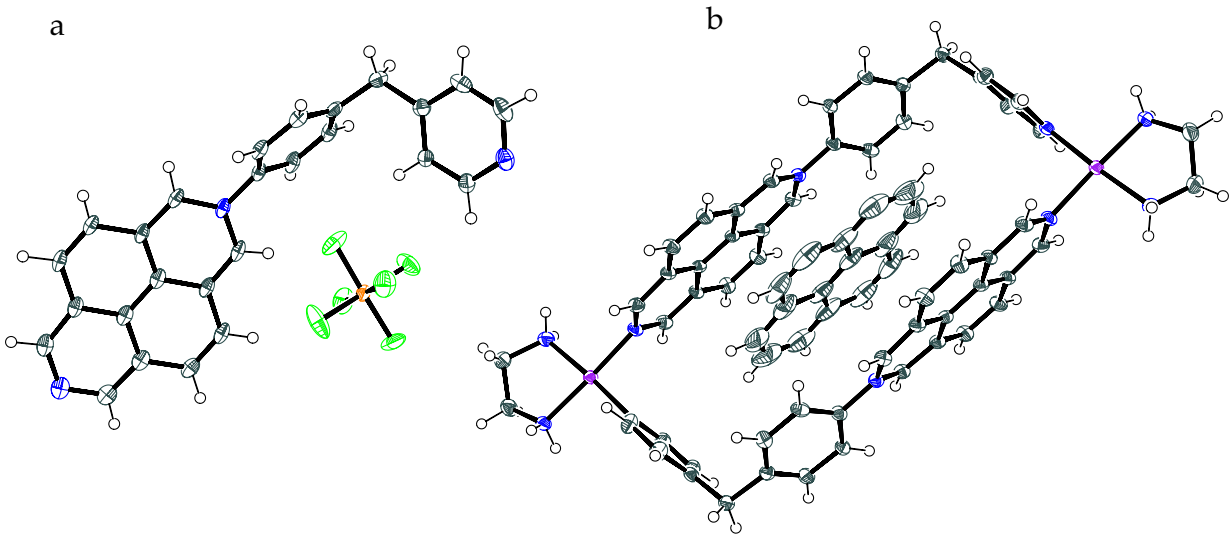

Figure 4.6: Crystal structures of (a) [DAzP]PF_6 and (b) the inclusion complex of the pyrene with the metallacycle $[Pt_2(DAzP)_2(en)_2](PF_6)_6$. Solvent molecules and counterions have been omitted for clarity. The color labelling scheme is as follows: carbon (dark grey), nitrogen (blue), fluorine (green), phosphorus (orange) and platinum (purple).

It was not possible to crystallize the metallacycle alone, but a crystal structure of its inclusion complex with a pyrene molecule was obtained. As a matter of fact, these rectangular metallacycles have proven to be receptors for polycyclic aromatic hydrocarbons (PAHs), such as pyrene, phenanthrene, triphenylene, and benzo[a]pyrene [202]. Their cavities present a nearly optimal size to form supramolecular complexes with PAHs through π-stacking and hydrophobic forces.

The formation of the 1:1 inclusion complexes in the solid state was confirmed by X-ray crystallography analysis of single crystals obtained by vapor diffusion of isopropyl ether into CH_3CN solutions of the pyrene and $[Pt_2(DAzP)_2(en)_2](PF_6)_6$ (Figure 4.6). The distance between the planes defined by the guest and the diazapirenium moieties is very close to the optimal separation maximizing π-π interactions. The metallacycle length and width are about 14.90 and 7.0 Å, respectively. The planes defined by the diazapyrene systems are parallel to each other and nearly perpendicular to the equat-

orial plane of the metallacycle defined by their four corners.

4.3 DNA interaction studies

In order to compare changes in the optical properties of DNA upon binding to the compounds [DAzP]NO_3 and [Pt_2(DAzP)$_2$(en)$_2$](NO_3)$_6$, titration experiments were performed using different spectroscopic techniques. Moreover the ability of these compounds to change the mobility of DNA in a electrophoretic experiment was evaluated as well as their capacity to inhibit the DNA amplification in a PCR assay.

4.3.1 Circular and linear dichroism

The CD spectrum of DNA in its native B-form is characterized by a positive band centered at 275 nm, a negative band at 240 nm, with the zero being around 258 nm (black solid line in Figures 4.7a and 4.8a). In the same way, B-DNA exhibits a characteristic LD spectrum with a typical negative band between 220 nm and 300 nm (black solid line in Figures 4.7b and 4.8b), caused by π-π^* transitions [70]. Spectral changes of these bands and, above all, the presence of induced bands (ICD and ILD) in others regions of the spectrum, provide a convenient tool for monitoring the interaction between the two compounds and the biopolymer.

In Figure 4.7 the CD (a) and LD (b) spectra of ct-DNA in the presence of increasing amounts of the [DAzP]NO_3, up to [DNA]/[DAzP] molar ratios of approximately 2:1, are shown. The titration was carried out adding increasing amounts of DAzP stock solutions to a ct-DNA solution with constant concentration. To ensure that, during the titration, the concentration of the DNA remained unaltered, for each addition of DAzP the same volume of a double-concentrated DNA solution was added. All the samples for which CD and LD spectrum was collected contained a fixed concentration of NaCl (10 mM) and sodium cacodylate buffer (1 mM).

The CD data obtained, with the presence of two ICD bands at approximately 320 and 420 nm separated by an isodichroic point at 378 nm, clearly demonstrate that DAzP binds the biological polymer acting as a further chromophore appended to the chiral backbone of the DNA double helix [70]. The DNA band centred at 240 nm is monotonously increased by the addition of the ligand probably as a consequence of an induced absorption by the ligand itself in that region. Nevertheless, the B-form of the polymer

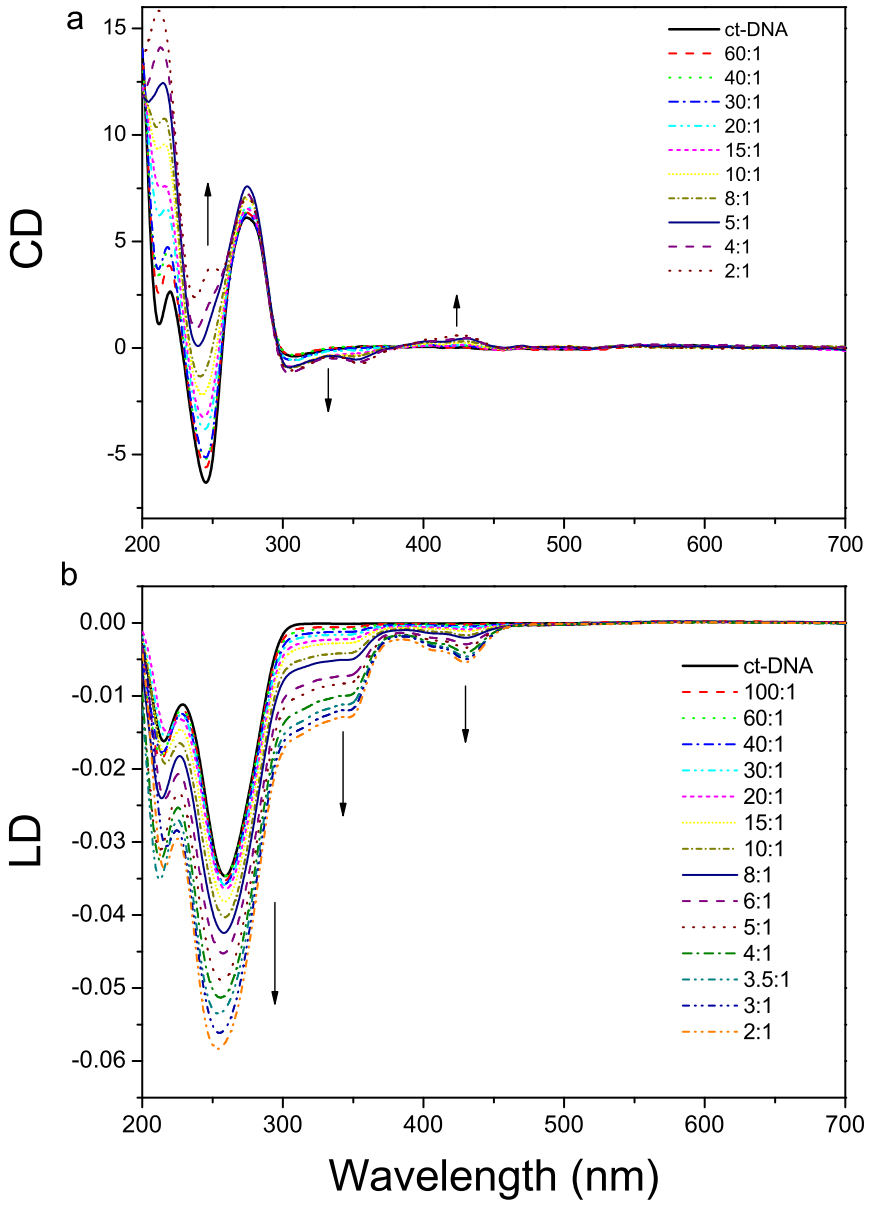

Figure 4.7: (a) CD of 100 μM ct-DNA and (b) LD of 300 μM ct-DNA, in 10 mM NaCl and 1 mM cacodylate buffer in the presence of increasing concentration of [DAzP]NO_3, in the range [DNA]:[DAzP] shown in the legend.

is preserved, as confirmed by the unmodified positive DNA band at 240 nm. The LD spectra in Figure 4.7b confirm the CD data indicating that the ligand is oriented in a

specific way by the polynucleotide. The presence of the two negative ILD bands (in the same region of the ICD bands) and the fact that the compound induces an enhancement of the DNA negative band clearly indicate an intercalative binding mode, as expected from the planar molecular geometry.

Changes in CD and LD spectra of DNA upon addition of $[Pt_2(DAzP)_2(en)_2](NO_3)_6$ are presented in Figure 4.8a and 4.8b respectively. The binuclear square complex has a strong effect on the DNA structure and presents a completely different behaviour with respect to DAzP. The modifications in the CD region between 200-300 nm are similar to those seen for $[DAzP]NO_3$ (Figure 4.7a) but, at the same molar ratios, the effect is stronger for the metallacycle. The ICD bands in the region 300-475 nm present a big intensity and in particular the one centred at 350 nm reaches almost the same intensity of the DNA negative band. In the LD spectra shown in Figure 4.8b it is possible to recognize the induced LD bands in the same positions seen in the CD spectra but both negative. Interestingly, the characteristic LD signal of DNA in the presence of the metallacycle decreases dramatically even at very small mixing ratios. This latter finding is consistent with bending/coiling of the DNA by $[Pt_2(DAzP)_2(en)_2](NO_3)_6$. As recently reported for iron and ruthenium supramolecular cylinders [78,189], the metallacyle induces the extent of DNA orientation in the experiment. The compaction of DNA due to the metallacycle presence is also confirmed by the precipitation occurring at molar ratios smaller than 8:1.

The binding constant of the $[DAzP]NO_3$-DNA system was determined by a method recently reported in the literature and using the following equation [203]:

$$y = 0.5R[A + B + x - \sqrt{(A + B + x)^2 - 4Bx}] \tag{4.1}$$

where A, B and R are fitting parameters, the binding constant is $K_b = 1/A$, while $B = B_T/n$ (where B_T is the total number of nitrogen bases and n the number of bases per binding site) and R represents the instrumental response sensitivity [203]). Fitting eqn 4.1 to CD and LD experimental data at 431 nm (see Figure 4.9) through a Levenberg-Marquardt least squares routine we obtain the K_b values for the ligand-DNA binding, equal to $(3.6 \pm 2) \times 10^5$ M^{-1} and $(5.3 \pm 0.5) \times 10^5$ M^{-1}, respectively. The good agreement of the constant value using two different spectroscopic techniques indicates the reliability of the data. The precipitation phenomenon during the metallacycle-DNA titration did not allow to calculate a binding constant for $[Pt_2(DAzP)_2(en)_2](NO_3)_6$ with the same set of experiments.

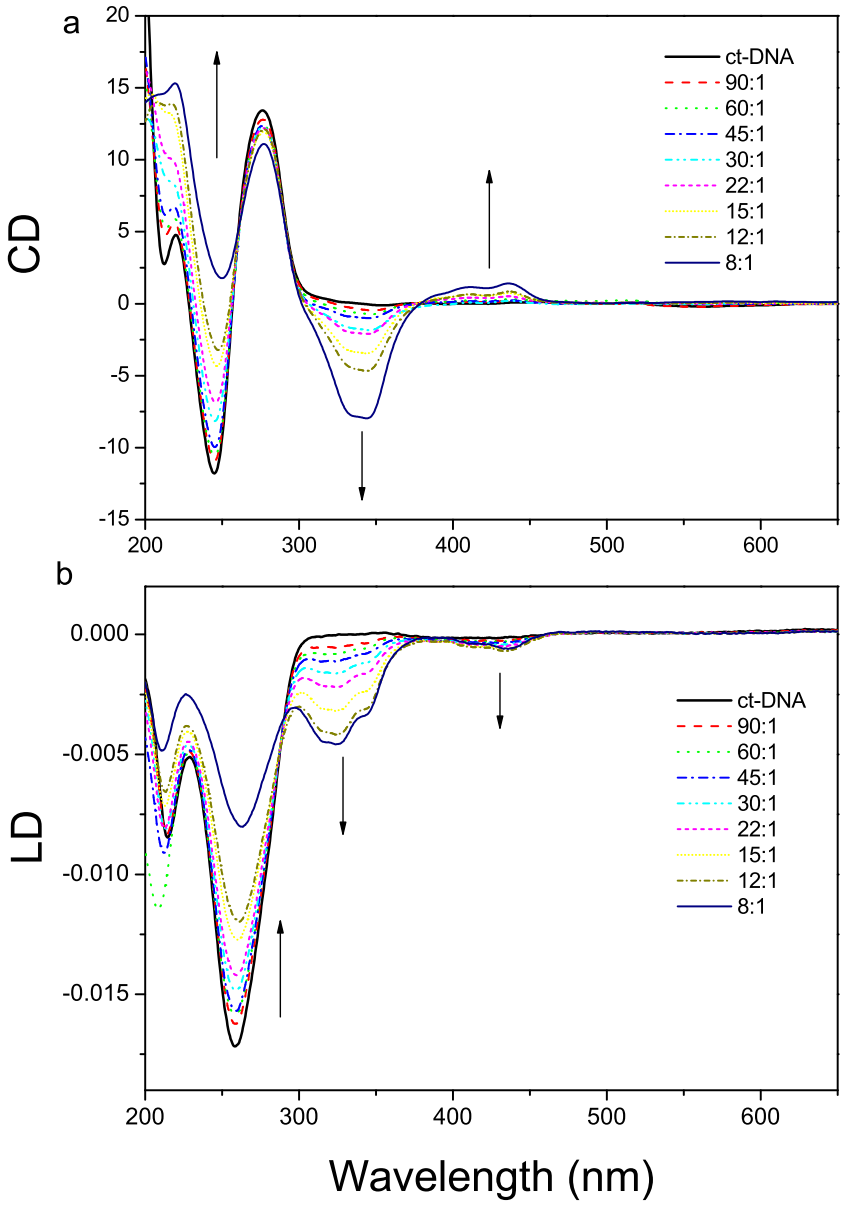

Figure 4.8: (a) CD of 150 μM ct-DNA and (b) LD of 150 μM ct-DNA, in 10 mM NaCl and 1 mM cacodylate buffer in the presence of increasing concentration of $[Pt_2(DAzP)_2(en)_2](NO_3)_6$, in the range [DNA]:[metallacycle] shown in the legend.

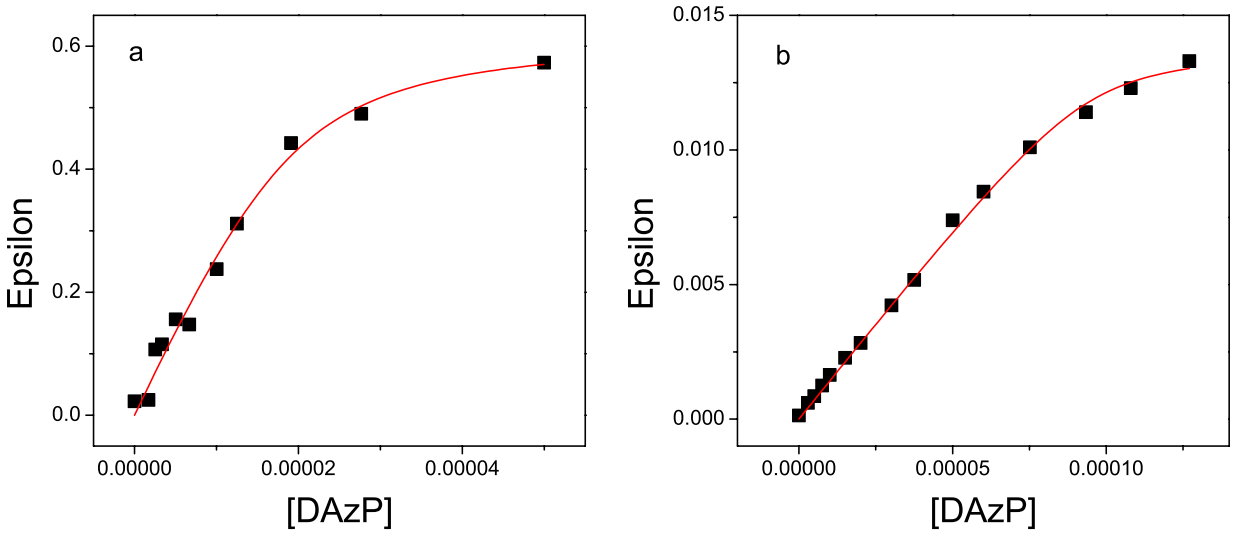

Figure 4.9: Titration data of DAzP derived by taking a vertical cross section at 431 nm in Figure 4.7a for CD and Figure 4.7b for LD experiment. The solid line is the theoretical fit of the data using eqn 4.1. In both graphs epsilon = y.

4.3.2 Fluorescence

In fluorescence spectroscopy investigations, of particular interest are molecules that can reversibly switch from a non-emissive to an emissive state [16].

Water solutions of compounds [DAzP]NO_3 and $[Pt_2(DAzP)_2(en)_2](NO_3)_6$ share an emission band at 439 nm when excited at 290 nm. DAzP is stable under irradiation and has a stronger emission with respect to the metallacycle. Furthermore, UV-vis experiments confirmed that the Pt^{II} complex is slightly light sensible. Binding of both compounds with the DNA helix was found to strongly quench the dyes fluorescence.

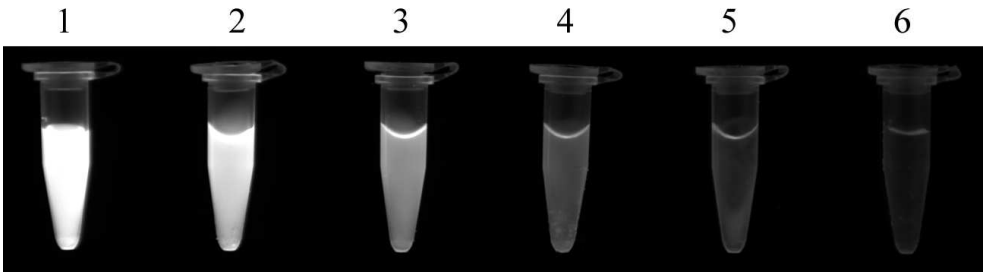

Figure 4.10: Effect of increasing concentration of ct-DNA on the luminescence of DAzP. Vial 1: DAzP 120 μM, Vials 2-6: [DNA]/[DAzP] 0.5:1; 1:1; 1.5:1; 2:1; 2.5:1.

In particular, water solutions of DAzP are luminescent when illuminated with a UV lamp (λ_{exc} = 312 nm) and a strong quenching is observed when DNA is added (see Fig-

ure 4.10). For these reasons fluorescence spectroscopy was used to further investigate the interaction between the two compounds and DNA.

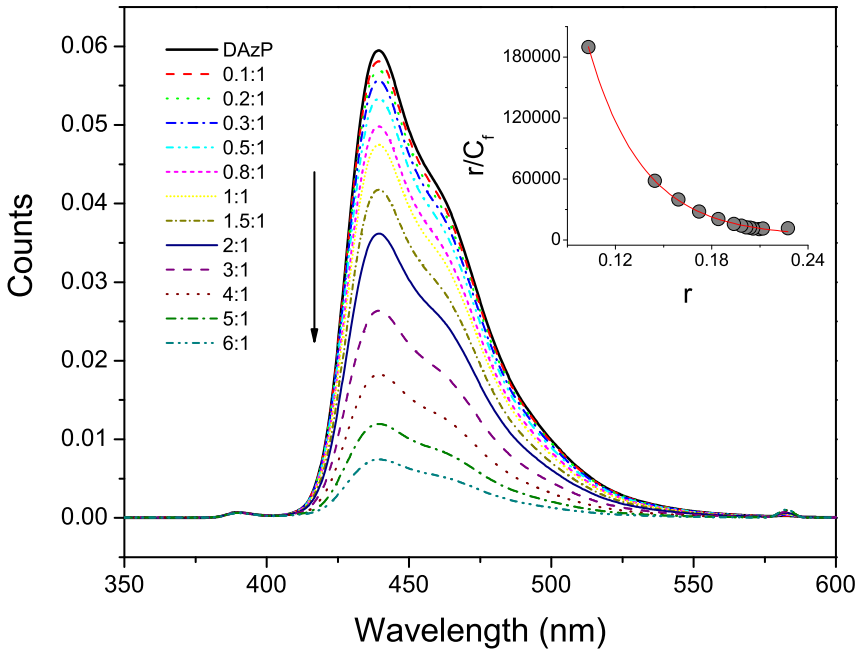

Figure 4.11: Fluorescence titration of 20 μM DAzP, in 10 mM NaCl and 1 mM cacodylate buffer in the presence of increasing concentration of ct-DNA, in the range [DNA]:[DAzP] shown in the legend. Inset: Scatchard plot of the fluorescence titration data at 439 nm using eqn 4.2.

Titration experiments were carried out by adding increasing amounts of DNA to a 20 μM solutions of the [DAzP]NO_3 ligand and of the Pt^{II} metallacycle. The decrease of the DAzP fluorescence due to the addition of DNA is presented in Figure 4.11. The spectral changes arise from changes in the environment of the fluorophore upon intercalating DNA.

Figure 4.12 shows the fluorimetric titration of the metallacycle with increasing amount of DNA. The trend is the same as seen in Figure 4.11 for DAzP, but the relatively poor emission of the complex and its light sensitivity prevented the possibility to obtain reproducible and accurate data to calculate the binding constant.

To obtain the value of the intercalation constant for the DAzP-DNA system from the

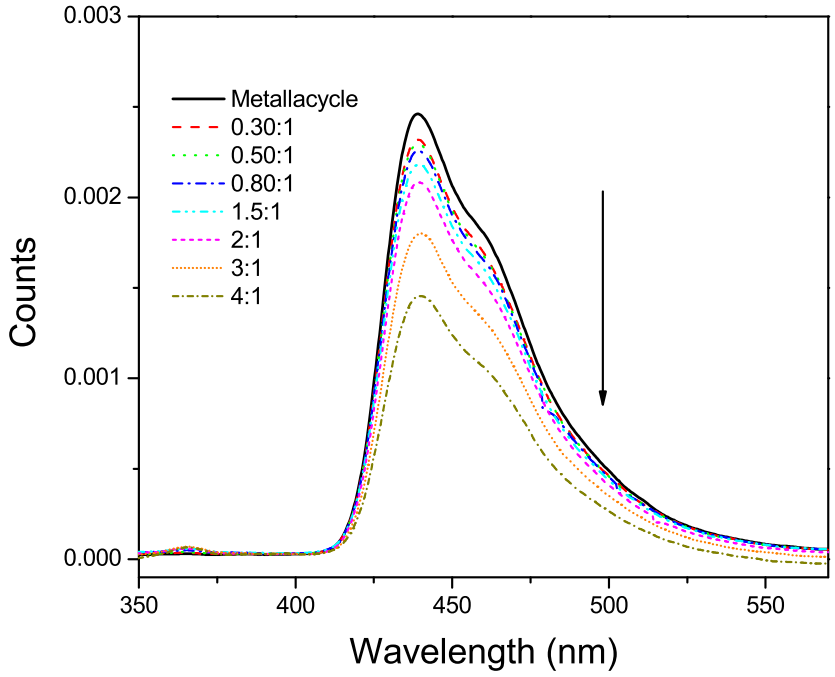

Figure 4.12: Fluorescence titration of 20 μM metallacycle, in 10 mM NaCl and 1 mM cacodylate buffer in the presence of increasing concentration of ct-DNA, in the range [DNA]:[metallacycle] shown in the legend.

fluorimetric titration the following equation was used [204–207]:

$$\frac{r}{C_f} = K_i(1 - nr)\left\{\frac{1 - nr}{1 - (n-1)r}\right\}^{n-1} \tag{4.2}$$

where r is the ratio between the concentration of the bound ligand (C_b) and the DNA, K_i is the intrinsic binding constant and n is the exclusion parameter in base pairs. C_b values were obtained subtracting C_f (the concentration of free ligand) to the total concentration of the ligand (C_t). C_f was determined according to the following equation [208, 209]:

$$C_f = C_t\frac{(\frac{I}{I_0} - P)}{(1 - P)} \tag{4.3}$$

where I_0 and I are the fluorescence intensities of the ligand in the absence and in presence of DNA, respectively. $P = I_{lim}/I_0$ was obtained from the minimum value of I (I_{lim})

at high DNA concentration and the initial value of I_0 in the absence of DNA.

In the inset of Figure 4.11 a Scatchard plot was constructed from r/C_f vs. r and the best fit of the data has returned a value of K_i equal to $(5.6 \pm 0.5) \times 10^5$ M^{-1}. This last value is in very good agreement with the ones obtained by CD and LD experiments.

4.3.3 Ethidium bromide displacement assays

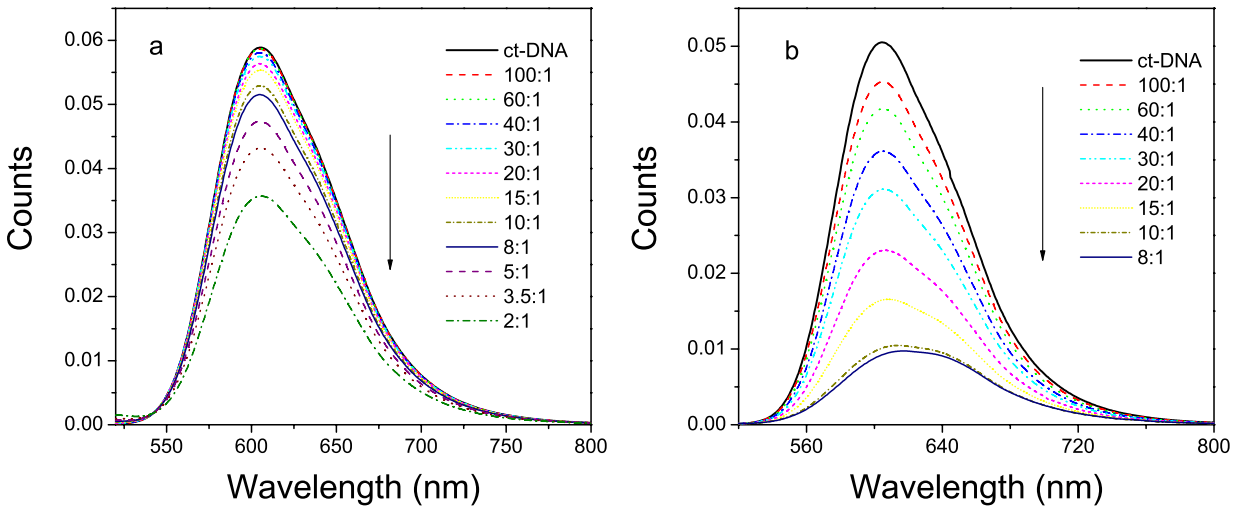

Figure 4.13: Displacement of ethidium bromide (10 μM) from ct-DNA (30 μM) by increasing concentration of (a) DAzP and (b) $[Pt_2(DAzP)_2(en)_2](NO_3)_6$, in the range [DNA]:[drug] shown in the legend.

In order to calculate the binding constant of the interaction between the metallacycle and the DNA, ethidium bromide (EB) fluorescence displacement assays were performed. It is well known that the intrinsic fluorescence intensity of DNA water solutions is very low. In the same way, EB water solutions present a very weak fluorescence that is enhanced by the addition of DNA because of its intercalation. The fluorescence intensity of EB intercalated into DNA can be quenched by the addition of another molecule due to decreasing of the binding sites of DNA available for EB. The titrations of the EB-DNA system with DAzP and the metallacycle are shown in Figure 4.13a and b, respectively. In both cases there is a fluorescence decrease. However, the effect of the metallacycle is stronger. Probably, while in the case of DAzP, that is an intercalator, there is only a replacement effect, the coiling produced by $[Pt_2(DAzP)_2(en)_2](NO_3)_6$ does not allow the EB to occupy most of the DNA binding sites. The apparent binding constant

for both compounds was calculated from:

$$K_{EB}[EB] = K_{app}[drug_{50\%}] \tag{4.4}$$

where *[drug$_{50\%}$]* is the concentration of DAzP or of the metallacycle at 50% reduction of fluorescence and K_{EB} is the binding constant for the ethidium bromide [210]. Using a value of $\approx 1.2 \times 10^6$ M^{-1} for K_{EB} [211, 212], the following binding constants were obtained: $(4.1 \pm 0.5) \times 10^5$ M^{-1} for DAzP and $(6.8 \pm 0.5) \times 10^6$ M^{-1} for $[Pt_2(DAzP)_2(en)_2](NO_3)_6$.

4.3.4 DNA Thermal Denaturation Analysis

Thermal denaturation profiles of calf thymus DNA solutions, in the presence of increasing amounts of compounds [DAzP]NO_3 and $[Pt_2(DAzP)_2(en)_2](NO_3)_6$, are shown in Figures 4.14a and b respectively. DNA-melting experiments were carried out by monitoring the absorbance of DNA (258 nm) at various temperatures in the absence and presence of the compounds at differents [DNA]:[drug] ratios. The temperature was elevated gradually from 20 to 95 °C at a rate of 0.5 °C per min.

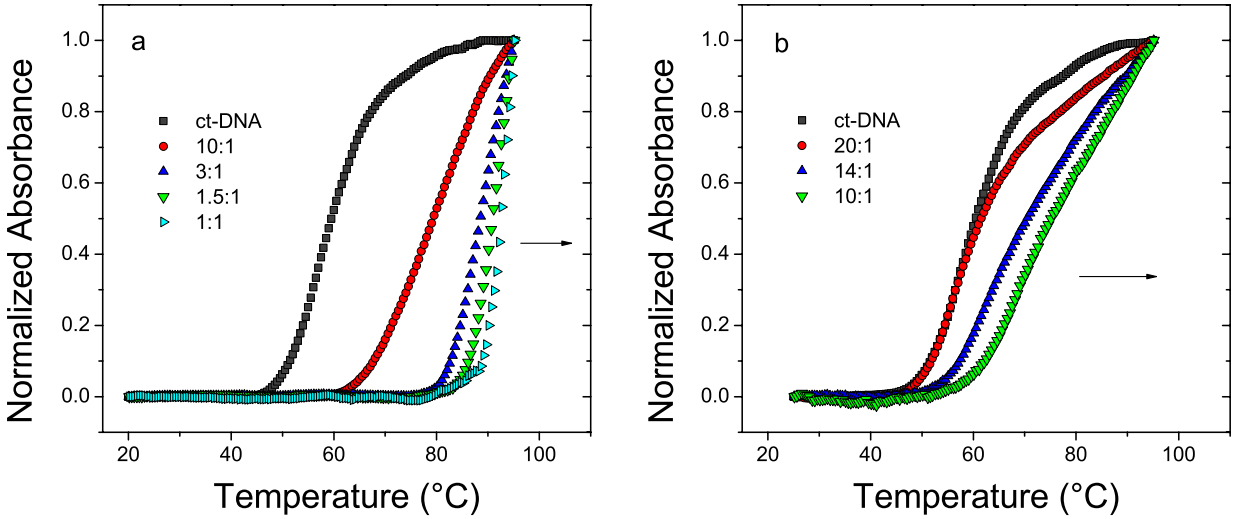

Figure 4.14: Thermal denaturation profiles of ct-DNA solutions (100 μM ct-DNA, 1.0 mM Tris-HCl, 20 mM NaCl) in the presence of increasing amounts of , (a) DAzP (ct-DNA, T_m= 59.7 $\pm$ 0.1; 10:1 T_m= 80.0 $\pm$ 0.1; 3:1, T_m= 89.0 $\pm$ 0.1; 1.5:1, T_m= 91.8 $\pm$ 0.2; 1:1, T_m= 92.3 $\pm$ 0.2 °C) and (b) metallacycle (ct-DNA, T_m= 60.2 $\pm$ 0.1; 20:1 T_m= 61.3 $\pm$ 0.2; 14:1, T_m= 70.6 $\pm$ 0.2; 10:1, T_m= 75.8 $\pm$ 0.3 °C

When the temperature is increased the double stranded DNA gradually dissociates into single strands. The DNA melting temperature (T_m) is defined as the temperature

where half of the total base pairs are unpaired and is obtained from a sigmoidal fit of the experimental data [67]. The ability of [DAzP]NO_3 to alter the thermal denaturation profile of DNA in a stronger way with respect to the metallacycle $[Pt_2(DAzP)_2(en)_2](NO_3)_6$ is another indication of the differences in the DNA binding mode. In fact, it is known that the intercalation of natural or synthesized compounds results in a strong stabilization of the double helix due to stacking interactions, thus in a considerable increase in the melting temperature of DNA [67–69]. The effect of DAzP results in an increase of the DNA melting temperature (59.7 $\pm$ 0.1 °C) of 20 °C at the ratio [DNA]/[DAzP] equal to 10:1. At the same ratio value, the Pt^{II} complex increases the DNA T_m of about 15 °C.

Although the binding of $[Pt_2(DAzP)_2(en)_2](NO_3)_6$ to DNA is very strong, as seen with other techniques, the general loss of planarity compared with [DAzP]NO_3 alone causes a smaller stabilization of the double strand. In the same way as for the CD and LD experiments, it was impossible to reach lower [DNA]:[metallacycle] ratios due to precipitation.

4.3.5 Gel electrophoresis

Plasmid Gel Electrophoresis. A gel electrophoresis experiment was performed in order to see how the gel mobility of negatively supercoiled plasmid is affected by the compounds [DAzP]NO_3 and $[Pt_2(DAzP)_2(en)_2](NO_3)_6$.

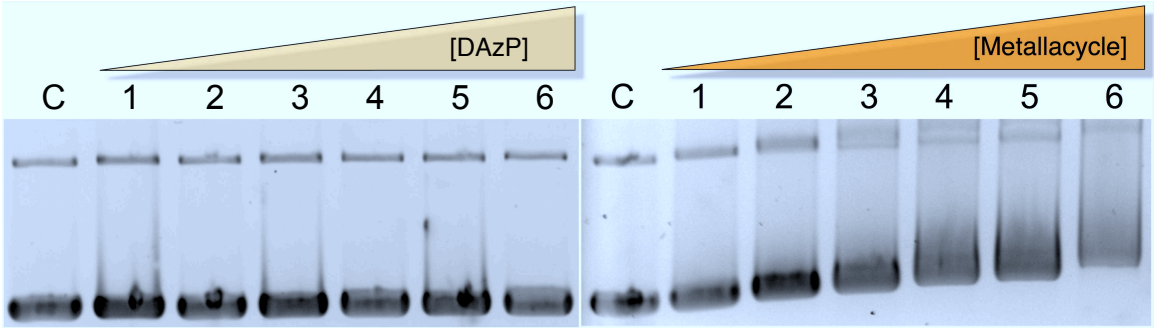

Figure 4.15: Agarose gel electrophoresis patterns for unwinding of supercoiled pBR322 plasmid DNA by (a) DAzP and (b) $[Pt_2(DAzP)_2(en)_2](NO_3)_6$. In each gel the top bands correspond to the circular plasmid form while the bottom bands to the supercoiled one. Lane C: DNA control; Lanes 1-6: [DNA]/[drugs] 20:1; 12:1; 8:1; 6:1; 5:1; 3:1.

The characteristic agarose gel pattern of plasmid DNA consists generally in two bands, one intense corresponding to the negatively-supercoiled DNA (lower band in Figure 4.15 a and b lane C) and another one to the open-circle DNA. It is well known

that molecules that are able to bind DNA could induce an unwinding of the duplex supercoils resulting in a decrease in the rate of migration through agarose gel [80, 81]. As shown in Figure 4.15 a and b, with the increase of the drug concentration (lanes 1-6), the intensity of the supercoiled DNA band decreases only when the metallacycle is added, while, in this experimental condition, DAzP has no effect.

PCR Gel Electrophoresis. As LD experiments showed $[Pt_2(DAzP)_2(en)_2](NO_3)_6$ coils dramatically DNA. To investigate whether this effect could prevent the replication of DNA, polymerase chain reaction (PCR) assays were performed. PCR is a straightforward technique which amplifies a double strand DNA mimicking in vitro the cellular replication process [85, 213, 214] (see Section 2.2.7).

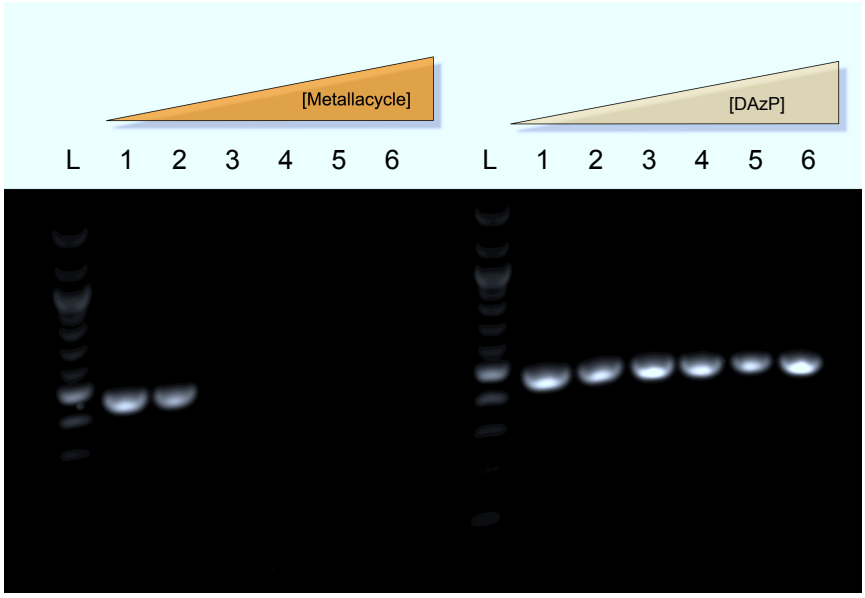

Figure 4.16: PCR inhibition assay with $[Pt_2(DAzP)_2(en)_2](NO_3)_6$ and DAzP at increasing concentration. L) 100 bp oligonucleotide ladders; 1) control (0 μM); 2) 0.05 μM; 3) 0.1 μM; 4) 0.3 μM; 5) 0.5 μM; 6) 1 μM.

It comprises three simple steps, repeated cyclically, required for any DNA synthesis reaction: (1) denaturation of the template, (2) annealing of primers to each original strand for new strand synthesis and (3) extension of the new DNA strands from the primers by a thermostable polymerase [85, 86]. In this PCR assay plasmidic pUC19 DNA was incubated with increasing concentration of both metallacycle and its DAzP ligand for 5 minutes at room temperature, then amplified. Agarose gel electrophoresis of the reaction products after 35 cycles, followed by ethidium bromide staining and UV

visualization, showed a single DNA product of the expected length (Figure 4.16).

Interestingly, the metallacycle is able to block completely the amplification of DNA even at 0.1 μM concentration. On the other hand DAzP does not affect at all the PCR. This result confirm that the binding of the metallacycle to DNA can prevent the regular activity of the polymerase and makes this compound a possible candidate as anticancer drug.

4.4 Cytotoxic Tests

The spectroscopic studies indicate the existence of a strong interaction between DNA and both DAzP and $[Pt_2(DAzP)_2(en)_2](NO_3)_6$, even if the mode of binding is different in the two cases. Gel electrophoresis studies and, above all, PCR experiments emphasize the potential role of $[Pt_2(DAzP)_2(en)_2](NO_3)_6$ as anticancer drug. In order to verify the biological activity of the two compounds, cytotoxic tests against different human cancer cell lines were performed (see Matherials and Methods, Section 4.6).

The IC_{50} values for the compound $[Pt_2(DAzP)_2(en)_2](NO_3)_6$ are presented in Table 4.1 and a range between 3.1 - 19.2 μM can be noticed. The anti-proliferative activities of the metallacycle is relatively selective in the 5 human cancer cell line, with the A-427 line being the most sensitive and the SISO line being the least. Interestingly, SISO is very sensitive to cisplatin but not to this compound. Likewise, of the 5 cell lines, A-427 is the least sensitive to cisplatin but the most sensitive to the metallacycle. Noteworthy is the observation that in the A-427 cell line $[Pt_2(DAzP)_2(en)_2](NO_3)_6$ has potency nearly as good as cisplatin. By contrast $[DAzP]NO_3$ was inactive.

Table 4.1: IC_{50} (μM) values of the analyzed compounds. Results are averages of three independent determinations with standard deviations.

Cell Line	Metallacycle	Cisplatin
SISO	19.24 ± 7.13	0.24 ± 0.05
DAN-G	11.76	0.53 ± 0.07
A-427	3.12 ± 1.22	1.27 ± 0.25
LCLC-103H	9.47 ± 3.12	1.09 ± 0.40
5637	7.61 ± 6.65	0.37 ± 0.08

4.5 Conclusions

The interaction with native DNA of a 2,7-diazapyrenium-based ligand and its Pt^{II} rectangular metallacycle was studied by means of different spectroscopic techniques. Qualitative and quantitative information was achieved. In particular, DAzP ligand was found to be an intercalator with a binding constant approximately equal to 5.0×10^5 M^{-1}, while the metallacycle produces a coiling of the biologic polymer with a binding constant of 7.0×10^6 M^{-1}.

Confirming the spectroscopic results, gel electrophoresis experiments highlight the stronger effect of the metallacycle on the DNA with respect to DAzP. $[Pt_2(DAzP)_2(en)_2](NO_3)_6$ is able to reduce the DNA electrophoretic mobility and, more interestingly, inhibits the DNA amplification (PCR assay) suggesting a possible use as anticancer drug.

As a matter of fact, the metallacycle resulted active towards 5 human cancer cell lines, with an activity comparable to that of cisplatin in one cell line.

4.6 Experimental

4.6.1 Materials and Method

All chemicals and solvents were purchased from Sigma–Aldrich, Fisher or Alfa Aesar and used as received. Deuterated solvents for NMR were supplied by Cambridge Isotope Laboratories, Inc. and Goss scientific.

Proton and carbon nuclear magnetic resonance spectra were recorded on a Bruker Avance 300 or Bruker Avance 500 equipped with a dual cryoprobe for ^1H and ^{13}C, using the residual protonated solvent as internal standard.

Mass spectrometry experiments were carried out in a LC-Q-q-TOF Applied Biosystems QSTAR Elite spectrometer for low- and high-resolution ESI.

Ultrapure water (18.2 MΩ, Fisher) was used in all UV-vis, circular and linear dichroism experiments and for electrophoresis gel. Lyophilized calf thymus DNA, purchased from Sigma-Aldrich, was resuspended in sodium cacodylate buffer ($Na(CH_2)_2AsO_2 \cdot 3H_2O$, pH 6.8 - 7.4) and dialyzed as described in the literature [144]. The DNA concentration was determined by UV-vis measurements using the molar extinction coefficient of ϵ_{260} = 7000 mol^{-1} dm^3 cm^{-1} per DNA base [135–138].

Spectroscopic studies

Stock solutions of 1 M NaCl, 1 M Tris-HCl and 100 mM sodium cacodylate buffer were prepared and, together with DNA stock, were used to obtain the final work solutions.

Absorption measurements were performed on a Varian Cary 5000 UV-vis double beam spectrophotometer or on a Varian UV-vis Cary 1E double beam spectrophotometer, both equipped with a Peltier temperature controller, using 1 cm pathlength cuvettes.

Circular dichroism spectra were collected using a Jasco J-810 spectropolarimeter in cuvettes of pathlength 1 cm. The following parameters were used: sensitivity, 100 mdeg; wavelength range, 200 -750 nm; data pitch, 0.5 nm; scanning mode, continuous; scanning speed, 200 nm min^{-1}; response, 0.1 s; bandwidth, 1.0; accumulation, 12. Linear dichroism spectra were collected using a Jasco J-810 spectropolarimeter. In particular, it was adapted for LD measurements with a flow Couette cell, ideal to give an orientation to long molecules such DNA [145]. The following parameters were used: sensitivity, 100 mdeg; wavelength range, 200-750 nm; data pitch, 0.5 nm; scanning mode, continuous; scanning speed, 500 nm min^{-1}; response, 0.25 s; bandwidth, 2.0; accumulation, 8.

The fluorescence spectra were recorded in a Shimadzu RF-5301 PC Fluorescence Spectrophotometer. DAzP, (λ_{exc} = 290 nm; range emission = 300-700 nm; resolution = 0.4 nm; speed = medium; excitation slit = 1.5; emission slit = 3; sensitivity = high). metallacycle, (λ_{exc} = 290 nm; Range emission = 300-700 nm; resolution = 0.4 nm; speed = medium; excitation slit = 1.5; emission slit = 5; sensitivity = high). All over the titration, the concentration of the DAzP/$[Pt_2(DAzP)_2(en)_2](NO_3)_6$ was kept constant while increasing amounts of DNA were added. All samples contained a fixed concentration of NaCl (10 mM) and sodium cacodylate buffer (1 mM). Luminescence was visualized using a UVtec-uvipro platinum system. EB displacement assay: DAzP and $[Pt_2(DAzP)_2(en)_2](NO_3)_6$, ($\lambda_{exc}$ = 500 nm; Range emission = 520-800 nm; resolution = 0.4 nm; speed = medium; excitation slit = 5; emission slit = 5; sensitivity = high). In this experiment the concentrations of DNA and EB were kept constants while increasing amounts of DAzP/$[Pt_2(DAzP)_2(en)_2](NO_3)_6$ were added. All samples contained a fixed concentration of NaCl (10 mM) and sodium cacodylate buffer (1 mM).

Gel electrophoresis

The electrophoresis experiments were performed through Electrophoresis Power Supply (EPS 301) system with the following parameters: voltage, 120 V; ampere, 190 mA; time, 2.5 h. Gel trays of 210 $\times$ 150 mm with a 15-toothed comb were used. In all of the electrophoresis experiments 1X Tris acetate (obtained by dilution of 10X TAE, supplied by SIGMA) was used as working buffer. In detail, the gel was prepared warming up 2 g of agarose (from USB corporation) in 200 mL of 1X TAE. pBR322 plasmide DNA (1mg/mL, New England Biolabs) was used to prepare the samples. The images of the gels were visualized and acquired using a UVtec-uvipro platinum system.

As concerns the PCR gel electrophoresis experiment, twelve reaction mixtures were prepared, all containing 1X NH_4 reaction buffer, $MgCl_2$ (1.5 mM), pUC19 plasmid DNA substrate (50 ng, Sigma Aldrich), Taq DNA polymerase (5U; Bioline), dNTPs (3 mM), the primers (0.4 μM each) pUC19F (5'-CGGTGAAAACCTCTGACACA -3') and M13 reverse (5'-CAGGAAACAGCTATGACC -3'; Alta Bioscience). The images of the gels were visualized and acquired using a UVtec-uvipro platinum system.

Cytotoxic Test

All stock solutions were prepared in DMSO and stored at -30 °C. Prior to testing stock solutions were removed from the freezer and serially diluted in DMSO 2-fold to the desired concentrations, giving the series of five dilutions. To investigate the cytotoxic potency of the compounds 5 different human cancer cell lines were used. SISO a cervical cancer cell line, 5637 from bladder cancer, A-427 and LCLC-103H a lung cancer cell lines and DAN-G a pancreas carcinoma cell line (see Table 4.2). All human cancer cell lines were obtained from the German Collection of Microorganisms and Cell Cultures (DSMZ, Braunschweig).

Cells were grown in medium containing 90% RPMI 1640 medium (Sigma, Taufenkirchen, Germany) and 10% FCS (Sigma), supplemented with penicillin G/streptomycin. Cells were kept at 37 °C in a water saturated atmosphere of 5% CO_2 air. Shortly before the cells reached confluence the cells were passaged.

Screening methods. The cells were seeded out in 96-well microtiter plates in 100 μl medium at a density of 1000 cells/well (LCLC-103H 250 cells/well). The plates were returned to the incubator for 24 h. The next day the stock solutions and the dilutions were directly diluted in medium 500-fold. 100 μl of the medium containing the compounds

Table 4.2: Human cancer cell lines used in the cytotoxic assay.

Cell Line	Patient (sex, age)	Origin	Doubling Time (h)
SISO	F, 67	Cervix adenocarcinoma	48
DAN-G	–	Pancreas carcinoma	42
A-427	M, 52	Lung carcinoma	38
LCLC-103H	M, 61	Large cell lung cancer	40
5637	M, 68	Urinary bladder carcinoma	30

were added to each well with a maximum DMSO concentration of 0.1% (v/v). After the complete incubation period of 96 h the medium was discarded and replaced for 25 min with a 1% glutaraldehyde buffer (PBS) solution to fix the cells. The fixing buffer was discarded and the cells were stored under PBS at 4 °C until staining. Staining was done with a 0.02% solution of Crystal Violet in water. The dye was added to each well and discarded after 30 min of staining, followed by 15 min washing with water. The cell-bound dye was redissolved in 70% ethanol/water. Optical density was measured at λ = 570 nm with an Anthos 2010 plate reader (Anthos, Salzburg, Austria). The corrected T/C values for the dose-response curves were calculated:

$$\frac{T}{C_{corr}} = \frac{(OD_{test} - OD_{t=0})}{(OD_{con} - OD_{t=0})} \times 100 \tag{4.5}$$

where OD_{test} is the mean optical density of the treated cells after staining, OD_{con} is the mean optical density of the controls and $OD_{t=0}$ is the mean optical density at the time the compounds were added. The IC_{50} values were calculated by a linear least-squares regression of the T/C_{corr} values versus the logarithm of the added compound concentration and extrapolating to the T/C_{corr} values of 50%.

X-ray crystallography

The structures were solved by direct methods and refined with the full-matrix least-squares procedure (SHELX-97)[28] against F^2. The X-ray diffraction data were collected on a Bruker X8 ApexII diffractometer. Non-solvent hydrogen atoms were placed in idealized positions with U_{eg}(H) = 1.2 U_{eg}(C) and were allowed to ride on their parent atoms. Solvent hydrogen atoms were placed in idealized positions with U_{eg}(H) = 1.5 U_{eg}(C) and were allowed to ride on their parent atoms.

4.6.2 Synthesis and characterization

Compounds **13**, **14** (see Figure 4.4) and 2,7-diazapyrene were prepared according to published procedures [215–218].

[DAzP]PF_6, 15a: a solution of 2-(2,4-dinitrobenzyl)-2,7-diazapiren-2-ium chloride (**13**·Cl) (1.03 g, 2.77 mmol) and 4-(pyridin-4-ylmethyl)aniline (**14**) (2.04 g, 11.07 mmol) in EtOH (75 mL) was refluxed for 3d, after cooling, the solvent was evaporated in vacuo. The resulting residue was dissolved in H_2O (200 mL) and extracted with EtOAc (200 mL). The organic layer was further extracted with H_2O (2×150 mL) and the combined aqueous extracts were washed with EtOAc (4×75 mL). The solvent was removed under reduced pressure to give a crude product, which was purified by column chromatography (SiO_2, acetone/NH_4Cl 1.5M/MeOH 5:4:1). The product-containing fractions were combined and the solvents were removed in vacuo. The residue was dissolved in H_2O/CH_3OH (95:5, 250 mL) and an excess of KPF_6 was added until no further precipitation was observed. The solid was filtered and washed with water to give [DAzP]PF_6 (0.97 g, 70%) as a dark yellow solid. Vapor diffusion of ethyl ether into a CH_3CN solution gave dark yellow crystals good for X-ray analysis.
^{1}H NMR (500 MHz, CD_3NO_2) δ (ppm): 4.68 (s, 2H), 7.84 (d, J = 8.6 Hz, 2H), 8.08 (d, J = 8.6 Hz, 2H), 8.11 (d, J = 6.7 Hz, 2H), 8.69 (d, J = 9.1 Hz, 2H), 8.82 (d, J = 6.8 Hz, 2H), 8.84 (d, J=9.1Hz, 2H), 9.91 (s, 2H), 9.92 (s, 2H).
^{13}C NMR (125 MHz, CD_3NO_2) δ (ppm): 42.1 (CH_2), 125.5 (C), 127.2 (CH), 127.3 (CH), 127.6 (C), 129.3 (CH), 130.4 (C), 130.6 (C), 133.1 (CH), 133.2 (CH), 139.3 (CH), 142.5 (CH), 142.7 (C), 144.8 (C), 149.9 (CH).
MS-ESI (m/z): 372.2 [M - PF_6^-]$^+$; elemental analysis calcd (%) for $C_{26}H_{18}F_6N_3P$: C, 60.35, H, 3.51, N, 8.12; found: C, 60.08, H, 3.86, N, 8.33.

[DAzP]NO_3, 15b: [DAzP]PF_6 (500.0 mg, 0.97 mmol) was dissolved in the minimum amount of CH_3CN and an excess of Bu_4NNO_3 was added until no further precipitation was observed. The white precipitate was filtered and washed with CH_3CN to yield [DAzP]NO_3 (356.0 mg, 85%) as a brown solid.
^{1}H NMR (500 MHz, D_2O) δ (ppm): 4.56 (s, 2H), 7.77 (d, J = 8.5 Hz, 2H,), 7.98 (m, 4H), 8.46 (d, J = 9.1 Hz, 2H), 8.56 (d, J = 9.1 Hz, 2H), 8.70 (d, J = 6.8 Hz, 2H), 9.57 (s, 2H), 9.95 (s, 2H).
^{13}C NMR (125 MHz, D_2O) δ (ppm): 40.5 (CH_2), 123.9 (C), 125.5 (CH), 126.1 (CH), 126.2 (C), 127.3 (CH), 128.0 (C), 128.7 (C),131.0 (CH), 131.6 (CH), 138.2 (CH), 141.1 (C), 141.2

(CH), 142.6 (C), 146.8 (CH), 161.5 (C).
MS-ESI (m/z): 372.2 [M - NO_3]$^+$; elemental analysis calcd (%) for $C_{26}H_{18}N_4O_3$: C, 71.88, H, 4.18, N, 12.90; found: C, 71.60, H, 3.88, N, 13.20.

[Pt_2(DAzP)$_2$(en)$_2$](PF_6)$_6$, 16a: A solution of [DAzP]NO_3 (120.0 mg, 0.276 mmol) and (en)Pt(NO_3)$_2$ (104.7 mg, 0.276 mmol) in H_2O (60 mL) was heated at 100 °C for 8d. Upon cooling to room temperature, an excess of KPF_6 was added until no further precipitation was observed. The solid was filtered to yield [Pt_2(DAzP)$_2$(en)$_2$](PF_6)$_6$ (281.7 mg, 96%) as a brown solid.
^{1}H NMR (500 MHz, CD_3NO_2) δ (ppm): 3.19 (m, 8H), 4.26 (s, 4H), 7.42 (d, J = 8.6 Hz, 4H), 7.51 (d, J = 6.8 Hz, 4H), 7.63 (d, J = 8.7 Hz, 4H), 8.63 (d, J = 9.2 Hz, 4H), 8.67 (d, J = 9.2 Hz, 4H), 8.82 (d, J = 6.8 Hz, 4H), 9.69 (s, 4H), 10.00 (s, 4H).
^{13}C NMR (125 MHz, CD_3NO_2) δ (ppm): 41.1 (CH_2), 49.8 (CH_2), 49.9 (CH_2), 126.2 (C), 126.3 (CH), 128.9 (C), 129.5 (CH), 130.0 (CH), 130.4 (C), 130.7 (C), 131.6 (CH), 132.3 (CH), 140.5 (CH), 143.6 (C), 144.7 (C) 151.1 (CH), 153.6 (CH), 156.7 (C).
HRMS-ESI (m/z): calcd for [M - 2PF_6^-]$^{2+}$ 917.1114; found 917.1085; calcd for [M - 3PF_6^-]$^{3+}$ 563.0860; found 563.0853; calcd for [M - 4PF_6^-]$^{4+}$ 386.0733; found 386.0749; calcd for [M - 5PF_6^-]$^{5+}$ 279.8657; found 279.8671. Elemental analysis calcd (%) for $C_{56}H_{52}F_{36}N_{10}P_6Pt_2$: C, 31.65, H, 2.47, N, 6.59; found: C, 31.84, H, 2.19, N, 6.33.

[Pt_2(DAzP)$_2$(en)$_2$](NO_3)$_6$, 16b: [Pt_2(DAzP)$_2$(en)$_2$](PF_6)$_6$ (95.0 mg, 0.0445 mmol) was dissolved in the minimum amount of CH_3CN and an excess of Bu_4NNO_3 was added until no further precipitation was observed. The white precipitate was filtered and washed with CH_3CN to yield [Pt_2(DAzP)$_2$(en)$_2$](NO_3)$_6$ (72.5 mg, 99%) as a brown solid.
^{1}H NMR (500 MHz, D_2O) δ (ppm): 2.93 (m, 8H), 4.16 (s, 4H), 7.39 (d, J = 8.6 Hz, 4H), 7.48 (m, 8H), 8.50 (d, J = 9.2 Hz, 4H), 8.57 (d, J = 9.2 Hz, 4H), 8.78 (d, J = 6.8 Hz, 4H), 9.70 (s, 4H), 9.95 (s, 4H).
^{13}C NMR (125 MHz, D_2O) δ (ppm): 39.8 (CH_2), 47.6 (CH_2), 47.6 (CH_2), 124.8 (CH), 125.0 (C), 127.3 (C), 127.7 (CH), 128.1 (CH), 128.8 (C), 129.0 (C), 129.7 (CH), 130.6 (CH), 139.0 (CH), 141.8 (C), 142.7 (C) 149.0 (CH), 151.6 (CH), 155.1 (C).
Elemental analysis calcd (%) for $C_{56}H_{52}N_{16}O_{18}Pt_2$: C, 41.33, H, 3.22, N, 13.77; found: C, 41.56, H, 3.08, N, 13.67.

Chapter 5

Curriculum Vitae

ALESSIO TERENZI

Dipartimento di Chimica Inorganica
e Analitica "S. Cannizzaro"
Università di Palermo
Viale delle Scienze, Parco d'Orleans
90128, Palermo, Italy

e-mail: aterenzi@unipa.it
Personal Website: Ph.D. website University of Palermo

Academic Curriculum

Jan. 2010 - Jun. 2010

Visiting student (six months) at the "School of Chemistry, University of Birmingham, UK", working on the study of interactions between metal complexes and DNA.

Jan. - July 2009

Visiting student (six months) at the "Quimica Fundamental" department, University of La Coruña, Spain, working on synthesis via metal-directed self-assembly of Palladium and Platinum metallacycles, catenanes and inclusion complexes.

Jan. 2008 -

Ph.D. student in Chemistry, University of Palermo.

Nov. 2007

Qualification to practice chemistry.

Oct. 2007

Master Degree in Chemistry. Final marks: 110/110 cum laude. Experimental thesis title: "The interaction of native calf thymus DNA with Fe^{III}-dipyrido[3,2-a:2',3'-c]phenazine".

Feb. - Oct. 2006

ERASMUS project: (8 months) La Coruña University (Spain).

List of Publications

1. A. Terenzi, G. Barone, A. Palumbo Piccionello, A. Guarcello, G. Giorgi, A. Pace - "*Synthesis and characterization of Cu^{II}, Ni^{II} and Zn^{II} complexes of 3,5-bis(2'-pyridyl)-1,2,4-oxadiazole and 3-(2'-pyridyl)5-(phenyl)-1,2,4-oxadiazole ligands*", Submitted.

2. A. Terenzi, C. Ducani, L. Male, G. Barone, M. J. Hannon, - "*DNA interaction studies by linear dichroism, gel electrophoresis and PCR of Cu^{II}, Ni^{II} and Zn^{II} functionalized Salphen complexes*" - Submitted.

3. A. Terenzi, C. Ducani, V. Blanco, C. Peinador, J. M. Quintela, P. J. Bednarski, G. Barone and M. J. Hannon - "*DNA binding studies and cytoxicity of a dinuclear Pt^{II} diazapyrenium-based metallo-supramolecular rectangular box*" - Submitted.

4. V. Blanco, M. D. García, A. Terenzi, E. Pía, A. Fernandez-Mato, C. Peinador, and J. M. Quintela, - "*Complexation and Extraction of PAHs to the Aqueous Phase with a Dinuclear Pt^{II} Diazapyrenium-Based Metallacycle*"- Chemistry: European Journal, 2010, 16, 12373 - 12380. DOI: 10.1002/chem.201002051

   Featured on the journal front cover: DOI: 10.1002/chem.201090203

5. A. Terenzi, G Barone, A. Palumbo Piccionello, G. Giorgi, A. Guarcello, P. Portanova, G. Calvaruso, S. Buscemi, N. Vivona, A. Pace, - "*Synthesis, characterization, cellular uptake and interaction with native DNA of a bis(pyridyl)-1,2,4-oxadiazole copper(II) complex*" - Dalton Transaction, 2010, 39, 9140 - 9145. DOI: 10.1039/c0dt00266f

6. G. Barone, A. Ruggirello, A. Silvestri, A. Terenzi, V. Turco Liveri, - "*Fluorescence emission and enhanced photochemical stability of Zn^{II}-5-triethyl ammonium methyl salicylidene ortho-phenylendiiminate interacting with native DNA*" - Journal of Inorganic Biochemistry, 2010, 104, 765 - 773. DOI:10.1016/j.jinorgbio.2010.03.012

7. G. Barone, N. Gambino, A. Ruggirello, A. Silvestri, A. Terenzi, V. Turco Liveri - "*Spectroscopic study of the interaction of Ni^{II}-5-triethyl ammonium methyl salicylidene ortho-phenylendiiminate with native DNA*" - Journal of Inorganic Biochemistry, 2009, 103, 731 - 737. DOI:10.1016/j.jinorgbio.2009.01.006

8. A.Terenzi, G. Barone, A. Silvestri, A. M. Giuliani, A. Ruggirello, V. Turco Liveri, - "*The interaction of native calf thymus DNA with Fe^{III}- dipyrido[3,2-a:2',3'-c]phenazine*" - Journal of Inorganic Biochemistry, 2009, 103, 1 - 9. DOI:10.1016/j.jinorgbio.2008.08.011

9. G. Barone, A. Longo, A. Ruggirello, A. Silvestri, A. Terenzi, V. Turco Liveri, - "*Confinement effects on the interaction of native DNA with Cu^{II}-5-triethyl ammonium methyl salicylidene ortophenylendiiminate in $C_{12}E_4$ liquid crystals*" - Dalton Trans., 2008, 4172 - 4178. DOI:10.1039/b804610g

Conferences and Workshops

1. A. Terenzi, G. Barone: "Complessi metallici e DNA nativo: interazione di intercalazione", Convegno Congiunto delle Sezioni Calabria e Sicilia della Società Chimica Italiana, Palermo (Italy), 2-3 Dicembre 2010, O34 of the Book of Abstracts.

2. G. Barone, A. Terenzi, R. Varsalona, M.L. Turco Liveri: "*The interaction of native calf thymus DNA with dipyrido[3,2-a:2',3'-c]phenazine and its heteroleptic Iron(III) complexes*", XXI Italian-Spanish Congress on Thermodynamics of Metal Complexes (ISMEC 2010), Bilbao (Spain), 7 -11 June 2010, page OC14 of the Book of Abstracts.

3. European summerschool in quantum chemistry (ESQC); 6 - 19 September 2009

4. G. Barone, A. Ruggirello, A. Silvestri, A. Terenzi, V. Turco Liveri: "*The interaction of native DNA with Ni^{II}, Cu^{II} and Zn^{II} complexes of 5-triethyl ammonium methyl salicylidene orthophenilendiimine*", XX Italian-Spanish Congress on Thermodynamics of Metal Complexes (ISMEC 2009), Tirrenia (Pisa), 7 - 11 June 2009, Book of Abstracts, OC19.

5. A. Terenzi, - "*Transition metal complexes as DNA-intercalators*" - Scuola Nazionale di Chimica Bioinorganica per Dottorandi - 14 - 16 Settembre 2008, Napoli, Book of Abstracts, P12.

6. G. Barone, N. Gambino, A. Ruggirello, A. Silvestri, A. Terenzi , V. Turco Liveri - "*Spectroscopic Study of the Interaction of Ni^{II}-5-triethyl Ammonium Methyl Salicylidene orto-phenylendiiminato with Native DNA*" - 9th European Biological Inorganic Chemistry Conference Eurobic9, 2-6 September, 2008, Wrocław, Poland, Book of Abstracts, P8.

7. A. Terenzi, G. Barone, G. Ruisi, A. Silvestri - "*The interaction of native calf thymus DNA with Fe(III)- dipyrido[3,2-a:2',3'-c]phenazine chloride*" - XXXV Congresso Nazionale della Divisione di Chimica Inorganica della Società Chimica Italiana, Milano, 3 - 7 Settembre 2007, Book of Abstracts, P24.

Appendix A

NMR spectra

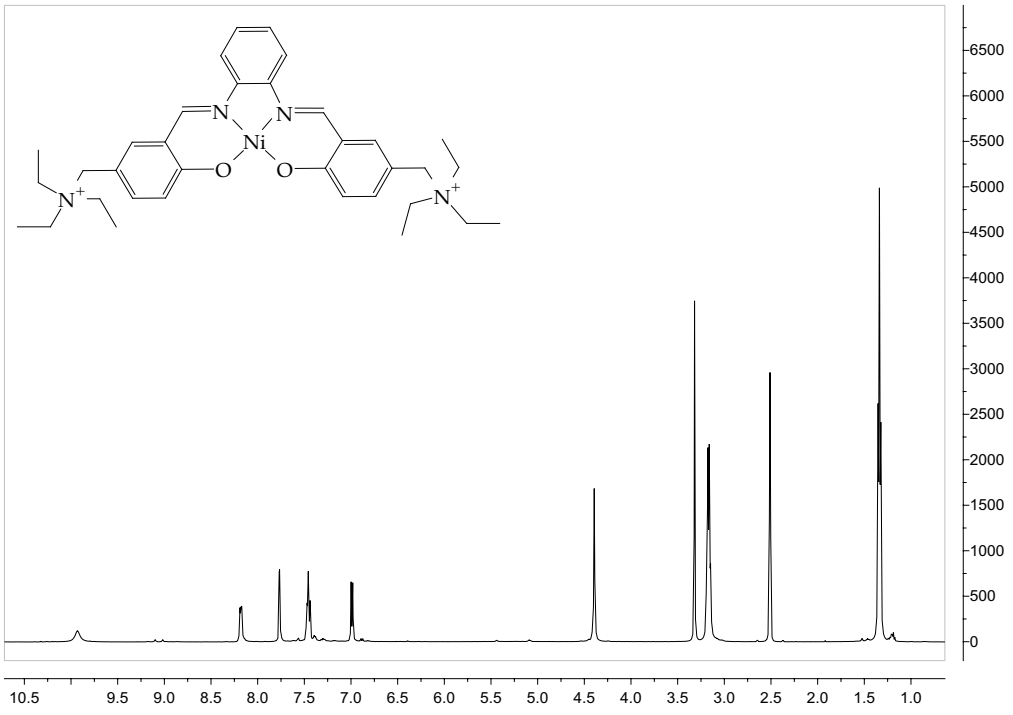

Figure A.1: ^{1}H NMR (500 MHz, DMSO) spectrum of the compound NiL^{2+}

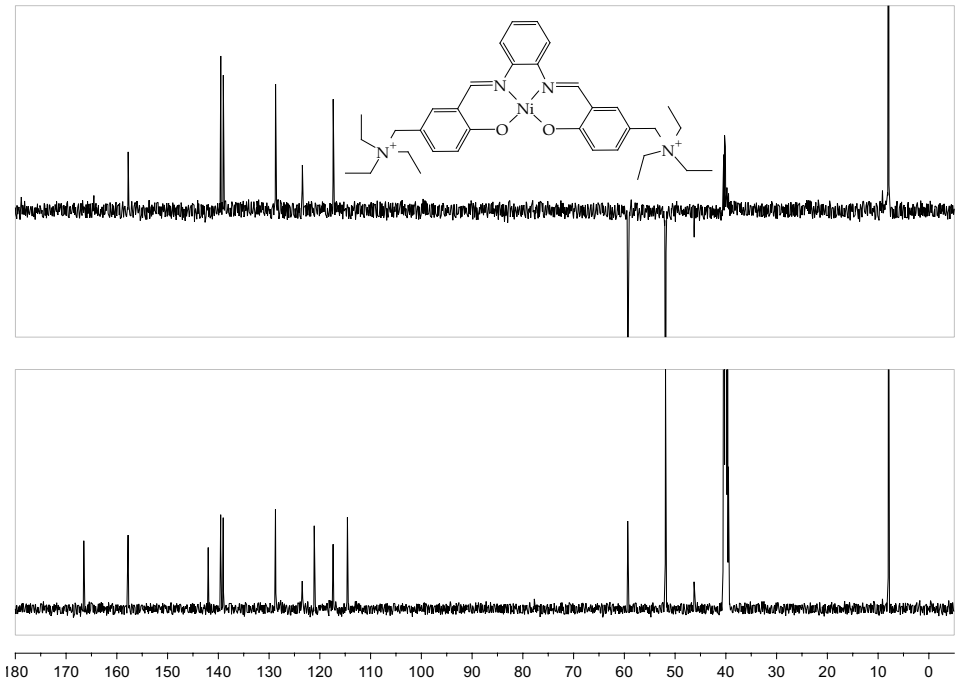

Figure A.2: ^{13}C NMR and DEPT (125 MHz, DMSO) spectra of the compound NiL^{2+}

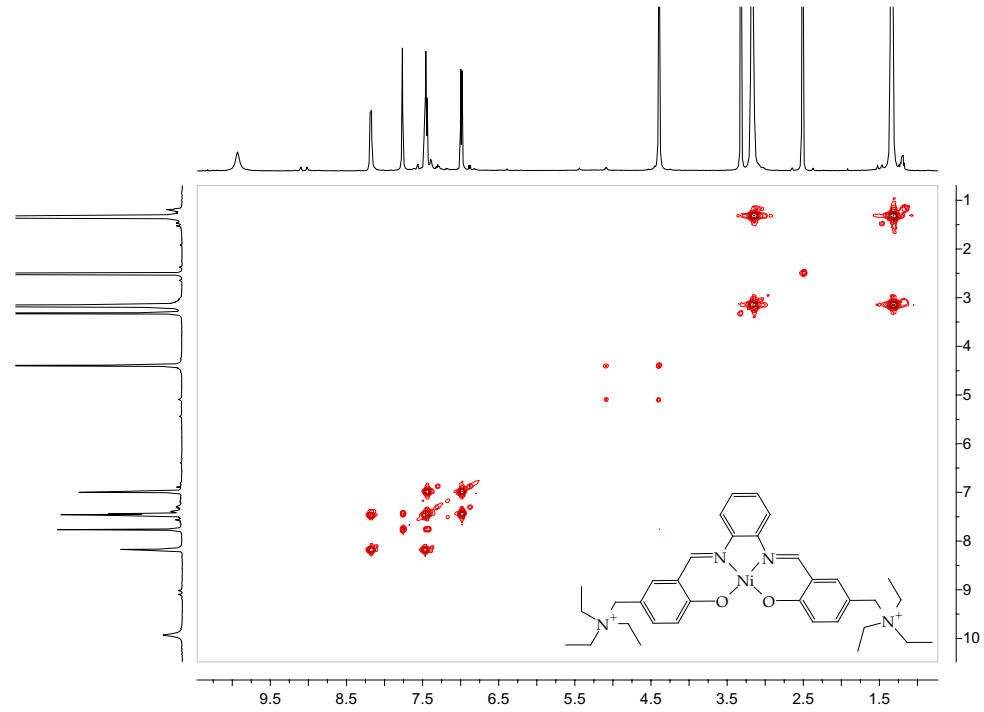

Figure A.3: COSY (500 MHz, DMSO) spectrum of the compound NiL^{2+}

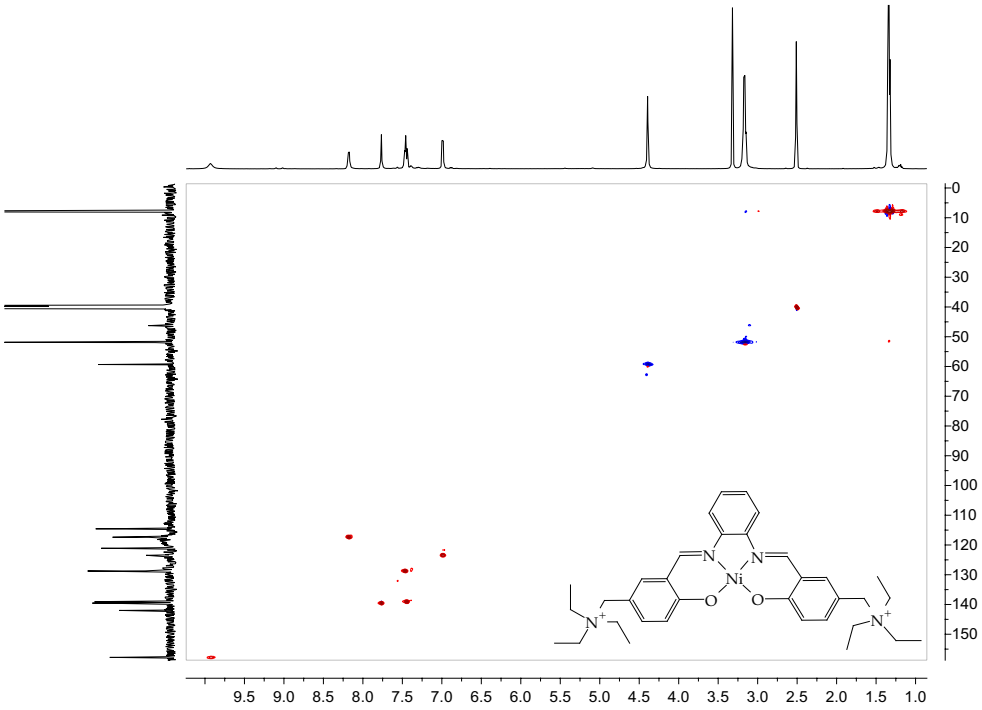

Figure A.4: HSQC (500 MHz, DMSO) spectrum of the compound NiL^{2+}

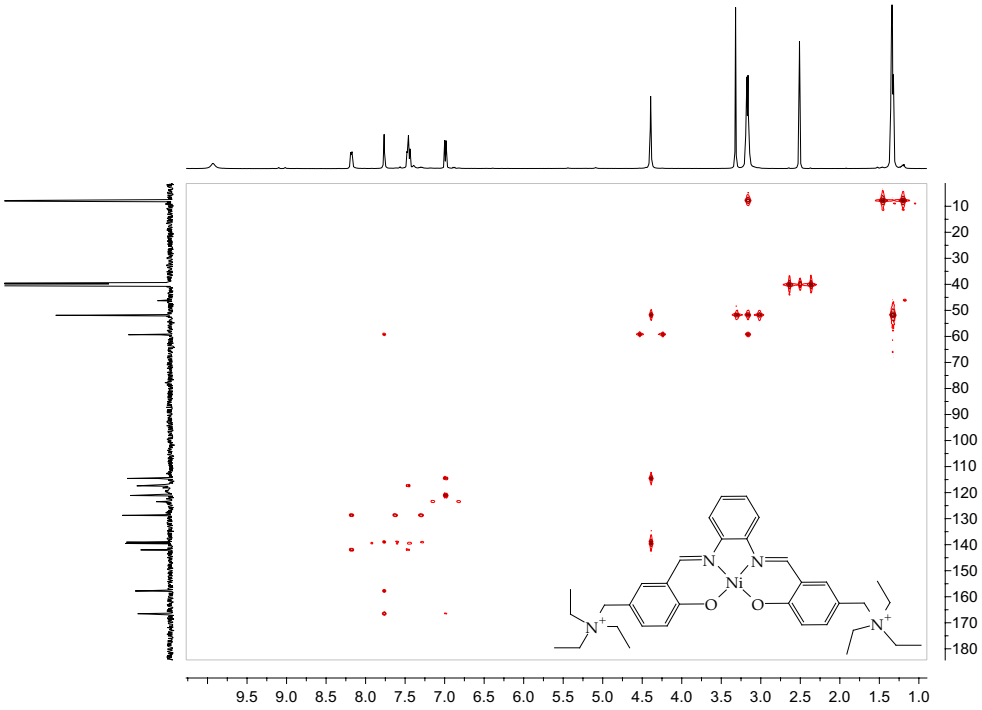

Figure A.5: HMBC (500 MHz, DMSO) spectrum of the compound NiL^{2+}

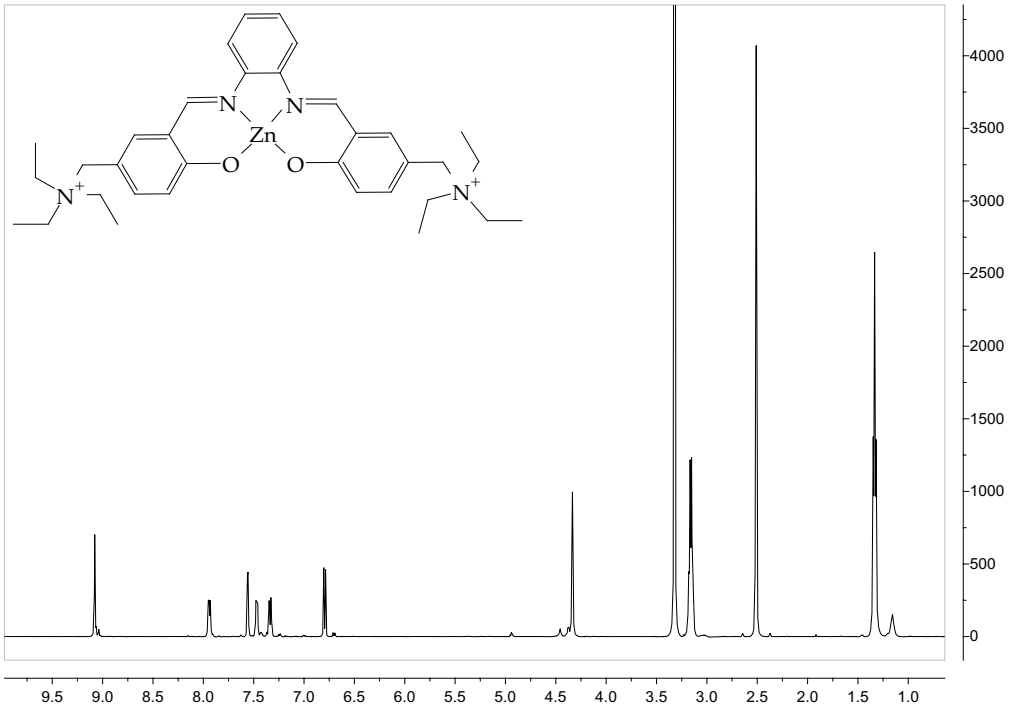

Figure A.6: ^{1}H NMR (500 MHz, DMSO) spectrum of the compound ZnL^{2+}

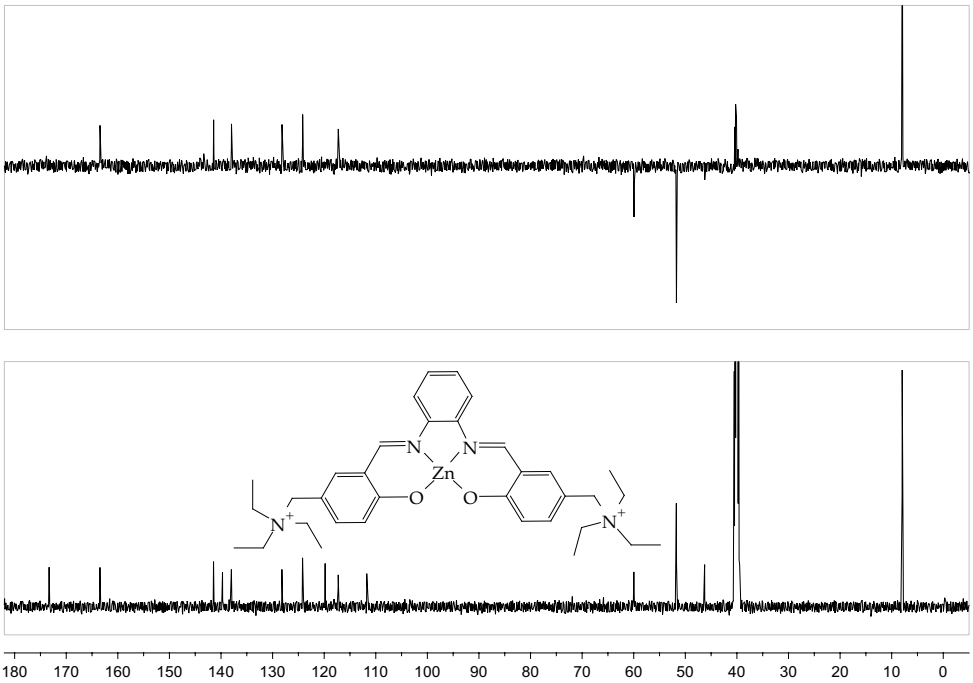

Figure A.7: ^{13}C NMR and DEPT (125 MHz, DMSO) spectra of the compound ZnL^{2+}

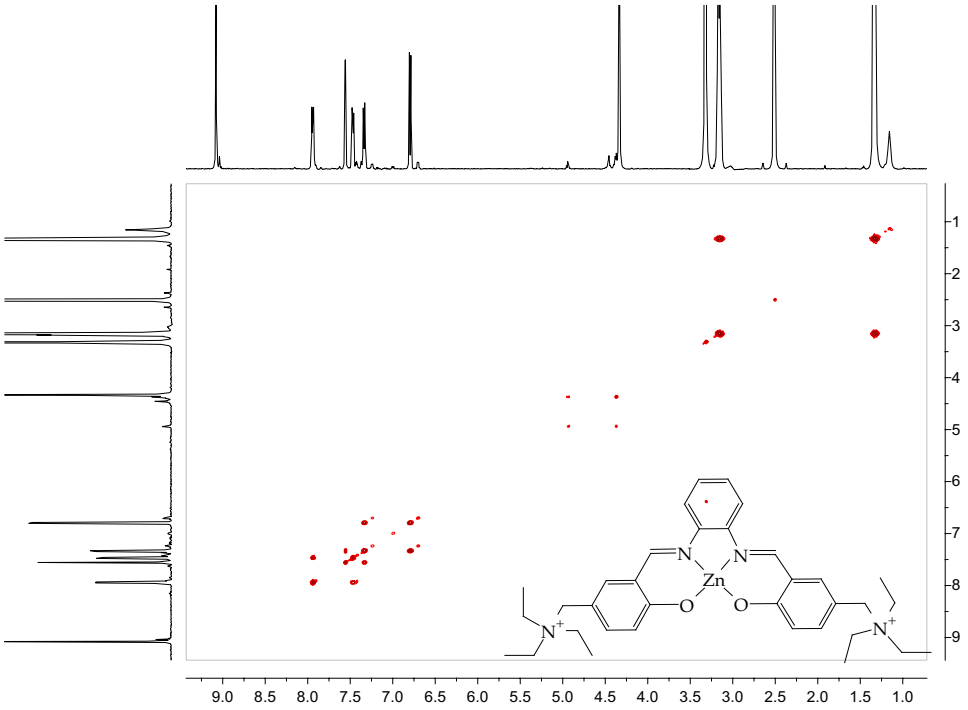

Figure A.8: COSY (500 MHz, DMSO) spectrum of the compound ZnL^{2+}

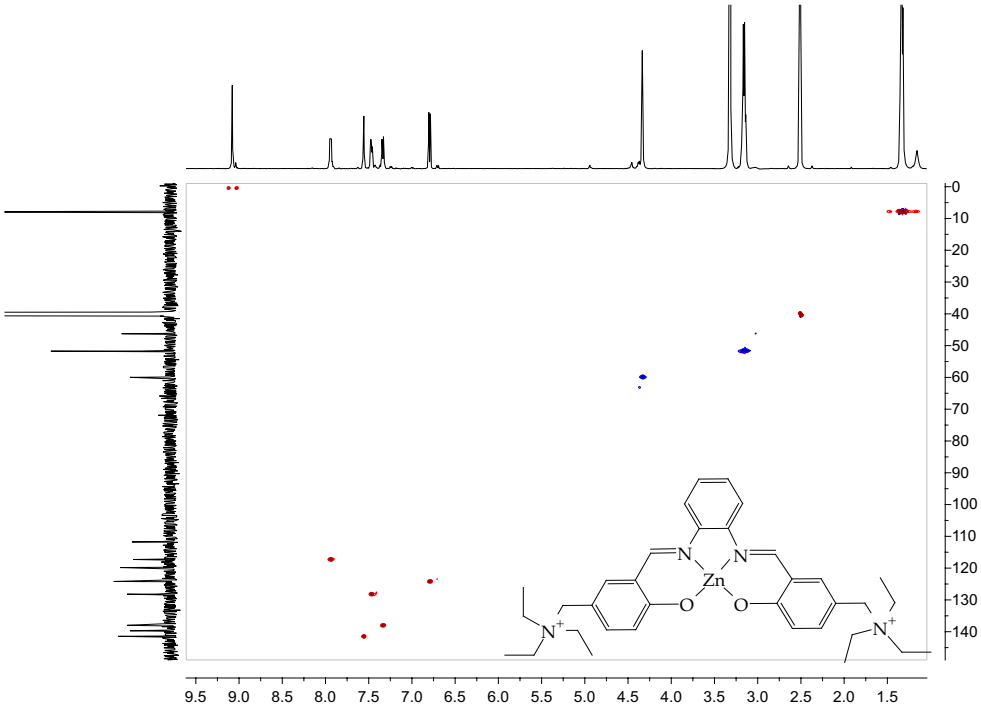

Figure A.9: HSQC (500 MHz, DMSO) spectrum of the compound ZnL^{2+}

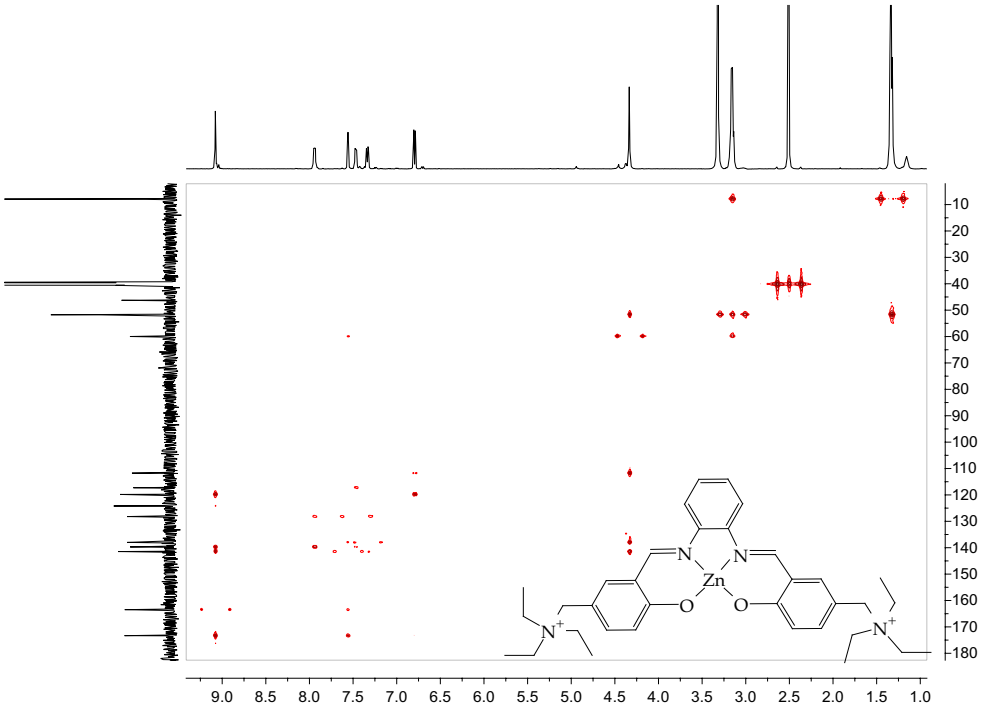

Figure A.10: HMBC (500 MHz, DMSO) spectrum of the compound ZnL^{2+}

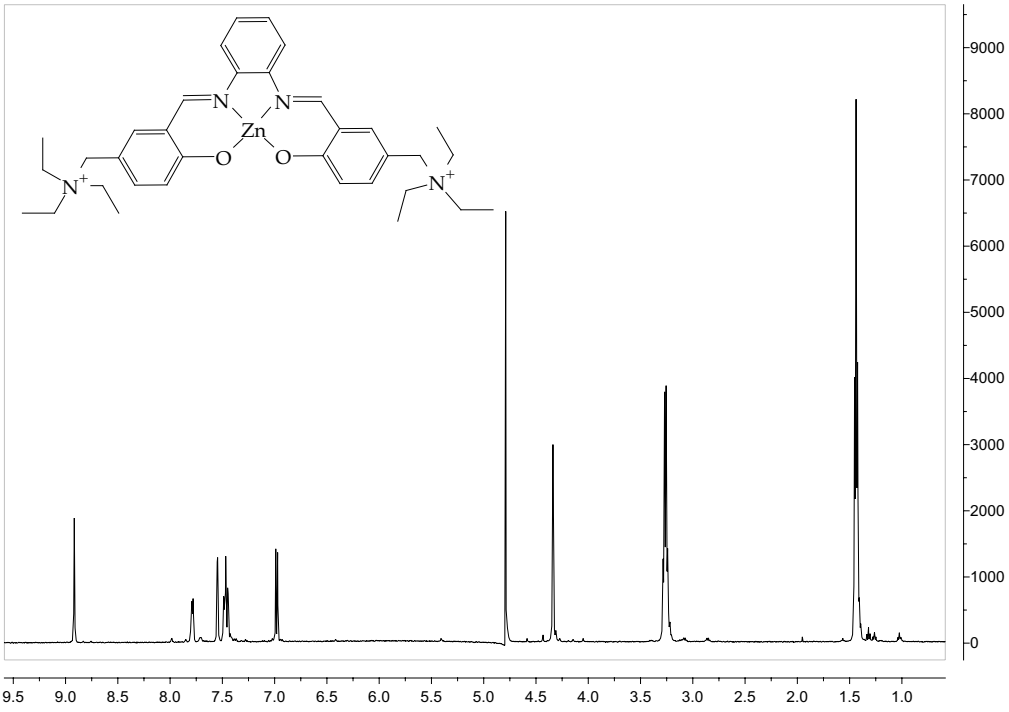

Figure A.11: ^{1}H NMR (500 MHz, D_2O) spectrum of the compound ZnL^{2+}

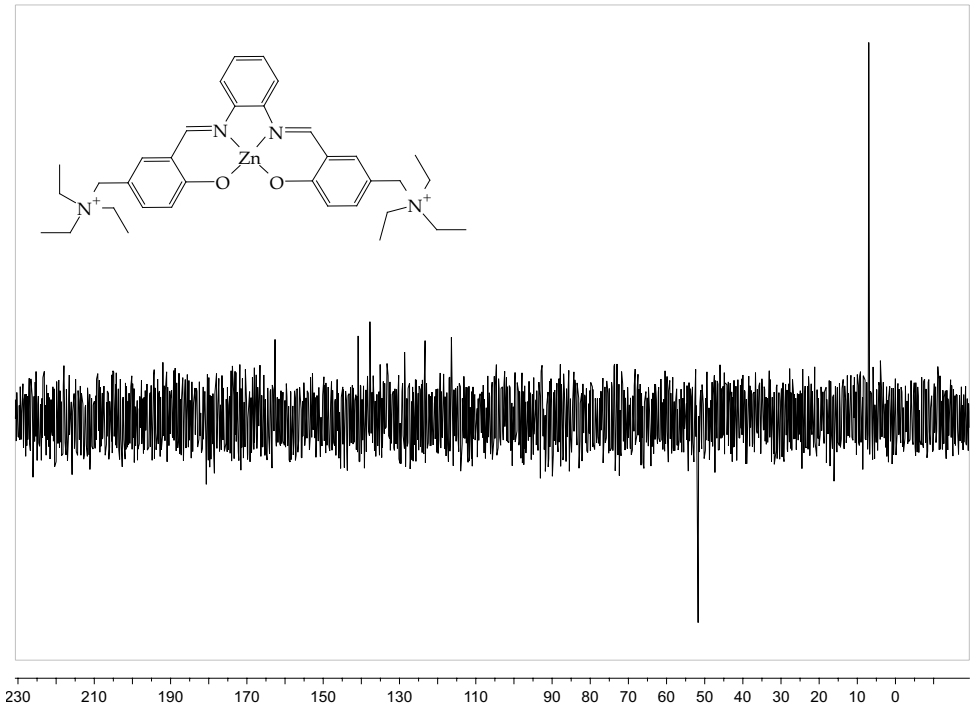

Figure A.12: DEPT ^{13}C NMR (125 MHz, D_2O) spectra of the compound ZnL^{2+}

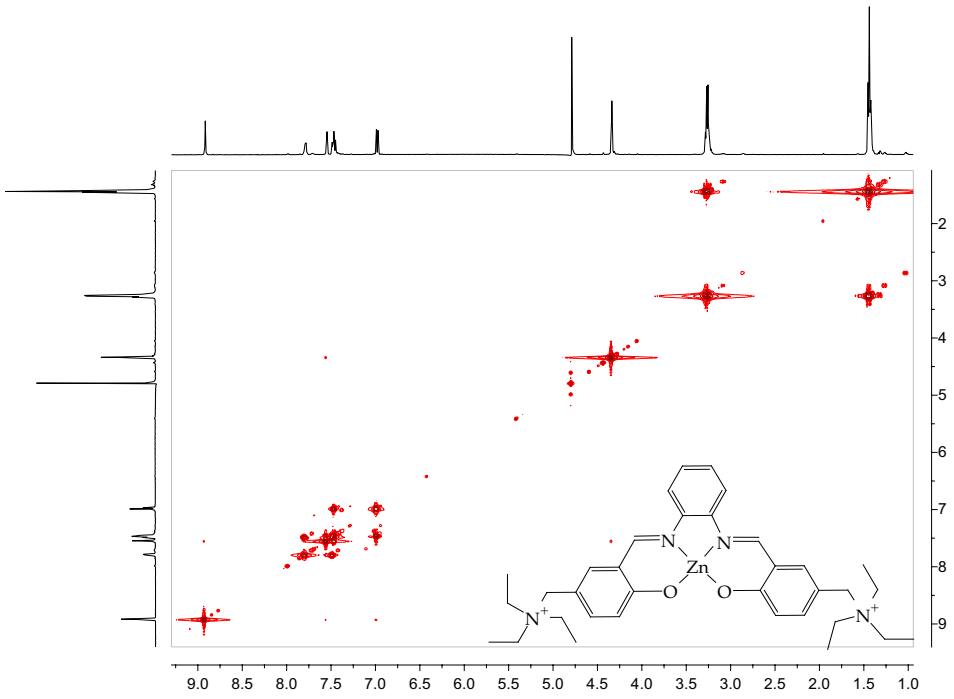

Figure A.13: COSY (500 MHz, D_2O) spectrum of the compound ZnL^{2+}

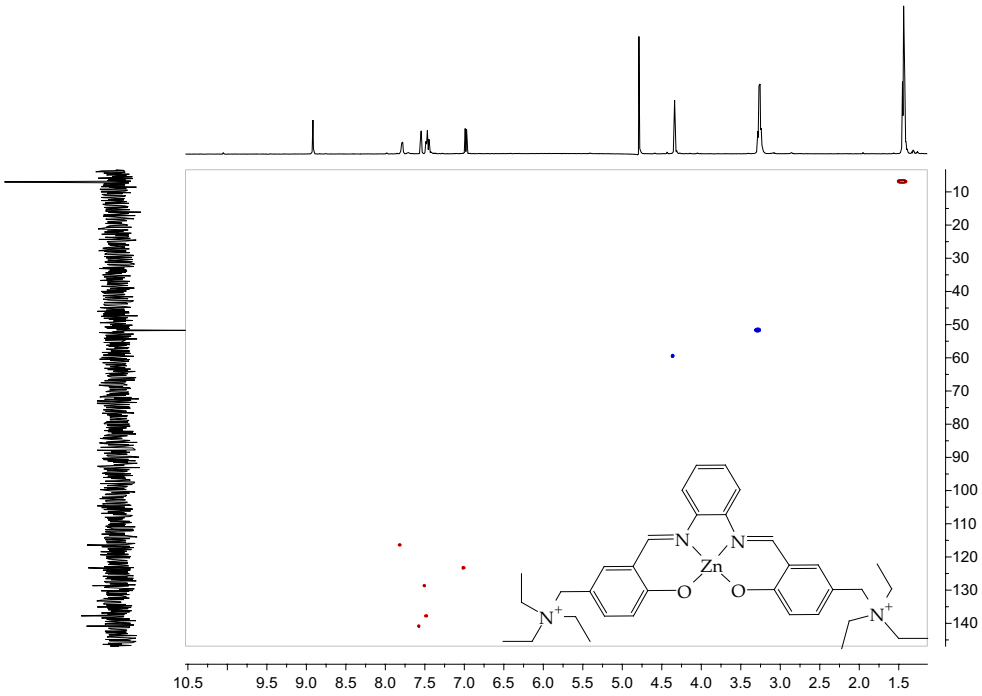

Figure A.14: HSQC (500 MHz, D_2O) spectrum of the compound ZnL^{2+}

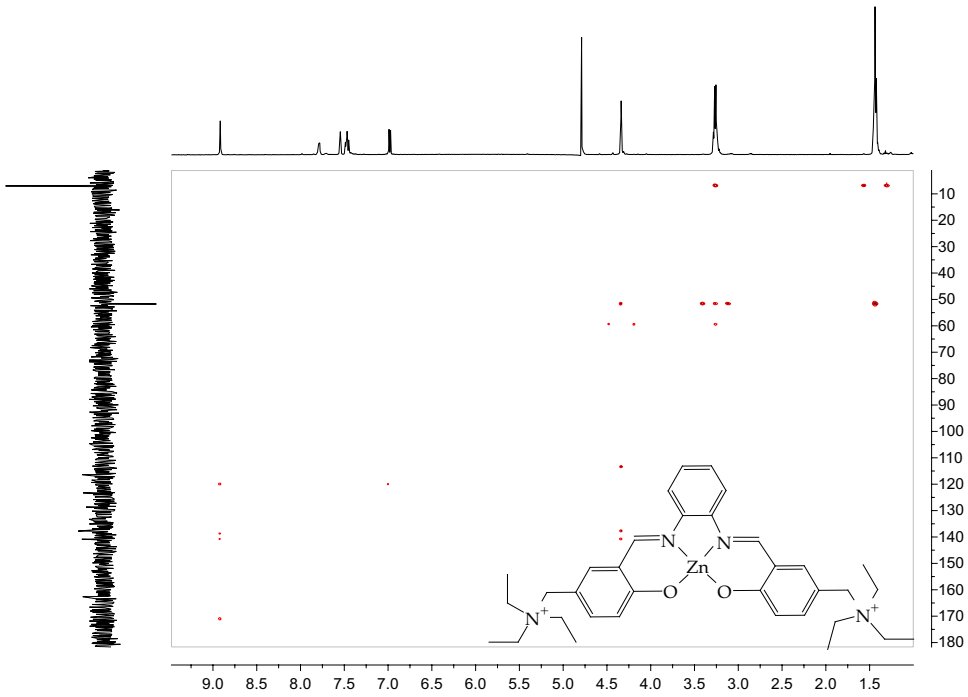

Figure A.15: HMBC (500 MHz, D_2O) spectrum of the compound ZnL^{2+}

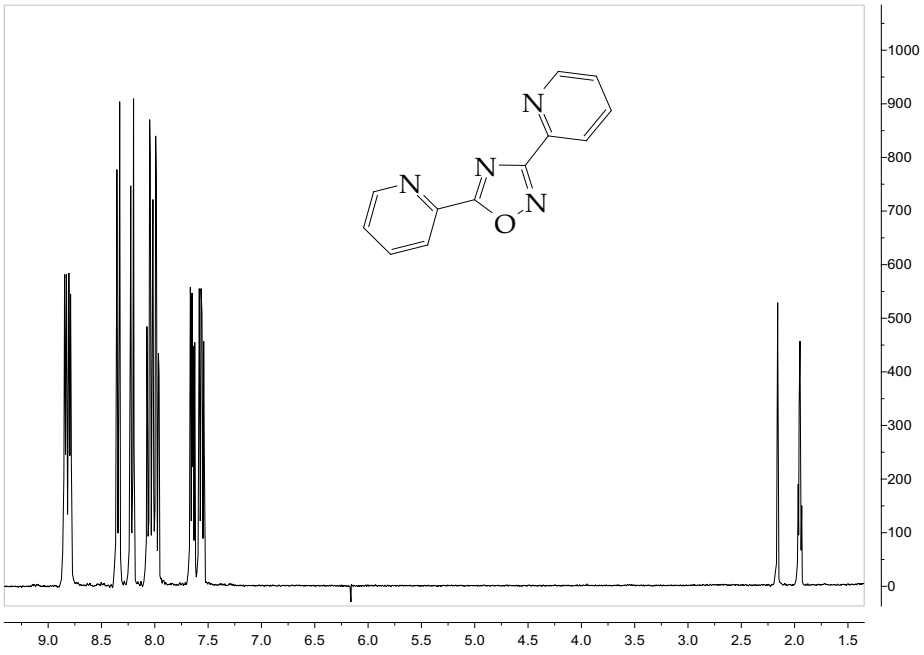

Figure A.16: ^{1}H NMR (300 MHz, CD_3CN) spectrum of the compound bipyOXA

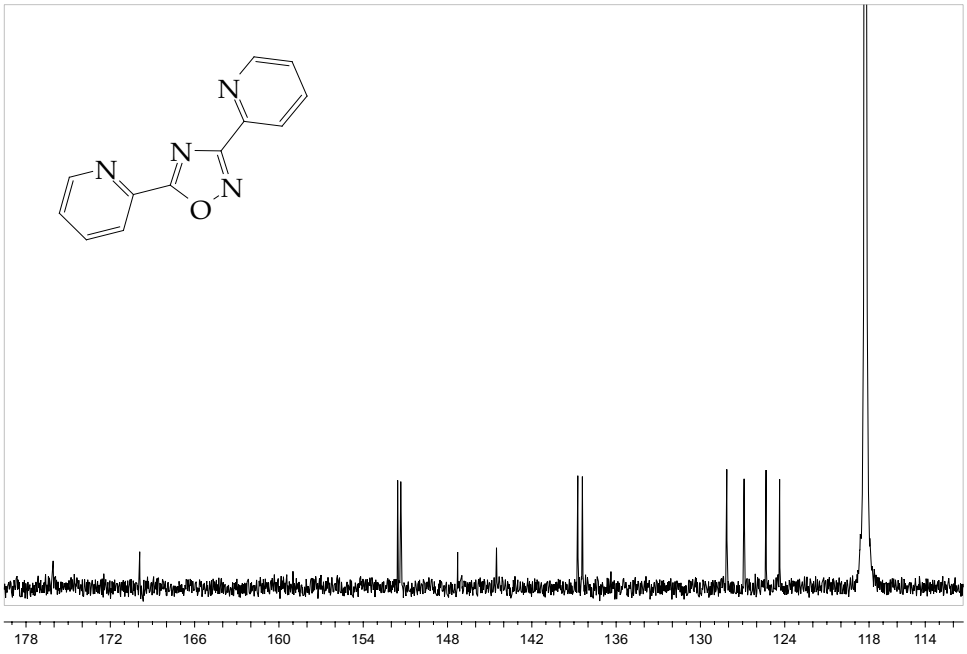

Figure A.17: ^{13}C NMR (75 MHz, CD_3CN) spectrum of the compound bipyOXA

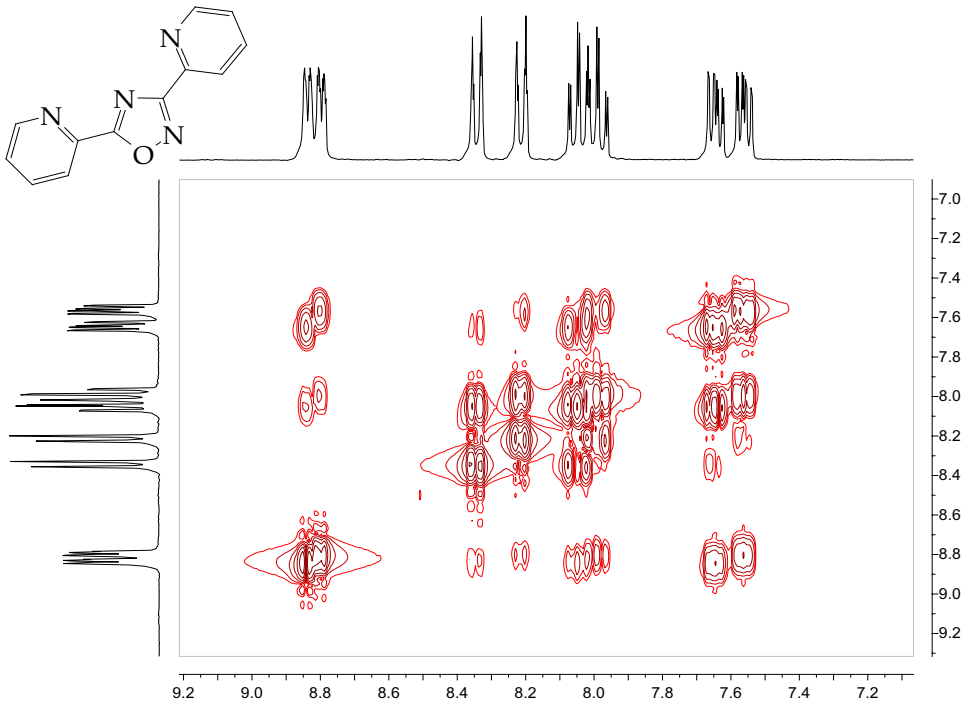

Figure A.18: COSY (300 MHz, CD_3CN) spectrum of the compound bipyOXA

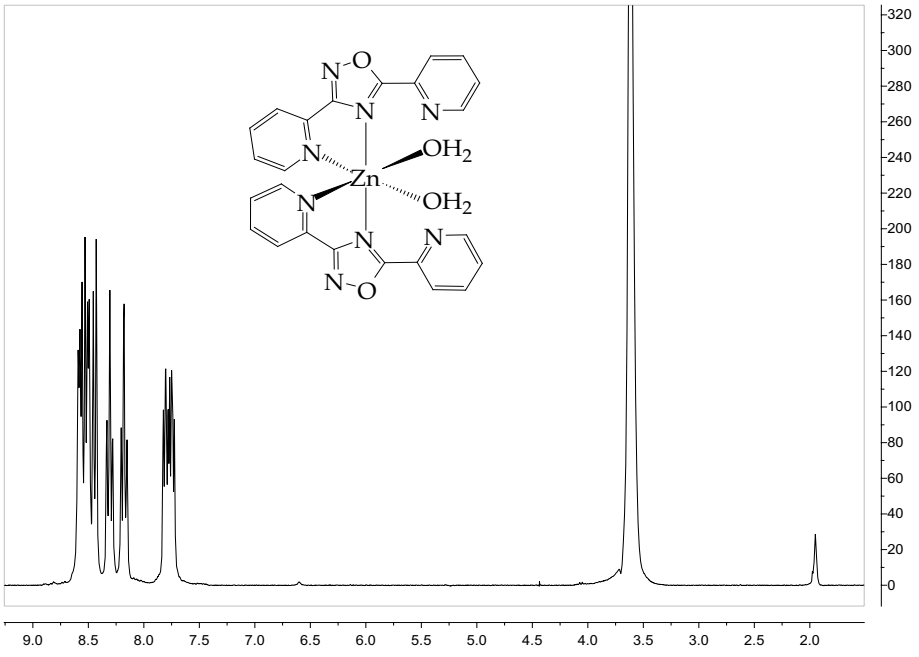

Figure A.19: ^{1}H NMR (300 MHz, CD_3CN) spectrum of the Zn^2 complex with bipyOXA

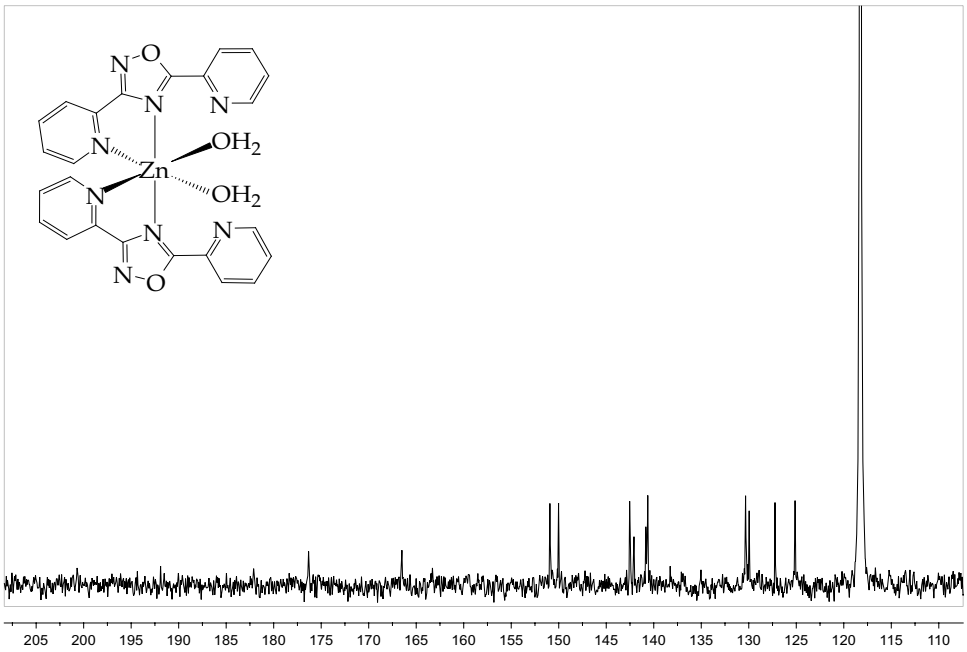

Figure A.20: ^{13}C NMR (75 MHz, CD_3CN) spectrum of the Zn^2 complex with bipyOXA

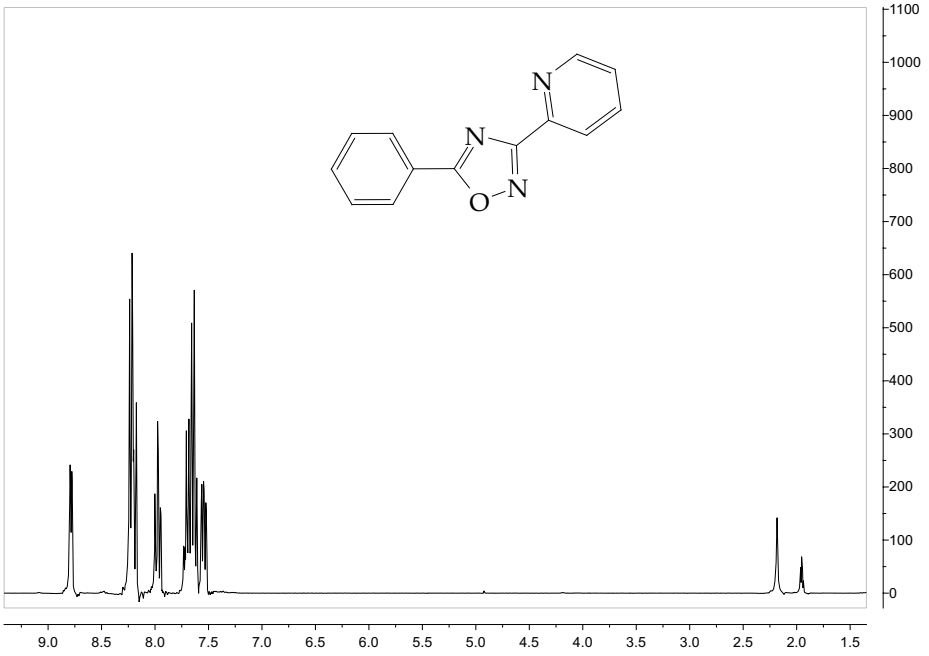

Figure A.21: ^{1}H NMR (300 MHz, CD_3CN) spectrum of the compound pyOXA

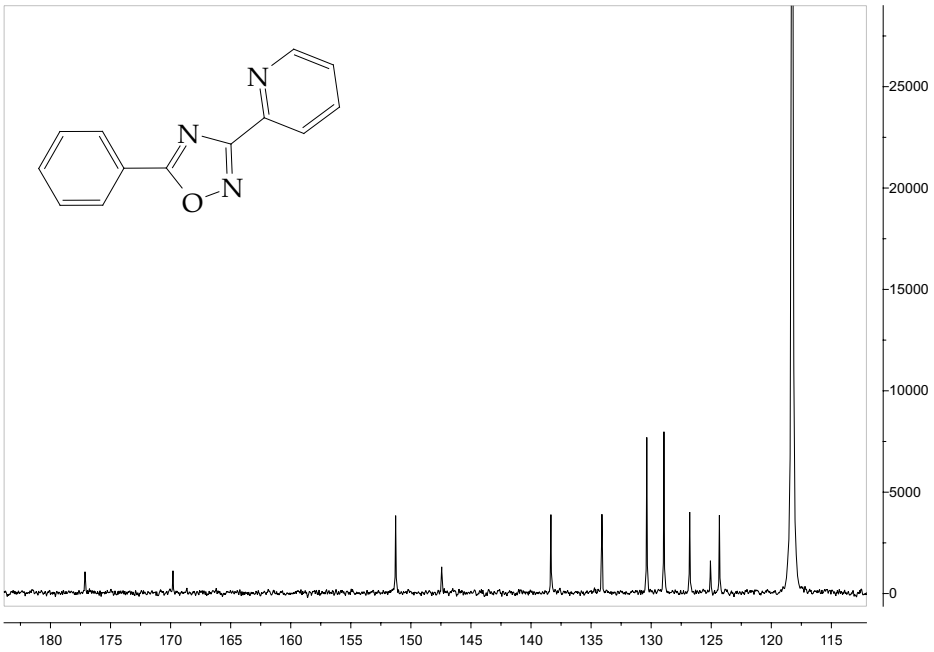

Figure A.22: ^{13}C NMR (75 MHz, CD_3CN) spectrum of the compound pyOXA

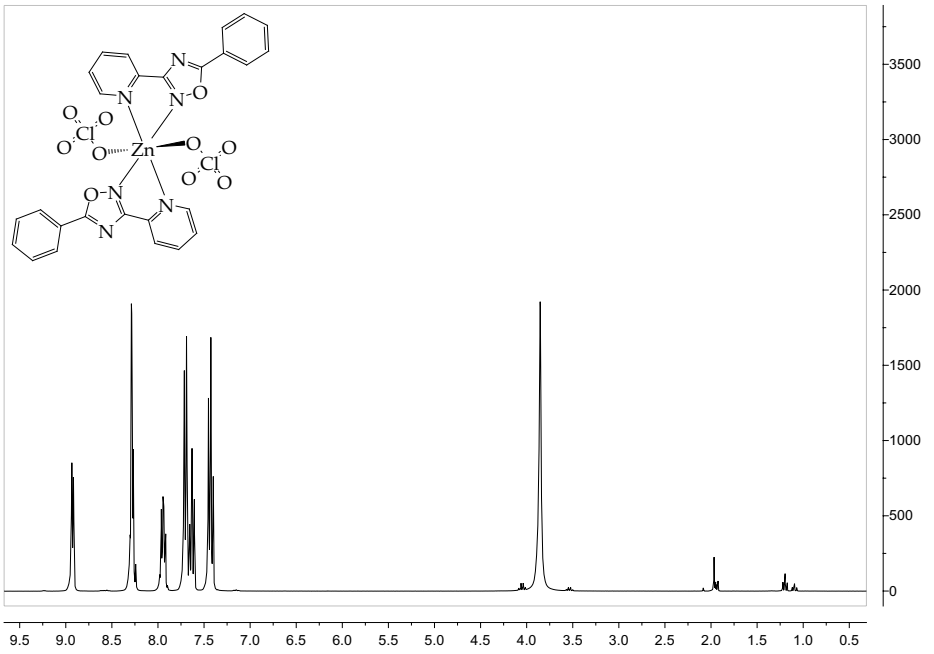

Figure A.23: ^{1}H NMR (300 MHz, CD_3CN) spectrum of the Zn^2 complex with pyOXA

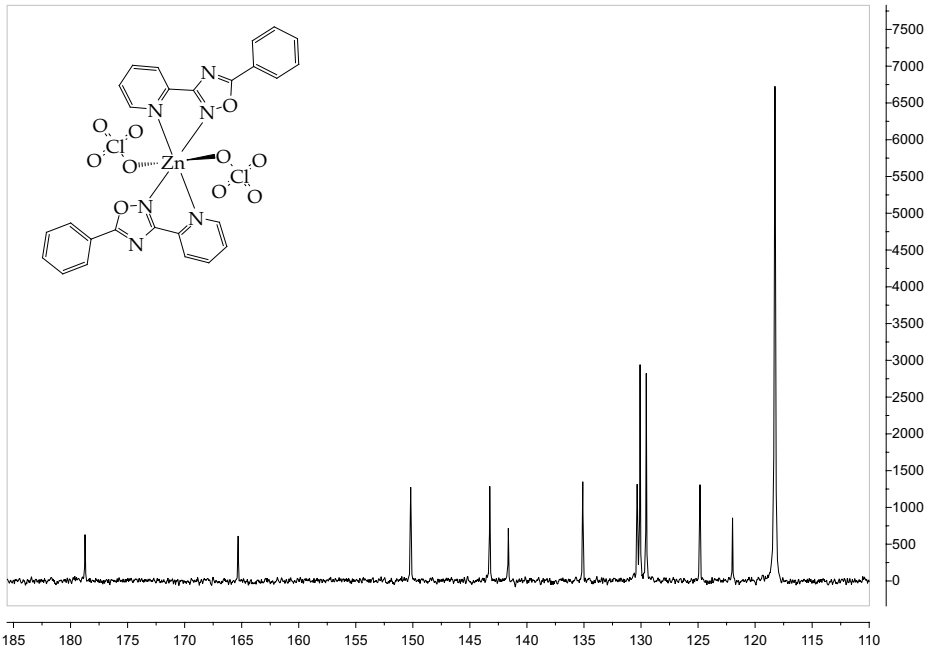

Figure A.24: ^{13}C NMR (75 MHz, CD_3CN) spectrum of the Zn^2 complex with pyOXA

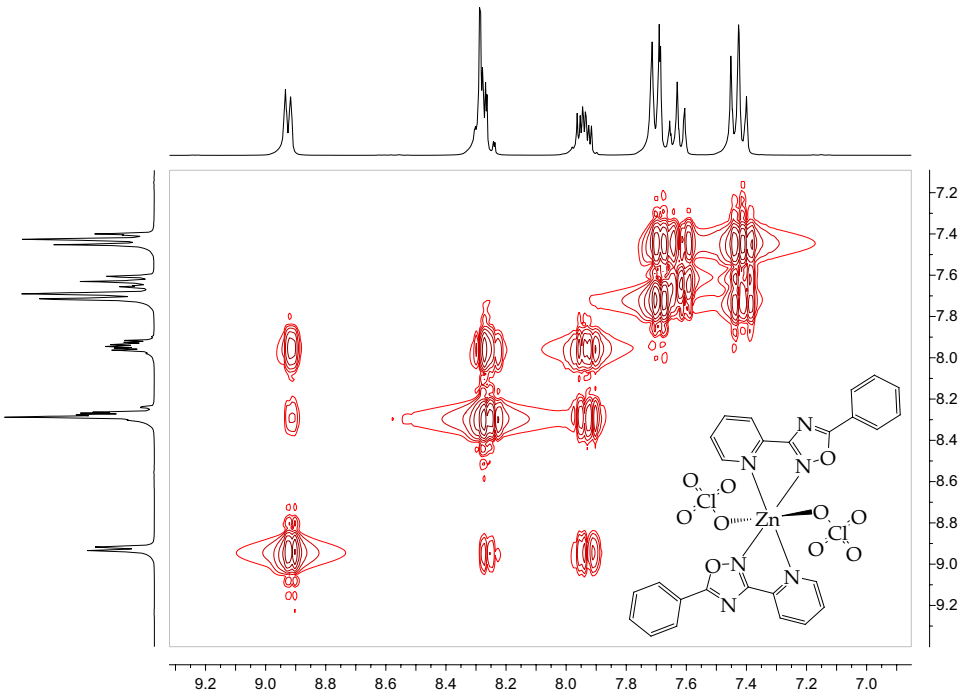

Figure A.25: COSY (300 MHz, CD_3CN) spectrum of the Zn^2 complex with pyOXA

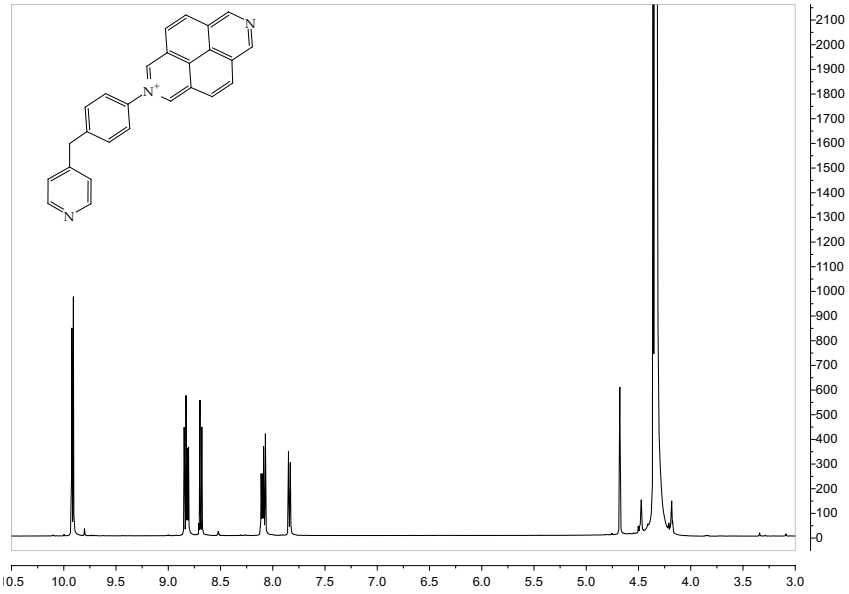

Figure A.26: ^{1}H NMR (500 MHz, CD_3NO_2) spectrum of the compound [DAzP]PF_6

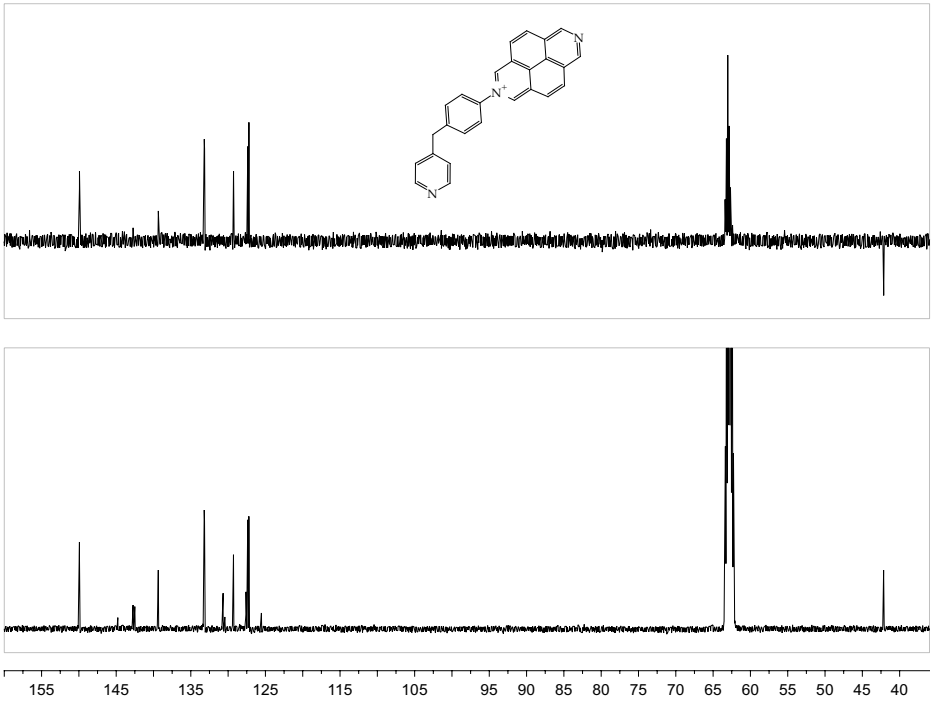

Figure A.27: ^{13}C NMR (125 MHz, CD_3NO_2) spectrum of the compound [DAzP]PF_6

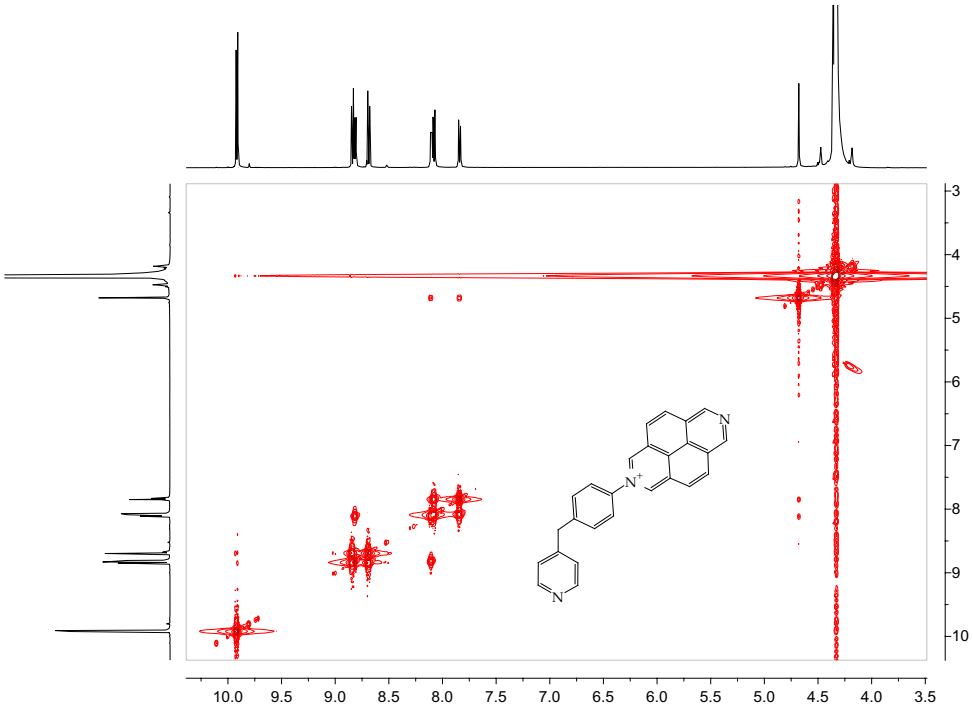

Figure A.28: COSY (500 MHz, CD_3NO_2) spectrum of the compound [DAzP]PF_6

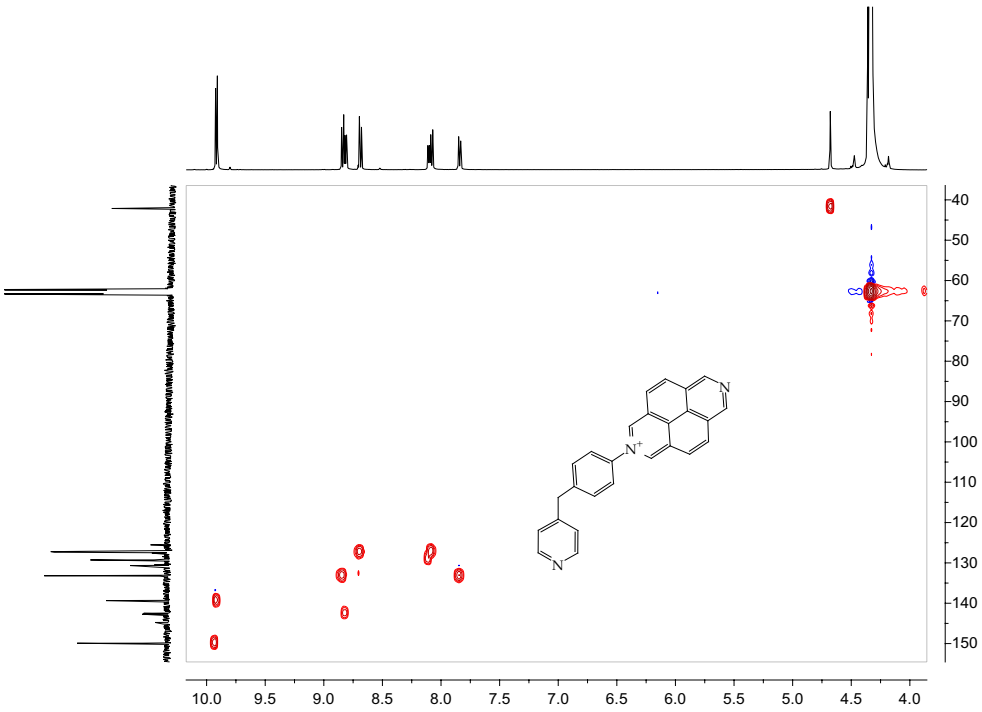

Figure A.29: HSQC (500 MHz, CD_3NO_2) spectrum of the compound [DAzP]PF_6

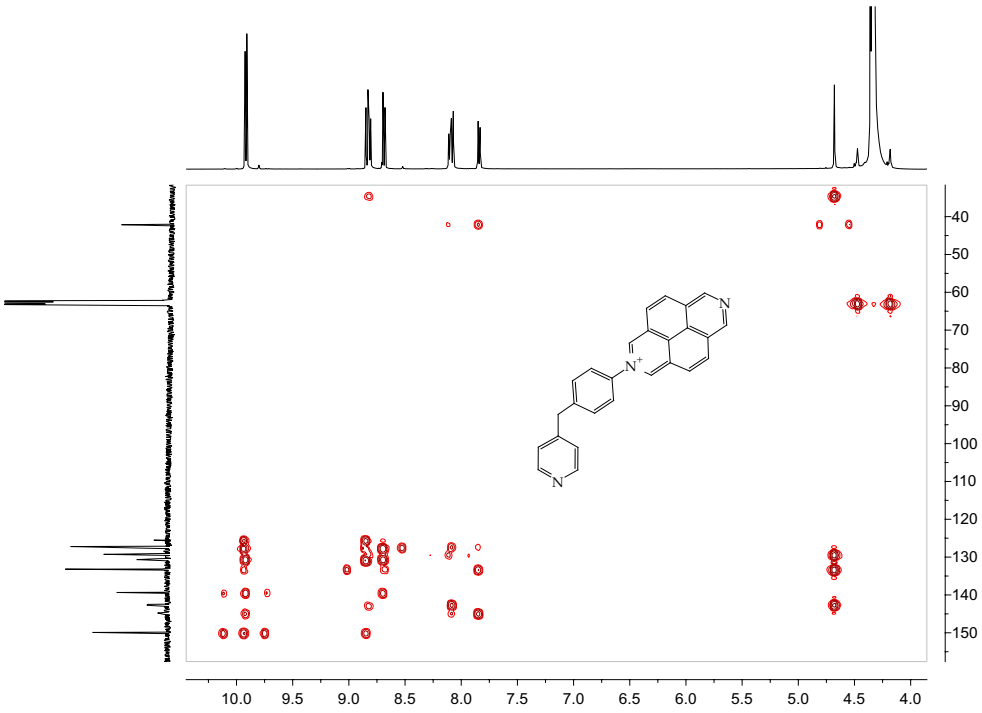

Figure A.30: HMBC (500 MHz, CD_3NO_2) spectrum of the compound [DAzP]PF_6

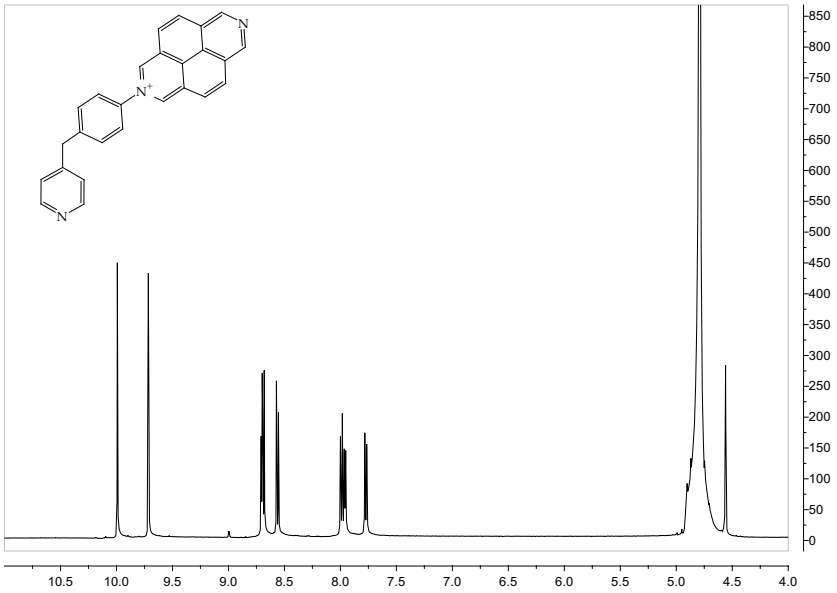

Figure A.31: ^{1}H NMR (500 MHz, D_2O) spectrum of the compound [DAzP]NO_3

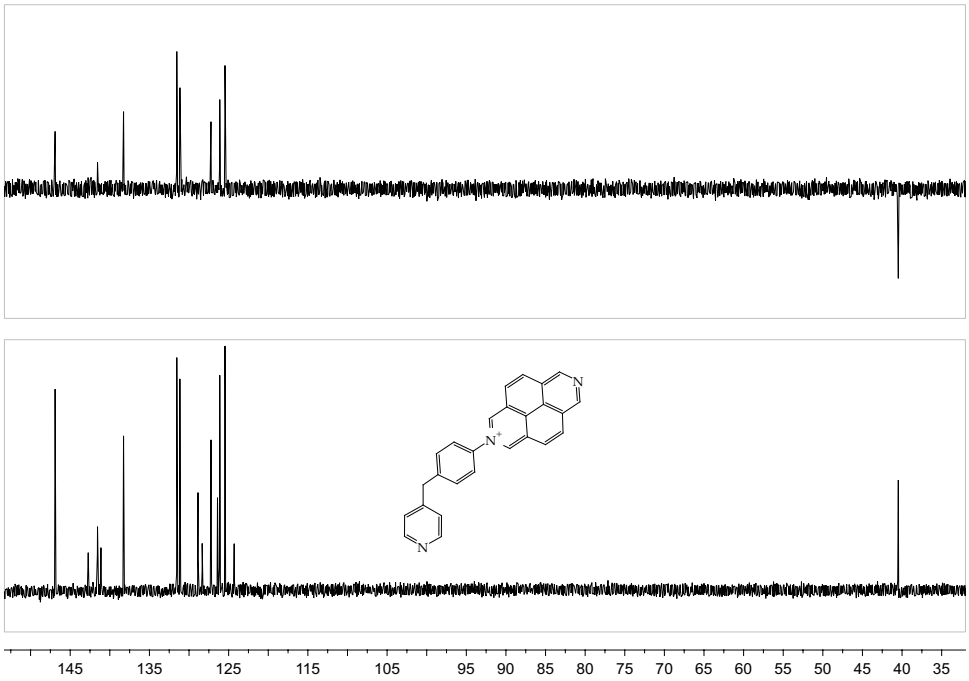

Figure A.32: ^{13}C NMR (125 MHz, D_2O) spectrum of the compound [DAzP]NO_3

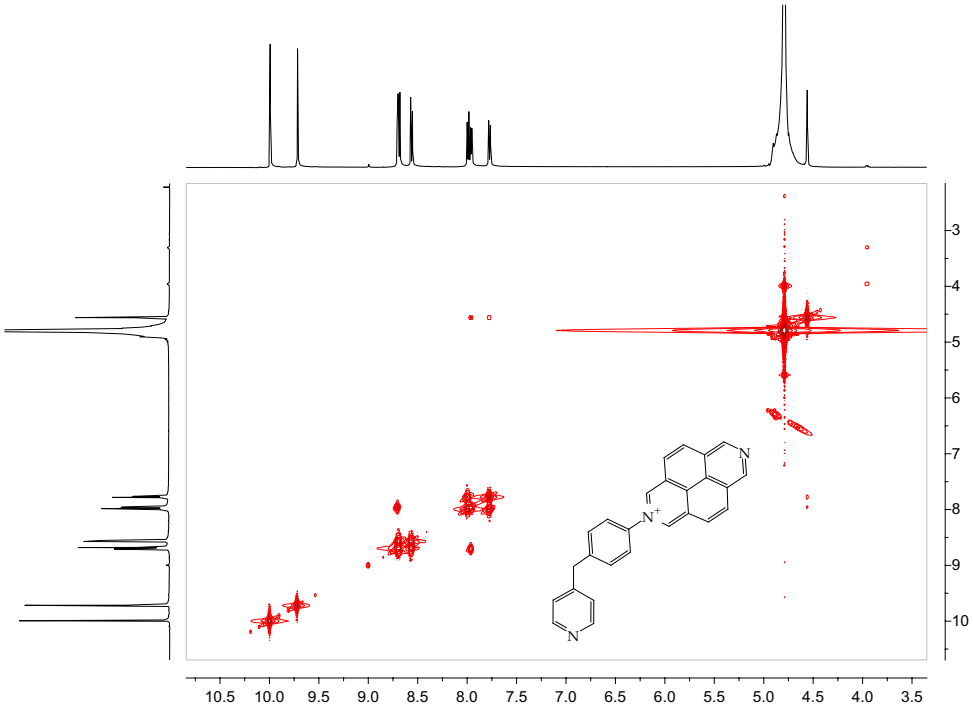

Figure A.33: COSY (500 MHz, D_2O) spectrum of the compound [DAzP]NO_3

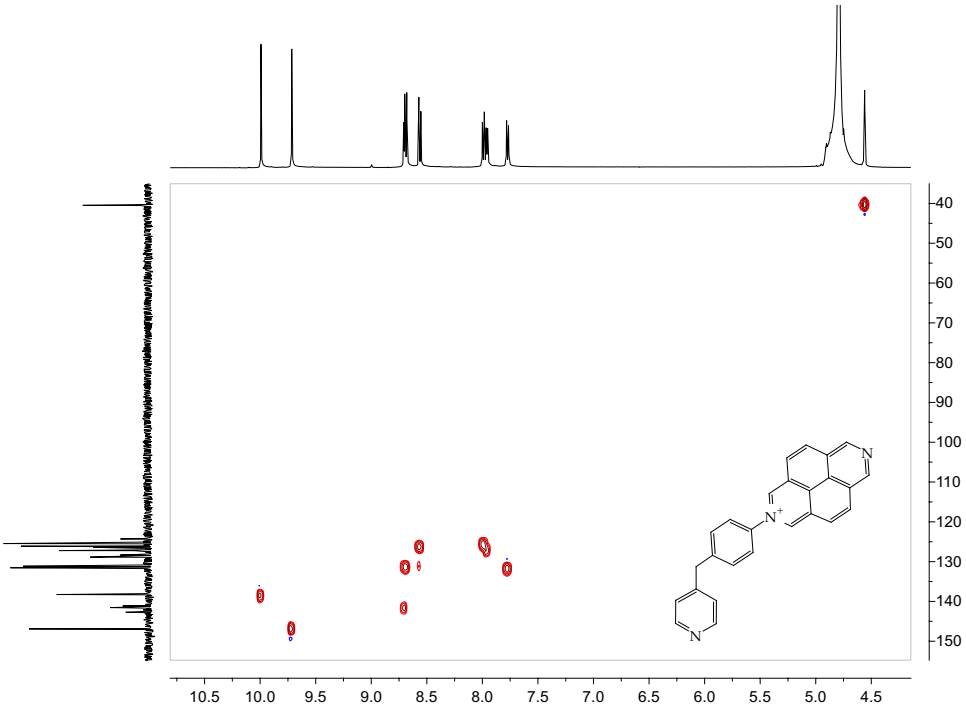

Figure A.34: HSQC (500 MHz, D_2O) spectrum of the compound [DAzP]NO_3

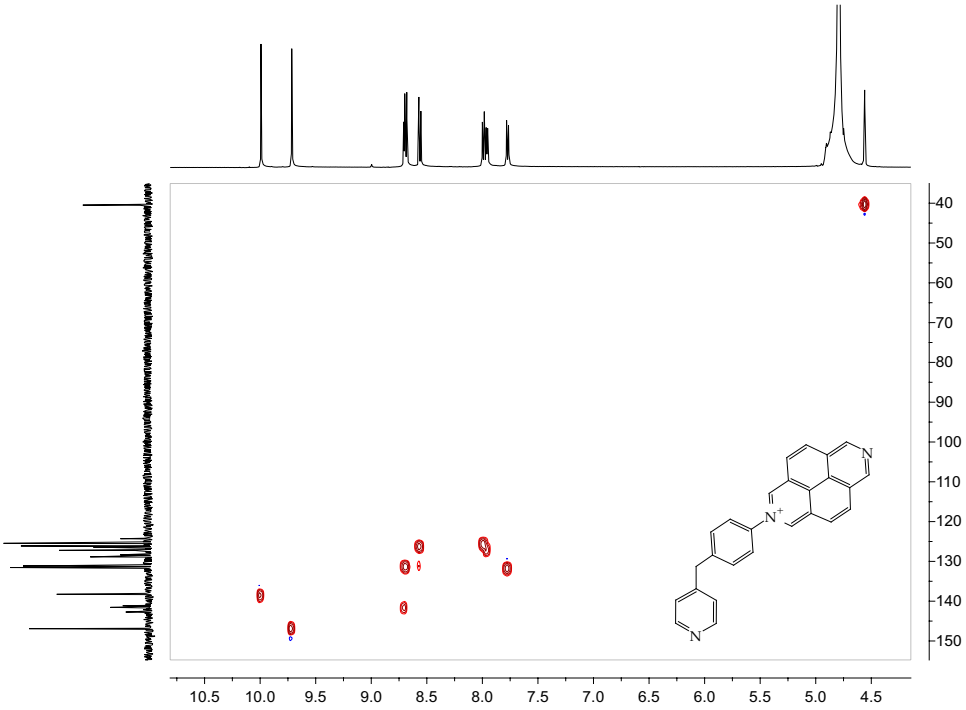

Figure A.35: HMBC (500 MHz, D_2O) spectrum of the compound [DAzP]NO_3

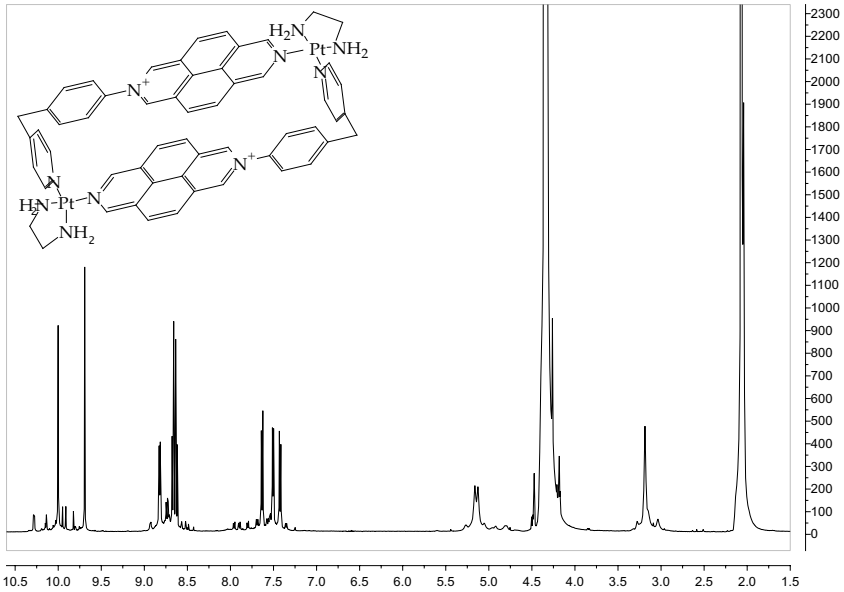

Figure A.36: ^{1}H NMR (500 MHz, CD_3NO_2) spectrum of the compound $[Pt_2(DAzP)_2(en)_2](PF_6)_6$

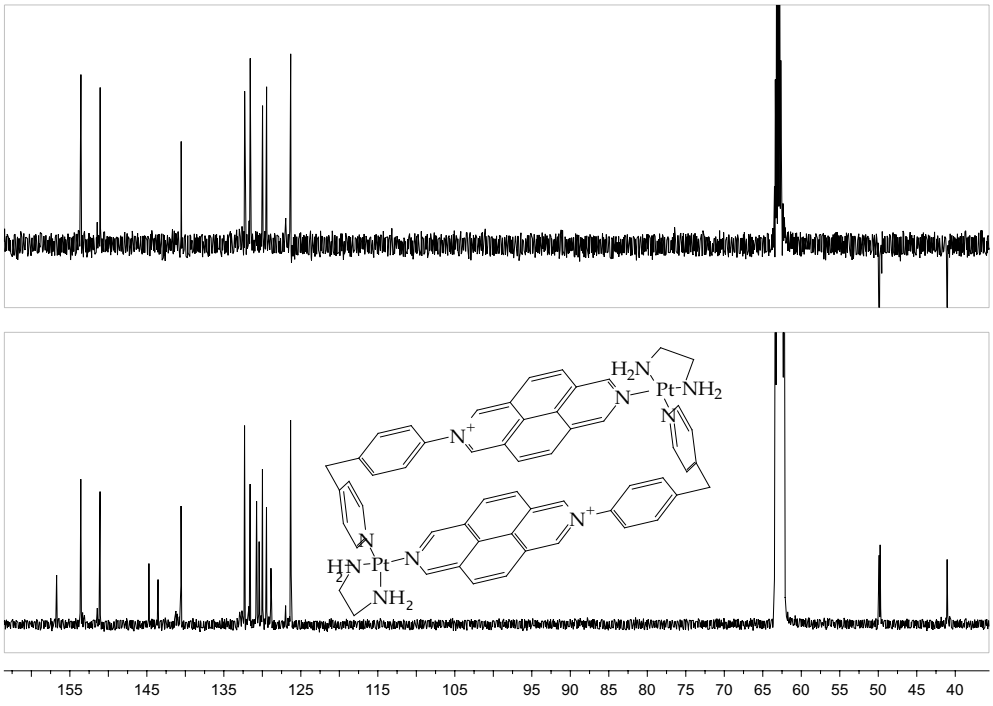

Figure A.37: ^{13}C NMR (125 MHz, CD_3NO_2) spectrum of the compound $[Pt_2(DAzP)_2(en)_2](PF_6)_6$

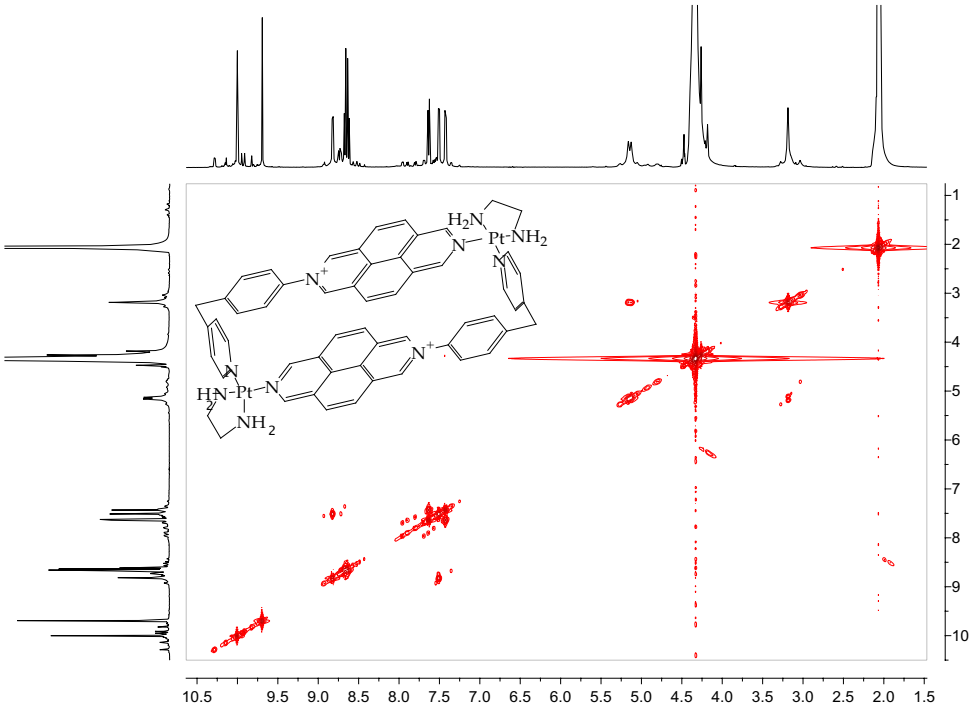

Figure A.38: COSY (500 MHz, CD_3NO_2) spectrum of the compound $[Pt_2(DAzP)_2(en)_2](PF_6)_6$

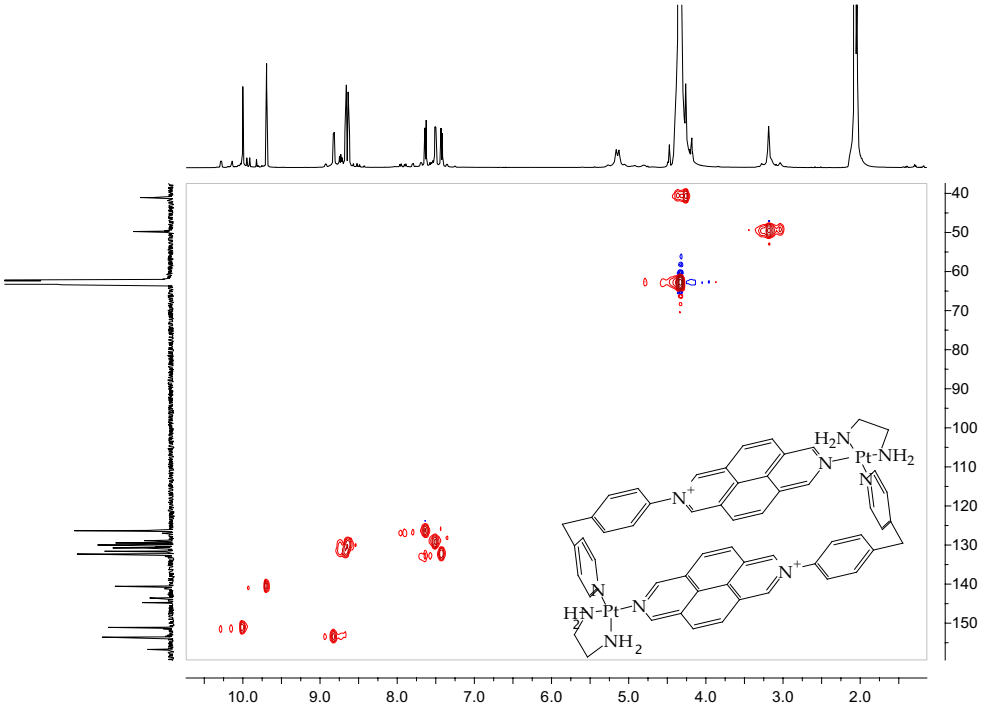

Figure A.39: HSQC (500 MHz, CD_3NO_2) spectrum of the compound $[Pt_2(DAzP)_2(en)_2](PF_6)_6$

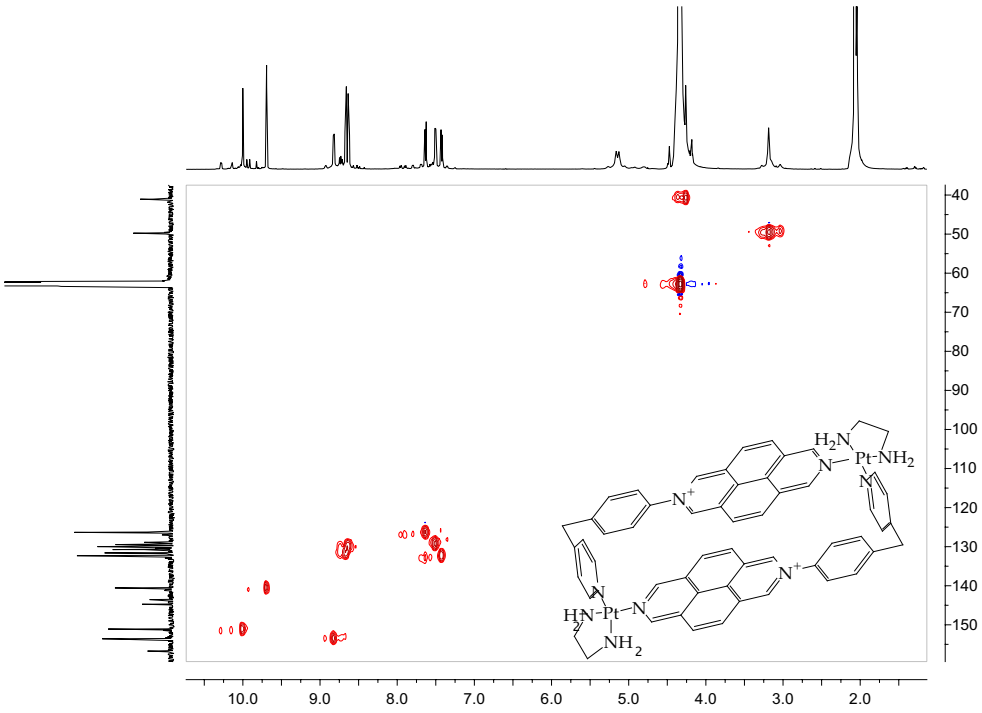

Figure A.40: HMBC (500 MHz, CD_3NO_2) spectrum of the compound $[Pt_2(DAzP)_2(en)_2](PF_6)_6$

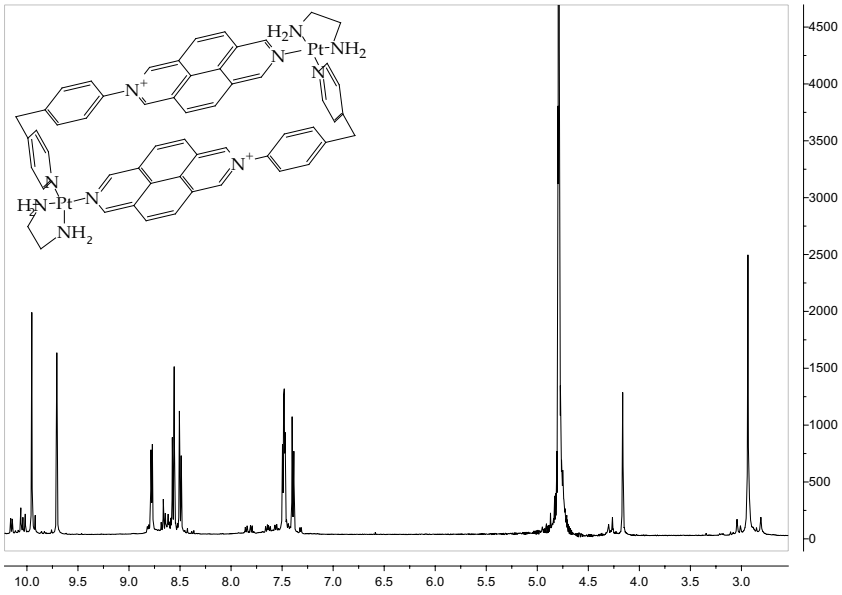

Figure A.41: ^1H NMR (500 MHz, D_2O) spectrum of the compound $[Pt_2(DAzP)_2(en)_2](NO_3)_6$

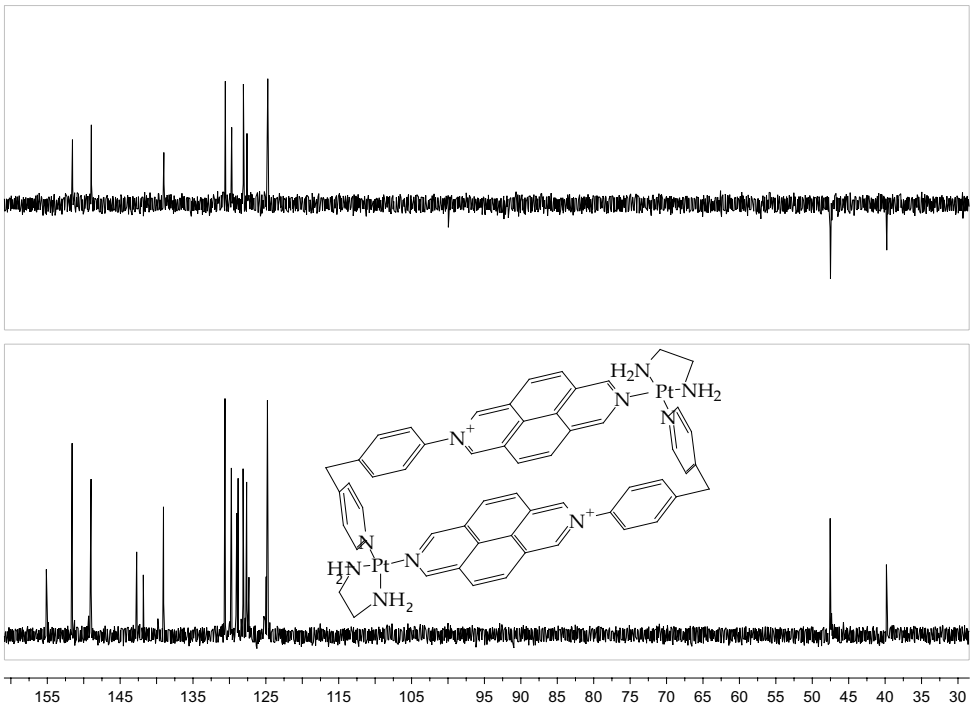

Figure A.42: ^{13}C NMR (125 MHz, D_2O) spectrum of the compound $[Pt_2(DAzP)_2(en)_2](NO_3)_6$

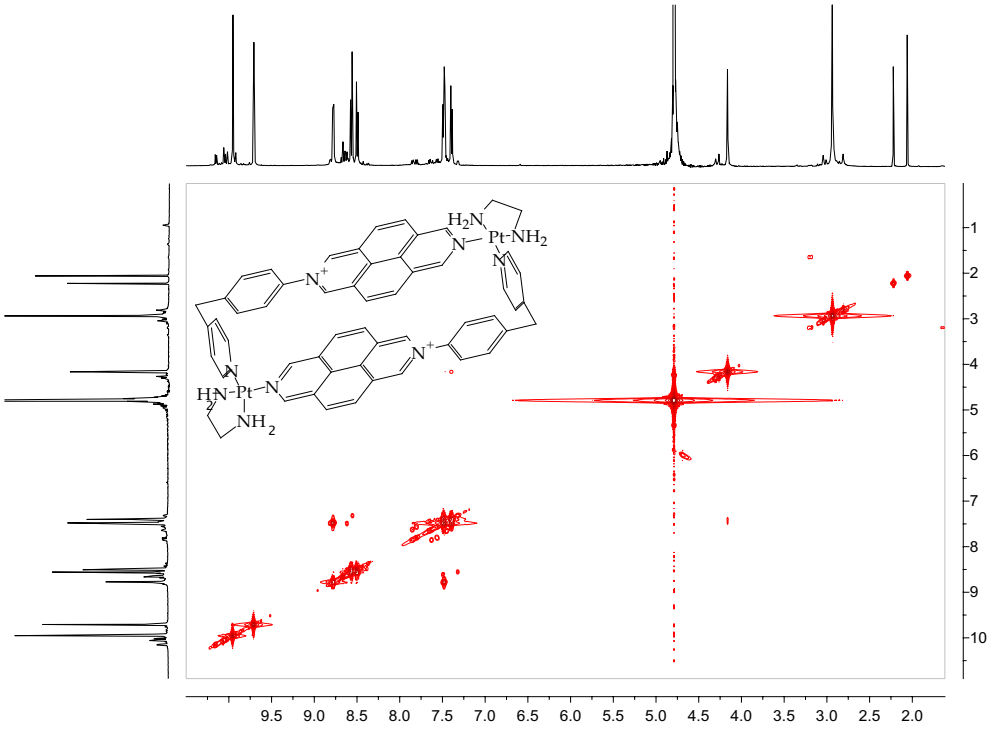

Figure A.43: COSY (500 MHz, D_2O) spectrum of the compound $[Pt_2(DAzP)_2(en)_2](NO_3)_6$

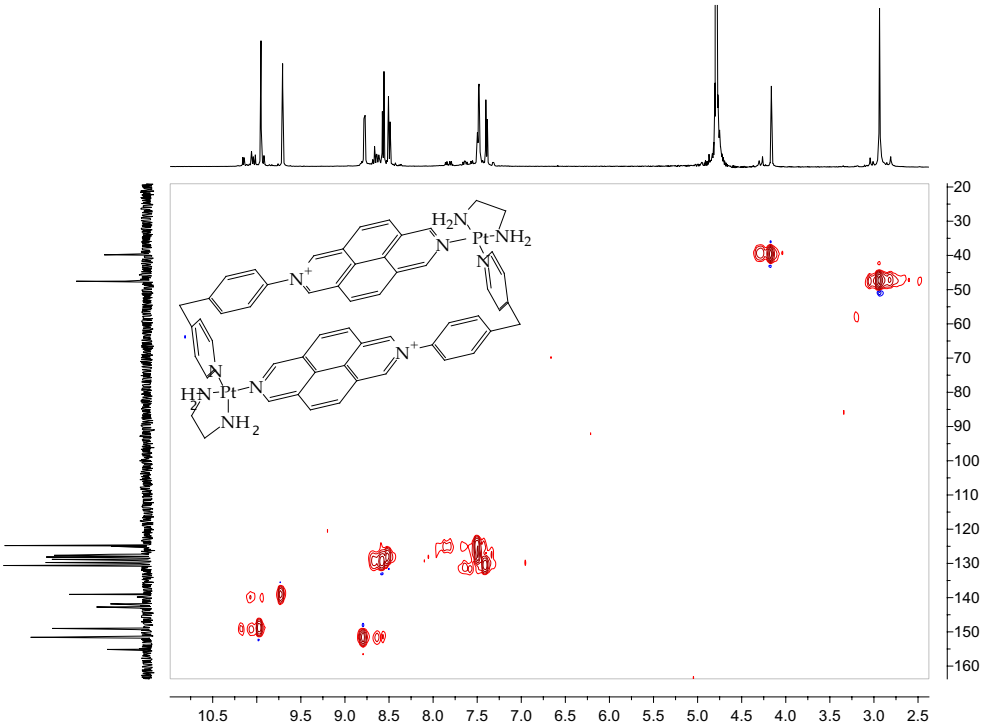

Figure A.44: HSQC (500 MHz, D_2O) spectrum of the compound $[Pt_2(DAzP)_2(en)_2](NO_3)_6$

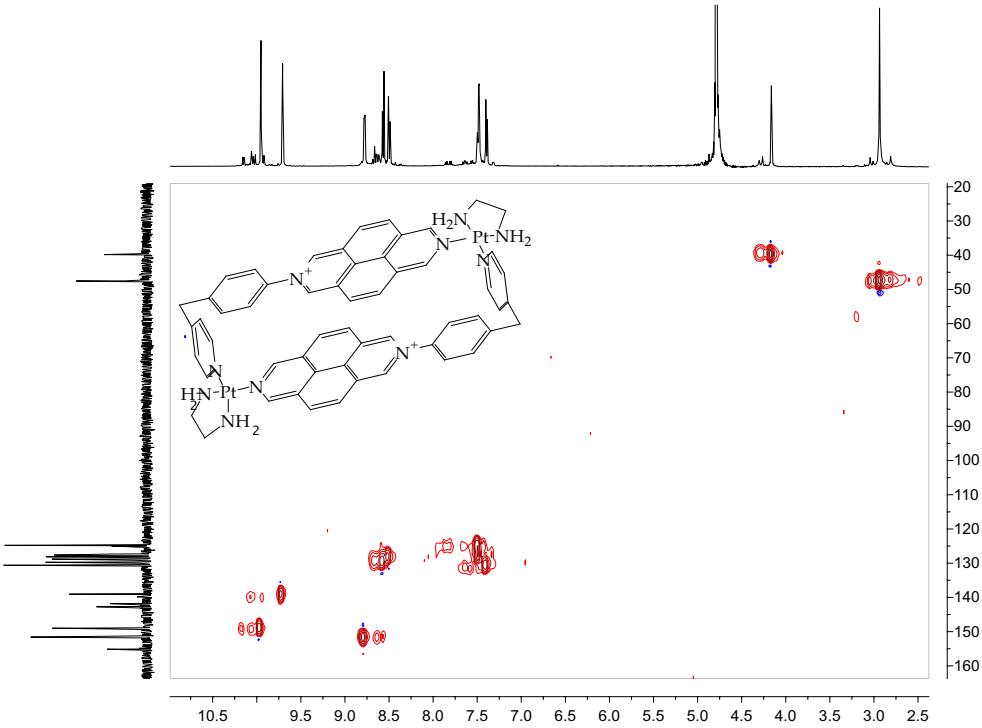

Figure A.45: HMBC (500 MHz, D_2O) spectrum of the compound $[Pt_2(DAzP)_2(en)_2](NO_3)_6$

Appendix B

X-Ray crystallographic data

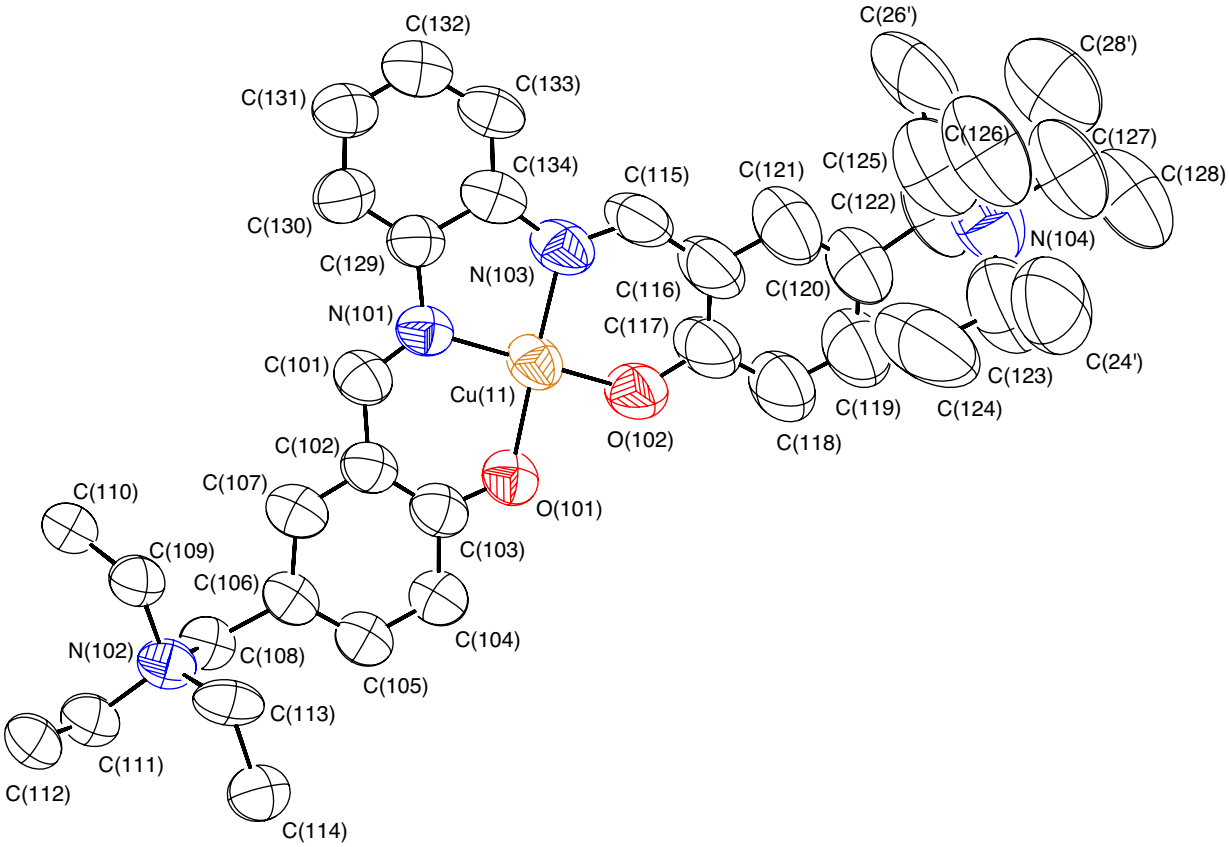

Figure B.1: Ortep view of the second of the two crystallographically independent copper complexes of CuL^{2+} with ellipsoids drawn at the 50 % probability level. Three methyl groups, C(124)/C(24'), C(126)/C(26') and C(128)/C(28') are disordered over two positions each. The perchlorate ions, benzene, nitromethane and water molecules and hydrogen atoms have been omitted for clarity.

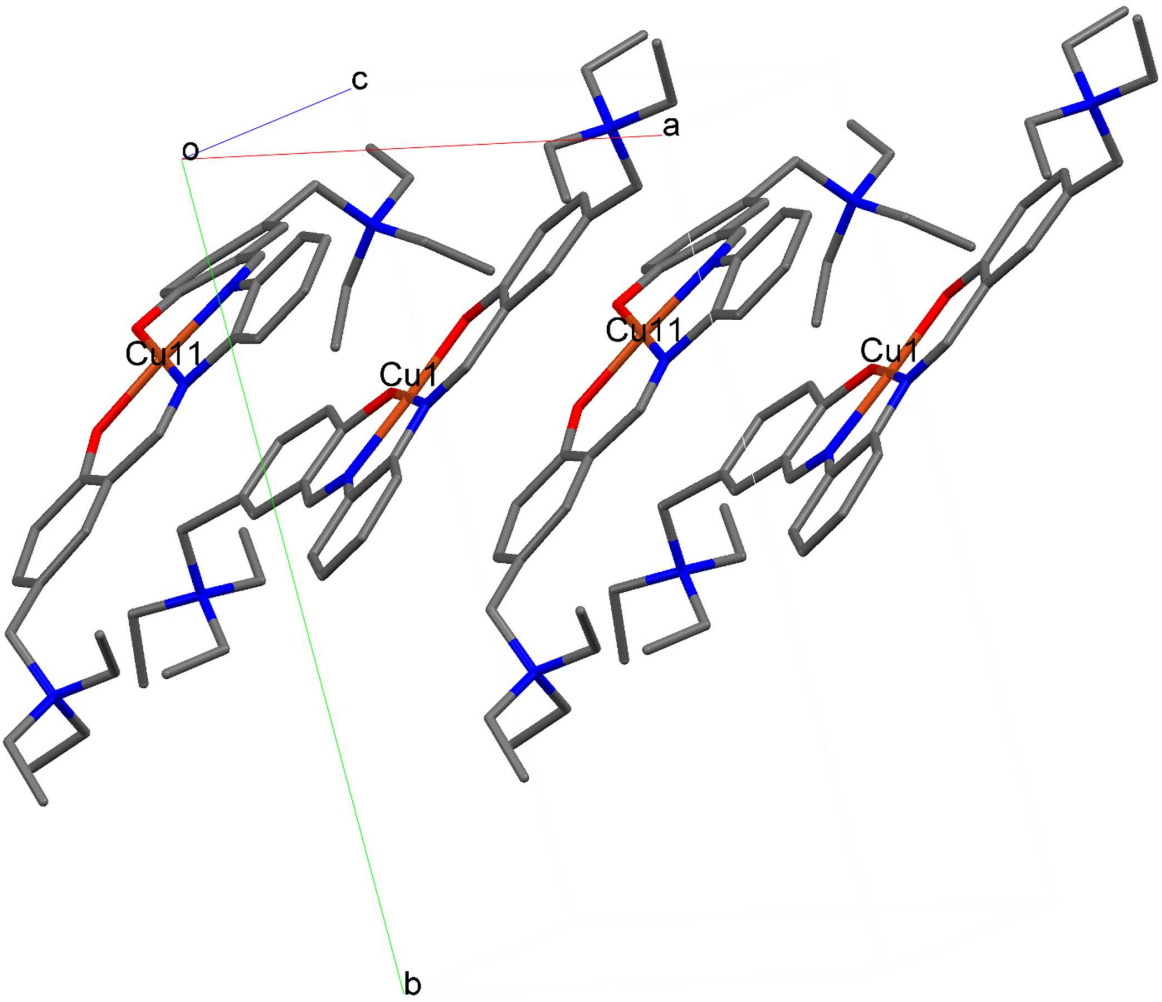

Figure B.2: The two crystallographically independent copper complexes of CuL^{2+} form columns in the (1 0 0) direction through intermolecular π-π stacking interactions with an interplanar distance of approximately 3.3 Å. The minor components of the disordered methyl groups, perchlorate ions, benzene, nitromethane and water molecules and hydrogen atoms have been omitted for clarity. Carbon atoms are coloured grey, nitrogen atoms blue, oxygen atoms red and copper atoms orange.

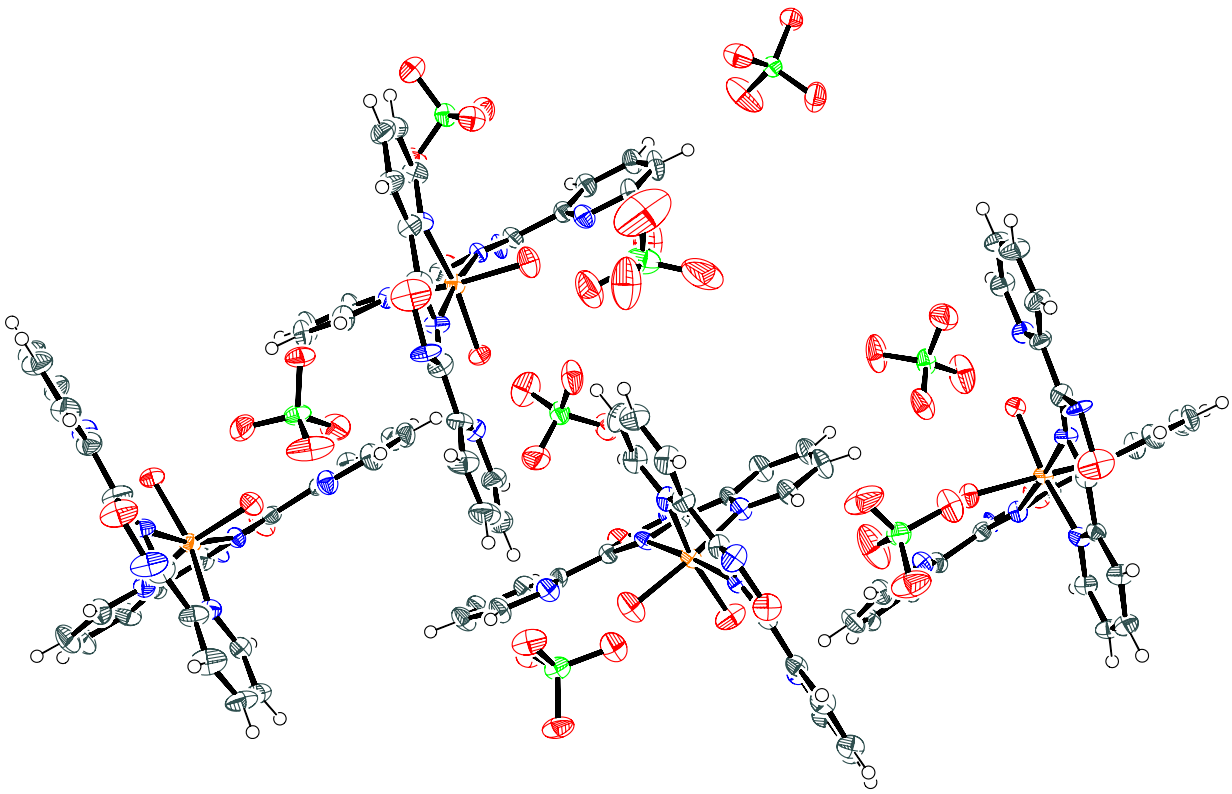

Figure B.3: View of the four crystallographically independent molecules of $[Cu(bipyOXA)_2(H_2O)_2]^{2+}$ constituting the asymmetric unit. Ellipsoids enclose 50% probability.The color labelling scheme is as follows: carbon (dark grey), nitrogen (blue), chlorine (green), copper (orange) and oxygen (red).

Bibliography

[1] V. Brabec and J. Kasparkova, "Modifications of DNA by platinum complexes - Relation to resistance of tumors to platinum antitumor drugs," *Drug Resistance Updates*, vol. 8, no. 3, pp. 131–146, 2005.

[2] M. J. Hannon, "Supramolecular DNA recognition," *Chemical Society Reviews*, vol. 36, no. 2, pp. 280–295, 2007.

[3] K. E. Erkkila, D. T. Odom, and J. K. Barton, "Recognition and reaction of metallointercalators with DNA," *Chemical Reviews*, vol. 99, no. 9, pp. 2777–2795, 1999.

[4] B. M. Zeglis, V. C. Pierre, and J. K. Barton, "Metallo-intercalators and metallo-insertors," *Chemical Communications*, no. 44, pp. 4565–4579, 2007.

[5] J. D. Watson and F. H. C. Crick, "Molecular Structure of Nucleic Acids - a Structure for Deoxyribose Nucleic Acid," *Nature*, vol. 171, no. 4356, pp. 737–738, 1953.

[6] J. D. Watson and F. H. C. Crick, "Genetical Implications of the Structure of Deoxyribonucleic Acid," *Nature*, vol. 171, no. 4361, pp. 964–967, 1953.

[7] L. S. Lerman, "Structural Considerations in Interaction of DNA and Acridines," *Journal of Molecular Biology*, vol. 3, no. 1, pp. 18–24, 1961.

[8] Rosenber.B, L. Vancamp, E. B. Grimley, and A. J. Thomson, "Inhibition of Growth or Cell Division in Escherichia Coli by Different Ionic Species of Platinium Complexes," *Journal of Biological Chemistry*, vol. 242, no. 6, pp. 1347–1350, 1967.

[9] B. Lippert, "Impact of Cisplatin on the recent development of Pt coordination chemistry: a case study," *Coordination Chemistry Reviews*, vol. 182, pp. 263–295, 1999.

[10] L. S. Lerman, "Structure of DNA-Acridine Complex," *Proceedings of the National Academy of Sciences of the United States of America*, vol. 49, no. 1, pp. 94–98, 1963.

[11] M. Waring, "Variation of the supercoils in closed circular DNA by binding of antibiotics and drugs: evidence for molecular models involving intercalation," *Journal of Molecular Biology*, vol. 54, no. 2, pp. 247–79, 1970.

[12] F. Gago, "Stacking interactions and intercalative DNA binding," *Methods*, vol. 14, no. 3, pp. 277–292, 1998.

[13] M. Howegrant and S. J. Lippard, "Binding of Platinum(II) Intercalation Reagents to Deoxyribonucleic-Acid - Dependence on Base-Pair Composition, Nature of the Intercalator, and Ionic-Strength," *Biochemistry*, vol. 18, no. 26, pp. 5762–5769, 1979.

[14] M. Howegrant, K. C. Wu, W. R. Bauer, and S. J. Lippard, "Binding of Platinum and Palladium Metallointercalation Reagents and Antitumor Drugs to Closed and Open Dnas," *Biochemistry*, vol. 15, no. 19, pp. 4339–4346, 1976.

[15] K. W. Jennette, S. J. Lippard, Vassilia.Ga, and W. R. Bauer, "Metallointercalation Reagents - 2-Hydroxyethanethiolato(2,2',2''-Terpyridine)-Platinum(II) Monocation Binds Strongly to DNA by Intercalation," *Proceedings of the National Academy of Sciences of the United States of America*, vol. 71, no. 10, pp. 3839–3843, 1974.

[16] A. E. Friedman, J. C. Chambron, J. P. Sauvage, N. J. Turro, and J. K. Barton, "Molecular Light Switch for DNA - $[Ru(Bpy)_2(Dppz)]^{2+}$," *Journal of the American Chemical Society*, vol. 112, no. 12, pp. 4960–4962, 1990.

[17] C. L. Kielkopf, K. E. Erkkila, B. P. Hudson, J. K. Barton, and D. C. Rees, "Structure of a photoactive rhodium complex intercalated into DNA," *Nature Structural Biology*, vol. 7, no. 2, pp. 117–121, 2000.

[18] A. Terenzi, G. Barone, A. Silvestri, A. M. Giuliani, A. Ruggirello, and V. Turco Liveri, "The interaction of native calf thymus DNA with Fe-III-dipyrido[3,2-a:2 ′,3′-c]phenazine," *Journal of Inorganic Biochemistry*, vol. 103, no. 1, pp. 1–9, 2009.

[19] A. Arola-Arnal, J. Benet-Buchholz, S. Neidle, and R. Vilar, "Effects of Metal Coordination Geometry on Stabilization of Human Telomeric Quadruplex DNA by Square-Planar and Square-Pyramidal Metal Complexes," *Inorganic Chemistry*, vol. 47, no. 24, pp. 11910–11919, 2008.

[20] J. E. Reed, A. Arola-Arnal, S. Neidle, and R. Vilar, "Stabilization of G-quadruplex DNA and inhibition of telomerase activity by square-planar nickel(II) complexes," *Journal of the American Chemical Society*, vol. 128, no. 18, pp. 5992–5993, 2006.

[21] A. Silvestri, G. Barone, G. Ruisi, D. Anselmo, S. Riela, and V. T. Liveri, "The interaction of native DNA with Zn(II) and Cu(II) complexes of 5-triethyl ammonium methyl salicylidene orto-phenylendiimine," *Journal of Inorganic Biochemistry*, vol. 101, no. 5, pp. 841–848, 2007.

[22] G. Barone, N. Gambino, A. Ruggirello, A. Silvestri, A. Terenzi, and V. Turco Liveri, "Spectroscopic study of the interaction of Ni-II-5-triethyl ammonium methyl salicylidene orthophenylendiiminate with native DNA," *Journal of Inorganic Biochemistry*, vol. 103, no. 5, pp. 731–737, 2009.

[23] M. de Rosa, D. de Sanctis, A. L. Rosario, M. Archer, A. Rich, A. Athanasiadis, and M. A. Carrondo, "Crystal structure of a junction between two Z-DNA helices," *Proceedings of the National Academy of Sciences of the United States of America*, vol. 107, no. 20, pp. 9088–9092, 2010.

[24] T. Da Ros, G. Spalluto, M. Prato, T. Saison-Behmoaras, A. Boutorine, and B. Cacciari, "Oligonucleotides and oligonucleotide conjugates: A new approach for cancer treatment," *Current Medicinal Chemistry*, vol. 12, no. 1, pp. 71–88, 2005.

[25] N. T. Thuong and C. Helene, "Sequence-Specific Recognition and Modification of Double-Helical DNA by Oligonucleotides," *Angewandte Chemie-International Edition in English*, vol. 32, no. 5, pp. 666–690, 1993.

[26] P. G. Baraldi, A. Bovero, F. Fruttarolo, D. Preti, M. A. Tabrizi, M. G. Pavani, and R. Romagnoli, "DNA minor groove binders as potential antitumor and antimicrobial agents," *Medicinal Research Reviews*, vol. 24, no. 4, pp. 475–528, 2004.

[27] T. A. Larsen, D. S. Goodsell, D. Cascio, K. Grzeskowiak, and R. E. Dickerson, "The structure of DAPI bound to DNA," *Journal of Biomolecular Structure and Dynamics*, vol. 7, no. 3, pp. 477–491, 1989.

[28] O. Dann, S. Lang, G. Lurding, W. Pfeifer, G. Bergen, R. Fernbach, and E. Demant, "Trypanocidal Diamidines with 3 Rings in 2 Isolated Ring-Systems," *Annalen Der Chemie-Justus Liebig*, vol. 760, no. Jun-J, pp. 37–40, 1972.

[29] B. Mildner, A. Metz, and P. Chandra, "Interaction of 4'-6-Diamidino-2-Phenylindole to Nucleic-Acids, and Its Implication to Their Template Activity in Rna-Polymerase Reaction of Escherichia-Coli Bacteria and of Friend-Virus Infected Mouse Spleen," *Cancer Letters*, vol. 4, no. 2, pp. 89–98, 1978.

[30] A. Kumar, S. S. D'Souza, S. L. Gaonkar, K. M. L. Rai, and B. P. Salimath, "Growth inhibition and induction of apoptosis in MCF-7 breast cancer cells by a new series of substituted-1,3,4-oxadiazole derivatives," *Investigational New Drugs*, vol. 26, no. 5, pp. 425–435, 2008.

[31] H. M. Coley, J. Sarju, and G. Wagner, "Synthesis and characterization of platinum(II) oxadiazoline complexes and their in vitro antitumor activity in platinum-sensitive and -resistant cancer cell lines," *Journal of Medicinal Chemistry*, vol. 51, no. 1, pp. 135–141, 2008.

[32] J. L. Mergny, G. Duvalvalentin, C. H. Nguyen, L. Perrouault, B. Faucon, M. Rougee, T. Montenaygarestier, E. Bisagni, and C. Helene, "Triple Helix Specific Ligands," *Science*, vol. 256, no. 5064, pp. 1681–1684, 1992.

[33] C. Escude, C. H. Nguyen, S. Kukreti, Y. Janin, J. S. Sun, E. Bisagni, T. Garestier, and C. Helene, "Rational design of a triple helix-specific intercalating ligand," *Proceedings of the National Academy of Sciences of the United States of America*, vol. 95, no. 7, pp. 3591–3596, 1998.

[34] S. C. M. Teixeira, J. H. Thorpe, A. K. Todd, H. R. Powell, A. Adams, L. P. G. Wakelin, W. A. Denny, and C. J. Cardin, "Structural characterisation of bisintercalation in higher-order DNA at a junction-like quadruplex," *Journal of Molecular Biology*, vol. 323, no. 2, pp. 167–171, 2002.

[35] J. C. Chambron, C. O. Dietrichbuchecker, V. Heitz, J. F. Nierengarten, J. P. Sauvage, C. Pascard, and J. Guilhem, "Transition-Metals as Assembling and Templating Species - from Catenanes and Knots to Organized Multi-Porphyrins Arrays," *Pure and Applied Chemistry*, vol. 67, no. 2, pp. 233–240, 1995.

[36] J. M. Lehn, *Supramolecular Chemistry, Concepts and Perspectives*. VCH Weinheim, 1995.

[37] M. J. Hannon, C. L. Painting, and W. Errington, "Self-assembly of supramolecular boxes," *Chemical Communications*, no. 3, pp. 307–308, 1997.

[38] M. J. Hannon, C. L. Painting, and W. Errington, "Controlled aggregation of supramolecular boxes," *Chemical Communications*, no. 18, pp. 1805–1806, 1997.

[39] M. Fujita, F. Ibukuro, K. Yamaguchi, and K. Ogura, "A Molecular Lock," *Journal of the American Chemical Society*, vol. 117, no. 14, pp. 4175–4176, 1995.

[40] A. Oleksi, A. G. Blanco, R. Boer, I. Uson, J. Aymami, A. Rodger, M. J. Hannon, and M. Coll, "Molecular recognition of a three-way DNA junction by a metallosupramolecular helicate," *Angewandte Chemie-International Edition*, vol. 45, no. 8, pp. 1227–1231, 2006.

[41] H. Schiff *Ann. Suppl.*, vol. 3, p. 343, 1864.

[42] D. A. Atwood and M. J. Harvey, "Group 13 compounds incorporating salen ligands," *Chemical Reviews*, vol. 101, no. 1, pp. 37–52, 2001.

[43] M. B. Smith and J. March, *March's Advanced Organic Chemistry: Reactions, Mechanisms, and Structure*. New York: Wiley, 2000.

[44] C. Baleizao and H. Garcia, "Chiral salen complexes: An overview to recoverable and reusable homogeneous and heterogeneous catalysts," *Chemical Reviews*, vol. 106, no. 9, pp. 3987–4043, 2006.

[45] A. Combes *Les Comptes Rendus de l'Academie des sciences - Institute de France*, vol. 108, p. 1252, 1889.

[46] L. Canali and D. C. Sherrington, "Utilisation of homogeneous and supported chiral metal(salen) complexes in asymmetric catalysis," *Chemical Society Reviews*, vol. 28, no. 2, pp. 85–93, 1999.

[47] S. J. Wezenberg and A. W. Kleij, "Material applications for salen frameworks," *Angewandte Chemie-International Edition*, vol. 47, no. 13, pp. 2354–2364, 2008.

[48] E. N. Jacobsen, *Comprehensive Organometallic Chemistry II*, vol. 12. New York: Pergamon, 1995.

[49] D. Anselmo, E. C. Escudero-Adan, J. Benet-Buchholz, and A. W. Kleij, "Isolation and characterization of a new type of mu-hydroxo-bis-Zn(salphen) assembly," *Dalton Transactions*, vol. 39, no. 37, pp. 8733–8740, 2010.

[50] P. H. Wooley and J. D. Whalen, "The Influence of Superoxide Scavenging Compound Ctc-23 on Type-Ii Collagen-Induced Arthritis in Mice," *Agents and Actions*, vol. 35, no. 3-4, pp. 273–279, 1992.

[51] A. Dalla Cort, P. De Bernardin, G. Forte, and F. Y. Mihan, "Metal-salophen-based receptors for anions," *Chemical Society Reviews*, vol. 39, no. 10, pp. 3863–3874, 2010.

[52] T. S. Lange, K. K. Kim, R. K. Singh, R. M. Strongin, C. K. McCourt, and L. Brard, "Iron(III)-salophene: an organometallic compound with selective cytotoxic and anti-proliferative properties in platinum-resistant ovarian cancer cells," *PLoS One*, vol. 3, no. 5, p. e2303, 2008.

[53] S. R. Doctrow, K. Huffman, C. B. Marcus, G. Tocco, E. Malfroy, C. A. Adinolfi, H. Kruk, K. Baker, N. Lazarowych, J. Mascarenhas, and B. Malfroyt, "Salen-manganese complexes

as catalytic scavengers of hydrogen peroxide and cytoprotective agents: structure-activity relationship studies," *Journal of Medicinal Chemistry*, vol. 45, no. 20, pp. 4549–4558, 2002.

[54] A. Silvestri, G. Barone, G. Ruisi, M. T. Lo Giudice, and S. Tumminello, "The interaction of native DNA with iron(III)-N,N'-ethylene-bis(salicylideneiminato)-chloride," *Journal of Inorganic Biochemistry*, vol. 98, no. 4, pp. 589–594, 2004.

[55] D. J. Gravert and J. H. Griffin, "Steric and electronic effects, enantiospecificity, and reactive orientation in DNA binding/cleaving by substituted derivatives of [SalenMn(III)]$^{+}$," *Inorganic Chemistry*, vol. 35, no. 17, pp. 4837–4847, 1996.

[56] J. G. Muller, L. A. Kayser, S. J. Paikoff, V. Duarte, N. Tang, R. J. Perez, S. E. Rokita, and C. J. Burrows, "Formation of DNA adducts using Nickel(II) complexes of redox-active ligands: a comparison of salen and peptide complexes," *Coordination Chemistry Reviews*, vol. 186, pp. 761–774, 1999.

[57] S. Routier, J. L. Bernier, M. J. Waring, P. Colson, C. Houssier, and C. Bailly, "Synthesis of a functionalized salen copper complex and its interaction with DNA," *Journal of Organic Chemistry*, vol. 61, no. 7, pp. 2326–2331, 1996.

[58] K. Sato, M. Chikira, Y. Fujii, and A. Komatsu, "Stereospecific Binding of Chemically-Modified Salen-Type Schiff-Base Complexes of Copper(II) with DNA [Salen=Bis(Salicyclidene)Ethylenediamine]," *Journal of the Chemical Society-Chemical Communications*, no. 5, pp. 625–626, 1994.

[59] A. J. Clarke, N. Yamamoto, P. Jensen, and T. W. Hambley, "Iron(III) complexes of fluorescent hydroxamate ligands: preparation, properties, and cellular processing," *Dalton Transactions*, no. 48, pp. 10787–10798, 2009.

[60] A. Hille, I. Ott, A. Kitanovic, I. Kitanovic, H. Alborzinia, E. Lederer, S. Wolfl, N. Metzler-Nolte, S. Schafer, W. S. Sheldrick, C. Bischof, U. Schatzschneider, and R. Gust, "[N,N'-Bis(salicylidene)-1,2-phenylenediamine]metal complexes with cell death promoting properties," *Journal of Biological Inorganic Chemistry*, vol. 14, no. 5, pp. 711–725, 2009.

[61] G. Barone, A. Ruggirello, A. Silvestri, A. Terenzi, and V. T. Liveri, "Fluorescence emission and enhanced photochemical stability of Zn-II-5-triethyl ammonium methyl salicylidene ortho-phenylendiiminate interacting with native DNA," *Journal of Inorganic Biochemistry*, vol. 104, no. 7, pp. 765–773, 2010.

[62] G. Barone, A. Longo, A. Ruggirello, A. Silvestri, A. Terenzi, and V. Turco Liveri, "Confinement effects on the interaction of native DNA with Cu(II)-5-

(triethylammoniummethyl)salicylidene ortho-phenylendiiminate in $C_{12}E_4$ liquid crystals," *Dalton Transactions*, no. 31, pp. 4172–4178, 2008.

[63] M. D. Hobday and T. D. Smith, "N,N'-Ethylenebis(Salicylideneiminato) Transition-Metal Ion Chelates," *Coordination Chemistry Reviews*, vol. 9, no. 3-4, pp. 311–337, 1973.

[64] T. Uno, K. Hamasaki, M. Tanigawa, and S. Shimabayashi, "Binding of meso-tetrakis(N-methylpyridinium-4-yl)porphyrin to double helical RNA and DNA center dot RNA hybrids," *Inorganic Chemistry*, vol. 36, no. 8, pp. 1676–1683, 1997.

[65] M. T. Carter, M. Rodriguez, and A. J. Bard, "Voltammetric Studies of the Interaction of Metal-Chelates with DNA .2. Tris-Chelated Complexes of Cobalt(III) and Iron(II) with 1,10-Phenanthroline and 2,2'-Bipyridine," *Journal of the American Chemical Society*, vol. 111, no. 24, pp. 8901–8911, 1989.

[66] S. R. Smith, G. A. Neyhart, W. A. Kalsbeck, and H. H. Thorp, "Electronic-Properties of Aquapolypyridyl Ruthenium Complexes Bound to DNA," *New Journal of Chemistry*, vol. 18, no. 3, pp. 397–406, 1994.

[67] M. J. Waring, "Complex Formation between Ethidium Bromide and Nucleic Acids," *Journal of Molecular Biology*, vol. 13, no. 1, pp. 269–274, 1965.

[68] J. M. Kelly, A. B. Tossi, D. J. Mcconnell, and C. Ohuigin, "A Study of the Interactions of Some Polypyridylruthenium(Ii) Complexes with DNA Using Fluorescence Spectroscopy, Topoisomerization and Thermal-Denaturation," *Nucleic Acids Research*, vol. 13, no. 17, pp. 6017–6034, 1985.

[69] G. A. Neyhart, N. Grover, S. R. Smith, W. A. Kalsbeck, T. A. Fairley, M. Cory, and H. H. Thorp, "Binding and Kinetics Studies of Oxidation of DNA by Oxoruthenium(IV)," *Journal of the American Chemical Society*, vol. 115, no. 11, pp. 4423–4428, 1993.

[70] A. Rodger and B. Norden, *Circular dichroism and linear dichroism*. Oxford chemistry masters 1, Oxford ; New York: Oxford University Press, 1997.

[71] M. J. Carvlin, N. Dattagupta, and R. J. Fiel, "Circular-Dichroism Spectroscopy of a Cationic Porphyrin Bound to DNA," *Biochemical and Biophysical Research Communications*, vol. 108, no. 1, pp. 66–73, 1982.

[72] J. E. B. Ramos, R. de Vries, and J. R. Neto, "DNA Psi-condensation and reentrant decondensation: Effect of the PEG degree of polymerization," *Journal of Physical Chemistry B*, vol. 109, no. 49, pp. 23661–23665, 2005.

[73] F. J. Meyeralmes and D. Porschke, "Mechanism of Intercalation into the DNA Double Helix by Ethidium," *Biochemistry*, vol. 32, no. 16, pp. 4246–4253, 1993.

[74] C. D. Byrne and A. J. de Mello, "Photophysics of ethidium bromide complexed to ct-DNA: a maximum entropy study," *Biophysical Chemistry*, vol. 70, no. 3, pp. 173–184, 1998.

[75] E. M. Talavera, P. Guerrero, F. Ocana, and J. M. Alvarez-Pez, "Photophysical and direct determination of binding constants of ethidium bromide complexed to E-coli DNA," *Applied Spectroscopy*, vol. 56, no. 3, pp. 362–369, 2002.

[76] R. Hochstrasser and D. Millar, "Fluorescence self-quenching of ethidium bromide intercalated in DNA," *Proceedings of SPIE*, vol. 1640, pp. 599–605, 1992.

[77] V. A. Izumrudov, M. V. Zhiryakova, and A. A. Goulko, "Ethidium bromide as a promising probe for studying DNA interaction with cationic amphiphiles and stability of the resulting complexes," *Langmuir*, vol. 18, no. 26, pp. 10348–10356, 2002.

[78] M. J. Hannon, V. Moreno, M. J. Prieto, E. Moldrheim, E. Sletten, I. Meistermann, C. J. Isaac, K. J. Sanders, and A. Rodger, "Intramolecular DNA coiling mediated by a metallosupramolecular cylinder," *Angewandte Chemie-International Edition*, vol. 40, no. 5, pp. 880–884, 2001.

[79] D. T. Rosa and D. Coucouvanis, "Crown-ether-functionalized nickel salicylaldimine complexes. Structural characterization of their potassium, cesium, and hexylammonium derivatives and their use in the transport of amino acids," *Inorganic Chemistry*, vol. 37, no. 10, pp. 2328–2329, 1998.

[80] S. F. Bellon, J. H. Coleman, and S. J. Lippard, "DNA Unwinding Produced by Site-Specific Intrastrand Cross-Links of the Antitumor Drug Cis-Diamminedichloroplatinum(II)," *Biochemistry*, vol. 30, no. 32, pp. 8026–8035, 1991.

[81] F. J. Ramos-Lima, O. Vrana, A. G. Quiroga, C. N. Navarro-Ranninger, A. Halamikova, H. Rybnickova, L. Hejmalova, and V. Brabec, "Structural characterization, DNA interactions, and cytotoxicity of new transplatin analogues containing one aliphatic and one planar heterocyclic amine ligand," *Journal of Medicinal Chemistry*, vol. 49, no. 8, pp. 2640–2651, 2006.

[82] J. K. Barton and A. L. Raphael, "Photoactivated Stereospecific Cleavage of Double-Helical DNA by Cobalt(III) Complexes," *Journal of the American Chemical Society*, vol. 106, no. 8, pp. 2466–2468, 1984.

[83] Y. M. Song, Q. Wu, P. J. Yang, N. N. Luan, L. F. Wang, and Y. M. Liu, "DNA Binding and cleavage activity of Ni(II) complex with all-trans retinoic acid," *Journal of Inorganic Biochemistry*, vol. 100, no. 10, pp. 1685–1691, 2006.

[84] S. Dhar, M. Nethaji, and A. R. Chakravarty, "Steric protection of a photosensitizer in a N,N-bis[2-(2-pyridyl)ethyl]-2-phenylethylamine-copper(II) bowl that enhances red light-induced DNA cleavage activity," *Inorganic Chemistry*, vol. 44, no. 24, pp. 8876–8883, 2005.

[85] R. A. Gibbs, "DNA Amplification by the Polymerase Chain-Reaction," *Analytical Chemistry*, vol. 62, no. 13, pp. 1202–1214, 1990.

[86] C. Ducani, A. Leczkowska, N. J. Hodges, and M. J. Hannon, "Noncovalent DNA-Binding Metallo-Supramolecular Cylinders Prevent DNA Transactions in vitro," *Angewandte Chemie-International Edition*, vol. 49, no. 47, pp. 8942–8945, 2010.

[87] G. B. Roy, "Synthesis and study of physico-chemical properties of a new chiral Schiff base ligand and its metal complex," *Inorganica Chimica Acta*, vol. 362, no. 6, pp. 1709–1714, 2009.

[88] T. Kawasaki, T. Kamata, H. Ushijima, M. Kanakubo, S. Murata, F. Mizukami, Y. Fujii, and Y. Usui, "Effects of diamine bridge length and substituents on the spectral properties of N,N '-bis(alpha-substituted salicylidene)diamines in solution," *Journal of the Chemical Society-Perkin Transactions 2*, no. 2, pp. 193–198, 1999.

[89] H. Kunkely and A. Vogler, "Optical properties of boron, gallium and gold complexes with salen ligands. Emission from intraligand excited states under ambient conditions," *Inorganica Chimica Acta*, vol. 321, no. 1-2, pp. 171–174, 2001.

[90] M. E. Germain and M. J. Knapp, "Turn-on Fluorescence Detection of H_2O_2 and TATP," *Inorganic Chemistry*, vol. 47, no. 21, pp. 9748–9750, 2008.

[91] K. E. Splan, A. M. Massari, G. A. Morris, S. S. Sun, E. Reina, S. T. Nguyen, and J. T. Hupp, "Photophysical and energy-transfer properties of (Salen)Zinc complexes and supramolecular assemblies," *European Journal of Inorganic Chemistry*, no. 12, pp. 2348–2351, 2003.

[92] M. E. Germain, T. R. Vargo, P. G. Khalifah, and M. J. Knapp, "Fluorescent Detection of Nitroaromatics and 2,3-Dimethyl 2,3-dinitrobutane (DMNB) by a Zinc Complex: (salophen)Zn," *Inorganic Chemistry*, vol. 46, no. 11, pp. 4422–4429, 2007.

[93] S. J. Wezenberg, E. C. Escudero-Adan, J. Benet-Buchholz, and A. W. Kleij, "Colorimetric discrimination between important alkaloid nuclei mediated by a bis-salphen chromophore," *Organic Letters*, vol. 10, no. 15, pp. 3311–3314, 2008.

[94] N. Turro, *Modern Molecular Photochemistry*. Menlo Park (CA): Benjamin-Cummings, 1978.

[95] H. Kunkely and A. Vogler, "Photochemistry of N,N′-bis(3,5-di-tert-butylsalicylidene)-1,2-diaminocyclohexane and its Co(II) complex in chloroform," *Journal of Photochemistry and Photobiology a-Chemistry*, vol. 138, no. 1, pp. 51–54, 2001.

[96] H. Kunkely and A. Vogler, "Photooxidation of N,N′-bis(3,5-di-tert-butylsalicylidene)-1,2-diamino hexane-manganese(III) chloride (Jacobsen catalyst) in chloroform," *Inorganic Chemistry Communications*, vol. 4, no. 12, pp. 692–694, 2001.

[97] T. Fukuda, F. Sakamoto, M. Sato, Y. Nakano, X. S. Tan, and Y. Fujii, "Photopromoted oxidative cyclization of an o-phenylene-bridged Schiff base via a manganese(III) complex, leading to a fluorescent compound, 2-(2-hydroxyphenyl)benzimidazole," *Chemical Communications*, no. 13, pp. 1391–1392, 1998.

[98] W. K. Dong, J. G. Duan, Y. H. Guan, J. Y. Shi, and C. Y. Zhao, "Synthesis, crystal structure and spectroscopic behaviors of Co(II) and Cu(II) complexes with Salen-type bisoxime ligands," *Inorganica Chimica Acta*, vol. 362, no. 4, pp. 1129–1134, 2009.

[99] A. Becke, "Density-functional thermochemistry. III. The role of exact exchange," *Journal of Chemical Physics*, vol. 98, pp. 5648–5652, 1993.

[100] N. Godbout, D. R. Salahub, J. Andzelm, and E. Wimmer, "Optimization of Gaussian-Type Basis-Sets for Local Spin-Density Functional Calculations .1. Boron through Neon, Optimization Technique and Validation," *Canadian Journal of Chemistry-Revue Canadienne De Chimie*, vol. 70, no. 2, pp. 560–571, 1992.

[101] C. Sosa, J. Andzelm, B. C. Elkin, E. Wimmer, K. D. Dobbs, and D. A. Dixon, "A Local Density Functional-Study of the Structure and Vibrational Frequencies of Molecular Transition-Metal Compounds," *Journal of Physical Chemistry*, vol. 96, no. 16, pp. 6630–6636, 1992.

[102] E. Runge and E. K. U. Gross, "Density-Functional Theory for Time-Dependent Systems," *Physical Review Letters*, vol. 52, no. 12, pp. 997–1000, 1984.

[103] R. E. Stratmann, G. E. Scuseria, and M. J. Frisch, "An efficient implementation of time-dependent density-functional theory for the calculation of excitation energies of large molecules," *Journal of Chemical Physics*, vol. 109, no. 19, pp. 8218–8224, 1998.

[104] R. Bauernschmitt and R. Ahlrichs, "Treatment of electronic excitations within the adiabatic approximation of time dependent density functional theory," *Chemical Physics Letters*, vol. 256, no. 4-5, pp. 454–464, 1996.

[105] M. E. Casida, C. Jamorski, K. C. Casida, and D. R. Salahub, "Molecular excitation energies to high-lying bound states from time-dependent density-functional response theory: Characterization and correction of the time-dependent local density approximation ionization threshold," *Journal of Chemical Physics*, vol. 108, no. 11, pp. 4439–4449, 1998.

[106] J. B. Foresman, M. Headgordon, J. A. Pople, and M. J. Frisch, "Toward a Systematic Molecular-Orbital Theory for Excited-States," *Journal of Physical Chemistry*, vol. 96, no. 1, pp. 135–149, 1992.

[107] R. J. Cave, K. Burke, and E. W. Castner, "Theoretical investigation of the ground and excited states of Coumarin 151 and Coumarin 120," *Journal of Physical Chemistry A*, vol. 106, no. 40, pp. 9294–9305, 2002.

[108] D. Jacquemin, E. A. Perpete, G. Scalmani, M. J. Frisch, I. Ciofini, and C. Adamo, "Absorption and emission spectra in gas-phase and solution using TD-DFT: Formaldehyde and benzene as case studies," *Chemical Physics Letters*, vol. 421, no. 1-3, pp. 272–276, 2006.

[109] D. Jacquemin, E. A. Perpete, X. Assfeld, G. Scalmani, M. J. Frisch, and C. Adamo, "The geometries, absorption and fluorescence wavelengths of solvated fluorescent coumarins: A CIS and TD-DFT comparative," *Chemical Physics Letters*, vol. 438, no. 4-6, pp. 208–212, 2007.

[110] V. Barone and M. Cossi, "Quantum calculation of molecular energies and energy gradients in solution by a conductor solvent model," *Journal of Physical Chemistry A*, vol. 102, no. 11, pp. 1995–2001, 1998.

[111] N. M. O'Boyle, A. L. Tenderholt, and K. M. Langner, "cclib: A library for package-independent computational chemistry algorithms," *Journal of Computational Chemistry, http://gaussum.sourceforge.net*, vol. 29, no. 5, pp. 839–845, 2008.

[112] M. Raguz and J. Brnjas-Kraljevic, "Resolved fluorescence emission spectra of PRODAN in ethanol/buffer solvents," *Journal of Chemical Information and Modeling*, vol. 45, no. 6, pp. 1636–1640, 2005.

[113] F. Ito, T. Kakiuchi, and T. Nagamura, "Excitation energy migration of acridine orange intercalated into deoxyribonucleic acid thin films," *Journal of Physical Chemistry C*, vol. 111, no. 19, pp. 6983–6988, 2007.

[114] A. Balducci, C. C. Hsieh, and P. S. Doyle, "Relaxation of stretched DNA in slitlike confinement," *Phys Rev Lett*, vol. 99, no. 23, p. 238102, 2007.

[115] T. Odijk, "DNA confined in nanochannels: Hairpin tightening by entropic depletion," *Journal of Chemical Physics*, vol. 125, no. 20, pp. –, 2006.

[116] M. Hayashi and Y. Harada, "Direct observation of the reversible unwinding of a single DNA molecule caused by the intercalation of ethidium bromide," *Nucleic Acids Research*, vol. 35, no. 19, pp. –, 2007.

[117] L. B. Hendry, V. B. Mahesh, E. D. Bransome, and D. E. Ewing, "Small molecule intercalation with double stranded DNA: Implications for normal gene regulation and for predicting the biological efficacy and genotoxicity of drugs and other chemicals," *Mutation Research-Fundamental and Molecular Mechanisms of Mutagenesis*, vol. 623, no. 1-2, pp. 53–71, 2007.

[118] F. Livolant and A. Leforestier, "Condensed phases of DNA: Structures and phase transitions," *Progress in Polymer Science*, vol. 21, no. 6, pp. 1115–1164, 1996.

[119] S. J. Lippard, P. J. Bond, K. C. Wu, and W. R. Bauer, "Stereochemical Requirements for Intercalation of Platinum Complexes into Double-Stranded Dnas," *Science*, vol. 194, no. 4266, pp. 726–728, 1976.

[120] T. Theophanides, "Interactions of Nucleic-Acids and Metals," *Canadian Journal of Spectroscopy*, vol. 26, no. 3, pp. 165–179, 1981.

[121] A. M. Pyle and J. K. Barton, "Probing Nucleic-Acids with Transition-Metal Complexes," *Progress in Inorganic Chemistry*, vol. 38, pp. 413–475, 1990.

[122] C. M. McIntosh, E. A. Esposito, A. K. Boal, J. M. Simard, C. T. Martin, and V. M. Rotello, "Inhibition of DNA transcription using cationic mixed monolayer protected gold clusters," *Journal of the American Chemical Society*, vol. 123, no. 31, pp. 7626–7629, 2001.

[123] W. H. Chu, M. Shinomiya, K. Y. Kamitori, S. Kamitori, R. G. Carlson, R. F. Weaver, and F. Takusagawa, "Role of D-Valine Residues in the Antitumor Drug Actinomycin-D - Replacement of D-Valines with Other D-Amino Acids Changes the DNA-Binding Characteristics and Transcription Inhibitory Activities," *Journal of the American Chemical Society*, vol. 116, no. 18, pp. 7971–7982, 1994.

[124] I. Haq, P. Lincoln, D. C. Suh, B. Norden, B. Z. Chowdhry, and J. B. Chaires, "Interaction of Delta-[Ru(Phen)$_2$Dppz]$^{2+}$ and Lambda-[Ru(Phen)$_2$Dppz]$^{2+}$ with DNA - a Calorimetric and Equilibrium Binding Study," *Journal of the American Chemical Society*, vol. 117, no. 17, pp. 4788–4796, 1995.

[125] P. K. L. Fu, P. M. Bradley, and C. Turro, "Stabilization of duplex DNA structure and suppression of transcription in vitro by bis(quinone diimine) complexes of rhodium(III) and ruthenium(II)," *Inorganic Chemistry*, vol. 42, no. 3, pp. 878–884, 2003.

[126] M. H. Kombrabail and G. Krishnamoorthy, "Fluorescence dynamics of DNA condensed by the molecular crowding agent poly(ethylene glycol)," *Journal of Fluorescence*, vol. 15, no. 5, pp. 741–747, 2005.

[127] B. Lindman and K. Thalberg, *Interactions of Surfactants with Polymers and Proteins*. Boca Raton, FL: CRC Press, 1993.

[128] D. J. Mitchell, G. J. T. Tiddy, L. Waring, T. Bostock, and M. P. Mcdonald, "Phase-Behavior of Polyoxyethylene Surfactants with Water - Mesophase Structures and Partial Miscibility (Cloud Points)," *Journal of the Chemical Society-Faraday Transactions I*, vol. 79, pp. 975–1000, 1983.

[129] B. Medhage, M. Almgren, and J. Alsins, "Phase-Structure of Poly(Oxyethylene) Surfactants in Water Studied by Fluorescence Quenching," *Journal of Physical Chemistry*, vol. 97, no. 29, pp. 7753–7762, 1993.

[130] E. Caponetti, P. D'Angelo, L. Pedone, and V. T. Liveri, "Fourier transform infrared and dielectric study of water-$C_{12}E_4$ liquid crystals," *Journal of Chemical Physics*, vol. 113, no. 19, pp. 8783–8790, 2000.

[131] G. Klose and Y. K. Levine, "Membranes of palmitoyloleoylphosphatidylcholine and C12E4 - A lattice model simulation," *Langmuir*, vol. 16, no. 2, pp. 671–676, 2000.

[132] V. Turco Liveri, *Nano-surface chemistry*, vol. 1. New York: M. Dekker, 2001.

[133] S. Osfouri, P. Stano, and P. L. Luisi, "Condensed DNA in lipid microcompartments," *Journal of Physical Chemistry B*, vol. 109, no. 42, pp. 19929–19935, 2005.

[134] V. G. Budker, P. M. Slattum, S. D. Monahan, and J. A. Wolff, "Entrapment and condensation of DNA in neutral reverse micelles," *Biophysical Journal*, vol. 82, no. 3, pp. 1570–1579, 2002.

[135] S. D. Kennedy and R. G. Bryant, "Manganese-Deoxyribonucleic Acid Binding Modes - Nuclear Magnetic-Relaxation Dispersion Results," *Biophysical Journal*, vol. 50, no. 4, pp. 669–676, 1986.

[136] E. Chargaff, C. F. Crampton, and R. Lipshitz, "Separation of Calf Thymus Deoxyribonucleic Acid into Fractions of Different Composition," *Nature*, vol. 172, no. 4372, pp. 289–292, 1953.

[137] E. Chargaff and R. Lipshitz, "Composition of Mammalian Desoxyribonucleic Acids," *Journal of the American Chemical Society*, vol. 75, no. 15, pp. 3658–3661, 1953.

[138] M. E. Reichmann, S. A. Rice, C. A. Thomas, and P. Doty, "A Further Examination of the Molecular Weight and Size of Desoxypentose Nucleic Acid," *Journal of the American Chemical Society*, vol. 76, no. 11, pp. 3047–3053, 1954.

[139] D. W. Dixon, N. B. Thornton, V. Steullet, and T. Netzel, "Effect of DNA scaffolding on intramolecular electron transfer quenching of a photoexcited ruthenium(II) polypyridine naphthalene diimide," *Inorganic Chemistry*, vol. 38, no. 24, pp. 5526–5534, 1999.

[140] A. Longo, G. Portale, W. Bras, F. Giannici, A. M. Ruggirello, and V. T. Liveril, "Structural characterization of frozen n-heptane solutions of metal-containing reverse micelles," *Langmuir*, vol. 23, no. 23, pp. 11482–11487, 2007.

[141] B. Prescott, C. H. Chou, and G. J. Thomas, "Raman Spectral Studies of Nucleic-Acids .15. Raman Spectroscopic Study of Complexes of Polylysine with Deoxyribonucleic-Acid and Polyriboadenylic Acid," *Journal of Physical Chemistry*, vol. 80, no. 11, pp. 1164–1171, 1976.

[142] M. Rasmusson and B. Akerman, "Dynamic mobility of DNA," *Langmuir*, vol. 14, no. 13, pp. 3512–3516, 1998.

[143] G. Caracciolo, D. Pozzi, H. Amenitsch, and R. Caminiti, "One-dimensional thermotropic dilatation area of lipid headgroups within lamellar lipid/DNA complexes," *Langmuir*, vol. 22, no. 9, pp. 4267–4273, 2006.

[144] P. McPhie *Methods in Enzymology*, vol. 22, pp. 23–32, 1971.

[145] A. Rodger, "Linear dichroism," *Methods Enzymol*, vol. 226, pp. 232–58, 1993.

[146] CrystalClear, *Rigaku Inc.* Texas: The Woodlands, 2008.

[147] Apex2, *Bruker AXS Inc.* Wisconsin: Madison, 2008.

[148] A. Altomare, M. C. Burla, M. Camalli, B. Carrozzini, G. L. Cascarano, C. Giacovazzo, A. Guagliardi, A. G. G. Moliterni, G. Polidori, and R. Rizzi, "EXPO: a program for full powder pattern decomposition and crystal structure solution," *Journal of Applied Crystallography*, vol. 32, pp. 339–340, 1999.

[149] G. M. Sheldrick, "A short history of SHELX," *Acta Crystallographica Section A*, vol. 64, pp. 112–122, 2008.

[150] L. Farrugia, "ORTEP-3 for Windows - a version of ORTEP-III with a Graphical User Interface (GUI)," *Journal of Applied Crystallography*, vol. 30, p. 565, 1997.

[151] C. F. Macrae, P. R. Edgington, P. McCabe, E. Pidcock, G. P. Shields, R. Taylor, M. Towler, and J. van De Streek, "Mercury: visualization and analysis of crystal structures," *Journal of Applied Crystallography*, vol. 39, pp. 453–457, 2006.

[152] T. Tanaka, K. Tsurutani, A. Komatsu, T. Ito, K. Iida, Y. Fujii, Y. Nakano, Y. Usui, Y. Fukuda, and M. Chikira, "Synthesis of new cationic Schiff base complexes of copper(II) and their selective binding with DNA," *Bulletin of the Chemical Society of Japan*, vol. 70, no. 3, pp. 615–629, 1997.

[153] S. J. Angyal, P. J. Morris, J. R. Tetaz, and J. G. Wilson, "The Sommelet Reaction .3. The Choice of Solvent and the Effect of Substituents," *Journal of the Chemical Society*, no. Aug, pp. 2141–2145, 1950.

[154] R. Palchaudhuri and P. J. Hergenrother, "DNA as a target for anticancer compounds: methods to determine the mode of binding and the mechanism of action," *Curr Opin Biotechnol*, vol. 18, no. 6, pp. 497–503, 2007.

[155] R. Cortesi and C. Nastruzzi, "Delivery systems for DNA-binding drugs as gene expression modulators," *Drug Discov Today*, vol. 6, no. 17, pp. 893–904, 2001.

[156] D. R. Boer, A. Canals, and M. Coll, "DNA-binding drugs caught in action: the latest 3D pictures of drug-DNA complexes," *Dalton Trans*, no. 3, pp. 399–414, 2009.

[157] L. H. Hurley, "DNA and its associated processes as targets for cancer therapy," *Nat Rev Cancer*, vol. 2, no. 3, pp. 188–200, 2002.

[158] A. K. Patra, T. Bhowmick, S. Roy, S. Ramakumar, and A. R. Chakravarty, "Copper(II) Complexes of L-Arginine as Netropsin Mimics Showing DNA Cleavage Activity in Red Light," *Inorganic Chemistry*, vol. 48, no. 7, pp. 2932–2943, 2009.

[159] A. K. Patra, S. Roy, and A. R. Chakravarty, "Synthesis, crystal structures, DNA binding and cleavage activity of L-glutamine copper(II) complexes of heterocyclic bases," *Inorganica Chimica Acta*, vol. 362, no. 5, pp. 1591–1599, 2009.

[160] C. Richardson and P. J. Steel, "The first metal complexes of 3,3'-bi-1,2,4-oxadiazole: a curiously ignored ligand," *Inorganic Chemistry Communications*, vol. 10, no. 8, pp. 884–887, 2007.

[161] A. Pace and P. Pierro, "The new era of 1,2,4-oxadiazoles," *Organic and Biomolecular Chemistry*, vol. 7, no. 21, pp. 4337–4348, 2009.

[162] M. H. Gezginci, A. R. Martin, and S. G. Franzblau, "Antimycobacterial activity of substituted isosteres of pyridine- and pyrazinecarboxylic acids," *Journal of Medicinal Chemistry*, vol. 44, no. 10, pp. 1560–1563, 2001.

[163] P. V. Fish, G. A. Allan, S. Bailey, J. Blagg, R. Butt, M. G. Collis, D. Greiling, K. James, J. Kendall, A. McElroy, D. McCleverty, C. Reed, R. Webster, and G. A. Whitlock, "Potent and selective nonpeptidic inhibitors of procollagen C-proteinase," *Journal of Medicinal Chemistry*, vol. 50, no. 15, pp. 3442–3456, 2007.

[164] Z. Li, W. R. Chen, J. J. Hale, C. L. Lynch, S. G. Mills, R. Hajdu, C. A. Keohane, M. J. Rosenbach, J. A. Milligan, G. J. Shei, G. Chrebet, S. A. Parent, J. Bergstrom, D. Card, M. Forrest, E. J. Quackenbush, L. A. Wickham, H. Vargas, R. M. Evans, H. Rosen, and S. Mandala, "Discovery of potent 3,5-diphenyl-1,2,4-oxadiazole sphingosine-1-phosphate-1 (S1P(1)) receptor agonists with exceptional selectivity against S1P(2) and S1P(3)," *Journal of Medicinal Chemistry*, vol. 48, no. 20, pp. 6169–6173, 2005.

[165] Y. Liao, H. Bottcher, J. Harting, H. Greiner, C. van Amsterdam, T. Cremers, S. Sundell, J. Marz, W. Rautenberg, and H. Wikstrom, "New selective and potent 5-HT1B/1D antagonists: Chemistry and pharmacological evaluation of N-piperazinylphenyl biphenylcarboxamides and biphenylsulfonamides," *Journal of Medicinal Chemistry*, vol. 43, no. 3, pp. 517–525, 2000.

[166] A. C. Leite, R. F. Vieira, M. M. D. R. de, D. J. Brondani, R. M. Srivastava, V. F. da Silva, and M. A. de Morais Junior, "Genotoxic activity of 3-[3-phenyl-1,2,4-oxadiazol-5-yl] propionic acid and its peptidyl derivatives determined by Ames and SOS response tests," *Mutat Res*, vol. 588, no. 2, pp. 166–71, 2005.

[167] H. Z. Zhang, S. Kasibhatla, J. Kuemmerle, W. Kemnitzer, K. Ollis-Mason, L. Qiu, C. Crogan-Grundy, B. Tseng, J. Drewe, and S. X. Cai, "Discovery and structure-activity relationship of 3-aryl-5-aryl-1,2,4-oxadiazoles as a new series of apoptosis inducers and potential anticancer agents," *Journal of Medicinal Chemistry*, vol. 48, no. 16, pp. 5215–5223, 2005.

[168] O. Adelfinskaya, V. C. Nashine, D. E. Bergstrom, and V. J. Davisson, "Efficient primer strand extension beyond oxadiazole carboxamide nucleobases," *Journal of the American Chemical Society*, vol. 127, no. 46, pp. 16000–16001, 2005.

[169] N. A. Bokach, A. V. Khripoun, V. Y. Kukushkin, M. Haukka, and A. J. L. Pombeiro, "A route to 1,2,4-oxadiazoles and their complexes via platinum-mediated 1,3-dipolar cycloaddition of nitrile oxides to organonitriles," *Inorganic Chemistry*, vol. 42, no. 3, pp. 896–903, 2003.

[170] M. Singh, V. Aggarwal, U. P. Singh, and N. K. Singh, "Synthesis, spectroscopic and crystal structure investigation of $[Cu(bzsmp)_2Cl_2]^-$; bzsmp=2-benzylsulfanyl-5-(2-methoxyphenyl)-1,3,4-oxadiazole: cyclization of N-2-[bis(benzylsulfanyl)methylene]-2-methoxybenzohydrazide to 2-benzylsulfanyl-5-(2-methoxyphenyl)-1,3,4-oxadiazole during complexation," *Polyhedron*, vol. 28, no. 1, pp. 195–199, 2009.

[171] F. Frausto da Silva and R. Williams, *The biological chemistry of the elements*. Oxford (U.K.): Clarendon Press, 1991.

[172] R. Williams and F. Frausto da Silva, *The natural selection of the chemical elements*. Oxford (U.K.): Clarendon Press, 1997.

[173] A. Siegel, H. Siegel, and R. Siegel, *Nickel and its surprising impact in nature*. New York (N.Y.): Wiley, 2007.

[174] W. Kaim and J. Rall, "Copper - A "modern" bioelement," *Angewandte Chemie-International Edition in English*, vol. 35, no. 1, pp. 43–60, 1996.

[175] H. M. Chen, J. A. Parkinson, O. Novakova, J. Bella, F. Y. Wang, A. Dawson, R. Gould, S. Parsons, V. Brabec, and P. J. Sadler, "Induced-fit recognition of DNA by organometallic complexes with dynamic stereogenic centers," *Proceedings of the National Academy of Sciences of the United States of America*, vol. 100, no. 25, pp. 14623–14628, 2003.

[176] A. Terenzi, G. Barone, A. P. Piccionello, G. Giorgi, A. Guarcello, P. Portanova, G. Calvaruso, S. Buscemi, N. Vivona, and A. Pace, "Synthesis, characterization, cellular uptake and interaction with native DNA of a bis(pyridyl)-1,2,4-oxadiazole copper(II) complex," *Dalton Transactions*, vol. 39, no. 38, pp. 9140–9145, 2010.

[177] X. H. Bu, H. Liu, M. Du, L. Zhang, Y. M. Guo, M. Shionoya, and J. Ribas, "New mononuclear, cyclic tetranuclear, and 1-D helical-chain Cu(II) complexes formed by metal-assisted hydrolysis of 3,6-di-2-pyridyl-1,2,4,5-tetrazine (DPTZ): Crystal structures and magnetic properties," *Inorganic Chemistry*, vol. 41, no. 21, pp. 1855–1861, 2002.

[178] M. Du, X. H. Bu, Y. M. Guo, H. Liu, S. R. Batten, J. Ribas, and T. C. W. Mak, "First Cu-II diamondoid net with 2-fold interpenetrating frameworks. The role of anions in the construction of the supramolecular arrays," *Inorganic Chemistry*, vol. 41, no. 19, pp. 4904–4908, 2002.

[179] P. Gomez-Saiz, J. Garcia-Tojal, M. A. Maestro, J. Mahia, F. J. Arnaiz, and T. Rojo, "Synthesis, crystal structure and spectroscopic properties of copper(II) complexes derived from 2-methylamino-5-pyridin-2-yl-1,3,4-oxadiazole," *Polyhedron*, vol. 21, no. 22, pp. 2257–2263, 2002.

[180] J. K. Barton, A. T. Danishefsky, and J. M. Goldberg, "Tris(Phenanthroline)Ruthenium(Ii) - Stereoselectivity in Binding to DNA," *Journal of the American Chemical Society*, vol. 106, no. 7, pp. 2172–2176, 1984.

[181] A. Wolfe, G. H. Shimer, and T. Meehan, "Polycyclic Aromatic-Hydrocarbons Physically Intercalate into Duplex Regions of Denatured DNA," *Biochemistry*, vol. 26, no. 20, pp. 6392–6396, 1987.

[182] D. E. V. Schmechel and D. M. Crothers, "Kinetic and Hydrodynamic Studies of Complex of Proflavine with Poly-A.Poly-U," *Biopolymers*, vol. 10, no. 3, pp. 465–471, 1971.

[183] G. L. Eichhorn and Y. A. Shin, "Interaction of Metal Ions with Polynucleotides and Related Compounds .12. Relative Effect of Various Metal Ions on DNA Helicity," *Journal of the American Chemical Society*, vol. 90, no. 26, pp. 7323–7328, 1968.

[184] J. Reynisson, G. B. Schuster, S. B. Howerton, L. D. Williams, R. N. Barnett, C. L. Cleveland, U. Landman, N. Harrit, and J. B. Chaires, "Intercalation of trioxatriangulenium ion in DNA: Binding, electron transfer, X-ray crystallography, and electronic structure," *Journal of the American Chemical Society*, vol. 125, no. 8, pp. 2072–2083, 2003.

[185] T. Mosmann, "Rapid colorimetric assay for cellular growth and survival: application to proliferation and cytotoxicity assays," *J Immunol Methods*, vol. 65, no. 1-2, pp. 55–63, 1983.

[186] F. Eloy and R. Lenaers, "Chemistry of Amidoximes and Related Compounds," *Chemical Reviews*, vol. 62, no. 2, pp. 155–183, 1962.

[187] A. Tomazic, M. Tisler, and B. Stanovnik, "Syntheses and Transformations of Some Heterocyclic Hydroxylamines," *Tetrahedron*, vol. 37, no. 9, pp. 1787–1793, 1981.

[188] D. Grant, R. Dahl, and N. D. P. Cosford, "Rapid multistep synthesis of 1,2,4-oxadiazoles in a single continuous microreactor sequence," *Journal of Organic Chemistry*, vol. 73, no. 18, pp. 7219–7223, 2008.

[189] G. I. Pascu, A. C. G. Hotze, C. Sanchez-Cano, B. M. Kariuki, and M. J. Hannon, "Dinuclear ruthenium(II) triple-stranded helicates: Luminescent supramolecular cylinders that bind and coil DNA and exhibit activity against cancer cell lines," *Angewandte Chemie-International Edition*, vol. 46, no. 23, pp. 4374–4378, 2007.

[190] M. Chas, D. Abella, V. Blanco, E. Pia, G. Blanco, A. Fernandez, C. Platas-Iglesias, C. Peinador, and J. M. Quintela, "Synthesis of new self-assembled Pd-II and Pt-II rectangular metallomacrocycles: A comparative study of their inclusion complexes," *Chemistry-a European Journal*, vol. 13, no. 30, pp. 8572–8582, 2007.

[191] D. Abella, V. Blanco, E. Pia, M. Chas, C. Platas-Iglesias, C. Peinador, and J. M. Quintela, "Stereoselective self-assembly of atropoisomeric Pd(II) metallocycles induced by an aromatic guest," *Chemical Communications*, no. 25, pp. 2879–2881, 2008.

[192] M. Fujita, "Metal-directed self-assembly of two- and three-dimensional synthetic receptors," *Chemical Society Reviews*, vol. 27, no. 6, pp. 417–425, 1998.

[193] M. Fujita, M. Tominaga, A. Hori, and B. Therrien, "Coordination assemblies from a Pd(II)-cornered square complex," *Accounts of Chemical Research*, vol. 38, no. 4, pp. 369–378, 2005.

[194] G. F. Swiegers and T. J. Malefetse, "New self-assembled structural motifs in coordination chemistry," *Chemical Reviews*, vol. 100, no. 9, pp. 3483–3537, 2000.

[195] P. J. Steel, "Ligand design in multimetallic architectures: Six lessons learned," *Accounts of Chemical Research*, vol. 38, no. 4, pp. 243–250, 2005.

[196] T. Sawada, M. Yoshizawa, S. Sato, and M. Fujita, "Minimal nucleotide duplex formation in water through enclathration in self-assembled hosts," *Nature Chemistry*, vol. 1, no. 1, pp. 53–56, 2009.

[197] Y. R. Zheng, H. B. Yang, K. Ghosh, L. Zhao, and P. J. Stang, "Multicomponent Supramolecular Systems: Self-Organization in Coordination-Driven Self-Assembly," *Chemistry-a European Journal*, vol. 15, no. 29, pp. 7203–7214, 2009.

[198] M. Mounir, J. Lorenzo, M. Ferrer, M. J. Prieto, O. Rossell, F. X. Aviles, and V. Moreno, "DNA interaction and antiproliferative behavior of the water soluble platinum supramolecular squares $[(en)Pt(N\text{-}N)]_4NO_3]^{8+}$ (en = ethylenediamine, N-N-4,4'-bipyridine or 1,4-bis(4-pyridyl) tetrafluoro benzene)," *Journal of Inorganic Biochemistry*, vol. 101, no. 4, pp. 660–666, 2007.

[199] M. Fujita, J. Yazaki, and K. Ogura, "Preparation of a Macrocyclic Polynuclear Complex, [(En)Pd(4,4'-Bpy)]4(No3)8, Which Recognizes an Organic-Molecule in Aqueous-Media," *Journal of the American Chemical Society*, vol. 112, no. 14, pp. 5645–5647, 1990.

[200] R. Kieltyka, P. Englebienne, J. Fakhoury, C. Autexier, N. Moitessier, and H. F. Sleiman, "A platinum supramolecular square as an effective G-quadruplex binder and telomerase inhibitor," *Journal of the American Chemical Society*, vol. 130, no. 31, pp. 10040–+, 2008.

[201] T. Zincke, "Dinitrophenyl pyridinium chloride and its conversion products," *Justus Liebigs Annalen Der Chemie*, vol. 330, no. 1/3, pp. 361–374, 1904.

[202] V. Blanco, M. D. Garcia, A. Terenzi, E. Pia, A. Fernandez-Mato, C. Peinador, and J. M. Quintela, "Complexation and Extraction of PAHs to the Aqueous Phase with a Dinuclear Pt-II Diazapyrenium-Based Metallacycle," *Chemistry-a European Journal*, vol. 16, no. 41, pp. 12373–12380, 2010.

[203] F. H. Stootman, D. M. Fisher, A. Rodger, and J. R. Aldrich-Wright, "Improved curve fitting procedures to determine equilibrium binding constants," *Analyst*, vol. 131, no. 10, pp. 1145–51, 2006.

[204] C. V. Kumar and E. H. Asuncion, "DNA-Binding Studies and Site-Selective Fluorescence Sensitization of an Anthryl Probe," *Journal of the American Chemical Society*, vol. 115, no. 19, pp. 8547–8553, 1993.

[205] Y. T. Wang, F. L. Zhao, K. A. Li, and S. Y. Tong, "Molecular spectroscopic study of DNA binding with neutral red and application to assay of nucleic acids," *Analytica Chimica Acta*, vol. 396, no. 1, pp. 75–81, 1999.

[206] J. D. Mcghee and P. H. V. Hippel, "Theoretical Aspects of DNA-Protein Interactions - Cooperative and Non-Cooperative Binding of Large Ligands to a One-Dimensional Homogeneous Lattice," *Journal of Molecular Biology*, vol. 86, no. 2, pp. 469–489, 1974.

[207] G. Scatchard, "The Attractions of Proteins for Small Molecules and Ions," *Annals of the New York Academy of Sciences*, vol. 51, no. 4, pp. 660–672, 1949.

[208] J. B. Chaires, N. Dattagupta, and D. M. Crothers, "Studies on Interaction of Anthracycline Antibiotics and Deoxyribonucleic-Acid - Equilibrium Binding-Studies on Interaction of Daunomycin with Deoxyribonucleic-Acid," *Biochemistry*, vol. 21, no. 17, pp. 3933–3940, 1982.

[209] A. Blake and A. R. Peacocke, "Interaction of Aminoacridines with Nucleic Acids," *Biopolymers*, vol. 6, no. 9, pp. 1225–1227, 1968.

[210] M. Lee, A. L. Rhodes, M. D. Wyatt, S. Forrow, and J. A. Hartley, "Gc-Base Sequence Recognition by Oligo(Imidazolecarboxamide) and C-Terminus-Modified Analogs of Distamycin Deduced from Circular-Dichroism, Proton Nuclear-Magnetic-Resonance, and Methidiumpropylethylenediaminetetraacetate-Iron(Ii) Footprinting Studies," *Biochemistry*, vol. 32, no. 16, pp. 4237–4245, 1993.

[211] C. Sanchez-Cano and M. J. Hannon, "Cytotoxicity, cellular localisation and biomolecular interaction of non-covalent metallo-intercalators with appended sex hormone steroid vectors," *Dalton Transactions*, no. 48, pp. 10765–10773, 2009.

[212] J. C. Peberdy, J. Malina, S. Khalid, M. J. Hannon, and A. Rodger, "Influence of surface shape on DNA binding of bimetallo helicates," *Journal of Inorganic Biochemistry*, vol. 101, no. 11-12, pp. 1937–1945, 2007.

[213] R. K. Saiki, D. H. Gelfand, S. Stoffel, S. J. Scharf, R. Higuchi, G. T. Horn, K. B. Mullis, and H. A. Erlich, "Primer-Directed Enzymatic Amplification of DNA with a Thermostable DNA-Polymerase," *Science*, vol. 239, no. 4839, pp. 487–491, 1988.

[214] M. Benedetti, C. Ducani, D. Migoni, D. Antonucci, V. M. Vecchio, A. Ciccarese, A. Romano, T. Verri, G. Ciccarella, and F. P. Fanizzi, "Experimental evidence that a DNA polymerase can incorporate N7-platinated guanines to give platinated DNA," *Angewandte Chemie-International Edition*, vol. 47, no. 3, pp. 507–510, 2008.

[215] J. M. Lehn, J. Blacker, and J. Jazwinski *European Patent Application*, vol. EP244320A119871104, 1987.

[216] W. J. Scot, A. Redman, J. Johnson, J. E. Wood, H. Paulsen, U. Khire, J. Dumas, R. A. Smith, W. Lee, H. Hatoum-Mokdad, B. Riedl, and L. T. B. *Australia Patent Application*, vol. 2006201959, 2006.

[217] P. R. Ashton, S. E. Boyd, A. Brindle, S. J. Langford, S. Menzer, L. Perez-Garcia, J. A. Preece, F. M. Raymo, N. Spencer, J. F. Stoddart, A. J. P. White, and D. J. Williams, "Molecular meccano Part 50 Diazapyrenium-containing catenanes and rotaxanes," *New Journal of Chemistry*, vol. 23, no. 6, pp. 587–602, 1999.

[218] A. J. Blake, G. Baum, N. R. Champness, S. S. M. Chung, P. A. Cooke, D. Fenske, A. N. Khlobystov, D. A. Lemenovskii, W. S. Li, and M. Schroder, "Long-range chain orientation in 1-D coordination polymers as a function of anions and intermolecular aromatic interactions," *Journal of the Chemical Society-Dalton Transactions*, no. 23, pp. 4285–4291, 2000.